Ping Wang · Chunsheng Wu
Ning Hu · K. Jimmy Hsia *Editors*

Micro/Nano Cell and Molecular Sensors

Science Press
Beijing

Springer

Micro/Nano Cell and Molecular Sensors

Ping Wang • Chunsheng Wu • Ning Hu
K. Jimmy Hsia
Editors

Micro/Nano Cell and Molecular Sensors

Science Press
Beijing

Springer

Editors
Ping Wang
Biosensor National Special Laboratory
Department of Biomedical Engineering
Zhejiang University
Hangzhou, China

Ning Hu
Biosensor National Special Laboratory
Department of Biomedical Engineering
Zhejiang University
Hangzhou, China

Chunsheng Wu
Institute of Medical Engineering
School of Basic Medical Sciences
Health Science Center
Xi'an Jiaotong University
Xi'an, China

K. Jimmy Hsia
Department of Biomedical Engineering
Carnegie Mellon University
Pittsburg, PA, USA

ISBN 978-981-10-1656-1 ISBN 978-981-10-1658-5 (eBook)
DOI 10.1007/978-981-10-1658-5

Library of Congress Control Number: 2016954427

Printed on acid-free paper

This Springer imprint is published by Springer Nature
The registered company is Springer Science+Business Media Singapore Pte Ltd.

Contents

Chapter 1
Introduction

Ping Wang, Chunsheng Wu, Ning Hu, and K. Jimmy Hsia

Abstract Rapid advancements in micro- and nanotechnologies have paved the way for the development of cell-/molecule-based biosensors at the micro/nano scale by providing novel micro/nano transducers and the integration of them with cells/molecules. In the recent decades, the integration of cells/molecules with micro/nano devices for the development of novel sensors with unique functions has attracted intensive interest and substantial research efforts. Exciting progress has been achieved due to the combination of micro/nano fabrication technologies with biotechnologies, which introduced new concepts and scientific paradigms to this area. Fast advancements in micro/nano structured devices are providing unprecedented opportunities to couple the devices with functional cells/molecules for the development of next generation of cell and molecular sensors. Micro/nano devices with novel designs at the micro/nano scale make it possible to integrate functional cells/molecules onto transducers with high efficiency and a negligible loss of functionality, which can improve the performances of sensors for the detection of responsive signals. Micro/nano cell and molecular sensors have become increasingly important and have found wide applications in a variety of areas. The topics covered by this book provide a comprehensive summary of the current state of micro/nano cell and molecular sensors as well as their future trend of development, which will be of great interest to the interdisciplinary research community active in this area. In this chapter, we will introduce the definition, characteristics, and types of micro/nano cell and molecular sensors.

Keywords Cell-based biosensor • Molecule-based biosensor • Micro/nano device

P. Wang (✉) • N. Hu
Biosensor National Special Laboratory, Department of Biomedical Engineering, Zhejiang University, Hangzhou, China
e-mail: cnpwang@zju.edu.cn

C. Wu
Institute of Medical Engineering, School of Basic Medical Sciences, Health Science Center, Xi'an Jiaotong University, Xi'an, China

K.J. Hsia
Department of Biomedical Engineering, Carnegie Mellon University, Pittsburg, PA, USA

P. Wang et al. (eds.), *Micro/Nano Cell and Molecular Sensors*,
DOI 10.1007/978-981-10-1658-5_1

1.1 Introduction

Nature is full of fascinating and complex phenomena involving cells/molecules that exhibit unique characteristics for the detection of special biological, biochemical, and biophysical signals with a high level of performance that currently cannot be matched by man-made devices. For example, at the cellular level, olfactory and taste cells are a specialized class of biological elements that can response to various chemical signals presented by taste substances and odorant molecules with ultrahigh performances [1–6]. As a result, they are being increasingly recognized as promising candidates for the development of chemical sensors [7–9]. Neurons and neural networks have also been proved to be ideal candidates for the development of electrical biosensors for chemical sensing with high sensitivity and fast response due to their unique capability of action potentials generation in response to electrical or chemical stimuli [10, 11]. Similarly, cardiomyocytes, a critical component of cardiac muscles, can respond to various chemical signals from different drugs through the generation of changes in cell membrane potential [12–14]. On the other hand, at the molecular level, various functional receptors and DNA molecules that are sensitive to specialized chemical/bioanalytical signals have also been considered as promising candidates for recognition and sensing elements in the development of chemical/bioanalytical sensors [15–17].

Rapid advancements in micro- and nanotechnologies have paved the way for the development of cell-/molecule-based biosensors at the micro/nano scale by providing novel micro/nano transducers and the integration of them with cells/molecules. In the recent decades, the integration of cells/molecules with micro/nano devices for the development of novel sensors with unique functions has attracted intensive interest and substantial research efforts [18–20]. Exciting progress has been achieved due to the combination of micro/nano fabrication technologies with biotechnologies, which introduced new concepts and scientific paradigms to this area. Fast advancements in micro/nano structured devices are providing unprecedented opportunities to couple the devices with functional cells/molecules for the development of next generation of cell and molecular sensors. Micro/nano devices with novel designs at the micro/nano scale make it possible to integrate functional cells/molecules onto transducers with high efficiency and a negligible loss of functionality, which can improve the performances of sensors for the detection of responsive signals. Micro/nano cell and molecular sensors have become increasingly important and have found wide applications in a variety of areas.

This book highlights key aspects and the future promises of micro/nano cell and molecular sensors. These key aspects can be grouped into two main categories: living cell analysis and molecular analysis. Figure 1.1 summarizes the current micro/nano cell and molecule-based biosensors that are developed by the integration of various cells/molecules with different micro/nano sensors such as microelectrode array (MEA), field-effect devices (FEDs), surface plasmon resonance (SPR), and electric substrate-impedance sensing (ECIS). For living cell analysis,

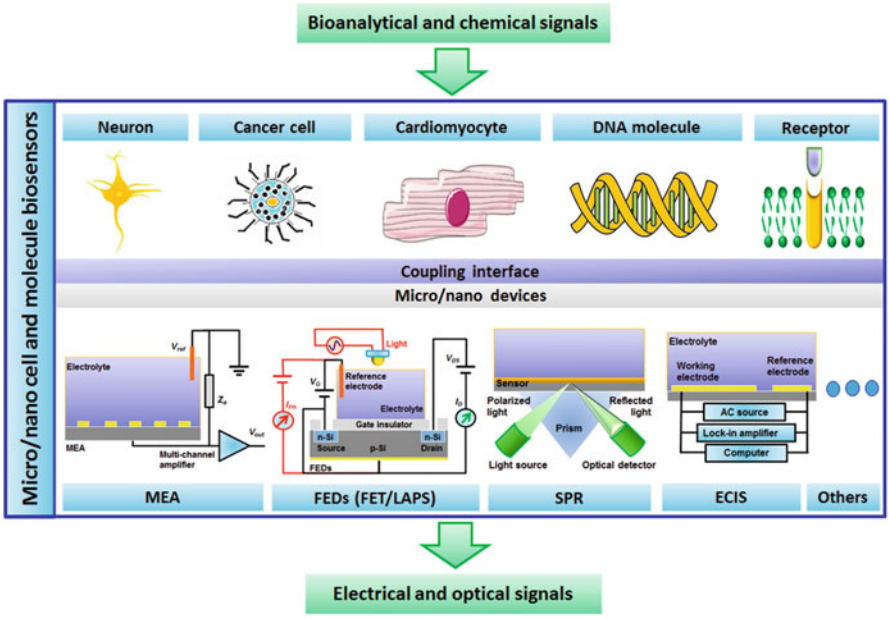

Fig. 1.1 Schematic diagram shows the basic configuration of micro/nano cell- and molecule-based biosensors

common micro/nano cell sensors are discussed to monitor the intra- and extracellular physiological signals, including the principle, design and fabrication, and application. The two main cell sensors, ECIS- and MEA-based sensors, are discussed in detail of their cell impedance and potential study, respectively. For neuron studies, neural network-based sensors are discussed, including the formation of neural networks on solid surface and their chemical sensing. Another aspect is micro/nano sensors for molecular analysis and their applications. For this, label-free DNA biosensors based on FEDs and their applications are introduced. Micro/nano electrochemical sensors are also described for ion sensing and measurement, which is applied in field environmental and food analysis. Moreover, the basic structures and properties of micro/nano materials are introduced in recent developments and applications in biomedicine and food analysis. At the end of this book, the future trend of micro/nano cell and molecular sensors is presented to demonstrate the potential of using the micro/nano electromechanical cell/molecular system and intelligent biosystem in biomimetic devices as well as for health care and rehabilitation.

The topics covered by this book provide a comprehensive summary of the current state of micro/nano cell and molecular sensors as well as their future trend of development, which will be of great interest to the interdisciplinary research community active in this area. In this chapter, we will introduce the definition, characteristics, and types of micro/nano cell and molecular sensors.

1.2 Micro/Nano Cell- and Molecule-Based Biosensors

Micro/nano cell- and molecule-based biosensors refer to the analytical devices that utilize functional cells or molecules as sensing elements and micro/nano scale transducers as physicochemical and biological detector for the detection of specific chemical and bioanalytical signals [21, 22]. In principle, any cell or molecule capable of generating detectable responses to specific stimuli can be used as sensing elements. For instance, excitable cells can generate membrane potential changes when exposed to specific stimuli such as odorants, taste substances, or drugs [12, 23–25]. If these cells are embedded into the transducers that are sensitive to surface potential changes such as FEDs, the responsive signals can thus be recorded by the transducers. By this approach, the specific target analytes can be detected by cell-based biosensors via the recording of cellular membrane potential changes measured at the surface of transducers. Similarly, molecules capable of generating responsive detectable signals upon stimulation can be embedded into the transducers for the detection of target analytes. For example, single-stranded DNA (ssDNA) molecules can be immobilized on the charge-sensitive transducers in order to detect complementary target ssDNA, which can provide information about the concentration and sequences of target ssDNA for the purpose of DNA analysis [26–28].

The integration of functional cells or molecules with micro/nano scale transducers is of great importance to the performance of micro/nano cell- and molecule-based biosensors. At the cell level, the surface of micro/nano transducers is quite different to conventional cell culture dish that is ideal for cell attachment due to its good surface hydrophilicity and proper surface charges. The surface of micro/nano transducers usually consists of silicon or conductive metals, which is not suitable for cell attachment due to the poor biocompatibility of these materials. This makes it a big challenge to obtain good contact between cell membrane and the surface of transducers. As a result, some research activities have been focused on the surface modification of micro/nano transducers for improving the coupling efficiency between cells and transducer surface [29–31]. As shown in Fig. 1.2, microfabricated microfences were employed to facilitate the trapping and immobilization of neurons on solid surfaces [30]. On the other hand, at the molecular level, functional immobilization of sensitive molecules on the surface of micro/nano transducers requires capturing molecules with high efficiency and maintaining their natural sensing functions. For example, hydrophobic environment is usually necessary in order to achieve functional immobilization of membrane receptors on transducer surface, which is crucial to maintain the natural structure and function of membrane receptors [15, 32]. At present, the molecule immobilization approaches mainly include three categories: physical adsorption, specific binding via antibodies, and covalent immobilization via chemical reactions. Each approach has advantages and disadvantages. It is important to choose appropriate approach for

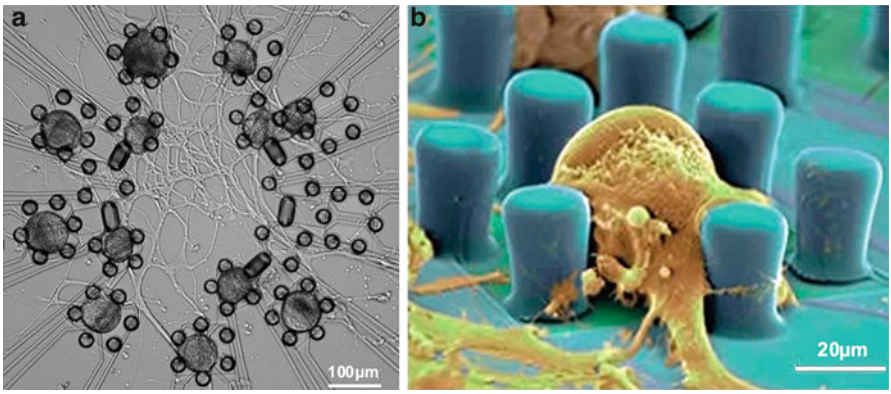

Fig. 1.2 Microfences were employed to precisely trap and immobilize neurons on solid surface. (**a**) Microfence array fabricated by polyimide with trapped neurons inside poles. (**b**) Single microfence trapped single neuron inside poles (Reproduced with permission from Ref. [30]. Copyright 2001 National Academy of Sciences, USA)

the coupling of molecules to transducers, which is crucial to the performance of the whole sensing systems.

In order to design and fabricate micro/nano devices that are suitable to be used as transducers for the detection of accurate signals from cells or molecules, it is necessary to study the mechanism and models of coupling between cells/molecules and micro/nano devices. When the cells or molecules are utilized as sensing elements for the detection of specific analytes, it is of great importance and highly essential to explore the mechanisms of cells/molecules sensing external stimulation and how the sensed signals couple to the transducers. Hence, the development of novel micro/nano devices usually involves considerable amount of basic research on the cellular and molecular sensing mechanisms as well as signal transduction mechanisms.

Micro/nano cell- and molecule-based biosensors have great potential to be used as the rapid, sensitive, low-cost tool for the detection of specific target analytes due to the unconventional integration of functional cells/molecules with micro/nano devices. Functional cells/molecules serve as sensing elements to receive signals from analytes, while micro/nano devices work as transducers that can convert the sensed signals by cells/molecules into electrical or optical output. At the cellular level, micro/nano cell-based biosensors have been used to detect many kinds of chemical and biological analytes by using different types of cells as sensing elements. As a result, micro/nano cell-based biosensors have great potential to be applied in a wide range of applications such as drug discovery, food safety, and environmental monitoring. On the other hand, micro/nano molecule-based biosensors also explored many potential applications and have shown promising prospects. Specifically, the combination of micro/nano field-effect devices with DNA molecules has resulted in the development of label-free DNA biosensors, which have been used for the detection of specific DNA sequences and attract more and

more attention due to their powerful capability for DNA assays and diagnostics and promising applications in a wide range of fields such as molecular diagnostics, gene analysis, and forensic detection.

1.3 Characteristics of Micro/Nano Cell- and Molecule-Based Biosensors

Micro/nano cell- and molecule-based biosensors show unique characteristics due to the unconventional utilization of micro/nano devices as transducers and the employment of natural functional cells or molecules as sensing elements. On the one hand, the sizes of micro/nano fabricated transducers are typically on the order of 10's to 100's of microns, which is much close to the sizes of cells and molecules. This could greatly improve the coupling efficiency of transducers with cells/molecules and result in the improvement in the performance of the whole sensing system. On the other hand, by using microscale or nanoscale devices as transducers, additional advantages are also provided such as significant reduction of sample and reagent consumption, increase in analyte transport, and high efficiency of signal transduction. Meanwhile, micro/nano devices also provide further miniaturization and automation, which could greatly improve the efficiency of detection processes by reducing the time and error compared to conventional manual operations. As a result, a variety of micro/nano cell and molecule-based biosensing platforms have been developed which utilize micro/nano devices as transducers for common analytical detection.

A major characteristic of the micro/nano cell and molecule-based biosensors is the integration of micro/nano devices with functional cells/molecules to develop novel approaches for the detection of specific analytes in a complex environment. Engineered sensing devices are great at detecting one particular chemical or analyte at a time, but perform poorly in a complex environment. Micro/nano cell- and molecule-based biosensors, however, utilize functional cells and molecules as sensing elements, which employ the unique natural function of cells and molecules. This makes micro/nano cell and molecule-based biosensors show similar performances for the detection of analyte with their natural sensing capability that is usually highly sensitive, specific to their target analytes, and performing equally well with multiple target analytes. One further advantage of using cells and molecules as sensing materials is resulted from features of their biological function, which is usually very fast. This characteristic contributes greatly to the fast responses of micro/nano cell and molecule-based biosensors to specific analytes. With the fast advancement in biotechnologies, it has become possible to modify cells and molecules to make them more suitable as sensing materials or even endow them with new functions. For example, cells can be genetically modified to express specific membrane receptors in order to achieve the capability of responding to the corresponding ligands. For this, chemical-sensitive receptors such as olfactory and

taste receptors have been expressed in a heterologous cell system to obtain functional cells that can respond to specific chemical signals such as odorants and tastants.

Micro/nano cell- and molecule-based biosensors have shown many advantages, which include high sensitivity and specificity, fast response, versatility, and high detection efficiency. Numerous applications have been explored by the combination of micro/nano device and functional cells or molecules, which include drug discovery, biomedicine, toxin detection, and environmental monitoring. Micro/nano cell and molecule-based biosensors have shown promising prospects and potential applications.

However, micro/nano cell and molecule-based biosensors also face some challenges, which hinder their further development and practical applications. One of the main problems is that the lifetime of micro/nano cell and molecule-based biosensors which limit their activity in the environment of coupling with transducers. Basically, it is difficult to maintain the natural environmental conditions that can make cells and molecules viable for a long period of time. To achieve this requires very strict controls on the physical and chemical parameters of environment. For mammalian cells, it is important to maintain an environment of certain temperature and CO_2 concentration in order to keep the cells alive and keep their responsive capability to specific target analytes. For this, large instruments like cell incubator are usually necessary, but this is difficult to realize in cell-based biosensors, especially when cells are integrated with micro/nano devices. For molecules, there are also some requirements on the environment in order to maintain their natural structure and functions. Specially, hydrophobic environment is crucial for membrane receptors to maintain their sensing capability to chemical signals. It thus needs to construct hydrophobic environment that is similar to cell membrane to make receptors work perfectly for specific analytic sensing, which has been proved to be difficult, especially on the surface of micro/nano transducers.

In order to utilize cells/molecules as sensing elements, it is crucial to couple the cells and molecules with the sensitive area of transducers, which has great influences on the performance of target analyte detection. This is another important problem faced by the development of micro/nano cell and molecule-based biosensors. To achieve the goal of high efficient coupling of cells/molecules with micro/nano devices, cells and molecules must be immobilized around or on the sensitive surface of the transducers without or with small influence on their natural sensing functions. With the fast advancement in microfabrication process and nanotechnologies, this challenge could be solved by the development of micro/nano devices that can provide interfaces with sizes in micro/nano scale and, consequently, greatly improve their coupling efficiency to cells and molecules because the sizes of cells and molecules are usually in micro/nano scale. Alternatively, the conventional devices modified with a layer of micro/nano materials may also facilitate their coupling with cells and molecules. For example, nanoparticles have been used to modify the surfaces of gold electrode in order to improve the coupling of microelectrodes with cells and thus facilitate the recording of cell

membrane potential changes by reducing the level of extracellular recording [33, 34].

Although micro/nano cell and molecule-based biosensors have shown potential applications in a wide range of fields, the theoretical mechanisms underlying their operation have not been completely understood. It is still not clear how the cells and molecules sensing target analytes, how the sensed signals are transmitted to the transducers, and how to accurately interpret the results. At present, the development of micro/nano cell and molecule-based biosensors means more opportunities as well as challenges in basic research and applications in order to overcome the commercialization barriers of further development.

1.4 Types of Micro/Nano Cell and Molecule-Based Biosensors

A variety of micro/nano cell and molecule-based biosensors have been developed by integrating functional cells and molecules with different transducers or analytical detection techniques such as microelectrode arrays (MEAs), field-effect transistors (FETs), light-addressable potentiometric sensors (LAPSs), and electric cell substrate-impedance sensing (ECIS) [35, 36]. Therefore, the types of micro/nano cell and molecule-based biosensors can be defined not only by the cells and molecules used as sensing elements but also by the micro/nano devices utilized as transducers. This book summarizes the state of the art in micro/nano cell and molecule-based biosensors for chemical sensing and biochemical analysis. Since many of micro/nano cell and molecule-based biosensors employ similar micro/nano devices as transducers, this book will introduce different types of micro/nano cell and molecule-based biosensors based on the types of devices that are used. In each chapter, the development and applications of different types of micro/nano cell and molecule-based biosensors will be introduced. Advantages and limitations as well as future opportunities and prospects of these micro/nano cell and molecule-based biosensors will be discussed.

In Chap. 2, novel micro/nano cell and molecule biosensors will be introduced by comparing the traditional cell and molecule-based biosensors with novel micro/nano cell and molecule biosensors that employ microfabrication process and nanotechnologies. Traditional devices such as MEAs, FETs, LAPSs, and ECISs have provided very useful platform for the development of cell and molecule-based biosensors for the detection of target analytes. However, these conventional devices suffer from some of their intrinsic limitations such as large sizes that are not compatible to the sizes of cells and molecules, which lead to the low efficiency of their coupling with cells and molecules. The fast progress in microfabrication process and nanotechnologies has paved the way for the development of novel devices with sizes in micro/nano scale, which has great potential to improve the performances of micro/nano cell and molecule-based biosensors. Figure 1.3 shows

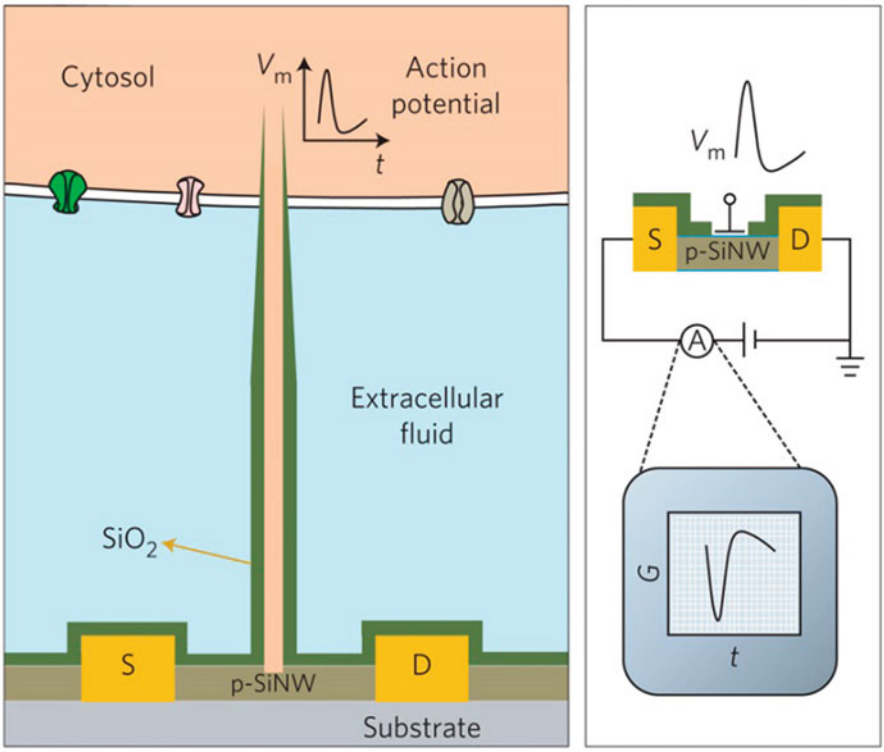

Fig. 1.3 Schematic diagram of a nanoscale FET for intracellular recordings of action potentials (Reproduced with permission from Ref. [37]. Copyright 2015 Nature Publishing Group)

an example of cells coupled with nanoscale FET for intracellular recording of action potentials [37]. Micro/nano devices with nanostructure or nanomaterial modified surfaces have proved to be suitable for the development of cell- and molecule-based biosensors with excellent performance. The combination of micro/nano devices with cells and molecules provides a novel approach for the development of micro/nano cell and molecule-based biosensors, which have shown characteristics of high sensitivity and low detection limit and rapid response and have great potential to be used in a wide range of fields.

In Chap. 3, the most recent advancement in field-effect devices (FEDs)-based DNA biosensors will be introduced. DNA biosensors have attracted more and more interest in recent decades due to their promising prospects and potential applications in a wide range of fields such as DNA diagnostics, gene analysis, fast detection of biological warfare agents, and forensic applications. However, the traditional DNA biosensors are usually developed using labeling strategies, which require the careful designing and labeling of DNA probe or target molecules with various markers (e.g., fluorescence or radiochemical). This has proven to be complicated, expensive, and time-consuming. To address this issue, label-free

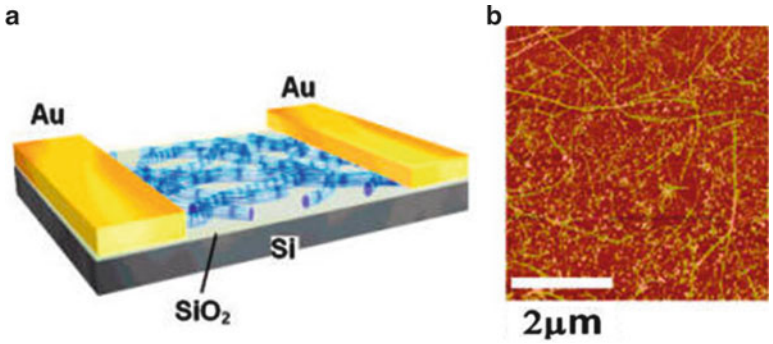

Fig. 1.4 (**a**) Schematic diagram of a FET modified with networks of carbon nanotubes for DNA sensing. (**b**) Atomic force microscope image of networks of carbon nanotubes on gate surface of FET (Reproduced with permission from Ref. [38]. Copyright 2007 American Chemical Society)

DNA biosensors have been developed. Among them, label-free DNA biosensors based on FEDs have shown significant promise, which utilize FEDs as charge-sensitive transducers for the label-free detection of DNA molecules based on their intrinsic molecular charges. Figure 1.4 shows a FET modified with networks of carbon nanotubes on its gate surface for DNA sensing [38]. Chapter 3 will introduce the signal generation and transduction mechanisms of DNA molecules and the basic principle of FED-based DNA biosensors. The coupling of DNA molecules with FEDs, the fabrication of FEDs, and the measurement setup will also be introduced in detail. Typical applications of FED-based DNA biosensors will be summarized in two aspects including the label-free DNA assays and detection of SNPs. Benefited from the fast advancement in the microfabrication process and nanotechnologies, FED-based DNA biosensors have shown some distinct advantages such as easy integration, mass production, and cost-effectiveness.

In Chap. 4, the mechanisms, development process, and applications of novel ECIS-based cell biosensors will be introduced with their most recent advancements. ECIS has proven to be a powerful biophysical technology for cellular analysis, which can monitor the growth status of cells cultured on sensor surface in a real-time and noninvasive manner based on the monitoring of electrode impedance changes induced by the physiological changes of cells cultured on the electrode surface. In recent decades, ECIS-based cell biosensors have attracted more and more attention due to their unique capability of monitoring various cellular events such as cell adhesion, cell growth, cell motility, and cell death. Figure 1.5 shows a cell-based ECIS integrated with a microfluidic chip for monitoring the migration of single cancer cell in three-dimensional matrixes [39]. In addition, ECIS-based cell biosensors have shown decisive advantages compared to traditional cell-based assays, including label-free detection, real-time monitoring, and noninvasive analysis. This chapter will introduce the measuring principles, sensor design and fabrication, measurement setup, and applications of ECIS-based cell biosensors. ECIS-based cell biosensors are characterized by their unique capability of

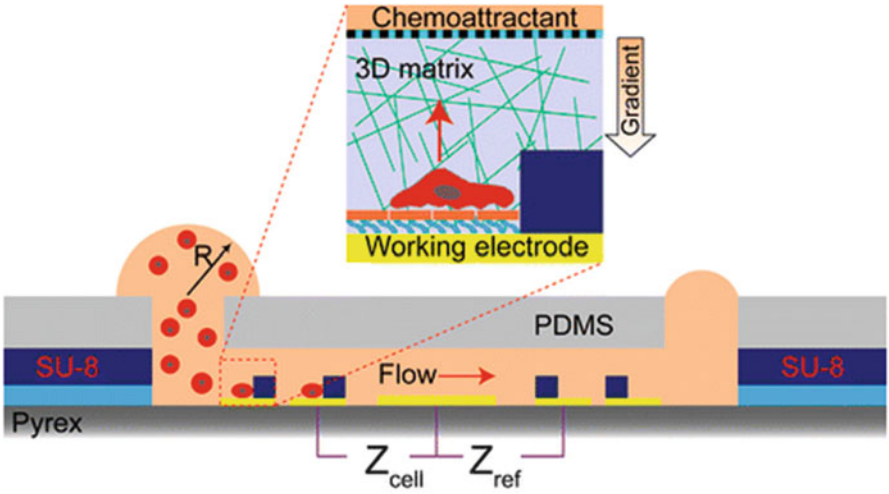

Fig. 1.5 Schematic diagram of an ECIS integrated with a microfluidic chip for monitoring single cancer cell migration in three-dimensional matrixes (Reproduced with permission from Ref. [39]. Copyright 2013 American Chemical Society)

performing fast, long-term, nondestructive, and high-throughput measurement, which have been demonstrated to be a valuable tool for cellular analysis and have great potentials to be applied in various fields such as drug screening, cancer research, and environmental pollutant identification.

In Chap. 5, novel MEA-based cell biosensors will be introduced, which is mainly focused on the principle and applications of MEA-based cell biosensors for extracellular recording of cardiomyocyte. The conventional techniques for cellular recording such as patch clamp usually suffer from the damage to cells, complex operations, and expensive instruments. The fast advancement in microfabrication process provides novel approaches for the development of novel micro/nano devices that are able to realize noninvasive and long-term cellular recordings. In recent decade, MEA have attracted more and more attention and achieved significant progress due to their promising prospects and broad range of applications. Especially, MEA-based biosensors that utilize cardiomyocyte as sensing elements provide a powerful and valuable tool for evaluation the influences of drugs and chemical stimuli on function of cardiomyocyte and their networks in a noninvasive and long-term manner with high throughput [40]. MEA devices are able to measure extracellular potential and impedance of cardiomyocytes [41]. In addition, MEA-based cell biosensors have shown decisive advantages by providing various affiliations to facilitate the cellular analysis such as the sample perfusion chamber, temperature controller, and various culture chambers, which makes it possible to perform a long-term measurement over several weeks or even months. MEA-based cell biosensors provide a promising platform for quantifying cellular events such as adhesion, spreading, growth, and motility, which is very useful in the

applications of cellular analysis including evaluation of environmental toxins and pharmacological drugs.

In Chap. 6, neuronal network-based biosensors will be introduced by focusing on the preparation of neuronal networks, various detection platforms, and their applications in biomedicine. Rapid advancement in semiconductor microfabrication technologies allows for the development of micro/nano devices that are more efficient and compatible with neurons and neuronal networks. The interface between neurons and micro/nano devices makes the signal transduction more efficient. This chapter will introduce the conventional devices such as FETs as well as the emerging micro/nano devices including graphene FET and nanowire FETs in detail. The combination of neuronal networks with micro/nano devices not only provides novel approaches for the research of mechanisms of neuron-to-neuron communications to explore the relation between the function of neuronal networks and the activity of individual neurons with high spatial and temporal resolution but also provides novel tools for applications in biomedicine such as drug screening, odor detection, and even toxicity detection in complex environment. Figure 1.6 is an example of nanowire FET array for recording the activities of neuronal networks with high temporal and spatial resolution [42]. The advantages of neuronal network-based biosensors are mainly originated from the features of neuronal networks such as spontaneous multichannel electrophysiological activities and fault tolerance. On the other hand, micro/nano devices provide further

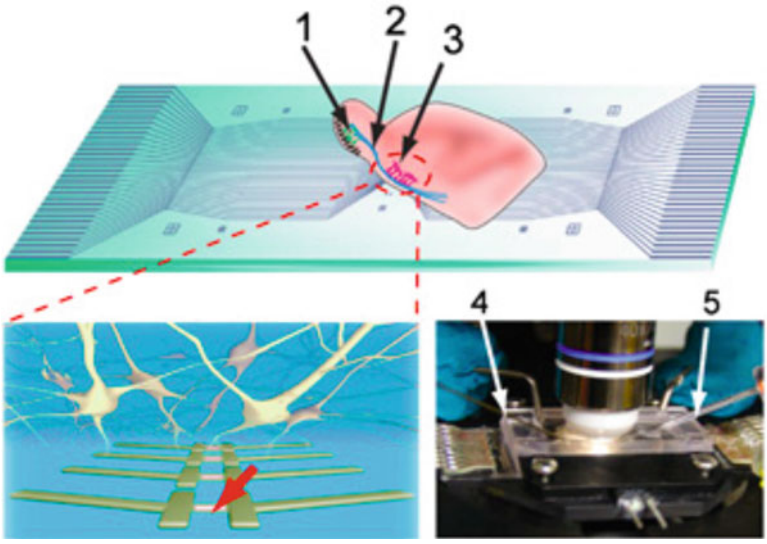

Fig. 1.6 Schematics of a silicon nanowire FET array fabricated on a transparent substrate for recording neuronal activities of pyramidal cell slice with high temporal and spatial resolution. Interconnected neurons and FETs are shown in *bottom left*. *Bottom right* is a photograph of the assembled sample chamber (Reproduced with permission from Ref. [42]. Copyright 2010 National Academy of Sciences, USA)

advantages of neuronal network-based biosensors such as lower signal detection limits and high signal-to-noise ratio.

In Chap. 7, the structures and properties of nanomaterials and their applications in micro/nano cell and molecule-based biosensors will be introduced. Nanomaterials refer to the materials that have at least one of their dimensions ranging in scale from 1 to 100 nm, which show unique physical and chemical features due to the quantum size effect, mini size effect, surface effect, and macro-quantum tunnel effect. Nanomaterials have been increasingly recognized as promising materials for the development of novel biosensors due to their powerful and valuable capability in improving the performances of biosensors. They can not only improve the coupling efficiency of cells and molecules with transducers but also provide good reaction microenvironment, accelerate the electron transfer process, and shorten the response time of signal [43–45]. Figure 1.7 shows the utilization of single-walled carbon nanotube (SWCNT) functionalized with flavin adenine dinucleotide (FAD) to facilitate the electrical coupling between glucose oxidase and Au electrode [46]. The utilization of nanomaterials in biosensors allows for the application of many new signal transduction technologies in the detection of cellular or molecular responses. In addition, the micro/nano devices functionalized with nanomaterials are able to perform rapid analysis of multiple substances in vivo

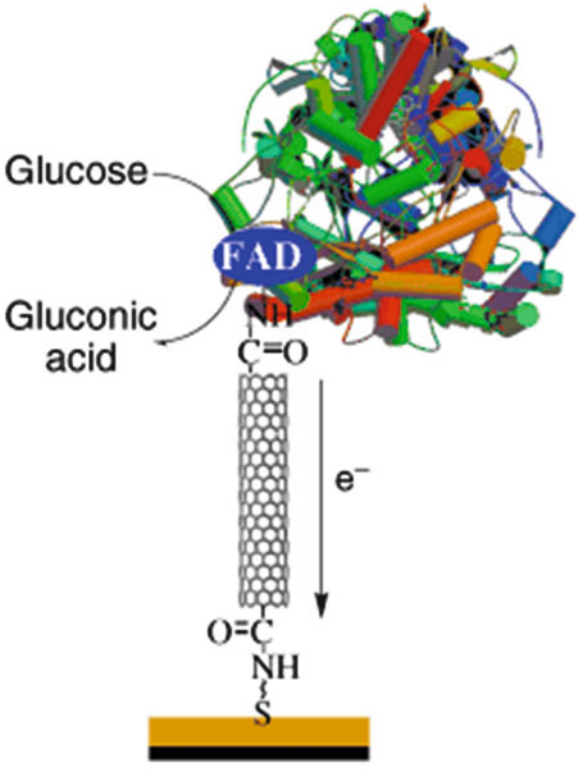

Fig. 1.7 Schematic diagram of single-walled carbon nanotube (SWCNT) functionalized with flavin adenine dinucleotide (FAD) was employed to realize the electrical contact between glucose oxidase and Au electrode (Reproduced with permission from Ref. [46]. Copyright 2015 John Wiley and Sons)

and in vitro due to their micro/nano scale sizes. Benefited from the discovery of more and more nanomaterials, micro/nano cell- and molecule-based biosensors obtain new opportunities to broaden their applications in a wide range of fields such as life science and engineering technology.

In Chap. 8, micro/nano electrochemical sensors for the detection of heavy metal ions in water environment will be introduced. Extensive heavy metals such as zinc, copper, cadmium, lead, mercury, and chromium is of great importance with regards to the human health and environmental protection due to their high toxicity, bioaccumulation, and non-biodegradability in water as ions. As a result, the detection of heavy metal ions is very important and essential in order to protect human and the environment from the harmful effects of heavy metal ions. However, the conventional approaches for heavy metal analysis as atomic absorption spectroscopy (AAS) and inductively coupled plasma mass spectroscopy (ICP-MS) are expensive, time-consuming, and not suitable for in-field measurement [47, 48]. Micro/nano electrochemical sensors provide novel approach to overcome these drawbacks, which are characterized with high sensitivity, rapid response, low detection limit, high signal-to-noise ratio, and cost-effectiveness. In addition, multiple heavy mental ions can be detected simultaneously due to the multiplex analysis capability of micro/nano electrochemical sensors. As a result, micro/nano electrochemical sensors for heavy mental ion sensing have been applied in a wide range of fields such as environment protection, water quality control, and food safety, which have shown promising prospects and commercialization potentials [49–51].

1.5 Summary

Micro/nano cell- and molecule-based biosensors have been increasingly recognized as a promising technology, which are characterized with high degree of sensitivity and specificity and rapid responses due to the utilization of cells and molecules as sensing elements and micro/nano devices as transducers. These biosensors have shown promising prospects and potential applications in a wide range of fields due to their unique capability of detecting a wide spectrum of target analytes. The use of cells and molecules as sensing elements makes it possible to directly receive functional qualitative or quantitative analytical information of analytes, which is very important in certain applications such as clinical diagnostics, pharmacology and drug screening, and toxicology and environmental monitoring. On the other hand, many of these biosensors employ nanomaterials or micro/nano devices to improve the performance of target analyte detection, which further advances the development of micro/nano cell and molecule-based biosensors and broaden their applications. The combination of micro/nano devices with cells and molecules also provide novel approaches to improving the flexibility and efficiency of analyte recognition and signal transduction.

Although many promising micro/nano cell- and molecule-based biosensors have been reported, there are still challenges that need to be addressed before these biosensors can achieve further development and practical applications. For example, it is highly essential and important to develop novel methods for the generation of functional cells and molecules with high quality that are suitable to be used as sensing elements. Moreover, methods for improving the integrity, life time, and stability of cell- and molecule-based biosensors are required. In addition, it is desirable to develop novel methods to enhance automation and make these biosensor systems more user-friendly. With the fast advancement in microfabrication process and nanotechnologies, enhanced robustness, sensitivity, and scalability are expected to be the features of next-generation micro/nano cell and molecule-based biosensors. All these progresses will help to make micro/nano cell- and molecule-based biosensors more useful for existing and new applications including biomedicine, food safety, environmental monitoring, and disease diagnosis.

References

1. Buck L, Axel R. A novel multigene family may encode odorant receptors: a molecular basis for odor recognition. Cell. 1991;65(1):175–87.
2. Nakamura T. Cellular and molecular constituents of olfactory sensation in vertebrates. Comp Biochem Physiol A Mol Integr Physiol. 2000;126(1):17–32.
3. Ache BW, Young JM. Olfaction: diverse species, conserved principles. Neuron. 2005;48 (3):417–30.
4. Gilbertson TA, Boughter JD, Zhang H, Smith DV. Distribution of gustatory sensitivities in rat taste cells: whole-cell responses to apical chemical stimulation. J Neurosci. 2001;21 (13):4931–41.
5. DeFazio RA, Dvoryanchikov G, Maruyama Y, Kim JW, Pereira E, Roper SD, Chaudhari N. Separate populations of receptor cells and presynaptic cells in mouse taste buds. J Neurosci. 2006;26(15):3971–80.
6. Chandrashekar J, Hoon MA, Ryba NJ, Zuker CS. The receptors and cells for mammalian taste. Nature. 2006;444(7117):288–94.
7. Wu C, Wang L, Zhou J, Zhao L, Wang P. The progress of olfactory transduction and biomimetic olfactory-based biosensors. Chin Sci Bull. 2007;52(14):1886–96.
8. Du L, Zou L, Zhao L, Wang P, Wu C. Biomimetic chemical sensors using bioengineered olfactory and taste cells. Bioengineered. 2014;5(5):326–30.
9. Wu C, Du L, Zou L, Zhao L, Huang L, Wang P. Recent advances in taste cell-and receptor-based biosensors. Sensors Actuators B. 2014;201:75–85.
10. Prasad S, Tuncel E, Ozkan M. Association of different prediction methods for determination of the efficiency and selectivity on neuron-based sensors. Biosens Bioelectron. 2006;21 (7):1045–58.
11. Morin F, Nishimura N, Griscom L, LePioufle B, Fujita H, Takamura Y, Tamiya E. Constraining the connectivity of neuronal networks cultured on microelectrode arrays with microfluidic techniques: a step towards neuron-based functional chips. Biosens Bioelectron. 2006;21(7):1093–100.
12. Wang T, Hu N, Cao J, Wu J, Su K, Wang P. A cardiomyocyte-based biosensor for antiarrhythmic drug evaluation by simultaneously monitoring cell growth and beating. Biosens Bioelectron. 2013;49:9–13.

13. Liu Q, Cai H, Xu Y, Xiao L, Yang M, Wang P. Detection of heavy metal toxicity using cardiac cell-based biosensor. Biosens Bioelectron. 2007;22(12):3224–9.
14. DeBusschere BD, Kovacs GT. Portable cell-based biosensor system using integrated CMOS cell-cartridges. Biosens Bioelectron. 2001;16(7):543–56.
15. Du L, Wu C, Liu Q, Huang L, Wang P. Recent advances in olfactory receptor-basedbiosensors. Biosens Bioelectron. 2013;42:570–80.
16. Sassolas A, Leca-Bouvier BD, Blum LJ. DNA biosensors and microarrays. Chem Rev. 2008;108(1):109–39.
17. Liu A, Wang K, Weng S, Lei Y, Lin L, Chen W, Lin X, Chen Y. Development of electrochemical DNA biosensors. TrAC Trends Anal Chem. 2012;37:101–11.
18. Ho C-M, Tai Y-C. Micro-electro-mechanical-systems (MEMS) and fluid flows. Annu Rev Fluid Mech. 1998;30(1):579–612.
19. Grayson ACR, Shawgo RS, Johnson AM, Flynn NT, Li Y, Cima MJ, Langer R. A BioMEMS review: MEMS technology for physiologically integrated devices. Proc IEEE. 2004;92 (1):6–21.
20. Bashir R. BioMEMS: state-of-the-art in detection, opportunities and prospects. Adv Drug Deliv Rev. 2004;56(11):1565–86.
21. Turner A, Karube I, Wilson GS. Biosensors: fundamentals and applications. 1987.
22. Liu Q. Cell-based biosensors: principles and applications (Artech House, 2014). 2014.
23. Wang P, Liu Q, Xu Y, Cai H, Li Y. Olfactory and taste cell sensor and its applications in biomedicine. Sensors Actuators A Phys. 2007;139(1):131–8.
24. Wu C, Chen P, Yu H, Liu Q, Zong X, Cai H, Wang P. A novel biomimetic olfactory-based biosensor for single olfactory sensory neuron monitoring. Biosens Bioelectron. 2009;24 (5):1498–502.
25. Wu C, Du L, Mao L, Wang P. A novel bitter detection biosensor based on light addressable potentiometric sensor. J Innov Opt Health Sci. 2012;5(02):1250008.
26. Kim D-S, Jeong Y-T, Park H-J, Shin J-K, Choi P, Lee J-H, Lim G. An FET-type charge sensor for highly sensitive detection of DNA sequence. Biosens Bioelectron. 2004;20(1):69–74.
27. Kataoka-Hamai C, Miyahara Y. Label-free detection of DNA by field-effect devices. Sensors J IEEE. 2011;11(12):3153–60.
28. Wu C, Bronder T, Poghossian A, Werner CF, Schöning MJ. Label-free detection of DNA using a light-addressable potentiometric sensor modified with a positively charged polyelectrolyte layer. Nanoscale. 2015;7(14):6143–50.
29. Chaniotakis N, Sofikiti N. Novel semiconductor materials for the development of chemical sensors and biosensors: a review. Anal Chim Acta. 2008;615(1):1–9.
30. Zeck G, Fromherz P. Noninvasive neuroelectronic interfacing with synaptically connected snail neurons immobilized on a semiconductor chip. Proc Natl Acad Sci. 2001;98 (18):10457–62.
31. Kotov NA, Winter JO, Clements IP, Jan E, Timko BP, Campidelli S, Pathak S, Mazzatenta A, Lieber CM, Prato M. Nanomaterials for neural interfaces. Adv Mater. 2009;21 (40):3970–4004.
32. Stenlund P, Babcock GJ, Sodroski J, Myszka DG. Capture and reconstitution of G protein-coupled receptors on a biosensor surface. Anal Biochem. 2003;316(2):243–50.
33. Xiao L, Liu Q, Hu Z, Zhang W, Yu H, Wang P. A multi-scale electrode array (MSEA) to study excitation–contraction coupling of cardiomyocytes for high-throughput bioassays. Sensors Actuators B. 2011;152(1):107–14.
34. Xiao L, Hu Z, Zhang W, Wu C, Yu H, Wang P. Evaluation of doxorubicin toxicity on cardiomyocytes using a dual functional extracellular biochip. Biosens Bioelectron. 2010;26 (4):1493–9.
35. Liu Q, Wu C, Cai H, Hu N, Zhou J, Wang P. Cell-based biosensors and their application in biomedicine. Chem Rev. 2014;114(12):6423–61.
36. Wu C, Lillehoj PB, Wang P. Bioanalytical and chemical sensors using living taste, olfactory, and neural cells and tissues: a short review. Analyst. 2015;140(21):7048–61.

37. Duan X, Gao R, Xie P, Cohen-Karni T, Qing Q, Choe HS, Tian B, Jiang X, Lieber CM. Intracellular recordings of action potentials by an extracellular nanoscale field-effect transistor. Nat Nanotechnol. 2012;7(3):174–9.
38. Gui EL, Li L-J, Zhang K, Xu Y, Dong X, Ho X, Lee PS, Kasim J, Shen Z, Rogers JA. DNA sensing by field-effect transistors based on networks of carbon nanotubes. J Am Chem Soc. 2007;129(46):14427–32.
39. Nguyen TA, Yin T-I, Reyes D, Urban GA. Microfluidic chip with integrated electrical cell-impedance sensing for monitoring single cancer cell migration in three-dimensional matrixes. Anal Chem. 2013;85(22):11068–76.
40. Navarrete EG, Liang P, Lan F, Sanchez-Freire V, Simmons C, Gong T, Sharma A, Burridge PW, Patlolla B, Lee AS. Screening drug-induced arrhythmia using human induced pluripotent stem cell–derived cardiomyocytes and Low-impedance microelectrode arrays. Circulation. 2013;128(11 suppl 1):S3–13.
41. Hu N, Fang J, Li H, Su K, Wang P. Dual-function microelectrode array system for simultaneously monitoring electromechanical integration status of cardiomyocytes, in Editor (Ed.)^(Eds.): Book dual-function microelectrode array system for simultaneously monitoring electromechanical integration status of cardiomyocytes (IEEE, 2015, edn.), p. 1519–22.
42. Qing Q, Pal SK, Tian B, Duan X, Timko BP, Cohen-Karni T, Murthy VN, Lieber CM. Nanowire transistor arrays for mapping neural circuits in acute brain slices. Proc Natl Acad Sci. 2010;107(5):1882–7.
43. Yang W, Ratinac KR, Ringer SP, Thordarson P, Gooding JJ, Braet F. Carbon nanomaterials in biosensors: should you use nanotubes or graphene? Angew Chem Int Ed. 2010;49(12):2114–38.
44. Pandey P, Datta M, Malhotra B. Prospects of nanomaterials in biosensors. Anal Lett. 2008;41(2):159–209.
45. Wang J. Nanomaterial-based electrochemical biosensors. Analyst. 2005;130(4):421–6.
46. Patolsky F, Weizmann Y, Willner I. Long-range electrical contacting of redox enzymes by SWCNT connectors. Angew Chem Int Ed. 2004;43(16):2113–7.
47. Welz B, Sperling M. Atomic absorption spectrometry. Weinheim: Wiley; 2008.
48. Jarvis KE, Gray AL, Houk RS. Handbook of inductively coupled plasma mass spectrometry. New York: Blackie; Chapman and Hall; 1991.
49. Schöning MJ, Kloock JP. About 20 years of silicon – based thin – film sensors with chalcogenide glass materials for heavy metal analysis: technological aspects of fabrication and miniaturization. Electroanalysis. 2007;19(19-20):2029–38.
50. Wan H, Ha D, Zhang W, Zhao H, Wang X, Sun Q, Wang P. Design of a novel hybrid sensor with microelectrode array and LAPS for heavy metal determination using multivariate nonlinear calibration. Sensors Actuators B. 2014;192:755–61.
51. Ha D, Hu N, Wu C, Kirsanov D, Legin A, Khaydukova M, Wang P. Novel structured light-addressable potentiometric sensor array based on PVC membrane for determination of heavy metals. Sensors Actuators B. 2012;174:59–64.

Chapter 2
Micro/Nano Biosensors for Living Cell and Molecule Analysis

Ning Hu, Jiaru Fang, and Ling Zou

Abstract The novel micro/nano cell and molecule biosensors are developed based on the traditional microfabrication and novel nanotechnology. Traditional biosensors, such as microelectrode array, impedance sensor, field-effect transistor, and light addressable potentiometric sensor, are useful tools in studying the cell biology and molecule analysis, while the nanobiosensor- and nanomaterial modified biosensors emerge gradually with the advance of nanotechnology. These nanobiosensor can achieve the single cell monitoring with high-quality signals, and nanomaterial modified biosensors have demonstrated excellent performance in cell and molecule applications. Combination of sensor detection technology and nanotechnology, the novel micro/nano cell, and molecule biosensors can explore a wide way in fields of biomedicine and environment monitoring.

Keywords Microbiosensor • Nanoscale FET • Nanobiosensor • Nanomaterial modified biosensor

2.1 Introduction

In recent year, micro/nano biosensors play a significant role in biomedicine researches. Micro/nano biosensors usually consist of two key components: one is living cells or bioactive molecules and the other is micro/nano structure sensor. Living cell is the basic unit of biological structures and functions and also the basic function unit of life activities. As shown in Fig. 2.1, living cells (e.g., myocytes, neurons, cancer cells) can be used to fabricate the cell-based biosensor to sensitively respond to intracellular and extracellular microenvironment changes. Most of adherent cells can attach and grow on the biosensor surface with characteristics of

N. Hu (✉) • J. Fang • L. Zou
Biosensor National Special Laboratory, Department of Biomedical Engineering, Zhejiang University, Hangzhou, China
e-mail: huning@zju.edu.cn

P. Wang et al. (eds.), *Micro/Nano Cell and Molecular Sensors*,
DOI 10.1007/978-981-10-1658-5_2

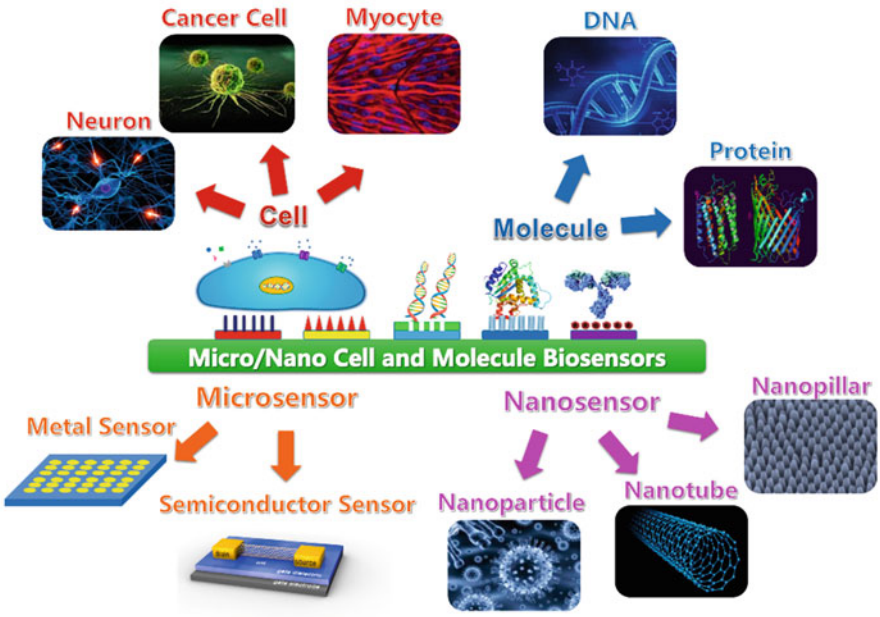

Fig. 2.1 Micro/nano cell and molecule biosensors

metabolism, proliferation, spreading, and migration, which can be converted into physical and chemical signals, such as changes of attachment or ion concentration, and the basic growth status can be monitored by the cell-based biosensors [1–6]. Besides, the electrogenic cells will spontaneously generate the action potential based on ion currents, which can be amplified and recorded in real time [7–10]. Furthermore, bioactive molecules (e.g., DNA, protein) can be used to fabricate the molecule-based biosensor to detect the target molecules (e.g., DNA, RNA, antigen) or molecule structure changes [11–13]. Micro/nano biosensor is another key element, which can record these various parameter changes induced by cells and molecules.

Traditional cell and molecule biosensors are commonly established by microstructure sensors, such as metal-based microelectrode array and semiconductor-based field-effect sensors for cellular potential, cellular growth, cellular metabolism, and target molecule detection. With the great advancement of nanotechnology, the nanostructure sensors are also employed for cell and molecule study. In the past decades, nanotechnology has greatly changed the state of science and technology. The former nanotechnology referred to precisely manipulating at the atoms and molecules levels, and now the nanotechnology is described as the manipulation of matter with at least one dimension sized within 1–100 nm [14–17]. The most common nanomaterials include nanoparticle, nanopore, nanotube, nanowire, etc. Now, nanotechnology is also playing a significant role in the development of cell and molecule biosensors. Performance of biosensors can be greatly enhanced by combining nanomaterials or nanostructures. Nanomaterials or nanostructures

present unique physical and chemical characteristics due to various effects. Based on their submicron dimensions, nanobiosensors have provided simple and rapid analytical methods for cells and molecules.

The integration of microfabrication, nanotechnology, biology, electronics, and photonics makes it possible to establish the novel micro/nano cell and molecule-based biosensors for wide applications. Many studies have been carried out to employ micro- and nano-based biosensors at the cellular or molecular level. Over the decades, micro/nano cell and molecule biosensors are developed to detect the biofunctional information of living cells and bioactive molecules. These novel biosensors have characteristics of high sensitivity, low detection limit, and rapid response, which have been widely applied in the fields of biomedicine, environmental monitoring, and pharmaceutical assessment.

2.2 Traditional Cell- and Molecular-Based Biosensors

2.2.1 Microelectrode Array

Microelectrode array (MEA) is a multisite and noninvasive metal-based biosensor for detecting extracellular potential of electrogenic cells (neurons and cardiomyocytes). In 1972, Thomas and his colleagues firstly reported that they employed MEA to record the signals of chicken cardiomyocytes [18]. Figure 2.2a

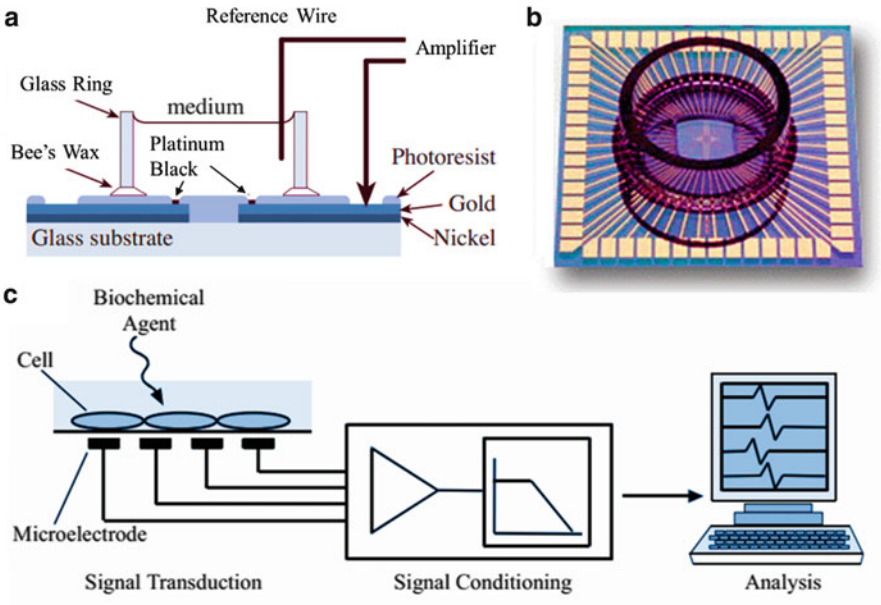

Fig. 2.2 Schematic of MEA (**a**), commercial MEA chip (**b**) and whole structure of detection system (**c**) (Reproduced with permission from Ref. [18]. Copyright 1972 Elsevier B.V.)

has shown the MEA designed by Thomas group. MEA was fabricated on the glass substrate by nikel and gold material, and patterns were formed by photoresist. Most of the metal was insulated by photoresist except microelectrode patterns. Meanwhile the bee wax was used to immobilize glass ring onto the glass substrate to form a cell culture chamber. Moreover, platinum black was electroplated on the electrode sites to enhance the signal-noise ratio (SNR) [19, 20]. Finally, the extracellular potential can be synchronously recorded from the multiple MEA. Researchers employed the MEA structure to carry out many experiments on cells, and also performance and fabrication of MEA are improved for the wide cell applications. Gross applied the polymer material to replace the photoresist insulator layer and record the extracellular potential of separate nerve tissue (brain nerve center of the snail) [21, 22]. The SiO_2 is used as insulator layer, and signals of separate neurons (neonatal rat sympathetic ganglion) are first detected [23]. Figure 2.2b is a commercial MEA chip produced by Multi Channel Systems GmbH.

Due to the practicability of MEA on recording extracellular potential, more studies and applications were explored based on the MEA. Figure 2.2c illustrates a typical MEA system, including MEA chip for signal transduction, amplification and filtering circuits for signal conditioning, and computer software for signal analysis. MEA platform can reflect the cellular responses to biochemical agents in microenvironment. A neuron-based biosensor was established to study the agent effects by spike signals, while the action potential profiles of cardiomyocytes can also be related with the different agents [24, 25]. Moreover, some portable cell-based biosensor instrument was designed for on-site rapid toxin detection [26]. Therefore, MEA is useful metal-based biosensor, which can be widely applied in field of pharmaceutical screening and toxin detection [27–29].

2.2.2 *Impedance Biosensor*

Impedance biosensor is another important metal-based biosensor for cell and molecule detection. The cells and molecules can be measured by electrochemical impedance spectroscopy (EIS), which measures the impedance of a medium as a function of frequency (Fig. 2.3). After the cells and molecules occupy the electrode sites, the ion current will be blocked, so the impedance values will be increased. The molecule (DNA, protein, etc.) concentrations can be calculated according to the Nyquist diagram, which has a low detection limit comparing with other methods. For cells, electric cell-substrate impedance sensing (ECIS) was proposed by Giaever and Keese in 1984, which can quantitatively evaluate the cellular morphology and motion to solve the problems of optical microscope [4].

ECIS detection system proposed by Giaever and Keese is presented in Fig. 2.4. The gold film electrodes were fabricated on standard polyethylene cell culture dish, including one large reference electrode (2 cm^2) and four small working electrodes (3×10^{-4} cm^2). Human lung fibroblasts (WI-38 and WI-38/VA-13) were selected to test this system. Lock-in amplifier is connected with a larger resistance to form a

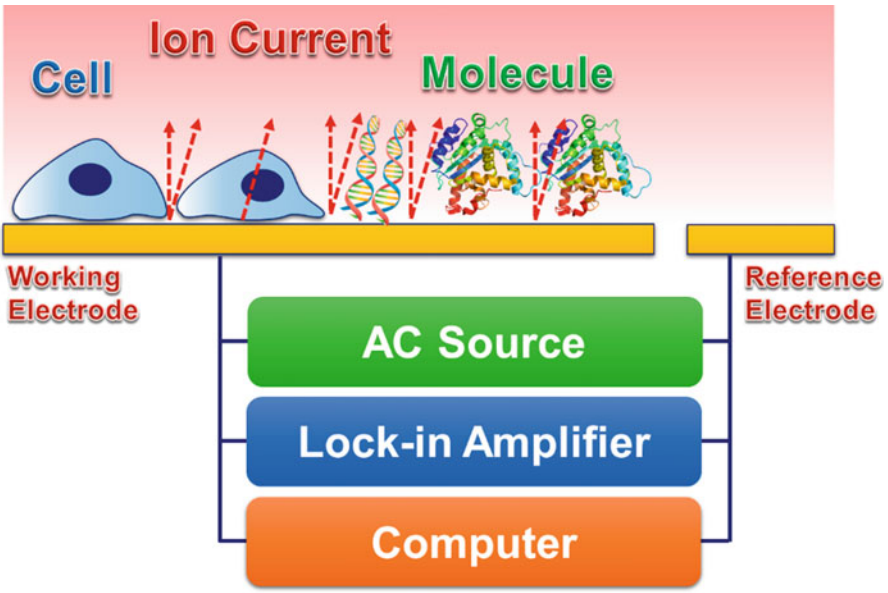

Fig. 2.3 Impedance sensor for the detection of cells and molecules

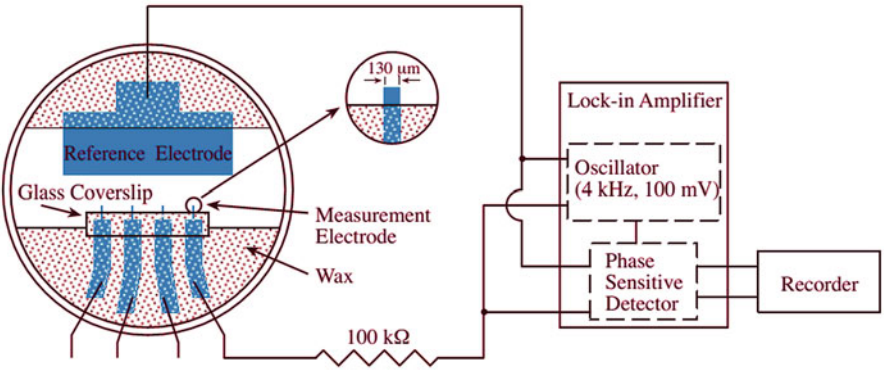

Fig. 2.4 Schematic of ECIS detection system (Reproduced with permission from Ref. [4]. Copyright 1984 National Academy of Sciences)

sinusoidal current source. Through the impedance of electrode and solution, the sinusoidal voltage can be detected by phase-sensitive lock-in amplifier. Impedance changes is mainly decided by small working electrode, while impedance changes of large electrodes can be ignored, so the impedance fluctuation of cell proliferation and cell migration can be dynamically monitored in real time. After the establishment of ECIS, many researches were implemented by this method for cell-based biosensor application: cell attachment, spreading, motion under different proteins

[30–33]; cell migration under various culture condition (temperature, glucose, CO_2, etc.) [34, 35]; and cell morphology under pulse AC field [36].

With the development of impedance sensor, various electrode patterns are designed for cell physiological study. However, there are only two basic structures of impedance sensors: monopolar electrode and interdigitated electrodes (IDEs) [37–40]. Monopolar electrode has been mentioned above, which can only detect impedance changes induced in a few cells or molecules. The monopolar electrodes have a high sensitivity, whereas the differences in cellular or molecular impedance are large for high-throughput bioassay. Moreover, large reference electrode results in space waste, which hampers the sensor miniaturization and integration. To address these problems and improve the utilization efficiency of electrodes, IDEs were explored for impedance detection. As shown in Fig. 2.5, reference electrode of IDEs is also employed. During the measurement, the reference electrode is equal with the working electrode, and coverage ratio of IDEs can reach 60 %, even 70 %. The cells cultured grow, attach, and proliferate on this impedance sensor, which can be measured by IDEs. Thus, the differences in cellular or molecular impedance-induced random location can be significantly reduced, so IDEs benefit to establish a high-consistency cell and molecule impedance sensor platform.

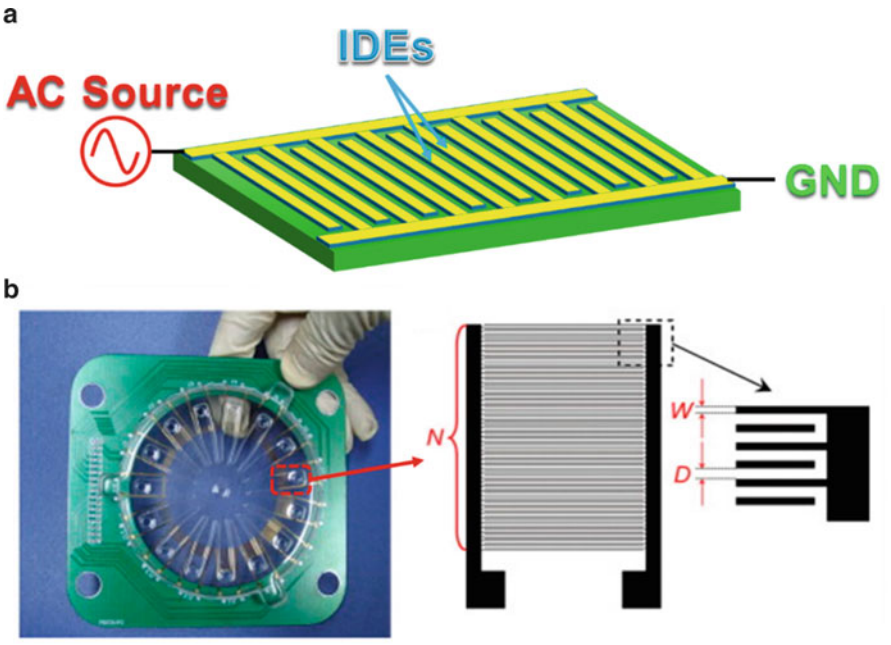

Fig. 2.5 Schematic of IDEs (**a**) and assembled sensing device (**b**) (Reproduced with permission from Ref. [41]. Copyright 2008 Elsevier B.V.)

2.2.3 *Field-Effect Transistor*

Field-effect transistor (FET) is a very interesting semiconductor-based biosensor, which can measure the conductance of a semiconductor as a function of an electrical field on the gate oxide surface. The early FET, a metal oxide semiconductor field-effect transistor (MOSFET), two n-type (p-type) diffusion source, and drain regions were fabricated in a p-type (n-type) silicon substrate. The SiO_2-insulating layer is fabricated on the structure, and a metal gate electrode is deposited on the insulating layer (left panel of Fig. 2.6a). MOFET was mainly used for gas detection, which was limited due to the metal layer. Consequently, a FET without metal layer was reported for measuring ion concentration in 1970, called ion-sensitive FET (ISFET) [42]. ISFET applied an electrolyte solution to replace the gate metal electrode of MOSFET. Reference electrode can be considered as the gate of the MOSFET (right panel of Fig. 2.6a).

In ISFET, electric current (I_{DS}) flows between the source and the drain via the channel. Like in case of MOSFET, the channel resistance depends on the electric field perpendicular to the direction of the current. As shown in Fig. 2.6b, when the drain-to-source voltage V_{DS} is much less than gate-to-source voltage V_{GS}, the V_{GS} will alter the channel resistance, and the drain current I_{DS} is proportional to the V_{GS}.

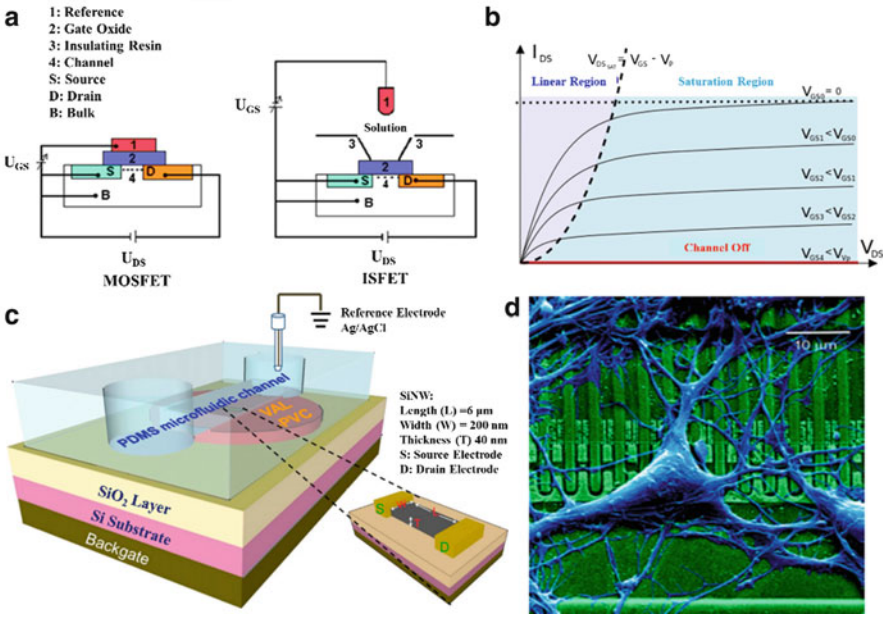

Fig. 2.6 Schematic of a MOSFET and an ISFET structure (**a**), typical characteristics of FET (**b**), FET detection system with microfluidic channels (**c**), neurons on a FET chip (**d**) (Reproduced with permission from Ref. [43]. Copyright 2012 Elsevier B.V., Ref. [44]. Copyright 2001 National Academy of Sciences)

In the case, FET operates in a linear mode as a variable resistor. If V_{DS} increases, a significant asymmetrical change will generate in the shape of channel. The shape of the inversion region becomes gradually pinched-off from the drain to source, and FET is in saturation mode.

Based on the characteristics of FET, it was widely adopted for molecule detection in extracellular microenvironment and cellular electrophysiology. The insulator layers of FET were fabricated by pH-sensitive material such as Al_2O_3, Si_3N_4, and Ta_2O_5 for pH detection [45–47]. Besides, organic films and other polymers were also used for other ion concentration monitoring [43, 48, 49]. For cell metabolism monitoring, the PDMS microfluidic channels or other microstructure will be combined with the FET, in order to enhance the sensitivity of FET (Fig. 2.6c). Besides, the FET can also be used for electrophysiology study of electrogenic cells. Fromherz groups cultured the neurons on a FET and recorded the action potential from the neurons [50, 51]. The past decades have witnessed significant improvement in semiconductor technology, which has led to both low-cost and robust performances of FET-based devices. With the development of FET, it has been a utility cell and molecule biosensor in field of biomedicine research and environment monitoring.

2.2.4 Light-Addressable Potentiometric Sensor

A LAPS is typically a conventional electrolyte/insulator/semiconductor (EIS) sensor, reported by Hafeman in 1988 as a semiconductor device for biochemical systems [52]. In the following decades, LAPS was another field-effect sensor widely studied in cell and molecule analysis, which is similar to ISFET. The LAPS is essentially a sensitive pH sensor. Figure 2.7a illustrates the common structure of LAPS chip. Silicon dioxide (SiO_2) and silicon dioxide (Si_3N_4) were formed on the silicon substrate as the insulating layer by thermal oxidation chemical vapor deposition (CVD). The insulating layer effectively separates the electrolyte from silicon substrate. With the interaction between electrolyte and groups on the LAPS surface, silanol (Si-OH) and silamine (Si-NH_2) are formed which can be changed into Si-O^- and Si-NH_3^+ according to the pH. Therefore, pH of solution can affect the sensor surface potential. When a voltage is applied onto the sensor, an electric field is formed in the LAPS. A photocurrent is created by the modulated infrared light illuminating at the backside of the sensor. At the atomic level, this photocurrent corresponds to a hole-electron pair creation by radiation absorption from the LED. Since a field potential is formed in the chip, holes and electrons move in opposite directions, resulting in the local current. The photocurrent can outflow from backside aluminum layer (Fig. 2.7b).

The amplitude of the photocurrent depends on the applied working potential and surface potential, and surface potential is determined by the pH of the electrolyte on the sensor chip. In the working mode, the applied voltage is selected as the most

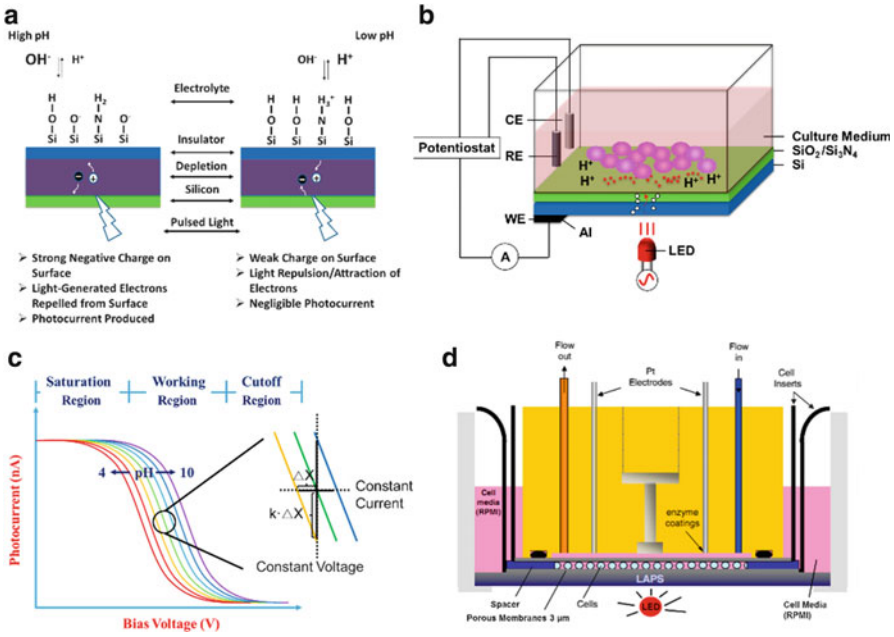

Fig. 2.7 (**a**) LAPS structure and principle. (**b**) Detection system. (**c**) P-V characteristic. (**d**) Multiparameter microphysiometer (Reproduced with permission from Ref. [2] Copyright 2013 Elsevier B.V., Ref. [53] Copyright 2000 Elsevier B.V., and Ref. [54] Copyright 2006 Elsevier B.V.)

sensitive point, by which the sensor can reflect the varying pH sensitively. The insulator surface is partially covered by silanol and few silamine, both of which can be considered as a function of pH. This feature of LAPS makes the surface potential pH-dependent from pH 2 to 11.

Photocurrent-voltage (P-V) characteristic curve can reflect the performance of LAPS. As shown in Fig. 2.7c, a group of the sigmoid curves are similar with a pH spectrum which reveals the relationship between the induced photocurrent and the bias voltage applied on LAPS under the different pH. Usually, the sigmoid curves have three regions. In cutoff region, there is no photocurrent. In saturation region, the photocurrent is close to maximum. In working region, the photocurrent increases linearly as bias voltage decreases for n-type LAPS. Conventionally, the method of LAPS pH detection was mainly by constant current detection mode, which monitors the change of inflection point voltage (ΔX). When photocurrent-voltage curve shifts toward positive potentials as the solution pH increases, the working voltage applied on reference electrode is correspondingly changed to keep the photocurrent constant, and thus the offset voltage ΔX can be measured. In some cases, the constant voltage detection mode was also performed for directly measuring the cellular and molecule study cases [55–57].

2.3 Novel Micro/Nano cell- and Molecular-Based Biosensors

2.3.1 Nanoscale FET

Nanostructure-based devices have been developed for the molecule and extracellular potential application [58–60]. Most of traditional biosensors, such as MEA and FET, can only remain at extracellular potential level. Although these tools were noninvasive, long-term, dynamic, and real-time, much information was changed or lost due to indirect measurement of action potential. Also, there is plenty of intracellular sensing methods, such as voltage-sensitive optical dye [61] and patch clamp [62]; however, the optical dye has limited signal-to-noise ratio, pharmacological side effects, and phototoxicity. The glass micropipettes size of patch clamp was relatively large, and the large pore of cell membrane resulted in irreversible damages to cells, which hampered the long-term experiments. Flexible nanoscale FET was reported by Lieber group in 2010 [63].

2.3.1.1 Fabrication of Nanoscale Device

For the fabrication of 3D flexible nanoFET, there are two design considerations: configuration synthesis and nanoFET fabrication. The silicon nanowire (SiNW) can be generated by variation of reactant pressure, and junction region can form the p-n diodes and FETs [64]. For fabrication of nanoFET, this methodology was employed to create FET probe configurations as shown in Fig. 2.8a. The top (60°) and middle (0°) FET cis-configuration of Fig. 2.8a can be inserted into a single cell, while the bottom FET trans-configuration of Fig. 2.8a is useless. The selective and reproducible synthesis of cis-linked units was achieved by controlling the junction length L in doubly kinked SiNWs (Fig. 2.8b). When L was about 50 nm, cis-linked will be dominant in growth of complex probe structures. NanoFET fabricated into the cis-linked nanowire was another key consideration during the synthesis (pink segments in Fig. 2.8a). To achieve the FET function, S/D segment is fabricated by heavy n++-type doping, while the FET segment is fabricated the light n-type doping.

For intracellular study, the nanoFET probe needs special fabrication to form a 3D device. As processes shown in Fig. 2.8c, the device is fabricated on the silicon substrate, deposited with polymethyl methacrylate (PMMA) layer and patterned by electron-beam lithography (EBL). Three hundred to 400 nm SU-8 layer is deposited over the chip surface, the functional kind nanowires FET is deposited on the SU-8, and then SU-8 layer is patterned by EBL as flexible support of metal interconnects. The Cr/Pd/Cr is thermally evaporated as the interconnects, and the 40–60 nm Si_3N_4 layer passivates metal interconnects by plasma-enhanced chemical vapor deposition (PECVD). The 3D nanoFET bends upward by removing the initial PMMA

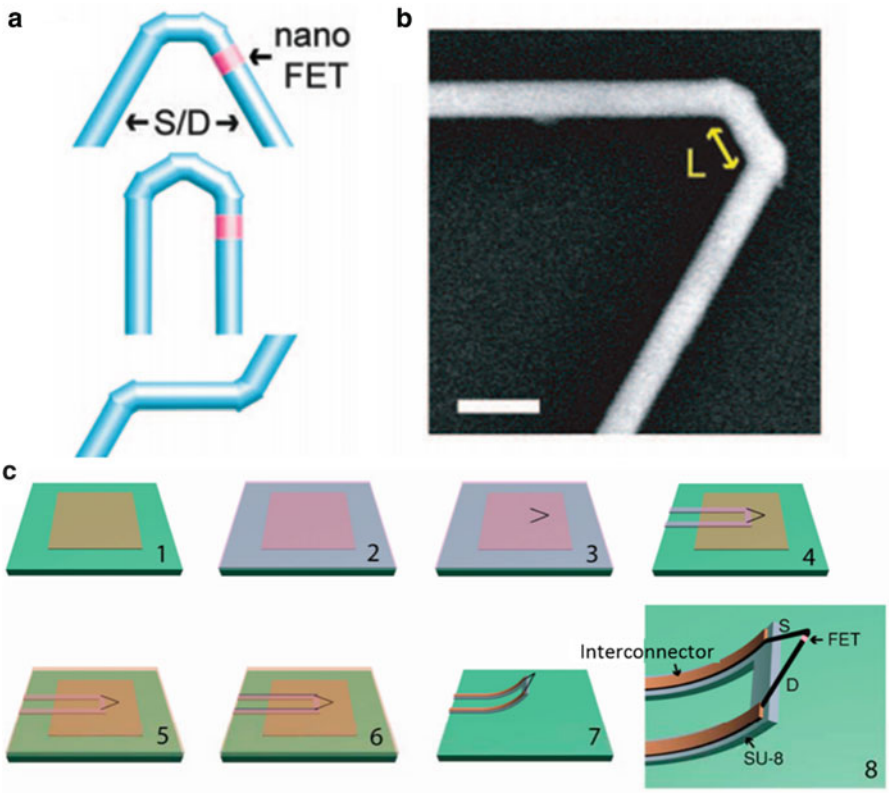

Fig. 2.8 (**a**) Synthesis of cis- (*top and middle*) and trans (*bottom*)-kinked SiNW probes. (**b**) SEM of kinked nanowire with a cis structure. (**c**) 3D flexible nanoscale FET probe fabrication. Scale bar: 200 nm (Reproduced with permission from Ref. [63]. Copyright 2010 AAAS)

layer after the lift-off process. Height and angle of the nanoFET probe can be tuned by changing the length and thickness of flexible support backbone.

To form a smaller probe for intracellular recording, a branched intracellular nanotube FET (BIT-FET) was synthesized based on the nanocluster-catalyzed vapor-liquid-solid (VLS) process [65]. Firstly, the silicon nanowire is fabricated to disperse on the SiO_2/Si growth substrate. Then Au nanodot is designed on the SiNW using EBL and thermal evaporation. Germanium nanowire (GeNW) is grown on the SiNW by the Au nanodot-catalyzed VLS process, as shown in c of Fig. 2.9. Subsequently, the metal contact points are fabricated by EBL on the SiNW at the two sides of GeNW. SiO_2 is deposited by atomic layer deposition (ALD) to cover the whole device surface, and the photoresist is used to cover device to expose the tip of GeNW. Then the SiO_2 of the tip is etched by buffered HF (BHF), and the isotropic BHF etching forms the tapered SiO_2 shell. After the photoresist lift-off, H_2O_2 is used to etch the Ge to form the SiO_2 nanotube. Thus, a BIT-FET device is completed.

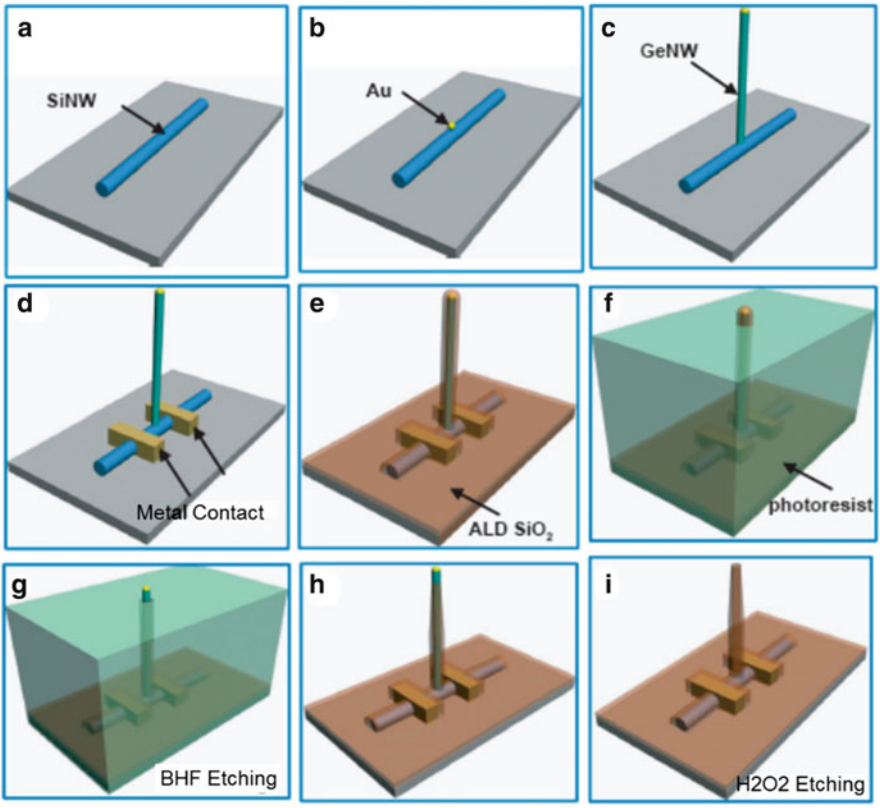

Fig. 2.9 Fabrication processes of the branched intracellular nanotube FET (Reproduced with permission from Ref. [66]. Copyright 2011 Nature publishing group)

2.3.1.2 Characterization and Application of Nanoscale FET Devices

3D flexible nanoFET function was tested by atomic force microscopy (AFM) and scanning gate microscopy (SGM) (Fig. 2.10a, b). The SGM images were recorded with Vtip of +10 V (left panel) and −10 V (right panel), respectively, and V_{SD} is set at 0.5 V. The dark and bright regions correspond to reduced and enhanced conductance, respectively. The SGM data demonstrate the successful synthetic integration of an n-type field-effect transistor (FET) immediately adjacent to the 60° probe tip, where the length of the FET is about 200 nm. Figure 2.10c is scanning electron microscope (SEM) image of 3D flexible device. It can be seen that the nanowire FET is fabrication on the tip of device. Moreover, the 3D nanoFET is sensitive to the pH. The solution pH changed from 7.5 to 6.7 by 0.1 pH unit step (Fig. 2.10d). The response of the FET is about 58 mV/pH which is near the Nernstian limit. Both of the SGM and pH tests prove the good performance of nanoFET.

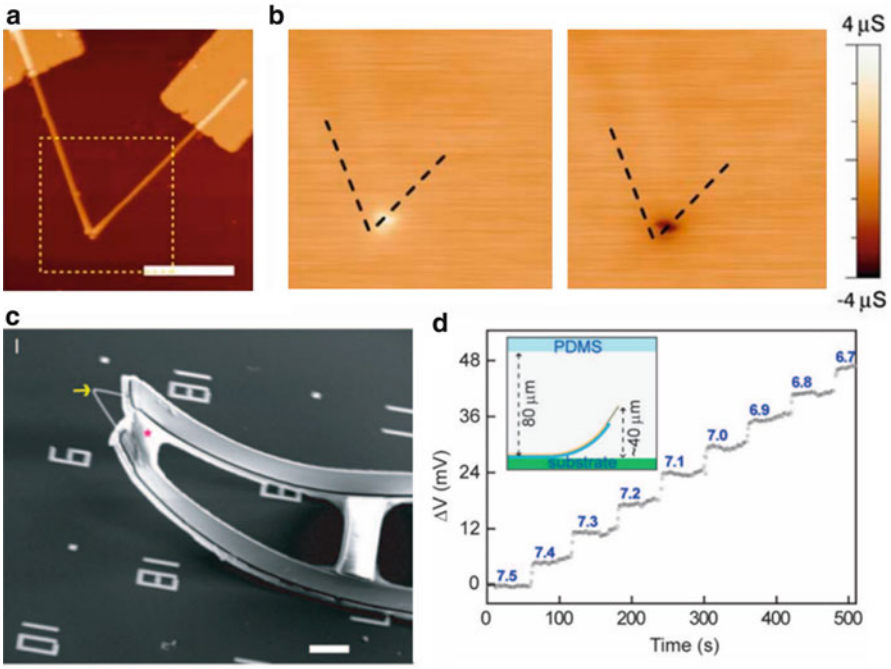

Fig. 2.10 Characterization of 3D flexible nanoFET device. (**a**) AFM images of nanowire FET. (**b**) SGM images of nanowire FET. (**c**) SEM image of 3D flexible device. (**d**) NanoFET pH detection. Scale bar 2 μm (**a**); 5 μm (Reproduced with permission from Ref. [63]. Copyright 2010 AAAS)

3D flexible nanoFET probe is designed for the single cell detection, so the intracellular recording is the most significant function as a nanoscale device. Usually, the electrogenic cells (e.g., cardiomyocytes and neurons) are useful study object for intracellular recording, due to their spontaneously firing signals. Cardiomyocytes can be cultured on PDMS culture chambers (Fig. 2.11a). When 3D nanoFET probes approach the cardiomyocytes, the extracellular potential can be recorded with a low signal-to-noise ratio (SNR). During the nanoFET probe inserting into the cardiomyocyte, the signals become larger. Finally, the action potentials remain the same shape with an average peak amplitude of 80 mV and duration of 200 ms (Fig. 2.11b). From the enlarged drawing of signals, it can be found that they have the similar features of amplitude, sign, and duration, which are reported for whole-cell patch clamp recordings from cardiomyocytes with five characteristic phases: (a) resting state, (b) rapid depolarization, (c) plateau, (d) rapid repolarization, and (e) hyperpolarization. 3D flexibility has many advantages: Electrical recording with 3D flexible nanoFET probes is convenient to use without electric circuit compensation, and the nanoprobes are chemically less invasive than glass micropipettes. The small size and biomimetic coating minimizes mechanical invasiveness; and the nanoFETs have high spatial and temporal resolution for intracellular recording.

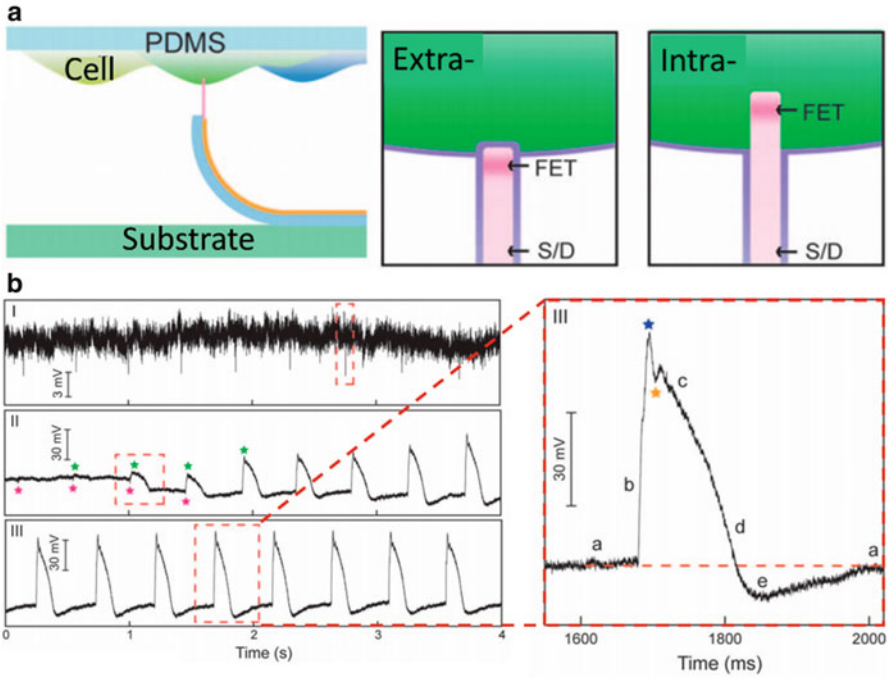

Fig. 2.11 Action potential recording by 3D flexible nanoFET device (**a**) extracellular and intracellular recording of the embryonic chicken cardiomyocyte cultured on the PDMS by nanoFET (*left panel*). (**b**) The signals of the nanoFET approaching and inserting into the cardiomyocyte (Reproduced with permission from Ref. [63]. Copyright 2010 AAAS)

To investigate performance of intracellular recording, the BIT-FET is used to record the cardiomyocytes cultured on polydimethylsiloxane (PDMS). The BIT-FET is modified with phospholipids to facilitate nanotube structure into cells for intracellular recording (Fig. 2.12a). The PDMS-cell sheet is gently touched on the nanotube of BIT-FET without any force. The signals change significantly as presented in Fig. 2.12c. The extracellular recording signals have a low SNR, while the intracellular recording signals have an amplitude of 75–100 mV and duration of 200 ms, which are similar features with the intracellular action potential of cardiomyocytes. The inverted signal peak is due to the p-type SiNW. The performance of nanoFET is excellent for intracellular recording with tiny invasive damage for cardiomyocytes.

2.3.2 Nanopillar and Nanotube Electrode Array

Action potential plays a significant role in nervous system and cardiovascular system, involving ion channels. Consequently, accurate measurement of action

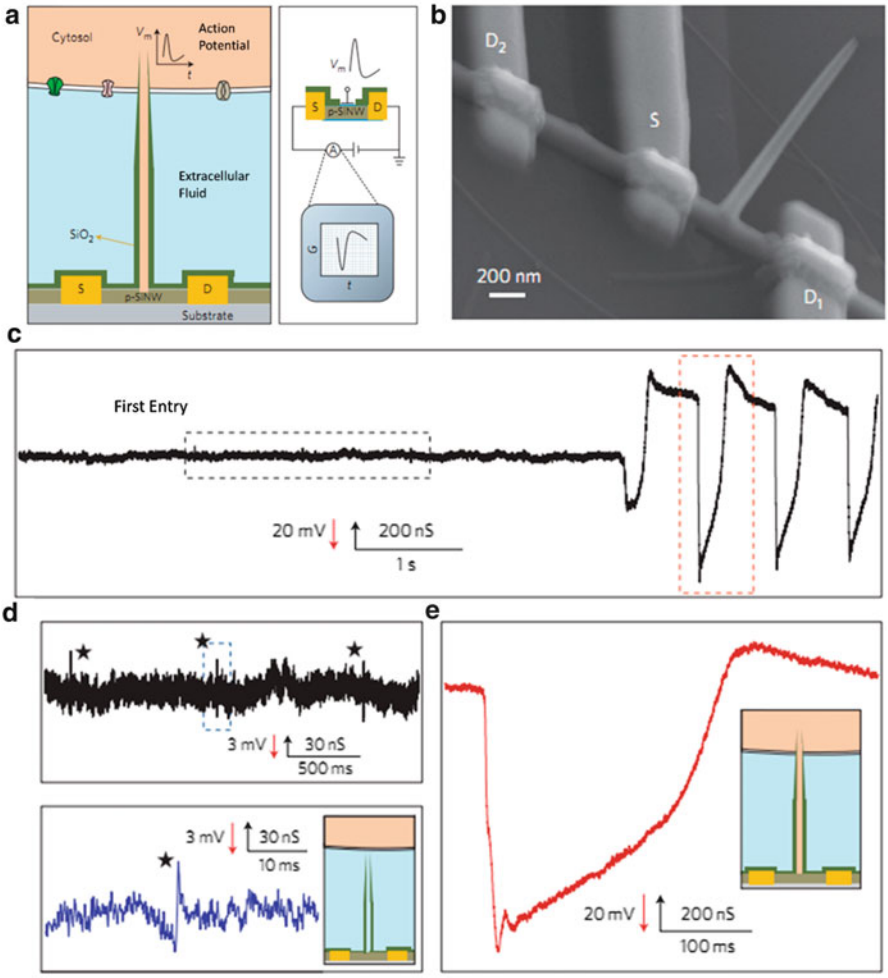

Fig. 2.12 (**a**) Schematic of BIT-FET recording system. (**b**) SEM image of a BIT-FET device (S-D1) and control device (S-D2). (**c**) Representative signals transition from the extracellular to intracellular recording. (**d**) Magnified view of signals in *black dashed rectangle* of (**c**). (**e**) Magnified view of signals *red dashed rectangle* of (**c**) (Reproduced with permission from Ref. [66]. Copyright 2011 Nature publishing group)

potential can help researchers study the cellular physiology and pharmacology further. Lots of work have been made for recording the action potential, such as patch clamp to measure the voltage or current across the cell membrane by forming a high ohm seal. However, this high seal is based on the invasive mode, which will limit the experiment time within several hours, and the complicated operation hampers it simultaneously record more than a cell [67]. To solve the experimental throughput, many sensors were developed extracellularly and intracellularly, such as FET, MEA, or nanoscale FET as mentioned above. Nanoscale FET has good

performance in cell and molecule investigation; however, the fabrication and manipulation of nanoscale FET are relatively complicated, especially for intracellular potentials detection. MEA is a utility tool for extracellular potential recording, which works in the noninvasive mode and allows a long-term recording [18, 23, 68]. However, the loose coupling between cell and microelectrode dramatically affects the signal quality and SNR. Moreover, the extracellular potential is quite different with the action potential recorded by intracellular recording. All these have limited the development application of these biosensors. Nanotechnology will change this situation due to the superiority of nanoscale materials. In following sections, two nanomaterials (nanopillar and nanotube) are employed to fabricate the vertical nanoscale electrodes array.

2.3.2.1 Fabrication of Nanoelectrode Array

To fabricate the nanoelectrode array, the basic structure of MEA needs to design, firstly, whose processes are the same with traditional MEA. The main processes are displayed in Fig. 2.13. A quartz wafer is patterned with 4×4 Pt/Ti microelectrode array. All the processes are operated by the standard photolithography methods. Then the passivated layer (Si_3N_4/SiO_2) is formed over the MEA surface by plasma-enhanced chemical vapor deposition. Five nanometer chromium layers are coated on the MEA as a protecting mask. The gallium-focused ion beam (FIB) is used for milling the holes with diameter of 250 nm through the Si_3N_4/SiO_2 insulation layer to reach the Pt microelectrode (Fig. 2.13b). To fabricate the nanopillars right at the holes on the MEA, FIB-assisted Pt is employed to create and connect the

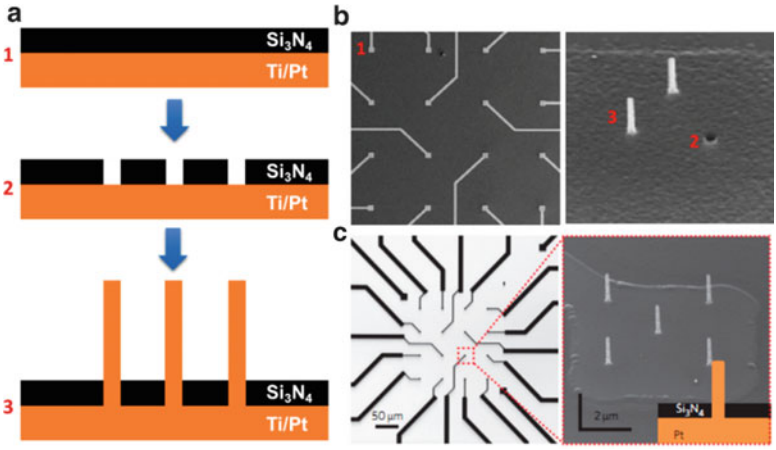

Fig. 2.13 (**a**) Fabrication of nanopillar electrode array. (**b**) Microelectrode array covered with insulation layer (*left panel*), milled hole, and nanopillar fabricated on the microelectrode (*right panel*). (**c**) Optical and SEM image of nanopillar electrode array (Reproduced with permission from Ref. [10]. Copyright 2012 Nature publishing group)

nanopillars to Pt pad under the insulation layer. Usually several nanopillars with the length of 1–2 μm and the diameter of 150–200 nm are created on one microelectrode. After the nanopillar electrode array fabrication, the Cr protection layer will be removed by CR14, and the device will be transparent except the electrode patterns. Figure 2.13c presents optical and SEM image of the completed nanopillar electrode array.

Nanotube is another useful nanostructure for fabrication of nanoscale electrode array. Figure 2.14a presents the main processes. To fabricate a nanotube electrode array, electrode pattern is firstly designed on the SiO_2/Si substrate and the Si_3N_4/SiO_2 is deposited over the device as the insulator layer. Then the nanoholes position is determined using electron beam lithography to etch through the insulator layer to contact the Pt electrode. Subsequently, the iridium oxide nanotubes can be formed in the nanoholes by electroporation. Finally, resist is removed to complete nanotube electrode array. IrOx is an interesting material to synthesize nanotube on the electrode array. Electrodeposition of IrOx can form the nanotube with hollow centers, while electrodeposition of metals will form the nanopillar structure [69–71]. From Fig. 2.14b, it can be seen that the IrOx nanotubes is formed as expected. Also, Au nanopillars were formed based on the same configuration.

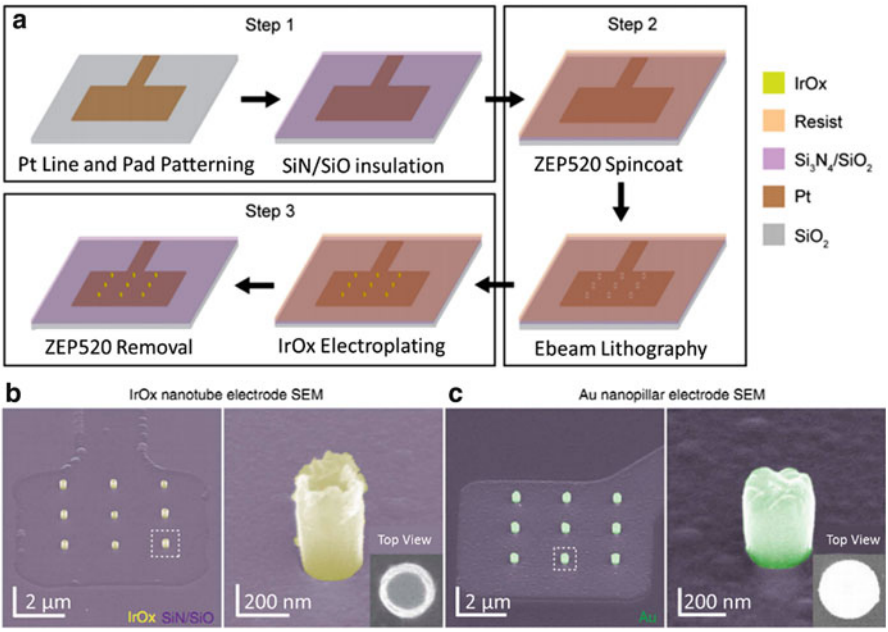

Fig. 2.14 (**a**) Fabrication of IrOx nanotube- or Au nanopillar-based electrode array with electroplating. (**b**) SEM image with false color by GNU image manipulation program (GIMP) (Reproduced with permission from Ref. [72]. Copyright 2014 Nature publishing group)

2.3.2.2 Characterization and Application of Nanoelectrode Array

To test the performance of nanopillar electrode array, cardiomyocytes are cultured on the electrode array. From the SEM images of cardiomyocyte cultured (Fig. 2.15a), it can be clearly seen that the nanopillars are engulfed by cells. Figure 2.15b shows the extracellular potential with two obvious features of extracellular recording. A shape of spike corresponds the first derivative of the action potential with an amplitude of ca. 100–200 μV. The noise is about 20–30 μV. Compared with the traditional MEA, the surface area of nanopillars is about 5–10 μm^2, which is significantly smaller than the microelectrode area of 400–2500 μm^2 [23]. However, the signals recorded from both electrode areas are similar with amplitude, while in the capacitive coupling nature of a solid-state electrode, the signal strength is related with the electrode area. Therefore, the record signals by nanopillar suggest that the engulfment of nanopillar has better sealing at the cell-electrode interface and compensates the smaller area.

A transient electroporation can greatly improve the quality of signals recorded by nanopillar electrode, due to significantly lower impedance between the electrode and the cell interior. Figure 2.15c shows a large signal obtained by the nanopillar electrode. A transient electroporation is in vitro technique to introduce exterior molecules into cells through the nanometer-sized pores in cell membrane under a high electric field [73–75]. The nanopillar electrodes are so sharp that they can form a large electrode field with a train transient voltage (2.5 V, 200 ms biphasic pulses for 1 s), which helps to increase the permeability of cell membranes. From the signals in Fig. 2.15c, the amplitudes of signals sharply increase to 11.8 mV after the electroporation, while the peak-to-peak noise is similar with that before electroporation; however, SNR increases to 590, which is a 100-fold SNR increase. Besides,

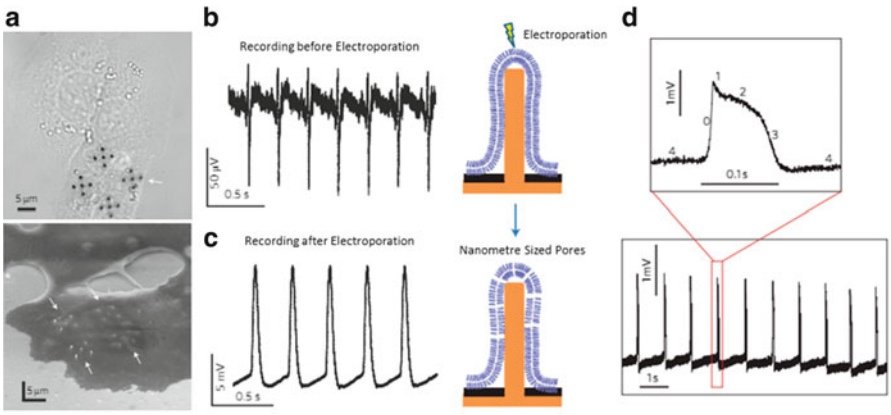

Fig. 2.15 (**a**) SEM images of cardiomyocytes on the nanopillar electrode array. (**b**) Representative extracellular signals recorded by nanopillar electrode. (**c**) Representative intracellular signals recorded by nanopillar electrode after the electroporation. (**d**) Magnified of a single action potential (Reproduced with permission from Ref. [10]. Copyright 2012 Nature publishing group)

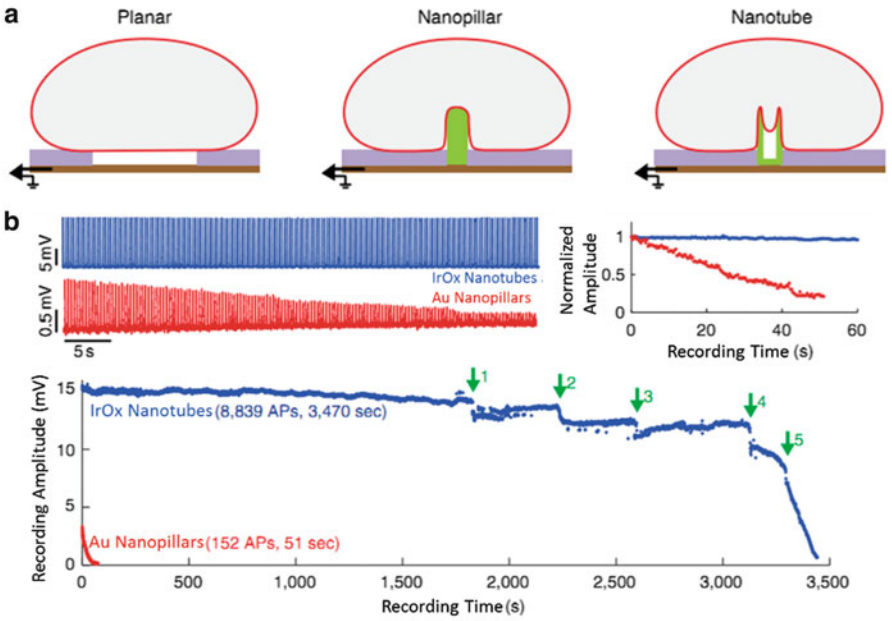

Fig. 2.16 (**a**) Three types of electrodes: planar, nanopillar, and nanotube. (**b**) Continue intracellular potential recording and analysis by IrOx nanotube and Au nanopillar electrode array (Reproduced with permission from Ref. [72]. Copyright 2014 Nature publishing group)

these intracellular potentials have the similar shape compared with action potentials.

Although the nanopillar-based electrode array can record the intracellular potentials, the amplitude of these signals will gradually decrease due to the rapid resealing of nanopore in the cell membrane [10]. As shown in Fig. 2.16, the gold nanopillar electrodes showed that the amplitude of recorded action potential also decreased after electroporation, which limits the experimental time for investigation. Meanwhile, the signals recorded by nanotube-based electrodes remain stable and can continue for 30 min as shown in Fig. 2.16b. In the next period, amplitude displays obvious sudden drop at different time points. Comparing with the nanopillar-based electrode array, nanotube-based electrode can record the intracellular potential with good quality in a long time.

The reason of long-term stable recording is spontaneous insertion of cell membrane into the nanotubes. After the electroporation, the nanopores of cardiomyocyte membrane reseal much slower, and information of nanopore in cell membrane can be measured by the patch clamp, so the quality of signals is better than that of nanopillar case. Figure 2.17 illustrates the comparison of intracellular potential of whole-cell current clamp and IrOx nanotube electrode. After the electroporation, the shape of signals of two methods is similar with each other at three different stages.

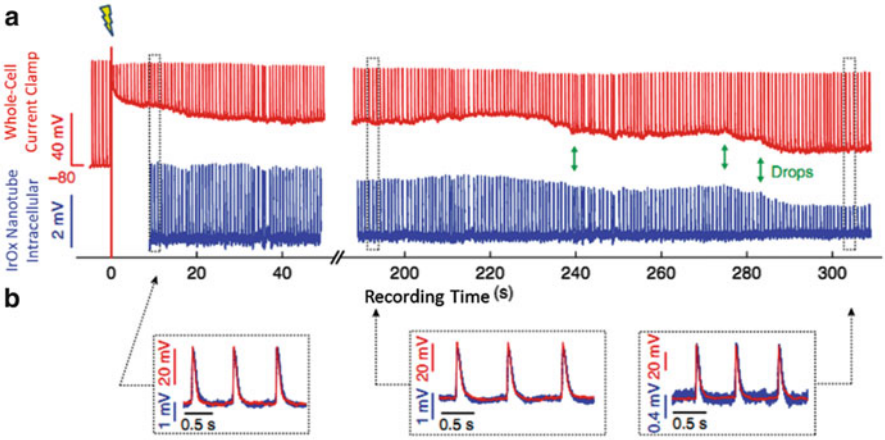

Fig. 2.17 Comparison of whole-cell current clamp and IrOx nanotube intracellular after the electroporation. (**a**) Long-term recording. (**b**) Comparison of signal shape (Reproduced with permission from Ref. [72]. Copyright 2014 Nature publishing group)

2.3.3 Nanomaterial Modified Biosensor

For molecule analysis, these biosensors are usually established by sensitive element (sensitive film, receptor, DNA, RNA, etc.) and sensors (FET, LAPS, impedance, etc.). To enhance the performance of biosensor, many nanomaterials are involved in the establishment of biosensors. Nanostructure biosensors have significant advantages in sensitivity for molecule analysis. Various nanomaterials and nanostructures play an important role in performance of biosensors. Nanomaterials, such as nanoparticle, nanotube, nanopore, and nanowire, have been widely applied in the molecule (e.g., DNA, protein, RNA, or other molecules) study [13, 76, 77]. The nanomaterial owns the advantages such as facile functionalization and biocompatibility. These nanomaterials highly attract the interest for various future applications in the field of biomedicine and analytical sciences.

2.3.3.1 Fabrication of Nanotube-Modified FET

Nanometer-scale sensors based on the nanotube FET have been used for highly sensitive chemical sensing. Significant progress of nanotube technology, which has great potential to produce low-cost and light-weight devices, has prompted the development of various sensing devices that are based on nanotubes [78–80]. When the target odorant molecules bind on the OR proteins, the equilibrium of the receptor protein may shift toward active receptor states, which have negative charges, resulting in an electrostatic fluctuation on the NT. FET is a utility tool in molecule analysis with its high sensitivity. Moreover, some nanomaterial can dramatically improve the performance of FET to a higher level. Figure 2.18

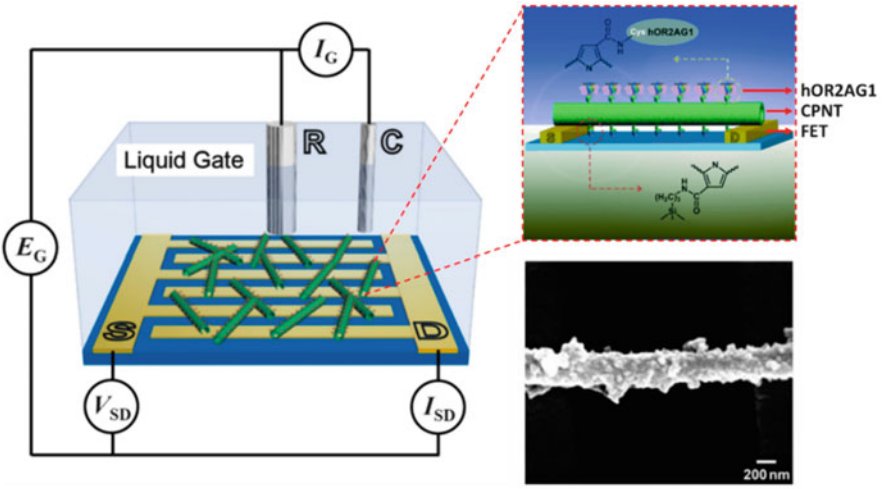

Fig. 2.18 Carboxylated polypyrrole nanotube-modified FET with human olfactory receptors (hORs) for target odorant detection (Reproduced with permission from Ref. [81]. Copyright 2009 John Wiley & Sons, Inc.)

presents a novel odorant biosensor based on the nanotube-modified FET with human olfactory receptors (hORs). FET is fabricated on a glass substrate with a structure of interdigitated microelectrode array (IDA) by a lithographic process. The IDA consisted of pairs of 25 fingers, in which the bands served as source (S) and drain (D) electrodes, respectively. The hOR2AG1 expressed by *Escherichia coli* is modified on the carboxylated polypyrrole nanotubes (CPNTs), while these CPNTs are modified on FET for signal amplification. The SEM image of a hOR2AG1-conjugated CPNT is presented in Fig. 2.18. The OR-CPNT FET responds to odorants by I_{DS} between source and drain of FET. Therefore, the nanomaterial modified FET will be a promising tool in molecular sensing field.

2.3.3.2 Characterization and Application of Nanotube-Modified FET

hOR2AG1-CPNT-modified FET can sensitively respond to the target gas, amyl butyrate (AB), as presented in Fig. 2.19a. It can be found that 400 fM AB can be easily detected by nanotube-modified FET, and responses to AB become large with increase of concentration. Specificity of hOR2AG1-CPNT FET is also important for odorant detection. To test the specificity of this FET, other odorants including butyl butyrate (BB), propyl butyrate (PB), and hexyl butyrate (HB) can be employed as the nontarget odorants. Results in Fig. 2.19b suggest that the high concentration (400 μM) of nontarget will induce on significant changes in FET response. Figure 2.19c displays that nontarget and target odorant molecules have the similar structures. However, the high performance hOR2AG1-CPNT FET can

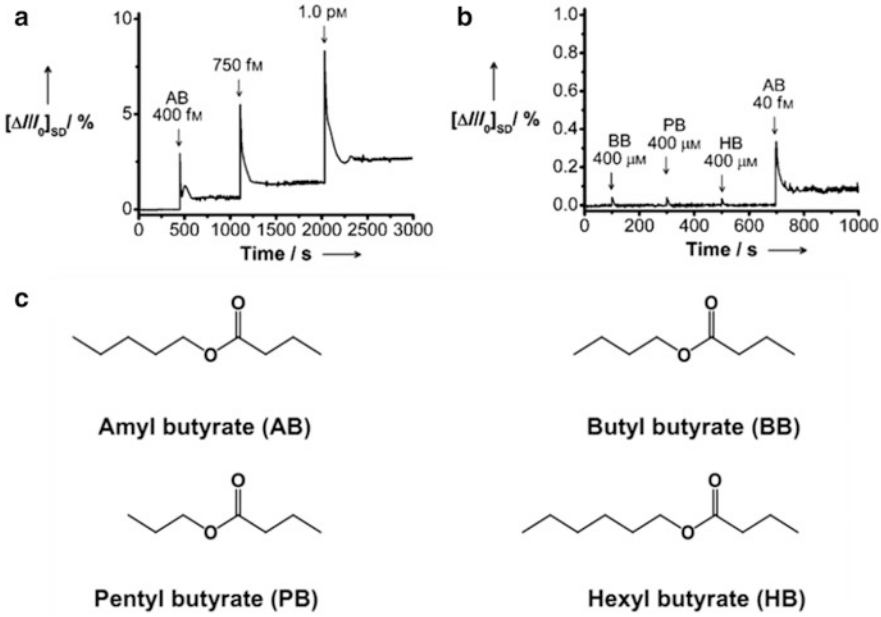

Fig. 2.19 (**a**) Real-time responses of OR-CPNT-modified FET for detecting the target odorant (*AB* amyl butyrate). (**b**) Comparison of nontarget (*BB* butyl butyrate, *PB* propyl butyrate, *HB* hexyl butyrate) and target odorants. (**c**) Structures of these odorants (Reproduced with permission from Ref. [81]. Copyright 2009 John Wiley & Sons, Inc.)

distinguish these different odorant molecules. It has been proven that hOR2AG1-CPNT FET can sensitively and selectively translate and amplify the hOR-odorant interaction into a detectable signal.

2.4 Summary

In this chapter, novel micro/nano cell and molecule biosensors are discussed based on the traditional biosensors and novel nanotechnology. Traditional biosensors, such as microelectrode array, impedance sensor, field-effect transistor, and light addressable potentiometric sensor, are useful tools in cell and molecule analysis, while the nanostructure and nanomaterial modified biosensors emerge gradually with the advance of nanotechnology. These nanostructure and nanomaterial modified biosensors have demonstrated the excellent performance in cell and molecule applications. By combining sensor technology with nanotechnology, the novel micro/nano cell, and molecule biosensors can explore a wide way in fields of biomedicine and environment monitoring.

References

1. Fanigliulo A, Accossato P, Adami M, Lanzi M, Martinoia S, Paddeu S, Parodi M, Rossi A, Sartore M, Grattarola M. Comparison between a LAPS and an FET-based sensor for cell-metabolism detection. Sensors Actuators B Chem. 1996;32(1):41–8.
2. Hu N, Wu C, Ha D, Wang T, Liu Q, Wang P. A novel microphysiometer based on high sensitivity LAPS and microfluidic system for cellular metabolism study and rapid drug screening. Biosens Bioelectron. 2013;40(1):167–73.
3. Giaever I, Keese CR. A morphological biosensor for mammalian cells. Nature. 1993;366 (6455):591–2.
4. Giaever I, Keese C. Monitoring fibroblast behavior in tissue culture with an applied electric field. Proc Natl Acad Sci. 1984;81(12):3761–4.
5. Giaever I, Keese CR. Micromotion of mammalian cells measured electrically. Proc Natl Acad Sci U S A. 1991;88(17):7896–900.
6. Keese CR, Wegener J, Walker SR, Giaever I. Electrical wound-healing assay for cells in vitro. Proc Natl Acad Sci U S A. 2004;101(6):1554–9.
7. Hess LH, Jansen M, Maybeck V, Hauf MV, Seifert M, Stutzmann M, Sharp ID, Offenhäusser A, Garrido JA. Graphene transistor arrays for recording action potentials from electrogenic cells. Adv Mater. 2011;23(43):5045–9.
8. Xiao L, Hu Z, Zhang W, Wu C, Yu H, Wang P. Evaluation of doxorubicin toxicity on cardiomyocytes using a dual functional extracellular biochip. Biosens Bioelectron. 2010;26 (4):1493–9.
9. Brüggemann D, Wolfrum B, Maybeck V, Mourzina Y, Jansen M, Offenhäusser A. Nanostructured gold microelectrodes for extracellular recording from electrogenic cells. Nanotechnology. 2011;22(26):265104.
10. Xie C, Lin Z, Hanson L, Cui Y, Cui B. Intracellular recording of action potentials by nanopillar electroporation. Nat Nanotechnol. 2012;7(3):185–90.
11. Zeng D, Zhang H, Zhu D, Li J, San L, Wang Z, Wang C, Wang Y, Wang L, Zuo X, Mi X. A novel ultrasensitive electrochemical DNA sensor based on double tetrahedral nanostructures. Biosens Bioelectron. 2015;71:434–8.
12. Li J, Lee E-C. Carbon nanotube/polymer composite electrodes for flexible, attachable electrochemical DNA sensors. Biosens Bioelectron. 2015;71:414–9.
13. Wang H-B, Zhang H-D, Chen Y, Liu Y-M. A fluorescent biosensor for protein detection based on poly(thymine)-templated copper nanoparticles and terminal protection of small molecule-linked DNA. Biosens Bioelectron. 2015;74:581–6.
14. Drexler KE. Engine of creation. The coming era of nanotechnology. New York: Anchor Books; 1986.
15. Drexler KE. Nanosystems: molecular machinery, manufacturing, and computation. New York: Wiley; 1992.
16. Sahoo S, Parveen S, Panda J. The present and future of nanotechnology in human health care. Nanomed Nanotechnol Biol Med. 2007;3(1):20–31.
17. Nel A, Xia T, Mädler L, Li N. Toxic potential of materials at the nanolevel. Science. 2006;311 (5761):622–7.
18. Thomas C, Springer P, Loeb G, Berwald-Netter Y, Okun L. A miniature microelectrode array to monitor the bioelectric activity of cultured cells. Exp Cell Res. 1972;74(1):61–6.
19. Gesteland R, Howland B, Lettvin J, Pitts W. Comments on microelectrodes. Proc IRE. 1959;47 (11):1856–62.
20. Robinson DA. The electrical properties of metal microelectrodes. Proc IEEE. 1968;56 (6):1065–71.
21. Gross G, Rieske E, Kreutzberg G, Meyer A. A new fixed-array multi-microelectrode system designed for long-term monitoring of extracellular single unit neuronal activity in vitro. Neurosci Lett. 1977;6(2):101–5.

22. Gross GW. Simultaneous single unit recording in vitro with a photoetched laser deinsulated gold multimicroelectrode surface. Biomed Eng IEEE Trans. 1979;5:273–9.
23. Pine J. Recording action potentials from cultured neurons with extracellular microcircuit electrodes. J Neurosci Methods. 1980;2(1):19–31.
24. Gross GW, Rhoades B, Jordan R. Neuronal networks for biochemical sensing. Sensors Actuators B Chem. 1992;6(1):1–8.
25. Borkholder D, DeBusschere BD, Kovacs G. An approach to the classification of unknown biological agents with cell based sensors. 1998.
26. DeBusschere BD, Kovacs GT. Portable cell-based biosensor system using integrated CMOS cell-cartridges. Biosens Bioelectron. 2001;16(7):543–56.
27. Gross GW, Rhoades BK, Azzazy HM, Wu M-C. The use of neuronal networks on multielectrode arrays as biosensors. Biosens Bioelectron. 1995;10(6):553–67.
28. Gross GW, Schwalm FU. A closed flow chamber for long-term multichannel recording and optical monitoring. J Neurosci Methods. 1994;52(1):73–85.
29. Rhoades BK, Gross GW. Potassium and calcium channel dependence of bursting in cultured neuronal networks. Brain Res. 1994;643(1):310–8.
30. Giaever I, Keese CR. Use of electric fields to monitor the dynamical aspect of cell behavior in tissue culture. Biomed Eng IEEE Trans. 1986;2:242–7.
31. Mitra P, Keese CR, Giaever I. Electric measurements can be used to monitor the attachment and spreading of cells in tissue culture. Biotechniques. 1991;11(4):504–10.
32. Keese CR, Giaever I. A whole cell biosensor based on cell-substrate interactions. In Editor (Ed.)^(Eds.): Book A whole cell biosensor based on cell-substrate interactions (IEEE, 1990, edn.), p. 500–501.
33. Keese CR, Giaever I. A biosensor that monitors cell morphology with electrical fields. Eng Med Biol Magaz IEEE. 1994;13(3):402–8.
34. Lo C-M, Keese CR, Giaever I. Monitoring motion of confluent cells in tissue culture. Exp Cell Res. 1993;204(1):102–9.
35. Lo C-M, Keese CR, Giaever I. pH changes in pulsed CO_2 incubators cause periodic changes in cell morphology. Exp Cell Res. 1994;213(2):391–7.
36. Ghosh PM, Keese CR, Giaever I. Morphological response of mammalian cells to pulsed ac fields. Bioelectrochem Bioenerg. 1994;33(2):121–33.
37. Xiao C, Lachance B, Sunahara G, Luong JH. Assessment of cytotoxicity using electric cell-substrate impedance sensing: concentration and time response function approach. Anal Chem. 2002;74(22):5748–53.
38. Wang L, Zhu J, Deng C, Xing W-l, Cheng J. An automatic and quantitative on-chip cell migration assay using self-assembled monolayers combined with real-time cellular impedance sensing. Lab Chip. 2008;8(6):872–8.
39. Ehret R, Baumann W, Brischwein M, Schwinde A, Stegbauer K, Wolf B. Monitoring of cellular behaviour by impedance measurements on interdigitated electrode structures. Biosens Bioelectron. 1997;12(1):29–41.
40. Chang B, Chen C, Ding S, Chen DC, Chang H. Impedimetric monitoring of cell attachment on interdigitated microelectrodes. Sensors Actuators B Chem. 2005;105(2):159–63.
41. Wang L, Wang H, Mitchelson K, Yu Z, Cheng J. Analysis of the sensitivity and frequency characteristics of coplanar electrical cell–substrate impedance sensors. Biosens Bioelectron. 2008;24(1):14–21.
42. Bergveld P. Development of an ion-sensitive solid-state device for neurophysiological measurements. IEEE Trans Biomed Eng. 1970;1:70–71c. BME-17.
43. Chang K-S, Sun C-J, Chiang P-L, Chou A-C, Lin M-C, Liang C, Hung H-H, Yeh Y-H, Chen C-D, Pan C-Y. Monitoring extracellular K+ flux with a valinomycin-coated silicon nanowire field-effect transistor. Biosens Bioelectron. 2012;31(1):137–43.
44. Fromherz P. Semiconductor chips with ion channels, nerve cells and brain. Phys E Low-Dimension Syst Nanostruct. 2003;16(1):24–34.

45. Ohtake T, Hamai C, Uno T, Tabata H, Kawai T. Immobilization of probe DNA on Ta_2O_5 thin film and detection of hybridized helix DNA using IS-FET. Jpn J Appl Phys. 2004;43(9A): L1137.
46. Ueno K, Inoue I, Akoh H, Kawasaki M, Tokura Y, Takagi H. Field-effect transistor on SrTiO3 with sputtered Al2O3 gate insulator, arXiv preprint cond-mat/0306436. 2003.
47. Finn A, Alderman J, Schweizer J. Towards an optimization of FET-based bio-sensors. Eur Cells Mater. 2002;4(Sup 2):21–3.
48. Oesch U, Caras S, Janata J. Field effect transistors sensitive to sodium and ammonium ions. Anal Chem. 1981;53(13):1983–6.
49. Bratov A, Abramova N, Domınguez C, Baldi A. Ion-selective field effect transistor (ISFET)-based calcium ion sensor with photocured polyurethane membrane suitable for ionised calcium determination in milk. Anal Chim Acta. 2000;408(1):57–64.
50. Zeck G, Fromherz P. Noninvasive neuroelectronic interfacing with synaptically connected snail neurons immobilized on a semiconductor chip. Proc Natl Acad Sci. 2001;98 (18):10457–62.
51. Fromherz P, Offenhausser A, Vetter T, Weis J. A neuron-silicon junction: a Retzius cell of the leech on an insulated-gate field-effect transistor. Science. 1991;252(5010):1290–3.
52. Hafeman DG, Parce JW, McConnell HM. Light-addressable potentiometric sensor for biochemical systems. Science. 1988;240(4856):1182–5.
53. Hafner F. Cytosensor® microphysiometer: technology and recent applications. Biosens Bioelectron. 2000;15(3):149–58.
54. Eklund SE, Snider RM, Wikswo J, Baudenbacher F, Prokop A, Cliffel DE. Multianalyte microphysiometry as a tool in metabolomics and systems biology. J Electroanal Chem. 2006;587(2):333–9.
55. Yicong W, Ping W, Xuesong Y, Gaoyan Z, Huiqi H, Weimin Y, Xiaoxiang Z, Jinghong H, Dafu C. Drug evaluations using a novel microphysiometer based on cell-based biosensors. Sensors Actuators B Chem. 2001;80(3):215–21.
56. Yicong W, Ping W, Xuesong Y, Qingtao Z, Rong L, Weimin Y, Xiaoxiang Z. A novel microphysiometer based on MLAPS for drugs screening. Biosens Bioelectron. 2001;16 (4):277–86.
57. Hu N, Ha D, Wu C, Cheng G, Yu H, Wang T, Wu J, Cai H, Liu Q, Wang P. Design of microphysiometer based on multiparameter cell-based biosensors for quick drug analysis. J Innov Opt Health Sci. 2012;5(01):1150005.
58. Qing Q, Pal SK, Tian B, Duan X, Timko BP, Cohen-Karni T, Murthy VN, Lieber CM. Nanowire transistor arrays for mapping neural circuits in acute brain slices. Proc Natl Acad Sci. 2010;107(5):1882–7.
59. Cohen-Karni T, Qing Q, Li Q, Fang Y, Lieber CM. Graphene and nanowire transistors for cellular interfaces and electrical recording. Nano Lett. 2010;10(3):1098–102.
60. Giljohann DA, Mirkin CA. Drivers of biodiagnostic development. Nature. 2009;462 (7272):461–4.
61. Scanziani M, Häusser M. Electrophysiology in the age of light. Nature. 2009;461 (7266):930–9.
62. Hamill OP, Marty A, Neher E, Sakmann B, Sigworth F. Improved patch-clamp techniques for high-resolution current recording from cells and cell-free membrane patches. Pflugers Arch. 1981;391(2):85–100.
63. Tian B, Cohen-Karni T, Qing Q, Duan X, Xie P, Lieber CM. Three-dimensional, flexible nanoscale field-effect transistors as localized bioprobes. Science. 2010;329(5993):830–4.
64. Tian B, Xie P, Kempa TJ, Bell DC, Lieber CM. Single-crystalline kinked semiconductor nanowire superstructures. Nat Nanotechnol. 2009;4(12):824–9.
65. Patolsky F, Zheng G, Lieber CM. Fabrication of silicon nanowire devices for ultrasensitive, label-free, real-time detection of biological and chemical species. Nat Protoc. 2006;1 (4):1711–24.

66. Duan X, Gao R, Xie P, Cohen-Karni T, Qing Q, Choe HS, Tian B, Jiang X, Lieber CM. Intracellular recordings of action potentials by an extracellular nanoscale field-effect transistor. Nat Nanotechnol. 2012;7(3):174–9.
67. Sakmann B. Single-channel recording. New York: Springer Science & Business Media; 2013.
68. Navarrete EG, Liang P, Lan F, Sanchez-Freire V, Simmons C, Gong T, Sharma A, Burridge PW, Patlolla B, Lee AS. Screening drug-induced arrhythmia using human induced pluripotent stem cell–derived cardiomyocytes and low-impedance microelectrode arrays. Circulation. 2013;128(11 suppl 1):S3–13.
69. Yamanaka K. Anodically electrodeposited iridium oxide films (AEIROF) from alkaline solutions for electrochromic display devices. Jpn J Appl Phys. 1989;28(4R):632.
70. Mafakheri E, Salimi A, Hallaj R, Ramazani A, Kashi MA. Synthesis of iridium oxide nanotubes by electrodeposition into polycarbonate template: fabrication of chromium (III) and arsenic (III) electrochemical sensor. Electroanalysis. 2011;23(10):2429–37.
71. Cogan SF, Ehrlich J, Plante TD, Smirnov A, Shire DB, Gingerich M, Rizzo JF. Sputtered iridium oxide films for neural stimulation electrodes. J Biomed Mater Res B Appl Biomater. 2009;89(2):353–61.
72. Lin ZC, Xie C, Osakada Y, Cui Y, Cui B. Iridium oxide nanotube electrodes for sensitive and prolonged intracellular measurement of action potentials. Nat Commun. 2014;5:1–10.
73. Zimmermann U, Pilwat G, Riemann F. Dielectric breakdown of cell membranes, Membrane transport in plants. Berlin: Springer; 1974. p. 146–53.
74. Neumann E, Schaefer-Ridder M, Wang Y, Hofschneider P. Gene transfer into mouse lyoma cells by electroporation in high electric fields. EMBO J. 1982;1(7):841.
75. Chang D, Reese TS. Changes in membrane structure induced by electroporation as revealed by rapid-freezing electron microscopy. Biophys J. 1990;58(1):1.
76. Zhai Y, Zhang Y, Qin F, Yao X. An electrochemical DNA biosensor for evaluating the effect of mix anion in cellular fluid on the antioxidant activity of CeO_2 nanoparticles. Biosens Bioelectron. 2015;70:130–6.
77. Zhou J, Du L, Zou L, Zou Y, Hu N, Wang P. An ultrasensitive electrochemical immunosensor for carcinoembryonic antigen detection based on staphylococcal protein A—Au nanoparticle modified gold electrode. Sensors Actuators B Chem. 2014;197:220–7.
78. Aleshin AN. Polymer nanofibers and nanotubes: charge transport and device applications. Adv Mater. 2006;18(1):17–27.
79. Kaiser AB. Electronic transport properties of conducting polymers and carbon nanotubes. Rep Prog Phys. 2001;64(1):1.
80. Li J, Lu Y, Ye Q, Cinke M, Han J, Meyyappan M. Carbon nanotube sensors for gas and organic vapor detection. Nano Lett. 2003;3(7):929–33.
81. Yoon H, Lee SH, Kwon OS, Song HS, Oh EH, Park TH, Jang J. Polypyrrole nanotubes conjugated with human olfactory receptors: high-performance transducers for FET-type bioelectronic noses. Angew Chem Int Ed. 2009;48(15):2755–8.

Chapter 3
Label-Free DNA Biosensors with Field-Effect Devices

Chunsheng Wu, Liping Du, Ling Zou, and Yulan Tian

Abstract In the recent decades, the detection of specific deoxyribonucleic acid (DNA) molecules has attracted more and more attention due to the fast increasing demand of DNA analysis, which plays very important roles in a wide range of applications such as molecular diagnostics, gene analysis, and environmental monitoring. Field-effect devices (FEDs) open up an exciting realm for the development of label-free DNA biosensors due to the fast advances in the microfabrication process. FED-based DNA biosensors have achieved significant advances and shown promising prospects and potential applications in many fields. In this chapter, the basic mechanisms and recent progress in the development of FED-based DNA biosensors will be reviewed in detail. For the first, the basic principle of FED-based DNA biosensors will be introduced, which will focus on the signal generation mechanisms of DNA hybridization and the signal transduction and readout by FEDs. In the second part, the design considerations of FED-based DNA biosensors will be discussed, which include the coupling of probe ssDNA FEDs, measurement solutions, and sensor system. Finally, the applications of FED-based DNA biosensors in two typical and important fields will be summarized, which are label-free DNA assays and detection of single nucleotide polymorphisms (SNPs). The development trends and the current main challenges of FED-based DNA biosensors will be provided and discussed in the final section.

Keywords DNA biosensor • Field-effect device • Label-free • DNA hybridization

C. Wu (✉) • L. Du
Institute of Medical Engineering, School of Basic Medical Sciences, Health Science Center, Xi'an Jiaotong University, Xi'an, China
e-mail: wuchunsheng@xjtu.edu.cn

L. Zou • Y. Tian
Biosensor National Special Laboratory, Department of Biomedical Engineering, Zhejiang University, Hangzhou, China

P. Wang et al. (eds.), *Micro/Nano Cell and Molecular Sensors*,
DOI 10.1007/978-981-10-1658-5_3

3.1 Introduction

In nature, deoxyribonucleic acid (DNA) molecules are double-stranded helices and consist of two long biopolymers made from repeating units of nucleotides including guanine (G), adenine (A), thymine (T), and cytosine (C) [1]. The main function of DNA molecules is carriers of life information, which store and encode the biological information for the development and functioning of almost all known living organisms. In the recent decades, the detection of specific DNA molecules has attracted more and more attention due to the fast increasing demand of DNA analysis, which plays very important roles in a wide range of applications such as molecular diagnostics, gene analysis, and environmental monitoring. This has led to many innovative and novel approaches for simple, cheap, and rapid detection of specific DNA molecules. In this context, DNA biosensors are one of the most attractive and promising approaches, which offer rapid and high sensitive tools for the detection of specific DNA molecules [2–8]. Basically, DNA biosensors consist of the probe DNA and electrodes, which function as sensitive elements and signal transducers, respectively. Probe DNA is usually single-stranded DNA (ssDNA) molecules with short sequences and immobilize onto the surface of transducers. Probe ssDNA can hybridize with its complementary ssDNA, which can generate a detectable signal that can be received by the transducer. Currently, DNA biosensors can be classified into two main categories based on their detection strategies, which are labeling strategies and label-free strategies. DNA biosensors exploit selective hybridization of probe ssDNA with its complementary target ssDNA for the generation of informative detectable signals. The labeling strategies usually require the careful designing and labeling of DNA probe or target molecules with various markers (e.g., fluorescence or radiochemical), which are complicated, expensive, and time-consuming. This obvious drawback results in various kinds of inconvenience and increase of the cost for DNA analysis.

To overcome this drawback, various label-free strategies have been proposed and proved to be an alternative and promising approach for the detection of specific DNA molecules by the utilization of different kinds of transduction methods such as optical, electrochemical, and photoelectrochemical approaches [9–13]. In particular, field-effect devices (FEDs) open up an exciting realm for the development of new generation of DNA biosensors due to the fast advances in the microfabrication process, which makes it possible to fabricate devices in micro/nano scale to facilitate the incorporation of sensitive elements at the molecular level as well as the achievement of highly sensitive and efficient signal transduction [14–18]. In addition, this also makes DNA biosensors cheaper, easier for integration and large-scale production. FED-based DNA biosensors are able to realize the label-free detection of DNA molecules by their intrinsic molecule charge with direct electrical readout. At present, FEDs with a structure of electrolyte–insulator–semiconductor (EIS) system, such as field-effect transistors (FETs), capacitive EIS sensors, and light-addressable potentiometric sensors (LAPSs), have been widely applied for the development of label-free DNA biosensors [19–25].

Since the backbone of DNA molecules is composed of alternating phosphate and sugar residues, DNA molecules are negatively charged in solution. The basic mechanism of FED-based DNA biosensors is a direct label-free electrical detection

of surface charge changes originated from the hybridization of probe ssDNA with its complementary target ssDNA, which occurs on the gate surface of the FEDs [14, 22, 26]. In a broad sense, FED-based biosensors are able to detect any charged molecules attached onto their gate surface including ssDNA as well as double-stranded DNA (dsDNA). As a result, FED-based DNA biosensors have great potential to be applied in a wide range of fields, for example, the detection of DNA-associated diseases, genetic analysis, drug screening, and DNA damage detection. However, the development of FED-based DNA biosensors also faces some challenges. One of the main challenges is the integration of FEDs with probe ssDNA with a high reliable and scalable process, which is crucial to the performances of sensor output. Moreover, the automation of the detection steps is also very important to the repeatability of DNA detection. The fast advancements in microfabrication technologies and nanotechnologies may promote the solving of these issues by providing novel micro/nano scale transducers, nanomaterials, and novel coupling technologies to enhance the performances of FED-based DNA biosensors.

FED-based DNA biosensors have achieved significant advances and shown promising prospects and potential applications in many fields. In this chapter, the basic mechanisms and recent progress in the development of FED-based DNA biosensors will be reviewed in detail. For the first, the basic principle of FED-based DNA biosensors will be introduced, which will focus on the signal generation mechanisms of DNA hybridization and the signal transduction and readout by FEDs. In the second part, the design considerations of FED-based DNA biosensors will be discussed, which include the coupling of probe ssDNA FEDs, measurement solutions, and sensor system. Finally, the applications of FED-based DNA biosensors in two typical and important fields will be summarized, which are label-free DNA assays and detection of single nucleotide polymorphisms (SNPs). The development trends and the current main challenges of FED-based DNA biosensors will be provided and discussed in the final section.

3.2 Principle of FED-Based DNA Biosensors

3.2.1 Mechanisms of DNA Hybridization and Signal Generation

DNA molecules contain extremely important genetic instructions and biological information for all living organisms, which are encoded by the use of the repeating unit of nucleotides. Natural DNA molecules usually exist as double-stranded helices due to the remarkable specificity of the interactions between complementary ssDNA molecules [1]. In addition, biological information stored in each strand of DNA molecules is the same, which duplicate the stored biological information. Figure 3.1 shows the chemical structure of dsDNA molecules that are formed by a pair of complementary ssDNA [27]. Basically, the backbone of ssDNA molecules consists of an alternating string of deoxyribose sugars and phosphate groups that are connected by special asymmetric bonds. This makes the backbone of ssDNA

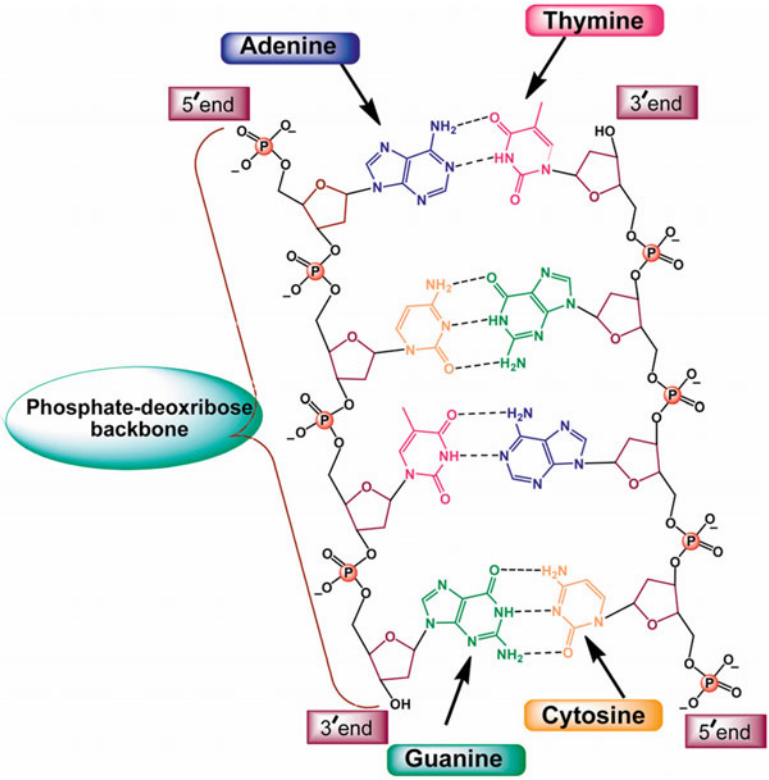

Fig. 3.1 Structure of dsDNA formed by the hybridization of complementary ssDNA molecules. *Dotted lines* indicate the hydrogen bonds between the bases (Reproduced with permission from Ref. [27]. Copyright 2012 Elsevier)

molecules pretty stable and resistant to cleavage. In addition, the asymmetric bonds lead to the polarity ssDNA sequence as indicated by the end labels 5′ and 3′, which makes DNA molecules form a direction in ssDNA molecules and antiparallel structure in dsDNA molecules. Therefore, the direction of each ssDNA in a dsDNA molecule is opposite to each other. Each sugar of the DNA backbone covalently binds with one of the four bases G, A, T, and C. The complementary ssDNA molecules are held tightly together via the noncovalent hydrogen bonds between the complementary bases as indicated by the dotted lines. In addition, each pair of complementary nucleotides is coiled round the same axis with a pitch of 3.4 nm and a radius of 10 nm, which forms a right-handed double helix [1]. The interactions between complementary nucleotides can be classified into two categories based on their origination of hydrogen bonds. One is the interaction between nucleotides of G and C, which forms three hydrogen bonds. The other one is the interaction between nucleotides of A and T, which forms two hydrogen bonds. As a result, the GC interactions are stronger than that of AT interactions, which partially contribute to the higher stability of higher GC-content dsDNA molecules compared

to the lower GC-content dsDNA molecules. In addition to the hydrogen bonds between complementary nucleotides, nucleotide-stacking interactions (the conjugated π bonds of nucleotide bases align perpendicular to the axis of the DNA molecule) also contribute partial to the stabilization of DNA double helix.

DNA hybridization refers to the formation of the dsDNA by base pairing between complementary strands. The remarkable specificity of the interactions between complementary nucleotides makes DNA a useful feature for the development of DNA biosensors. For this, hybridization between complementary ssDNA should be able to generate detectable signals that can be received by the related transducers. For labeling strategies, the most commonly used signal generation approach is to label the ssDNA molecules using fluorescent dye. The amount of hybridized ssDNA can be detected by the measurement of fluorescent signals before and after DNA hybridization. On the other hand, the label-free strategies usually rely on the detection of physical changes before and after ssDNA hybridization, for instance, the mass or charge changes of DNA molecules. In case of label-free DNA biosensors using FEDs as transducers, the basic mechanism is based on the detection of intrinsic molecular charge changes on their gate surface, which originated from the hybridization of negatively charged target ssDNA with probe ssDNA that is immobilized on the gate surface of FEDs [14, 15]. Probe ssDNA is usually a short-length ssDNA with a few tens of base pairs (~10 nm), which can be carefully designed to control the interactions and hybridization with desired target ssDNA. In this length scale, ssDNA molecules are stiff and straight, which are favorable for the hybridization with its complementary ssDNA. Because the backbone of DNA molecules is negatively charged in solution, the hybridization of target ssDNA with probe ssDNA will change the charge distribution on the gate surface of FEDs. This charge change will alter the channel conductance under the gate surface, which can be detected by monitoring the channel current. By this approach, label-free DNA detection can be realized based on the detection of DNA intrinsic charges using FEDs as transducer for the monitoring of surface charge changes.

3.2.2 Label-Free Detection of DNA Hybridization with FEDs

With the fast advances in the microfabrication process, more and more FEDs have been applied in DNA biosensors. The extreme capabilities of FEDs for surface charge sensing have been utilized for the label-free detection of DNA molecules based on their intrinsic charges. At present, various types of FEDs have been involved in the development of DNA biosensors [19–25, 28–37]. All the FEDs require the conversion of DNA hybridization signals into detectable signals by FEDs. The most direct and convenient strategies are usually involved in the recording of surface charge change signals originated from hybridization of ssDNA molecules. The hybridization of probe ssDNA molecules immobilized on the surface of FEDs with their complementary target ssDNA molecules can

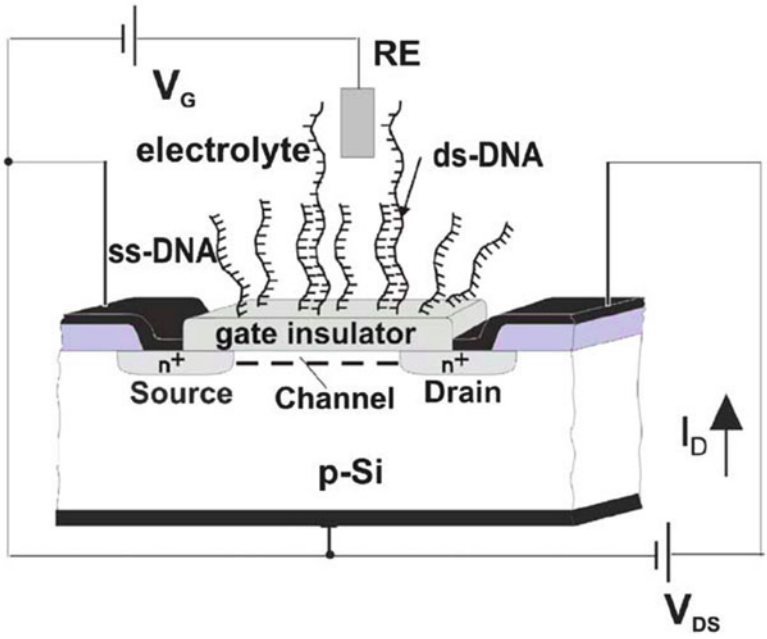

Fig. 3.2 Schematic diagram of DNA biosensors using FET device as transducer for the detection of surface charge changes originated from the DNA hybridization events occurred on its gate surface (Reproduced with permission from Ref. [14]. Copyright 2005 Elsevier)

generate the charge changes due to the negatively charged DNA backbone. The charge changes can be detected by the charge-sensitive devices, FEDs. In this section, label-free detection of DNA molecules with two types of FEDs will be introduced, which are field-effect transistors (FETs) and light-addressable potentiometric sensors (LAPSs).

FETs have become one of the most commonly used FEDs for the label-free detection of biomolecules, which have also been widely applied in the development of label-free DNA biosensors. FETs can efficiently record the surface potential changes originating from the DNA hybridization that occurred on their gate surfaces. Figure 3.2 shows the basic configuration of FET with probe ssDNA immobilized on its gate surface via the electrolyte solution, where a reference electrode is also put into the electrolyte solution [14]. The potential of gate surface will change due to the redistribution of surface charge changes when the target ssDNA hybridized with probe ssDNA. The surface potential changes will couple to the gate of FET, which will modulate the channel conductance between the source and drain electrode. The channel conductance changes can be measured by recording the changes in the drain current that are the output of FET signals and dependent on the surface charge changes resulting from DNA hybridization.

FETs can provide a particular powerful tool for label-free DNA detection to meet the special requirements on the development of DNA biosensors. For instance,

FETs usually have a high input impedance, which makes it very convenient to be used as a transducer to combine with DNA molecules to develop DNA biosensors. In addition, FETs hold the decisive advantages of miniaturization due to the fast development of microfabrication process, which makes it possible to miniaturize the whole sensor system to a portable sensor system that can be used to detect the specific DNA molecules in fields, for example, the development of point-of-care systems for the detection of bacterial DNA markers.

LAPSs are another type of commonly used FEDs that are sensitive to the changes of the surface potential, which are semiconductor-based sensors that use light to flexibly define the gate area for localized surface potential detection. The decisive advantage of LAPSs originated from their ability to perform spatially resolved measurements, which is useful for monitoring surface charge changes due to the hybridization of DNA molecules occurring on the surface of LAPSs. Figure 3.3 shows the basic mechanism of the LAPS with a structure of electrolyte–insulator[SiO_2]–semiconductor[Si] for the label-free detection of DNA molecules based on their intrinsic molecular charges [19]. Figure 3.3a shows the layer structure of LAPS as well as the measurement setup of a multi-spot LAPS system, where an LED array was employed as the light source for the realization of multi-spot measurement. As shown in Fig. 3.3b, the immobilization of probe ssDNA and hybridization of probe ssDNA with its complementary target ssDNA will induce the shifts of photocurrent–bias voltage curve. The basic principle of LAPS operation is based on the photoelectric effect of semiconductors. During illumination of the modulated light with a certain wavelength, LAPS semiconductor produces electro-hole pairs due to the adsorption of light energy. A DC bias voltage is applied to LAPS chip via a reference electrode and working electrode to generate a depletion layer at the insulator/semiconductor interface by avoiding the rapid recombination of electron and hole. As a result, the AC photocurrent is generated and can be detected by peripheral circuit to serve as the output of the sensor signals. In addition, the width of depletion layer is a function of the surface potential value of the local illuminated area, which can be electrically read out through the AC photocurrent. When the probe ssDNA molecules or target ssDNA molecules attach onto the LAPS surface, the local surface potential of LAPS can generate the corresponding changes due to the redistribution of surface charges. These changes can be detected by the measurement of photocurrent fluctuation, which can be indicated by the shift of photocurrent–bias voltage curves as shown in Fig. 3.3b. Because the DNA molecules are negatively charged in solution, the immobilization of probe ssDNA and the hybridization of target ssDNA will introduce more negative charges to the sensor surface. This will lead to the shift of the photocurrent–bias voltage curves in the direction of more positive bias voltages.

Compared with FET, the main advantage of LAPSs originated from its flexible gate defined by light illumination, which overcomes the limitation of discrete gate of FETs. This allows for the measurement of desirable target spots by simply focusing the light to the local area, which avoids the complicated molecular positioning on the gate surface of FETs. In addition, the LAPS setup with a LED array is able to realize multi-spot measurement, where the measurement spots can

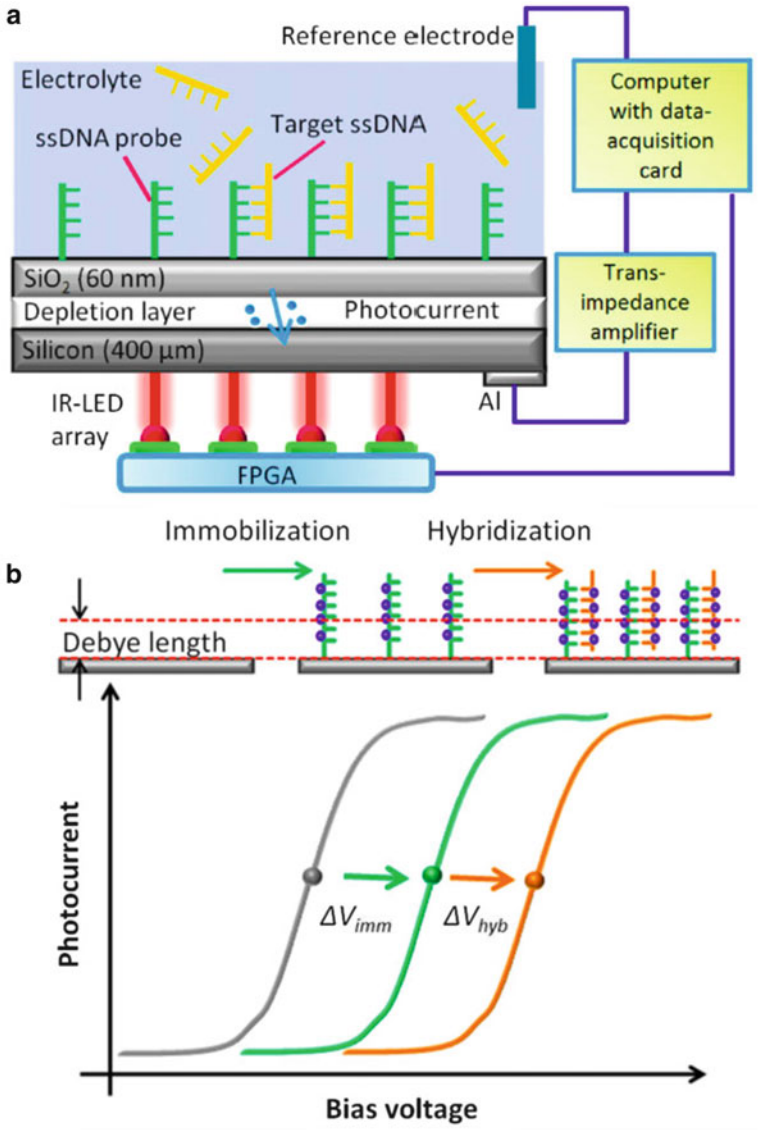

Fig. 3.3 Schematic diagrams showing (**a**) the configuration of DNA biosensors based on LAPSs and (**b**) expected shifts of typical photocurrent–voltage curves induced by DNA immobilization and hybridization occurred on the sensor surface (Reproduced with permission from Ref. [19]. Copyright 2014 WILEY-VCH Verlag GmbH & Co. KGaA, Weinheim)

be determined by the illumination area of each LED. Basically, the modulation frequency of each LED is different, which results in the modulation of generated photocurrent on each measurement spot at the different frequency of corresponding LED. Therefore, the local surface potential changes of multi-spots can be measured

in a parallel manner, where the recorded overall photocurrent is a superposition of all illuminated spots. Photocurrent amplitudes of each measured spots, which are associated with local surface potentials of corresponding spot, can be separated and determined from the overall photocurrent by the fast Fourier transformation (FFT). This makes it possible for the realization of simultaneous measurement of multiple spots, which is favorable for the development of light-addressable DNA chips.

In general, both FETs and LAPSs are only sensitive to surface charge changes that occur within the Debye length from the sensitive surface. Therefore, the detection of charge changes originated from the probe ssDNA immobilization and target ssDNA hybridization is limited by the Debye length. On the other hand, the Debye length is strongly influenced by the ionic strength of the solution used during the measurement. In principle, the lower the ionic strength of the solution, the longer the Debye length. This leads to a higher sensitivity for the detection of DNA molecular charges. As a result, to achieve higher output signals, the solution with low ionic strength is usually utilized as a measurement solution for the detection of ssDNA immobilization and hybridization.

3.3 Design and Fabrication of FEDs for DNA Sensing

The basic mechanism of FED-based biosensors for label-free DNA detection is to employ the extreme high charge sensitivity of FEDs for the detection of DNA molecules based on their intrinsic molecular charges. The coupling of a highly specialized probe ssDNA with a transducer can generate potential devices and instruments that can be used for a wide range of applications associated with highly sensitive detection of DNA molecules. For this purpose, it is necessary to achieve effective coupling of ssDNA probes with FEDs, which can not only maintain their natural structure and functions to serve as the sensitive elements for target ssDNA hybridization but also provide high efficiency for the transduction of hybridization signals into detectable signals by FEDs. On the other hand, FEDs should be built to convert the DNA hybridization signals into the readable signals by the peripheral circuits. In this section, the coupling of DNA molecules with FEDs for the label-free DNA detection will be introduced. By the following, we will focus on two types of FEDs, which are FETs and LAPSs. We will introduce the fabrication of FETs and LAPSs for the development of label-free DNA biosensors. Both of them can record the electrical responsive signals originated from DNA molecules attached onto the sensor surface. The related measurement setup and peripheral circuits are required for the construction of the sensor systems to realize the label-free detection of DNA molecules.

3.3.1 Coupling of DNA Molecules with FEDs

The coupling of DNA molecules with FEDs is crucial to develop a DNA biosensor, which has great influences on the performances of whole DNA-sensing system. Usually, the coupling of DNA molecules with FEDs is realized by the immobilization of probe ssDNA on their sensitive surfaces. To achieve the optimal performances including the high sensitivity and selectivity, it is important to immobilize the probe ssDNA with high stability as well as to avoid the nonspecific adsorption. Basically, the methods employed for the immobilization of probe ssDNA on the sensitive surface of FEDs include the adsorption, covalent attachment, and biotin–(strept)avidin interaction [5, 15].

The simplest immobilization method for probe ssDNA immobilization is adsorption, which is mainly based on the physical interactions between probe ssDNA molecules and sensitive surface of FEDs, particularly the electrostatic interaction [20, 22]. The main advantage of this method is that the modification of probe ssDNA is not required for the sake of immobilization. Probe ssDNA molecules are negatively charged in solution at a physiological pH, while the surfaces of majority of FEDs are also negatively charged. In order to immobilize probe ssDNA on the surface of FEDs by electrostatic interactions, it is necessary to adsorb a positively charged layer onto the sensor surface. The adsorption is a very simple and convenient approach for probe ssDNA immobilization. However, this method also has some direct influences on the performances of DNA biosensors, which usually lead to the lower stability and repeatability due to the difficulties in controlling the amount of DNA immobilization as well as the chemical and physical properties of modification layer on sensor surface. In addition, this method also suffers from the steric hindrance of the probe ssDNA, which results in the low-efficiency hybridization of probe ssDNA with target ssDNA.

To overcome the drawback of adsorption method, covalent binding method was employed as an alternative method for the probe ssDNA immobilization on the gate surface of FEDs to achieve the high efficient hybridization. The stable and homogeneous immobilization of probe ssDNA on the gate surface of FEDs is necessary for the detection of hybridization signals with low background signals. Covalent binding can not only achieve stronger and robust bond between probe ssDNA and gate surface of FEDs but also provide an approach to control the surface density of probe ssDNA immobilization, which is important to enhance the performance of the whole DNA-sensing system. In order to design and fabricate a DNA biosensor with high performance, it is essential to immobilize probe ssDNA on the gate surface of FEDs with an optimal surface density due to the electrostatic repulsion between probe ssDNA and target ssDNA. Basically, the hybridization efficiency of probe ssDNA with complementary target ssDNA decreases greatly with the increase of probe ssDNA surface density. In addition, higher surface density of probe ssDNA also leads to the decrease in hybridization stability due to the steric hindrance. On the other hand, the sensitivity of DNA biosensors increases with the decreases in the probe ssDNA distance due to the lower charge screening effect.

Therefore, to design a DNA biosensor with higher performance, it is highly essential and favorable to optimize the surface density of probe ssDNA with regard to the detection sensitivity.

The gate surfaces of FEDs usually consist of oxide (e.g., SiO_2, Ta_2O_5), nitride (e.g., Si_3N_4), or gold. As a result, various chemical reactions have been employed for the covalent immobilization of probe ssDNA on the gate surface of FEDs. In order to covalently immobilize probe ssDNA to oxide and nitride surfaces that contain hydroxyl groups, silane coupling agents is usually employed to modify the surface with siloxane layers that can tether functionalized probe ssDNA to the surface. Siloxane layers often terminate with various functional moieties such as amines, thiols, and aldehydes, which can be used to covalently bind with terminal-modified probe ssDNA. (3-Aminopropyl)triethoxysilane (APTES) is a kind of aminosilane, which is commonly used to modify oxide and nitride surfaces with amines. Figure 3.4 shows the mechanisms of amino-modified probe ssDNA immobilization on the gate surface of FEDs using APTES as silane agent [19, 28]. The surfaces modified with amine can be used to covalently bind with amino-modified probe ssDNA via the homobifunctional cross-linking agents such as glutaraldehyde and succinic anhydride. However, both of the activity sites of the homobifunctional cross-linker molecules may bind to the siloxane layer, which results in the losing of their capability of reaction with amino-modified probe ssDNA. On the other hand, the surfaces modified with APTES can react with heterobifunctional cross-linking agents, which can avoid the intralayer cross-linking. For instance, N-maleimidocaproyl-oxysulfosuccinimide ester (sulfo-EMCS) and sulfosuccinimidyl 4-(N-maleimidomethyl) cyclohexane-1-carboxylate (sulfo-SMCC) can be used to functionalize the APTES-modified surfaces for the sake of immobilization of thiol-modified probe ssDNA. On the contrary, the use of 3-mercaptopropyltrimethoxysilane (MPTMS) for surface modification makes it possible to covalently immobilize thiolated or acrylic phosphoramidite-modified probe ssDNA on the oxide and nitride surfaces. Direct immobilization of amine-functionalized probe ssDNA is also possible by the use of trimethyloxysilane aldehyde as a silane coupling agent.

For the FEDs with gold-gate surfaces, thiol-modified probe ssDNA is usually utilized to directly bind to the gold surfaces via covalent bonds. Figure 3.5 shows the mechanism of thiol-modified probe ssDNA immobilization on the gold surface of FEDs [37–39]. In addition, the alkyl thiols can be used to control the surface density and orientation of probe ssDNA on gold surfaces by mixing thiolated probes and alkyl thiols with a proper ratio during probe ssDNA immobilization.

Biotin–streptavidin binding has also been applied to the coupling of probe ssDNA with the gate surface of FEDs for the development of DNA biosensors [40]. Basically, one molecule of avidin and streptavidin can provide four binding sites for biotin, which are a kind of noncovalent binding but with very high affinity [41]. This makes it possible to form strong and robust biotin–(strept)avidin complex even in changing solution environments. This approach usually modified the gate surface of FEDs with a layer of avidin to allow the capture of biotinylated probe ssDNA. Due to the stable and robust binding between avidin and biotin, the

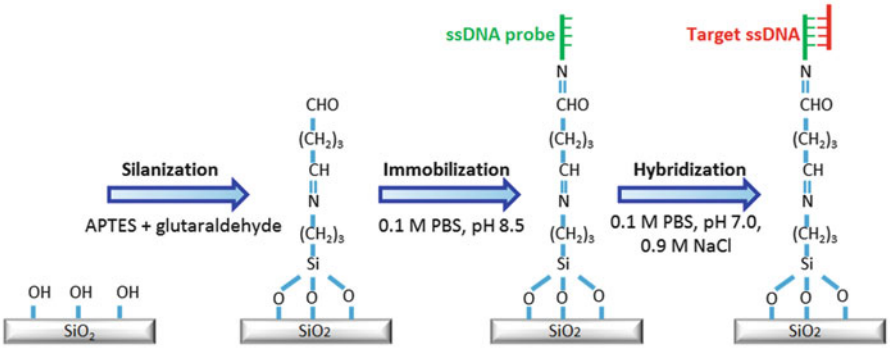

Fig. 3.4 Mechanisms of amino-modified probe ssDNA immobilization on the gate surface of FEDs that consists a layer of SiO_2. The hybridization of probe ssDNA with its complementary target ssDNA is also shown (Reproduced with permission from Ref. [19]. Copyright 2014 WILEY-VCH Verlag GmbH & Co. KGaA, Weinheim)

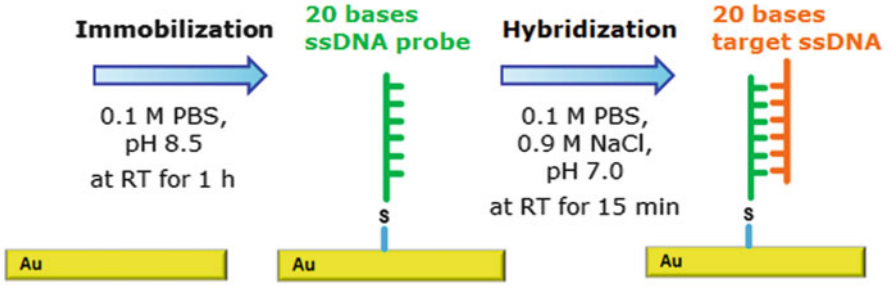

Fig. 3.5 Schematic diagram of thiol-modified probe ssDNA immobilization on the gold surface via gold–thiol bond and its hybridization with complementary target ssDNA [39]

immobilized probe ssDNA is stable even after multiple washing steps and pH value changes. This could potentially contribute to the repeatability and reproducibility of DNA biosensors.

3.3.2 Fabrication of FEDs for DNA Sensing

In the recent decades, microfabrication process has achieved fast advancements, which make it possible to design and fabricate various precise FEDs for the special objects and applications [42, 43]. This also advances the development of DNA biosensors that use FEDs as transducers for the detection of DNA molecules based on their intrinsic molecular charges. In principle, the basic function of the transducers is related to the detection of hybridization of probe ssDNA with its complementary target ssDNA and transmission of detected hybridization signals to the

peripheral circuits for further processing such as signal amplification, data collection, data storage, and data display. Therefore, the transducers for DNA biosensors require the high efficient and robust coupling with probe ssDNA, which is not only referred to the stable immobilization, but more importantly referred to the signal transduction. There are two main typical FEDs which have been used as transducers and applied in the development of DNA biosensors, which are FETs and LAPSs, respectively. Both of them have been successfully applied in the detection of specific DNA hybridization signals, which proves their potential capability of being used as transducers in DNA biosensors. By the following, the fabrication process of FETs and LAPSs that are used as transducers in DNA biosensors will be briefly introduced.

FETs have been successfully applied in the development of DNA biosensors, where they can not only realize the electrical detection of DNA hybridization but also realize the transduction of hybridization signal to the detectable electrical signals by the peripheral circuits [16, 25, 28, 31, 32, 44]. FET devices are usually fabricated on the basis of silicon wafer by the standard microfabrication process. For the first, the silicon wafer is thermally grown with an insulator layer with proper thickness to serve as the gate surface of FET devices. For some FETs, a layer of Si_3N_4 is further deposited to the top of oxide layer via plasma-enhanced chemical vapor deposition (PECVD) process. For the next step, a passivation layer consisting of polyimide is usually formed for the fixation with a printed circuit board. The source and drain electrodes are fabricated using conventional photolithography process. Finally, the fabricated FET devices are encapsulated with a conventional epoxy resin to form a detection chamber for DNA sensing. Basically, only the gate surface of FET devices is exposed to the solution of detection chamber, which allows for probe ssDNA immobilization and target ssDNA hybridization occurring on the gate surface and consequently can be detected by the FETs. Based on this approach, the electrical signals of DNA hybridization can be coupled to the gate electrode of FET and then converted into the output signals of FET. The transduced signals can then be output via the source and drain electrodes of FET, which make it possible for the signals to be further amplified and processed by the peripheral circuits. Figure 3.6 shows an example of FET device fabrication for DNA sensing by 0.5 μm standard complementary metal–oxide–semiconductor (CMOS) technology, where the key fabrication steps are shown [25]. In this FET device, the gate was formed by polysilicon (PolySi) and tungsten silicide (WSix), then opened by plasma etching, and finally deposited by a layer of Cr/Au for the immobilization of thiol-modified probe ssDNA molecules.

The sensor systems of FET-based DNA biosensors usually consist of peripheral circuits for the signal processing and analysis and sample introduction setup for DNA sample addition to the detection chamber in solution. During measurement, DNA sample is introduced to the detection chamber via a constant flow generated by the sample introduction setup, where a suction pump is generally utilized. If the DNA sample contains the complementary target ssDNA that can hybridize with the probe ssDNA immobilized on the gate surface of the FET devices, the surface charge distribution will change accordingly due to the negatively charged target

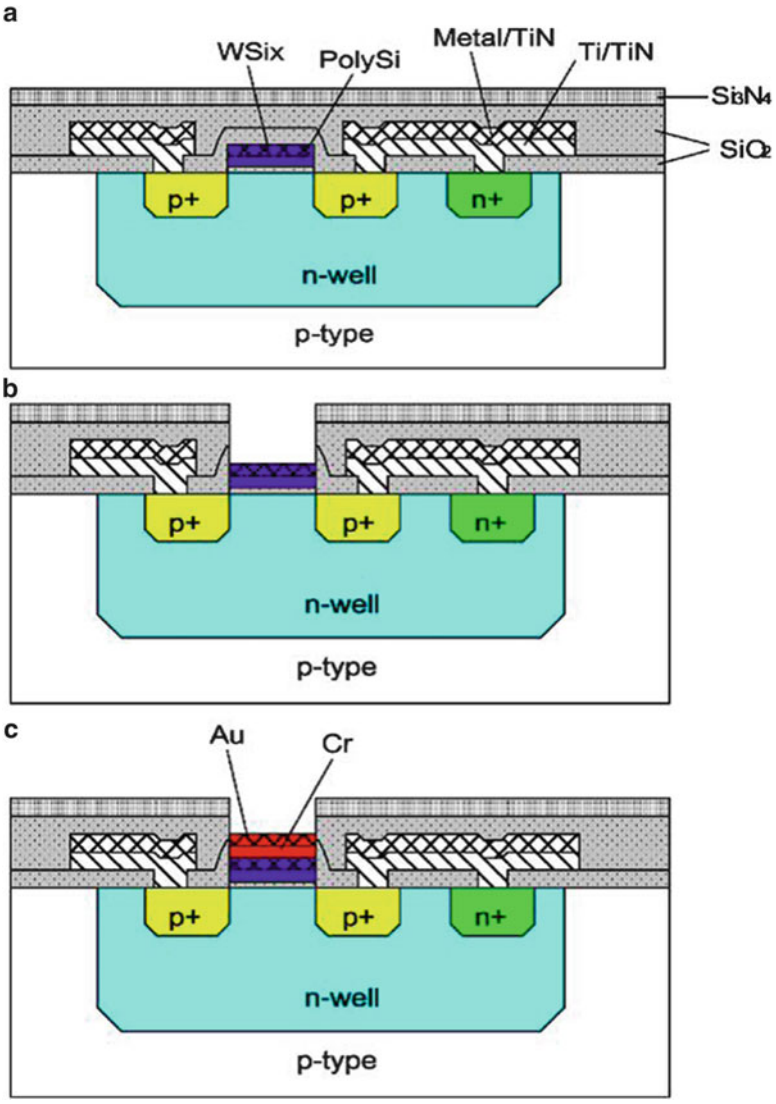

Fig. 3.6 Schematic diagram shows the key fabrication steps of FET devices for the development of DNA biosensors, which include (**a**) p-channel metal–oxide–semiconductor FET fabrication based on 0.5 μm standard complementary metal–oxide–semiconductor (CMOS) technology, (**b**) SiO_2/Si_3N_4 plasma etching for gate opening, and (**c**) Cr/Au formation by lift-off process (Reproduced with permission from Ref. [25]. Copyright 2004 Elsevier)

ssDNA molecules attached onto the gate surface of FETs. This will result in the generation of corresponding electrical signals and readout by FETs with the help of a reference electrode that is put into the solution in detection chamber. With this measurement setup, the hybridization signals of probe ssDNA with target ssDNA

can be measured by recording the output of FET signals that the drain current commonly used. In the following, the output signals of FET devices will be amplified and collected by the peripheral circuits. In a certain concentration range of target ssDNA molecules, if different concentrations are introduced to the detection chamber, the FET device can record the different electrical responses. In this way, the target ssDNA can be determined in a quantitative manner.

The LAPS devices are another type of commonly used transducers for the development of label-free DNA biosensors [19–21, 39, 45]. LAPS is a silicon-based FED that is sensitive to the surface charge change, which can overcome the limitations of FETs due to its flexible gate surface defined by the addressable light illumination on LAPS surface [46, 47]. As a result, the fabrication of LAPS chip is much simpler and convenient compared with FETs. LAPS chip is often fabricated on silicon wafer, which usually consists of a SiO_2 layer on the top of silicon layer to serve as an insulation layer. The insulation layer is prepared by thermal oxidation. For some LAPS chips, an additional layer of Ta_2O_5 or Si_3N_4 is further developed on the top of insulation layer to enhance the sensitivity of LAPS chip. The rear side of LAPS chip is usually deposited with a layer of Al after removing the oxide layer to serve as ohmic contact. For the backside illumination measurement setup, it is necessary to etch the Al layer to form a window for the light illumination. The fabricated wafer was cut into separate chips with small sizes. Finally, the LAPS chip was then mounted in a detection chamber for measurement.

One of the measurement setups of DNA biosensors using LAPS chips as the transducers is shown in Fig. 3.8, which is a multi-spot LAPS measurement setup suitable for simultaneous monitoring of the surface charge changes from multiple spots [19]. In this measurement setup, the light source is a 4×4 infrared LED array that can generate a light array at a wavelength of 950 nm and a diameter around 2 mm. Each LED is controlled independently and simultaneously by a field-programmable gate array (FPGA) that can generate unique modulation frequency for each LED in a certain frequency range. A reference electrode was put into the solution in the detection chamber for the recording of photocurrent as well as for the application of bias voltage to the LAPS chip. The recorded photocurrent is then amplified by a transimpedance amplifier and collected by a data-acquisition card and sent to the computer for further processing and analysis. The whole measurement setup is usually controlled by the customized software developed on the basis of LabVIEW. To reduce the influences of ambient light and environmental factors on the measurements, it is necessary to shield the setup in a Faraday box.

Another kind of LAPS measurement setup that uses a modulated laser as the light source is also applied for the development of DNA biosensors [39, 45]. The laser can generate a light with a wavelength of 780 nm and a diameter of 70 μm. During measurement, the laser is working in a scanning manner in two dimensions to achieve multiple spot measurements and in some cases the spatial resolution. In a measurement setup that uses nanomotor to control the movement of laser, the stepwise laser movement can be as low as 40 nm and the scanning area could reach 18 mm^2. Except for the light source, the other components of the measurement setup are similar to that of multi-spot LAPS measurement setup.

For the detection of hybridization between probe ssDNA and complementary target ssDNA, the photocurrent vs. bias voltage curves (*I–V* curves) are recorded before and after the introduction and incubation with DNA samples. The shift of the *I–V* curves (achieved from the comparison of the *I–V* curves recorded before and after the DNA hybridization) along the voltage axis is used as a quantitative indicator to characterize the DNA hybridization events occurring on the LAPS surface. In addition, the shifts of *I–V* curves can be monitored in a real-time manner in a constant photocurrent mode. This makes it possible to monitor the DNA hybridization on the sensor surface in a real-time manner.

3.4 Application of FED-Based DNA Biosensors

DNA biosensors have shown promising prospects and have great potential to be applied in a wide range of fields such as DNA diagnostics, gene analysis, fast detection of biological warfare agents, and forensic applications. Increasing interest in the development of DNA biosensors and their widely used applications are related to their capability of detecting hybridization events between probe ssDNA and its complementary target ssDNA with high sensitivity and specificity. FED-based DNA biosensors are characterized with label-free, fast, and direct electrical detection of hybridization of probe ssDNA with its complementary target ssDNA. The decisive advantage of FED-based DNA biosensors originated from their capability of label-free detection of DNA molecules based on their intrinsic molecular charges, which avoid the complicated, time-consuming, and costive labeling process. In addition, the FED-based DNA biosensors are connected with microfabrication production manner. By the following, we briefly introduce some typical applications of FED-based DNA biosensors, which mainly include label-free DNA assays and detection of SNPs.

3.4.1 Label-Free DNA Assays

With the fast development of biotechnology and medical diagnostics, the devices that are capable of continuously and selectively detecting specific DNA molecules are increasingly demanded, which can provide helpful information for the detection and identification of many diseases such as infection and genetic diseases. FED-based DNA biosensors have been applied for the label-free DNA assays, which aim to rapidly and reliably detect specific DNA sequences from complex samples. Compared with typical methods such as optical measurements and electrochemical measurements, DNA assays with FED devices have the advantages of less requirements on expensive equipment, direct electrical signal readout, and easy integration with semiconductor circuit chip and mass production. As a result, FED-based DNA biosensors have been tried to be applied in the label-free DNA

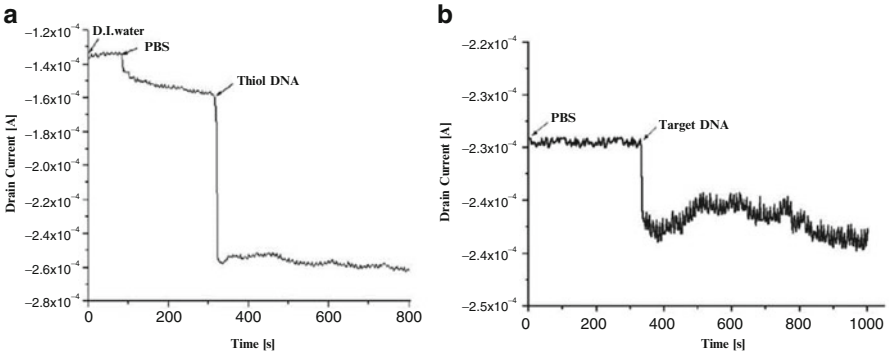

Fig. 3.7 The detection of thiol-modified probe ssDNA immobilization on the gate surface of FET device and hybridization of probe ssDNA with its complementary target ssDNA in a real-time manner by monitoring changes in drain current (Reproduced with permission from Ref. [25]. Copyright 2004 Elsevier)

assays. At present, there are mainly two categories of FEDs that have been utilized as transducers for the development of DNA biosensors for label-free DNA sensing based on their intrinsic molecular charges, which are FETs and LAPSs.

FET-based DNA biosensors for label-free DNA assays have attracted considerable attention due to their decisive advantages in miniaturization, standardization, and suitable integration with measurement circuit. An FET-based DNA biosensor has been developed for the detection of probe ssDNA immobilization and target ssDNA hybridization on the gate surface of FETs [25]. Based on the intrinsic molecular charge of DNA molecules, the changes in electrochemical potential at the gate resulting from the attachment of negatively charged DNA molecules onto the gate surface can be measured by the monitoring of changes in the drain current of FETs. In addition, the potential changes of gate surface can be measured in a real-time manner by continuously recording the variation of the drain current induced by DNA charge due to the field effect.

Based on this approach, the immobilization of probe ssDNA on the gate surface of FET as well as the hybridization of probe ssDNA with its complementary target ssDNA can be monitored in real time as shown in Fig. 3.7 [25]. It is indicated that both probe ssDNA immobilization and target ssDNA hybridization occurring on the gate surface of FET increase the magnitude of drain current due to the negative charge of DNA molecules. But the increase in magnitude of drain current resulting from probe ssDNA immobilization is larger than that of target ssDNA hybridization, which may be due to the hybridization efficiency that is not sufficient to form 100 % dsDNA. In addition, the amount of probe ssDNA immobilized on the gate surface of FET can be determined by the voltage induced by DNA charge, which can be extracted from the drain current investigating the electrical characteristic of FETs. It is estimated that the number of probe ssDNA immobilized on one unit of gate surface is 3.81×10^{12} (Nm^{-2}) if the probe ssDNA molecules are ideally immobilized on the gold layer of FET gate. On the other hand, the immobilization

of probe ssDNA and hybridization of probe ssDNA with target ssDNA are further validated by mass spectrometry using quartz crystal microbalance (QCM) measurement. These results confirmed that FET-based DNA biosensors are suitable to be used as novel label-free tools for the detection of specific DNA molecules by monitoring the changes in drain current of FET originated from the attachment of charged DNA molecules onto the gate surface of FET.

On the other hand, LAPS-based DNA biosensors have also been applied for the label-free electrical detection of DNA immobilization and hybridization. Based on a multi-spot LAPS measurement setup (4×4 spots), the LAPS signal can be simultaneously recorded from 16 spots on LAPS surfaces by using a 4×4 LED array as the light source [19]. The photocurrent–bias voltage curves (*I–V* curves) were recorded after each step of surface modification, which includes the steps of surface silanization, probe ssDNA immobilization, BSA blocking, and complementary target ssDNA hybridization. In addition, in order to improve the sensor signal by reducing the screening effects of solution ions, low ionic strength measuring solution (0.2 mM PBS, pH 7) was utilized as measurement solution. It is indicated that, for the same LAPS surface, nearly similar shape of the *I–V* curves can be recorded from all 16 spots, although the amplitude of photocurrent shows smaller differences that are probably due to the different modulation frequencies used for each LED. On the contrary, for LAPS surfaces with different modifications, the obvious shifts of *I–V* curves can be observed as shown in Fig. 3.8, where it shows

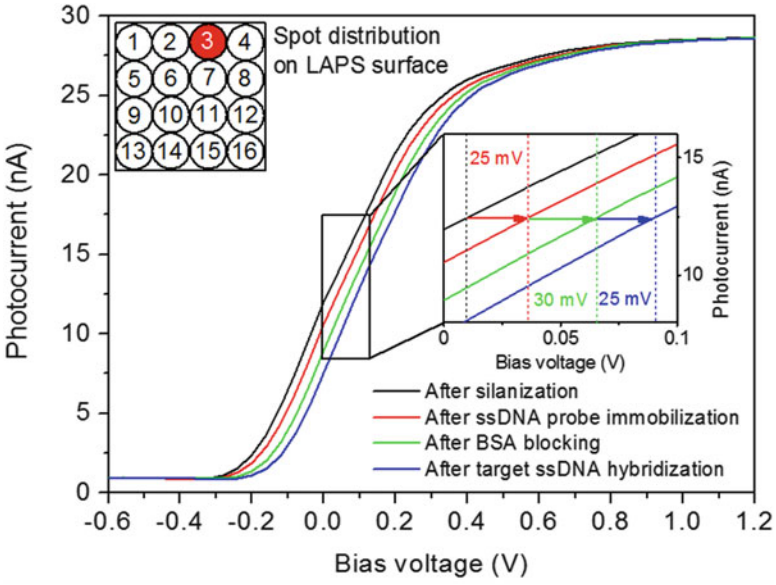

Fig. 3.8 Shifts of photocurrent–bias voltage curves (*I–V* curves) recorded by LAPS from the single spot 3 on LAPS surfaces after silanization, after probe ssDNA immobilization, after BSA blocking, and after hybridization of probe molecules with complementary target ssDNA (Reproduced with permission from Ref. [19]. Copyright 2014 WILEY-VCH Verlag GmbH & Co. KGaA, Weinheim)

the LAPS signals recorded from one spot after different surface modifications such as after silanization, after probe ssDNA immobilization, after BSA blocking, and after target ssDNA hybridization. In addition, 25 mV shifts of LAPS *I–V* curves along the voltage axis can be registered for the probe ssDNA immobilization and complementary target ssDNA hybridization. The direction of *I–V* curve shift is the positive direction of bias voltage, which indicates more negatively charged gate surface. This is in good agreement with the fact that DNA molecules are negatively charged in the solution. Also, the BSA blocking induces a 30 mV LAPS *I–V* curve shift to the direction of more positive bias voltages due to the attachment of negatively charged BSA molecules onto the LAPS surface.

Furthermore, the specificity of this LAPS-based DNA biosensor was demonstrated by the use of fully mismatched ssDNA to the probe ssDNA immobilized on the LAPS surface. The measurement results show that a much smaller LAPS *I–V* curve shift (~5 mV) can be observed for fully mismatched ssDNA, which indicates a good specificity for the complementary ssDNA detection. The smaller LAPS signal is probably due to the unspecific adsorption of mismatched ssDNA on the LAPS surface. These results demonstrate that LAPS-based DNA biosensors can be used as a promising platform for label-free DNA assays based on their intrinsic molecular charge. Especially, the LAPS-based DNA biosensors have great potential to be developed into DNA chips that can be used for DNA assays in a high-throughput manner due to their capability of multi-spot measurement and light addressability, which could potentially contribute to the development of light-addressable DNA chips.

An improved LAPS-based DNA biosensor has also been developed, which employs a simple layer-by-layer (LbL) technique for the probe ssDNA immobilization on the LAPS surface [20]. In this DNA biosensor, LAPS surface was modified with a thin layer of weak polyelectrolyte poly(allylamine hydrochloride) (PAH), which is positively charged and used to modify the negatively charged LAPS surface (SiO_2 layer) for the sake of adsorption of negatively charged probe ssDNA molecules onto the PAH layer. The local surface potential changes in each measurement spot induced due to the surface modification steps (i.e., PAH adsorption, probe ssDNA immobilization, nonspecific adsorption of mismatched ssDNA, hybridization with cDNA) were determined from the shifts of *I–V* curves along the voltage axis. The main advantages of LbL technique originate from its simple, fast, and efficient capability of constructing well-defined ultrathin films by electrostatically assembling the repetitive, sequential adsorption of polyions with alternating charge, which has been widely applied for the modification of various surfaces for different purposes [48–51]. In addition, the immobilization of probe ssDNA by LBL technique leads to the orientation of DNA molecules being flat on the sensor surface other than standing up, which results in the distribution of more DNA molecular charges closer to the sensor surface within the Debye length, thus contributing to the enhancement of sensitivity for DNA detection based on its molecular charges. Moreover, this method could potentially accelerate the hybridization of probe ssDNA with its complementary ssDNA due to the reduction in electrostatic repulsion between DNA molecules. Therefore, the DNA hybridization

signals could be enhanced due to the lower Debye screening effect and the electrostatic repulsion.

This LAPS-based DNA biosensor has been applied for the label-free detection of DNA immobilization and hybridization based on their intrinsic molecular charge by simultaneously recording the shifts of *I–V* curves from 16 spots of LAPS after each step of surface modification, which includes the PAH adsorption, probe ssDNA immobilization, and target ssDNA hybridization. The local surface potential changes in each measurement spot induced originating from the charge molecules attached onto the LAPS surface were determined by monitoring the shifts of *I–V* curves along the voltage axis. In addition, the real-time monitoring of surface charge changes originating from the attachment of PAH and DNA molecules onto the sensor surface can be realized by recording the long-term shifts of LAPS *I–V* curves in a constant photocurrent mode. That is, if the photocurrent of LAPS is set at constant (e.g., 20 nA), the shifts of LAPS *I–V* curves can be monitored in a real-time manner by plotting the potential changes of bias voltage versus time.

Figure 3.9 shows the mean constant photocurrent responses of the LAPS recorded before and after PAH adsorption, after probe ssDNA immobilization, after nonspecific adsorption of fully mismatched ssDNA molecules, and after hybridization of probe ssDNAs with complementary target cDNAs (5 μM). It is indicated that the mean response signals for DNA immobilization and hybridization

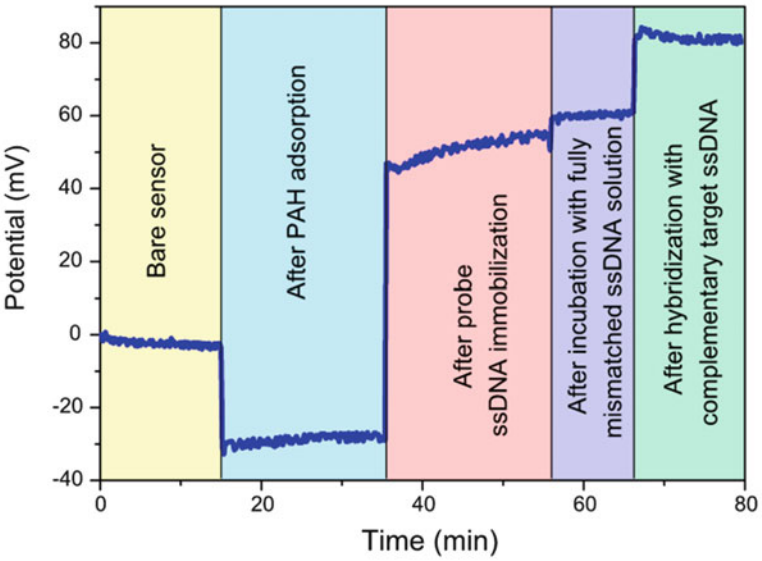

Fig. 3.9 Detection of DNA immobilization and hybridization by a LAPS-based DNA biosensor with layer-by-layer technique. Real-time mean response of DNA biosensor to PAH adsorption, probe ssDNA immobilization, nonspecific adsorption of fully mismatched ssDNA molecules, and hybridization of probe ssDNAs with complementary target cDNAs (Reproduced with permission from Ref. [20]. Copyright 2015 Royal Society of Chemistry)

are 83 mV and 32 mV, respectively. On the contrary, only 5 mV signal can be recorded induced by the nonspecific adsorption of fully mismatched ssDNAs, which confirms that this DNA biosensor is able to differentiate between complementary and mismatched DNA sequences. This also demonstrates a good specificity of this biosensor for the detection of specific DNA molecules. In addition, this LAPS-based DNA biosensor has been applied for the detection of complementary target ssDNA at different concentrations, which ranged from 0.1 nM to 5 μM. It is indicated that the DNA hybridization signals increase with the increasing of the target ssDNA concentrations. The detectable concentration is as low as 0.1 nM, at which 5 mV DNA hybridization signal can be obtained.

It is suggested that this LAPS-based DNA biosensor could be used as a promising tool for the label-free detection of DNA immobilization and hybridization. Due to their small sizes and compatibility with advanced micro- and nanofabrication technologies, LAPS-based DNA biosensors offer new opportunities for label-free DNA chips with direct electronic readout for fast, simple, and inexpensive real-time analysis of nucleic acid samples. In addition, it has great potential to be further developed into light-addressable DNA chips by the immobilization of different probe ssDNAs on each spot of LAPS chip.

3.4.2 Label-Free Detection of SNPs

FED-based DNA biosensors have been explored to be applied in the label-free detection of SNPs that is a single nucleotide variation in DNA sequence from members of a biological species or paired chromosomes. SNPs are critical for a wide range of fields such as forensic science, personalized medicine, and evaluation of susceptibility to certain diseases (e.g., Alzheimer disease) [52–57]. Therefore, the detection of SNPs has attracted more and more interest due to their promising prospects, which can provide useful and helpful information for many biomedical research and applications. It is thus highly essential and favorable to develop novel DNA biosensors that are able to detect the SNPs. FED-based DNA biosensors make it possible and attractive to directly label-free detect the SNPs based on their intrinsic molecular charge. In addition, the detection of SNPs by FED-based DNA biosensors is rapid and cost effective.

An FET-based DNA biosensor was reported to be able to be applied in the label-free detection of the point mutations in short DNA sequences based on the detection of DNA hybridization using their intrinsic molecular charges [32]. The use of FET devices as transducers allows for the fast and fully electronic readout of DNA hybridization signals originating from the negatively charged target ssDNA molecules hybridized with probe ssDNA immobilized on the gate surface of FET devices. In addition, a time-resolved DC readout is used in order to overcome the drawback of conventional FETs, where FET signals are influenced by many factors such as sensor drift, temperature drift, and electrolyte composition or pH value. This FET-based DNA biosensor consisted of an FET microarray and the gate

surface of each FET was immobilized with different probe ssDNA molecules. The probe ssDNA molecules can be classified into two main categories: perfect matched probe ssDNA and single-base mismatched probe ssDNA. The microarray configuration also allows a differential AC readout, which contributes to the stability of sensor signals and thus a reliable readout. As shown in Fig. 3.10, the potentiometric responses of different units of FET array where different probe ssDNA molecules were immobilized on their gate surface to the same target ssDNA with differential, time-resolved readout using the FET unit with fully mismatched probe ssDNA immobilized on its gate surface as a reference. It is indicated that only two mismatches in 20 bp sequences can be distinguished. In addition, the hybridization time was elongated due to the use of low ionic strength buffer as measurement solution, which can range from several 10 min to even hours. It is suggested that the FET-based DNA biosensors have great potential to be used as a tool for the detection of SNPs with further development and improvement with regard to the sensitivity and stability.

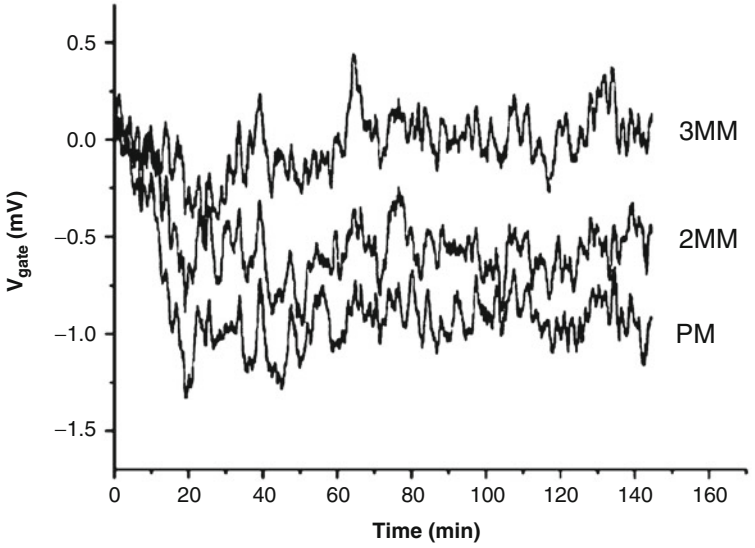

Fig. 3.10 Responses of FET array-based DNA biosensors, where the gate surface of each FET was immobilized with different probe ssDNAs, to same target ssDNA. PM: probe ssDNA molecules with sequences that are perfectly matched with target ssDNA. 2MM and 3MM represent the probe ssDNA molecules with sequences that contain only two and three bases mismatched to the target ssDNA, respectively. An FET unit with fully mismatched probe ssDNA immobilized on its gate surface was employed as a reference to ensure a stable signal. The target ssDNA was introduced to the gate surface of FET at $t = 0$ (Reproduced with permission from Ref. [32]. Copyright 2007 Elsevier)

3.5 Summary

The detection of specific DNA sequences for DNA assays and diagnostics has attracted more and more interest in the recent decades, which also promotes the research and development of DNA biosensors, especially the label-free DNA biosensors. At present, various DNA biosensors have been developed by the utilization of FEDs as transducers for the label-free detection of DNA molecules based on their intrinsic molecular charges. In addition, FED-based DNA biosensors have been applied in many fields and shown promising prospects. Compared with conventional DNA biosensors, DNA biosensors using FEDs as charge-sensitive transducers have advantages that are not able to be achieved with those using other devices as transducers. For the first, the fabrication of FEDs is compatible with the microfabrication process. With the fast advances in microfabrication techniques, it is possible to design and fabricate various precise FEDs for the sake of coupling with DNA molecules with high efficiency as well as to achieve better signal transduction. In addition, the easy integration with circuits makes it possible to have a higher level of miniaturization for the development of portable devices for label-free DNA detection in field. This can greatly facilitate their practical applications and broaden their applicable fields. Furthermore, FED-based DNA biosensors also benefited from the fast advancement in the microfabrication and nanotechnologies, which makes the mass production possible and could reduce the cost significantly. Finally, a large number of DNA molecules can provide sufficient sensing spaces for the development of FED-based DNA biosensors in order to detect different desired DNA molecules. The fast advancement in these fields also provides novel approaches for the design and fabrication of next generation of FED-based DNA biosensors. In this chapter, we firstly introduced the signal generation and transduction mechanism of DNA molecules and the basic principle of FED-based DNA biosensors. Then, the coupling of DNA molecules with FEDs, the fabrication of FEDs used for the development of FED-based DNA biosensors, and the measurement setup were introduced in detail. The DNA biosensors using FETs and LAPSs as transducers were introduced. By the following, we summarize the typical applications of FED-based DNA biosensors in two aspects, which include the label-free DNA assays and detection of SNPs.

In the future, the development trends of FED-based DNA biosensors are based on the novel designs to better utilize the unique capability of DNA molecules and FEDs for the detection of charge changes originated from the molecular interactions such as DNA hybridization. For example, the design and fabrication of novel transducers can be used to record the responses of probe ssDNA in a more efficient and reliable manner. In addition, the development of FED array-based DNA biosensors that could realize parallel detection of multiple DNA samples is also a very important direction due to the widely used applications of DNA microarrays, which are a powerful tool for DNA analysis for a broad range of fields. However, there are also some challenges in the further development of FED-based DNA biosensors. For instance, how to couple probe ssDNA molecules onto the sensor surface with

controllable density to optimize the performance of biosensors for DNA hybridization? How to improve the efficiency of signal transduction of FEDs as well as the stability of output signals? On the other hand, with the fast development of nanotechnologies, the development of various nanomaterials might provide novel desired function for the development of DNA biosensors with special functions such as carbon nanotubes and graphenes [58–64]. In order to achieve in-field measurement, the sensor systems for FED-based DNA biosensors should have higher level of integration to realize further miniaturization. In addition, it will be useful to investigate and optimize the hybridization conditions in order to improve the sensor stability by a more stable structure of dsDNA molecules. Benefiting from the fast development of nano- and biotechnologies, the next generation of FED-based DNA biosensors is expected to be more powerful and more efficient, with even more intelligence.

References

1. Watson JD, Crick FH. Molecular structure of nucleic acids. Nature. 1953;171(4356):737–8.
2. Cosnier S, Mailley P. Recent advances in DNA sensors. Analyst. 2008;133(8):984–91.
3. Downs ME, Kobayashi S, Karube I. New DNA technology and the DNA biosensor. Anal Lett. 1987;20(12):1897–927.
4. Perumal V, Hashim U. Advances in biosensors: principle, architecture and applications. J Appl Biomed. 2014;12(1):1–15.
5. Sassolas A, Leca-Bouvier BD, Blum LJ. DNA biosensors and microarrays. Chem Rev. 2008;108(1):109–39.
6. Teles F, Fonseca L. Trends in DNA biosensors. Talanta. 2008;77(2):606–23.
7. Vo-Dinh T. Development of a DNA biochip: principle and applications. Sensors Actuators B Chem. 1998;51(1):52–9.
8. Wei F, Lillehoj PB, Ho C-M. DNA diagnostics: nanotechnology-enhanced electrochemical detection of nucleic acids. Pediatr Res. 2010;67(5):458–68.
9. Zhao W-W, Xu J-J, Chen H-Y. Photoelectrochemical DNA biosensors. Chem Rev. 2014;114 (15):7421–41.
10. Kerman K, Kobayashi M, Tamiya E. Recent trends in electrochemical DNA biosensor technology. Meas Sci Technol. 2004;15(2):R1.
11. Drummond TG, Hill MG, Barton JK. Electrochemical DNA sensors. Nat Biotechnol. 2003;21 (10):1192–9.
12. Peng H-I, Miller BL. Recent advancements in optical DNA biosensors: exploiting the plasmonic effects of metal nanoparticles. Analyst. 2011;136(3):436–47.
13. Dolatabadi JEN, Mashinchian O, Ayoubi B, Jamali AA, Mobed A, Losic D, Omidi Y, de la Guardia M. Optical and electrochemical DNA nanobiosensors. TrAC Trends Anal Chem. 2011;30(3):459–72.
14. Poghossian A, Cherstvy A, Ingebrandt S, Offenhäusser A, Schöning MJ. Possibilities and limitations of label-free detection of DNA hybridization with field-effect-based devices. Sensors Actuators B Chem. 2005;111:470–80.
15. Kataoka-Hamai C, Miyahara Y. Label-free detection of DNA by field-effect devices. Sensors J IEEE. 2011;11(12):3153–60.
16. Sakata T, Kamahori M, Miyahara Y. DNA analysis chip based on field-effect transistors. Jpn J Appl Phys. 2005;44(4S):2854.

17. Matsumoto A, Miyahara Y. Current and emerging challenges of field effect transistor based bio-sensing. Nanoscale. 2013;5(22):10702–18.
18. Schöning MJ, Poghossian A. Bio FEDs (Field-Effect Devices): state-of-the-art and new directions. Electroanalysis. 2006;18(19–20):1893–900.
19. Wu C, Bronder T, Poghossian A, Werner CF, Bäcker M, Schöning MJ. Label-free electrical detection of DNA with a multi-spot LAPS: first step towards light-addressable DNA chips. Phys Status Solidi (a). 2014;211(6):1423–8.
20. Wu C, Bronder T, Poghossian A, Werner CF, Schöning MJ. Label-free detection of DNA using a light-addressable potentiometric sensor modified with a positively charged polyelectrolyte layer. Nanoscale. 2015;7(14):6143–50.
21. Zong X-l, Wu C-s, Wu X-l, Lu Y-f, Wang P. A non-labeled DNA biosensor based on light addressable potentiometric sensor modified with TiO_2 thin film. J Zhejiang Univ Sci B. 2009;10(11):860–6.
22. Poghossian A, Ingebrandt S, Abouzar M, Schöning MJ. Label-free detection of charged macromolecules by using a field-effect-based sensor platform: experiments and possible mechanisms of signal generation. Appl Phys A Mater Sci Process. 2007;87(3):517–24.
23. Lee K-H, Lee JO, Choi S, Yoon J-B, Cho G-H. A CMOS label-free DNA sensor using electrostatic induction of molecular charges. Biosens Bioelectron. 2012;31(1):343–8.
24. Barbaro M, Bonfiglio A, Raffo L, Alessandrini A, Facci P, Barák I. A CMOS, fully integrated sensor for electronic detection of DNA hybridization. Electron Device Lett IEEE. 2006;27 (7):595–7.
25. Kim D-S, Jeong Y-T, Park H-J, Shin J-K, Choi P, Lee J-H, Lim G. An FET-type charge sensor for highly sensitive detection of DNA sequence. Biosens Bioelectron. 2004;20(1):69–74.
26. Cherstvy A. Detection of DNA hybridization by field-effect DNA-based biosensors: mechanisms of signal generation and open questions. Biosens Bioelectron. 2013;46:162–70.
27. Premkumar T, Geckeler KE. Graphene–DNA hybrid materials: assembly, applications, and prospects. Prog Polym Sci. 2012;37(4):515–29.
28. Uslu F, Ingebrandt S, Mayer D, Böcker-Meffert S, Odenthal M, Offenhäusser A. Labelfree fully electronic nucleic acid detection system based on a field-effect transistor device. Biosens Bioelectron. 2004;19(12):1723–31.
29. Song K-S, Zhang G-J, Nakamura Y, Furukawa K, Hiraki T, Yang J-H, Funatsu T, Ohdomari I, Kawarada H. Label-free DNA sensors using ultrasensitive diamond field-effect transistors in solution. Phys Rev E. 2006;74(4):041919.
30. Zhao L, Cao D, Gao Z, Mi B, Huang W. Label-free DNA sensors based on field-effect transistors with semiconductor of carbon materials. Chin J Chem. 2015;33(8):828–41.
31. Guo S-R, Lin J, Penchev M, Yengel E, Ghazinejad M, Ozkan CS, Ozkan M. Label free DNA detection using large area graphene based field effect transistor biosensors. J Nanosci Nanotechnol. 2011;11(6):5258–63.
32. Ingebrandt S, Han Y, Nakamura F, Poghossian A, Schöning MJ, Offenhäusser A. Label-free detection of single nucleotide polymorphisms utilizing the differential transfer function of field-effect transistors. Biosens Bioelectron. 2007;22(12):2834–40.
33. Barbaro M, Bonfiglio A, Raffo L, Alessandrini A, Facci P, Barák I. Fully electronic DNA hybridization detection by a standard CMOS biochip. Sensors Actuators B Chem. 2006;118 (1):41–6.
34. Xia D, Yan J, Hou S. Fabrication of nanofluidic biochips with nanochannels for applications in DNA analysis. Small. 2012;8(18):2787–801.
35. Gui EL, Li L-J, Zhang K, Xu Y, Dong X, Ho X, Lee PS, Kasim J, Shen Z, Rogers JA. DNA sensing by field-effect transistors based on networks of carbon nanotubes. J Am Chem Soc. 2007;129(46):14427–32.
36. Sakata T, Miyahara Y. Detection of DNA recognition events using multi-well field effect devices. Biosens Bioelectron. 2005;21(5):827–32.
37. Shin JK, Kim DS, Park HJ, Lim G. Detection of DNA and protein molecules using an FET-type biosensor with gold as a gate metal. Electroanalysis. 2004;16(22):1912–8.

38. Hu K, Lan D, Li X, Zhang S. Electrochemical DNA biosensor based on nanoporous gold electrode and multifunctional encoded DNA – Au bio bar codes. Anal Chem. 2008;80 (23):9124–30.
39. Wu C, Bronder T, Poghossian A, Werner CF, Schoening MJ. DNA-hybridization detection using light-addressable potentiometric sensor modified with gold layer. in Editor (Ed.)^(Eds.): 'Book DNA-hybridization detection using light-addressable potentiometric sensor modified with gold layer' (VDE, 2014, edn.), p. 1–4.
40. Hahm J-i, Lieber CM. Direct ultrasensitive electrical detection of DNA and DNA sequence variations using nanowire nanosensors. Nano Lett. 2004;4(1):51–4.
41. Diamandis EP, Christopoulos TK. The biotin-(strept) avidin system: principles and applications in biotechnology. Clin Chem. 1991;37(5):625–36.
42. Ho C-M, Tai Y-C. Micro-electro-mechanical-systems (MEMS) and fluid flows. Annu Rev Fluid Mech. 1998;30(1):579–612.
43. Voldman J, Gray ML, Schmidt MA. Microfabrication in biology and medicine. Annu Rev Biomed Eng. 1999;1(1):401–25.
44. Gao A, Lu N, Dai P, Li T, Pei H, Gao X, Gong Y, Wang Y, Fan C. Silicon-nanowire-based CMOS-compatible field-effect transistor nanosensors for ultrasensitive electrical detection of nucleic acids. Nano Lett. 2011;11(9):3974–8.
45. Wu C, Poghossian A, Werner CF, Bronder T, Bäcker M, Schöning M, Wang P. A9-An application of a scanning light-addressable potentiometric sensor for label-free DNA detection. Tagungsband, 2013, p. 164–168.
46. Owicki JC, Bousse LJ, Hafeman DG, Kirk GL, Olson JD, Wada HG, Parce JW. The light-addressable potentiometric sensor: principles and biological applications. Annu Rev Biophys Biomol Struct. 1994;23(1):87–114.
47. Hafeman DG, Parce JW, McConnell HM. Light-addressable potentiometric sensor for biochemical systems. Science. 1988;240(4856):1182–5.
48. Sukhorukov GB, Donath E, Lichtenfeld H, Knippel E, Knippel M, Budde A, Möhwald H. Layer-by-layer self assembly of polyelectrolytes on colloidal particles. Colloids Surf A Physicochem Eng Asp. 1998;137(1):253–66.
49. Kovtyukhova NI, Ollivier PJ, Martin BR, Mallouk TE, Chizhik SA, Buzaneva EV, Gorchinskiy AD. Layer-by-layer assembly of ultrathin composite films from micron-sized graphite oxide sheets and polycations. Chem Mater. 1999;11(3):771–8.
50. Caruso F, Trau D, Möhwald H, Renneberg R. Enzyme encapsulation in layer-by-layer engineered polymer multilayer capsules. Langmuir. 2000;16(4):1485–8.
51. Lvov Y, Decher G, Moehwald H. Assembly, structural characterization, and thermal behavior of layer-by-layer deposited ultrathin films of poly (vinyl sulfate) and poly (allylamine). Langmuir. 1993;9(2):481–6.
52. Carlson CS, Eberle MA, Rieder MJ, Yi Q, Kruglyak L, Nickerson DA. Selecting a maximally informative set of single-nucleotide polymorphisms for association analyses using linkage disequilibrium. Am J Hum Genet. 2004;74(1):106–20.
53. Halushka MK, Fan J-B, Bentley K, Hsie L, Shen N, Weder A, Cooper R, Lipshutz R, Chakravarti A. Patterns of single-nucleotide polymorphisms in candidate genes for blood-pressure homeostasis. Nat Genet. 1999;22(3):239–47.
54. Wang DG, Fan J-B, Siao C-J, Berno A, Young P, Sapolsky R, Ghandour G, Perkins N, Winchester E, Spencer J. Large-scale identification, mapping, and genotyping of single-nucleotide polymorphisms in the human genome. Science. 1998;280(5366):1077–82.
55. Rafalski A. Applications of single nucleotide polymorphisms in crop genetics. Curr Opin Plant Biol. 2002;5(2):94–100.
56. Sachidanandam R, Weissman D, Schmidt SC, Kakol JM, Stein LD, Marth G, Sherry S, Mullikin JC, Mortimore BJ, Willey DL. A map of human genome sequence variation containing 1.42 million single nucleotide polymorphisms. Nature. 2001;409(6822):928–33.
57. Syvänen A-C. Accessing genetic variation: genotyping single nucleotide polymorphisms. Nat Rev Genet. 2001;2(12):930–42.

58. Kerman K, Saito M, Tamiya E, Yamamura S, Takamura Y. Nanomaterial-based electrochemical biosensors for medical applications. TrAC Trends Anal Chem. 2008;27(7):585–92.
59. Kochmann S, Hirsch T, Wolfbeis OS. Graphenes in chemical sensors and biosensors. TrAC Trends Anal Chem. 2012;39:87–113.
60. Pumera M. Graphene in biosensing. Mater Today. 2011;14(7):308–15.
61. Min SK, Kim WY, Cho Y, Kim KS. Fast DNA sequencing with a graphene-based nanochannel device. Nat Nanotechnol. 2011;6(3):162–5.
62. Wohlstadter JN, Wilbur JL, Sigal GB, Biebuyck HA, Billadeau MA, Dong L, Fischer AB, Gudibande SR, Jameison SH, Kenten JH. Carbon nanotube-based biosensor. Adv Mater. 2003;15(14):1184–7.
63. Balasubramanian K, Burghard M. Biosensors based on carbon nanotubes. Anal Bioanal Chem. 2006;385(3):452–68.
64. Chen C-P, Ganguly A, Lu C-Y, Chen T-Y, Kuo C-C, Chen R-S, Tu W-H, Fischer WB, Chen K-H, Chen L-C. Ultrasensitive in situ label-free DNA detection using a GaN nanowire-based extended-gate field-effect-transistor sensor. Anal Chem. 2011;83(6):1938–43.

Chapter 4
Micro/Nano Cell-Substrate Impedance Biosensors

Yulan Tian, Ling Zou, and Ping Wang

Abstract Electrical cell–substrate impedance sensing (ECIS) is a powerful biophysical technology that can realize realtime noninvasive monitoring of the cells in vitro cultured physiological changes including cell adhesion, growth, motility, death, and so on. The changes of cells cultured on the electrode microarray will be induced by internal and external stimulation. In this chapter, the ECIS cell impedance model, ECIS cell growth detection principle, ECIS cell pulsation measuring principle, processing procedures of the ECIS sensor chip, and ECIS instrumentation system design are introduced. Then the method of enhancing the adhesion of a cell on the gold electrode's surface is stated; the most used method is chemical surface modification. The ECIS sensor has attracted more and more attention because of its many advantages such as being noncontact, realtime, noninvasive, and so on. Therefore, the ECIS technology provides a good platform for noninvasively and instantaneously detecting and analyzing cell responses to chemical and biological agents. The application of the ECIS sensor is presented in the rest of this chapter, including drug screening of verapamil by using rat cardiomyocytes, environment monitoring such as drinking water supplies from chemical contaminants, food analysis such as the shellfish poisoning (PSP) toxins in fish or shellfish, cancer research, and other applications. ECIS has the characteristics of being a fast, long-term, nondestructive, and high-throughput measurement, which makes it a promising development direction.

Keywords Electric cell–substrate impedance sensing (ECIS) • Cell impedance model • ECIS chip fabrication • Drug screening • Food analysis

Y. Tian • L. Zou • P. Wang (✉)
Biosensor National Special Laboratory, Department of Biomedical Engineering, Zhejiang University, Hangzhou, China
e-mail: cnpwang@zju.edu.cn

P. Wang et al. (eds.), *Micro/Nano Cell and Molecular Sensors*,
DOI 10.1007/978-981-10-1658-5_4

4.1 Introduction

Electrical cell–substrate impedance sensing (ECIS), developed by Giaever and Keese in the 1980s [1–4], is a powerful biophysical technology that can realize realtime noninvasive monitoring of the growth status of in vitro cultured cells. Generally, ECIS sensors are developed by immobilizing cells on an array of electrodes on an insulative substrate such as glass and plastic [5–8]. The electrode microarray is incorporated into the bottom of a cell-culture well [9, 10]. Over the last few decades, variations of the ECIS instruments were introduced to monitor cellular events including cell adhesion, growth, motility, death, and so on. The physiological changes of cells cultured on the electrode microarray will be induced by internal and external stimuli. Thus, the electrode impedance can reflect the physiological state of cells on the electrode. Research on cellular activity and heterogeneity is better at the single-cell level than cell cluster. Therefore, more and more attention has been paid in the ECIS technology based on the single cell [11–14]. Compared to traditional cell-based assays (e.g., WST-1, XTT/MTT, BrdU, CFSE) which are laborious, time-consuming, invasive, and have unitary information, ECIS technology has the advantages of label-free detection, realtime monitoring, and noninvasive analysis. The ECIS technique has proven to be a valuable tool in biomedical applications such as drug screening, cancer research, and environmental pollutant identification [15–20].

Recently, with the development of micro–nanomachining technology and nanomaterials sciences, the research and application of the ECIS sensor have been greatly accelerated [21]. An overview of the fabrication and measurement principles of the ECIS sensor and the application in biomedicine and food analysis are introduced in this chapter.

4.2 Theory of Cell Impedance Biosensors

4.2.1 ECIS Cell Impedance Model

The cell membrane is considered as a complex structure of high capacitance and low conductance. The cell membrane is mainly composed of a phospholipid baitlayer with thickness about 7 nm; the conductivity of phospholipids' baitlayer is very low, and above the phospholipid baitlayer there are distributed various types of channels; water molecules and ions can import and exit by a special channel only, and the magnitude of membrane conductivity is 10^{-6} S/m. The hydration is formed on the surface of the cell membrane, and the whole cell is charged with a certain charge. Because the cell membrane is thin, it has a high capacitance value; the range is about 1 μF/cm^2 [22]. By changing the membrane permeability to control the internal environment, the destruction of the cell membrane can cause the death of the cell. The cell is filled with many kinds of particles such as nuclear

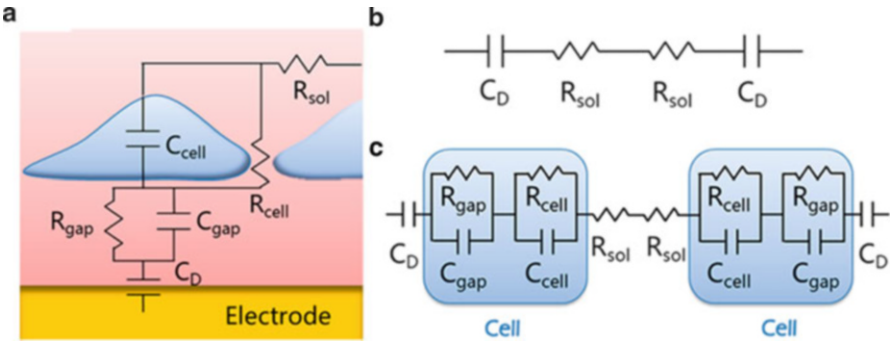

Fig. 4.1 (**a**) Simplified model of cell on ECIS. (**b**) The equivalent model of cell-free ECIS. (**c**) The equivalent model of ECIS covered with cell (Reproduced with permission from Ref. [29]. Copyright 2014 American Chemical Society)

mitochondria and other charged molecules. Thus, the inner membrane of the cell is highly conductive and the membrane is highly insulated.

In the attached cell [23], growth and proliferation [24] on the ECIS electrode block the ion current, which causes the change of impedance. The simplified model [25, 26] of cells on ECIS is shown in Fig. 4.1a. In general, the equivalent impedance circuit is used to represent the real impedance model, to interpret widely and analyze impedance data acquired from experiment. With the development of ECIS, more and more cell research uses interdigitated electrode structure [1]; this is beneficial to improve the performance of the cell impedance sensor. Figure 4.1b is an equivalent circuit model of the impedance of the ECIS for the case of a noncell attachment on the fork. Where C_D is the Helmholtz double-layer interface capacitance, R_{sol} is the expansion resistance of the cell culture fluid. The cells grow on the electrode and its simplified equivalent circuit model as shown in Fig. 4.1c, compared to the equivalent circuit model of the noncell, increases the cell capacitance C_{cell} and resistance R_{cell} and capacitance C_{gap} and resistance R_{gap} between the cell and substrate. Based on the equivalent circuit model of the free cell and cell, the impedance spectroscopy of ECIS is obtained (Fig. 4.1d), and the sensitivity of its corresponding ECIS cell impedance detection is also obtained (Fig. 4.1e).

Suppose the interdigital electrode has N branches; the total impedances of the electrodes can be expressed by Formula (4.1) [27]:

$$Z_{ele}(f) = \frac{R_S + (j2\pi f C_D)^{-1}}{2N} \tag{4.1}$$

The characteristic frequency of the equivalent circuit is shown in Formula (4.2):

$$f_{low-ele} \approx \frac{1}{2\pi R_S C_D} \tag{4.2}$$

The cell covered electrode impedance can be expressed by Formula (4.3):

$$Z_{\text{cell-ele}}(f) = \frac{1}{N}\left(Z_{\text{ele}}(f) + \frac{2}{{R_{\text{gap}}}^{-1} + \left(j2\pi f C_{\text{gap}}\right)^{-1}} + \frac{2}{{R_{\text{cell}}}^{-1} + \left(j2\pi f C_{\text{cell}}\right)^{-1}}\right) \tag{4.3}$$

The characteristic frequency of the equivalent circuit is shown in Formula (4.4)

$$f_{\text{low-cell}} \approx \frac{1}{2\pi\left(R_S + R_{\text{cell}} + R_{\text{gap}}\right)C_D} \tag{4.4}$$

In order to study the frequency characteristics of the interdigital electrodes, Wang et al. define three significant frequencies, f_{low}, f_{middle}, and f_{high}, from the equivalent circuit model, and based on the three frequencies, the whole impedance spectrum range is divided into four parts: I, II, III, IV [28]. When the excitation frequency is below the f_{low}, regardless of whether cells attach on the ECIS electrode, its impedance is mainly determined by the Helmholtz electric double-layer interface capacitance C_{D}, in this frequency range, ECIS sensitivity is lower, with the frequency decreasing, and sensitivity decreases further, close to zero. The range of frequencies below f_{low} is defined for zone I. Compared to the low frequency range, when the frequency is high enough and higher than f_{high}, the impedance of the ECIS electrode is determined by the solution expanded resistance R_{sol} regardless of the ECIS electrode cell. In this frequency range, the sensitivity of ECIS is also lower; with the frequency increasing, sensitivity decreases further, and close to zero. The range of frequencies higher than f_{high} is defined as the IV region. Best suited for cell impedance measurement frequency range are regions II and III, and when the working frequency of ECIS is between f_{high} and f_{low}, the effect of the cell on ECIS impedance change plays a major role. At the lower operating frequency range (II), the change of ECIS impedance caused by C_{cell} and R_{cell} is more than C_{gap} and R_{gap}. At the high operating frequency range (III), the change of ECIS impedance caused by R_{cell} and C_{cell} is more than that of R_{gap} and C_{gap}. By the ECIS cell impedance model, it is easy to find the suitable working frequency range of the ECIS sensor, which is helpful for optimizing the processing and design of the sensor.

The lower frequency flow and upper bound frequency f_{high} are calculated by Formulas 4.5 and 4.6:

$$f_{\text{low}} = \frac{1}{5}\frac{1}{2\pi\left(R_s + R_{\text{cell}} + R_{\text{gap}}\right)C_D} \tag{4.5}$$

$$f_{\text{high}} = \frac{1}{5}\frac{\left(C_D^{-1} + C_{\text{cell}}^{-1} + C_{\text{gap}}^{-1}\right)}{2\pi R_s} \tag{4.6}$$

4.2.2 Detection Principle of Cell Growth and Pulse

When we put the cell suspension into the cavity of the impedance chip, the cell will fall to the surface of the impedance electrode due to gravity. Initially, the contact area of the cell and the electrode is small. Then the cell becomes flat, and the contact area of the electrode becomes larger. This is a passive cell adhesion on the electrode and the extension, the contact process, is similar to the process of a drop of oil dropping on a substrate. In the next active adhesion phase, the cell is further stretched on the electrode, the cytoskeleton is reorganized, and the shape of the cell is changed from the circular to an irregular polygon shape. Because of the electrical insulation of the cell membrane, the current path between the working electrode and the electrode is hindered, so that the total impedance is increased. The more cells adhere, the greater is the impedance. After cell adhesion is finished, the cells continue to spread and proliferate on the electrode, and form a dense single-cell layer. This process will lead to a sustained increase in impedance. Then, due to increased environmental pressure of cells, such as limited growth space, the accumulation of liquid nutrient depletion, the cell metabolic product of culture, some cells undergo apoptosis and necrosis, detached from the sensor, releasing toxins that promote the electrode on the other cells' apoptosis, finally causing the death of all the cells in the system. This process impedance gradually decreases until close to zero. Therefore, the cell impedance sensor can be used to monitor the whole process of adhesion, spreading, proliferation, and apoptosis in the surface of the cell.

The ECIS sensor can detect the physiological state of the cells on its surface [30–32]. Compared to the single electrode, the reference electrode and the working electrode of interdigital electrodes play an equivalent function, and the utilization of the space impedance electrode is improved. In cell experiments, the principle of cell impedance with a single electrode is similar to an interdigitated electrode, and we mainly use interdigital electrodes, therefore the detection principle of the interdigital electrodes is introduced. When a sinusoidal AC voltage with a small amplitude is loaded at both ends of the interdigital electrodes, an ionic current is formed between the interdigital electrodes. As shown in Fig. 4.2a, when the interdigital electrodes don't have cells, its impedance is minimal, also known as the baseline impedance. When the cells grow and attach on the interdigital electrodes, they inhibit the ion current, thereby causing an increase of the impedance. The more the number of cells on the electrode impedance, the greater the degree of hindering the ion current and the impedance is. In addition, the size of ECIS impedance is closely related to the adhesion of the cell, and the tighter the cell and the electrode attachment, the more the impedance is, and the tighter the cells' contact with each other, the tighter the impedance is.

Regarding mammalian cell growth on the electrode surface by adherent growth style, with its coverage on the electrode surface, impedance properties of the electrode will change and cell morphology will change, and cell mobile and intercellular contact will lead to changes in the impedance of the electrode. The

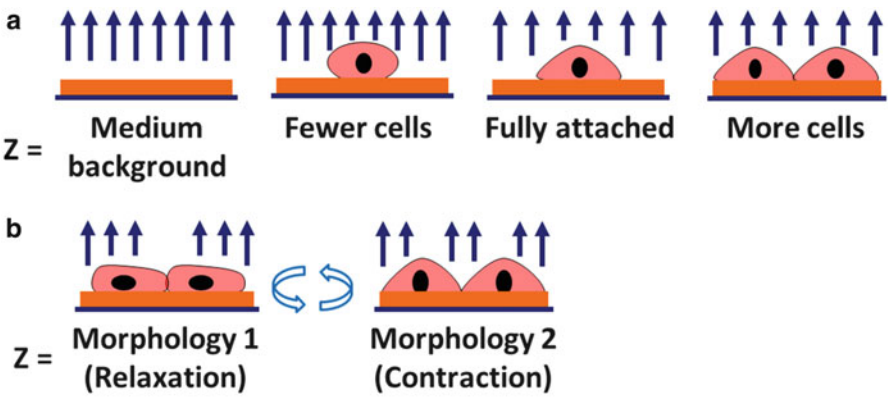

Fig. 4.2 Principle of ECIS sensor detecting cell and pulse. (**a**) Growth: substrate impedance without cells, fewer cells, more cells, and strongly attached cells. (**b**) Pulse: substrate impedance with cell contraction and relaxation of cardiomyocytes

cell impedance sensor (ECIS) monitors the changes of cell attachment and cell morphology by detecting the change of impedance. Due to the capacitance characteristics of the cells, when applying low-frequency AC excitation, the current tends to flow from the intercellular space and the gap of cells and electrodes. Therefore, under the conditions of low frequency excitation, ECIS more reflects the coverage area of cells on the electrode and the case of cells attached to the electrode, and tightness of the cells' connections. When high-frequency AC is excited, the current tends to flow from the cell membrane and the cytoplasm, therefore, under the conditions of high-frequency excitation, ECIS can reflect intracellular information.

The ECIS sensor can detect the impedance of the cell, and can record the important information of the physiological state of the cell on the electrode in realtime. When the cells are under the effect of external stimulus, physiological state changes can be reflected from the cell impedance detection of ECIS. Therefore, the EC1S sensor is often used in cell experiments for indicating the changes of physiological state such as cell growth, proliferation, morphological change, degree of adherence, and death and other physiological changes.

The basic function of the ECIS sensor is to monitor the physiological state of cell growth and attachment in realtime. For some cells with particular behavior (such as rhythmic pulsatile myocardial cells), the ECIS sensor can further expand the function of the detection of cell attachment and morphology [33–36]. Because myocardial cells' characteristics of excitation contraction coupling produce rhythmic contraction and relaxation [37], it will produce rhythmic contraction and relaxation, resulting in changes of the extent of contact tightness between myocardial cells and electrodes, and changes in cell morphology; these changes are more rapid compared to slow cell growth state change, and can cause rapid changes in impedance, which can be detected by the ECIS sensor (see Fig. 4.2b).

The ECIS sensor for the detection of myocardial cell beats is a new type of ECIS function application. Using neonatal rat myocardial cells and myocardial cell line, combined with the ECIS sensor, a sensor detection platform can be established for research on myocardial cells in vitro culture and cardiomyocyte sensor platforms can be further used in medical pharmacology experiments [38].

4.2.3 Cell Index

Using the cell impedance sensors to monitor the growth state of the cells, researchers have proposed a new parameter called the cell index CI [38], which can characterize a particular frequency point, the system impedance changes:

$$\mathrm{CI} = \frac{Z_{\mathrm{cell}} - Z_0}{Z_0} \tag{4.7}$$

where Z_0 represents the empty chip impedance before the cell inoculation, and Z_{cell} indicates the impedance value of the cells' presence. Compared with the previous section which mentioned normalized impedance variations, normalized impedance changes in data processing only to characterize its own changing trends, all with their own first data as a benchmark for statistics; the resulting curves use "1" as the starting point when mapping. CI results already exclude the background noise of the chip and the influence of blank chip impedance, and at the same time can evaluate the impedance magnitude of the cell under different contexts of surface treatment. The magnitude of the CI values will vary with the different growth states of the cell: small CI values characterizing the number of the cells attached to the electrode surface are small; the increase of CI values represents the increase of the number of cells attached on the surface of the electrode, the cell attached degree, and cells adhered to the attached area. In general, the CI is simpler than the normalized impedance changes to reflect the state of the cells. And the CI measurement system is more intelligent, operation is simpler, and follow-up data processing has been completed in the measurement process, saving a lot of human resources. Thus we can use CI to record the results of the experiment.

4.3 ECIS-Based Biosensors and Measurement

4.3.1 Chip Fabrication

ECIS-based biosensors employ cells as primary transducers for signal generation. Cells are cultured on a substrate that comprises both conductive and insulative materials in a classic ECIS device. Figure 4.3a shows the processing procedures of a

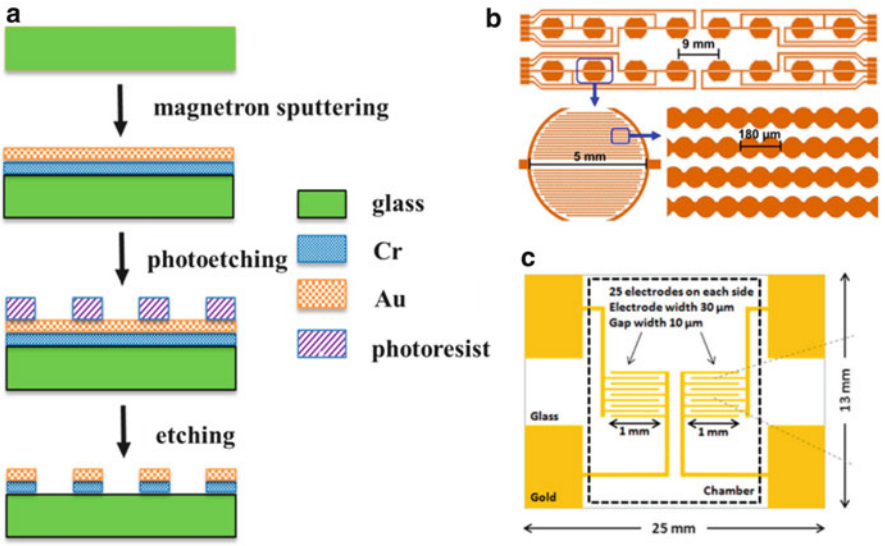

Fig. 4.3 (**a**) The fabrication of ECIS sensor chip. (**b**) Design of the glass chip with the micropatterned interdigitated electrodes (Reproduced with permission from Ref. [39]. Copyright 2014 AIP Publishing LLC). (**c**) The layout of IDEs structured coplanar ECIS sensor chip

sensor chip. The sensor chip is fabricated on a sterilized Pyrex glass 7740 (Corning). A 20 nm thick Cr layer is sputtered on a glass matrix to enhance the strength adhesion between the Au layer and the glass, and then 300 nm Au is sputtered on the Cr layer as the electrode material. Subsequently, the interdigitated electrodes (IDEs) array, leads, and pads are fabricated with UV lithography and etching technology. The sensor chip is then fixed on a printed circuit board (PCB) and a multiwell chamber made of PET material is sealed on the sensor chip to form a cell culture chamber.

The core structure of an ECIS sensor chip is electrodes and interconnecting conduits. Typically, monopolar structure electrodes and interdigitated electrodes are primarily used for impedance sensing. The application of a monopolar electrode not only limits the effective sensing area, but also hampers the miniaturization of ECIS sensors. Hence, IDEs are widely researched and put into application nowadays in ECIS devices (Fig. 4.3b,c).

4.3.2 Surface Modification

Although gold electrodes have good biocompatibility, surface treatments are still applied prior to cell cultures. Most of the cell adhesion enhancements conducted in an ECIS device are done by chemical surface modification, which includes different functional groups and biomacromolecules on the membrane surface [6, 16,

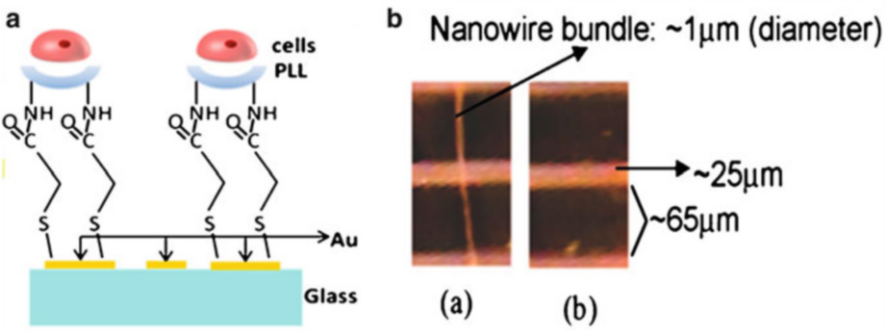

Fig. 4.4 (**a**) The schematic diagram of carboxylate groups' modified chip surface for guiding cell adhesion (Reproduced with permission from Ref. [6]. 2013 Sensors and Actuators A: Physical.). (**b**) (*a*) Gold microelectrode crossed with TiO_2 nanowire bundle (*a*) and without TiO_2 nanowire bundle (*b*) (Reproduced with permission from Ref. [45]. Copyright 2008 American Chemical Society)

40]. Self-assembled monolayers (SAMs) with different surface functional groups were formed after a series of complex chemical reactions, such as hydroxyl (OH), carboxyl (COOH), amine (NH2), and methyl (CH3) groups. Zhou et al. have used NHS ester-terminated alkanethiol SAM which formed a biocompatible layer for PLL on gold electrodes to investigate that the covalently bound poly-l-lysine (PLL) on electrodes improved cell adhesion on the electrodes (Fig. 4.4a). Some extracellular matrix (ECM) proteins were coated onto the substrates, which also can improve cell adhesion. For example, Guo et al. constructed a smart functional biomimetic film sensor by covalently bonding RGD-peptide on a graphene surface that can significantly boost cell adhesion and growth for realtime electrochemical detection [41].

Furthermore, recently the role of microtopography in controlling cell adhesion is becoming increasingly important. Some research indicates that cell attachment is greatly enhanced by roughness modifications compared to a smooth surface [42, 43]. And unique micro- or nanopattern designs showed an increase in attachment on pit-patterned surfaces [44].

Nanocrystalline materials are a new area in materials science because they possess some special functions in sound, light, electric, magnetic, and heat, and advanced performance, such as small-size effect, surface and boundary effect, quantum-size effect, and so on. Semiconductor nanocrystals, such as CdS quantum dots (QDs), were widely used to modify the biosensor surface.

4.3.3 Detection System

The ECIS detection system often includes a signal generator module, amplification and filter module, and data acquisition module (Fig. 4.5a). By applying a sinusoidal

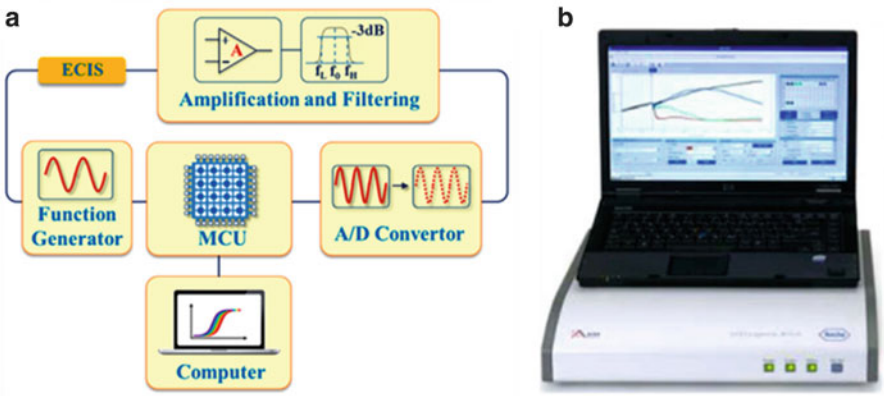

Fig. 4.5 (**a**) Block diagram of ECIS detection system (Reproduced with permission from Ref. [47]. Copyright 2013 Elsevier). (**b**) High time-resolution detection system developed by ACEA Biosciences

voltage generated by the signal generator module, an ion current is formed between the electrodes. Then the current signal is converted to a voltage signal by the amplification and filter module. Subsequently, the signals can be recorded by the data acquisition module. Finally, the digital signals are transferred to a computer by signal processing. Many factors result in signal noise in practical measures, including electronic instrumentation, interference from external sources, pH, and temperature [46]. Lock-in amplifiers are utilized because they can detect small AC signals and single out the component of a signal at a specific reference frequency and phase. Figure 4.5b shows a typical ECIS sensor detection system, both of which include the electrochemical analyzer and computer.

4.4 Application in Biomedicine and Food Analysis

ECIS sensors have attracted more and more attention because they have many advantages such as noncontact, realtime, are noninvasive, and so on. The conventional cell-based assays such as 3-(4,5-dimethylthiazol-2-yl)-2,5-diphenyltetrazolium bromide test (MTT), neutral red uptake (NRU), and ATP and lactate dehydrogenase (LDH) measurement are based on single endpoints, which would miss some important information due to the endpoint assay [48, 49]. Furthermore, classic endpoint assays take too long a period in time, have complex operation and many steps, including cell lysis or fixation, and are treated using different chemical reagents. Therefore, ECIS technology provides a good platform for noninvasively and instantaneously detecting and analyzing cell responses to chemical and biological agents.

Over the past several decades, many ECIS sensors have been successfully used in biomedicine and food analysis, and some commercially available systems have been developed and applied to many fields [16, 50–52]. This section focuses on introducing application of the ECIS sensor in biomedicine and food analysis, such as drug screening, environment monitoring, food analysis, and clinical diagnostics.

4.4.1 Drug Screening

The effect of drugs on growth and proliferation of cancer cells is a pivotal issue in developing effective and safe anticancer drug therapies. ECIS technology can monitor cell activities in a realtime and label-free way, therefore, ECIS sensors are used in drug screening by using various cancer cell line models [10, 53].

The ECIS sensor can provide realtime kinetic impedance measurement information throughout the whole experiment. Different growth states of cancer cells may be seen after several different drugs' effect on the cancer cells.

The result of different drugs for cancer cells can be learned from the CI curves after the drugs are added to the cells, and the characteristics of the sensor for realtime monitoring can also be used to obtain a detailed understanding of its role in the process of change.

Early and effective drug-screening methods are required in the field of biotechnology and the pharmaceutical industry for predicting drug-induced cardiotoxicity and reducing late-stage drug attrition [54]. Cardiotoxicity accounts for about one third of safety-based withdrawn pharmaceuticals [55]. Earlier and broader screening is a validated approach to improve cardiovascular safety as demonstrated with human ether-a-go-go–related gene (hERG) screening to reduce drug-induced arrhythmia [38, 56, 57]. But novel in vitro assays are needed to address other mechanism research of cardiovascular function, including contractility, heart rate, toxicity, hypertrophy, and non-hERG arrhythmia. Therefore, the EICS systems for predicting drug-induced cardiotoxicity are meaningful in the pharmaceutical and biotechnology industries to decrease late-stage drug attrition.

RTCA technology is an advanced ECIS technology that significantly explores the high sample rate and high-throughput detection [58]. Therefore, it can record the rapid-changing impedance signals and facilitate the monitoring of the cardiomyocytes' beating status. RTCA technology provides an efficient approach to establish a high-performance cardiomyocyte-based biosensor.

Figure 4.6a shows a typical CI curve of myocardial cells; firstly, due to cell growth, adhesion, cells grow in an exponential way. Subsequently, due to the regular pulsation of the myocardial cells, the amplitude of CI curves presents periodic changes, as part of the blue line in the graph shows.

Generally, cell impedance technology is used to study cell growth and drug experiments in vitro. Moreover, high temporal resolution impedance detection technology can monitor the morphology and adhesion changes induced by cardiomyocyte rhythmic beating in realtime.

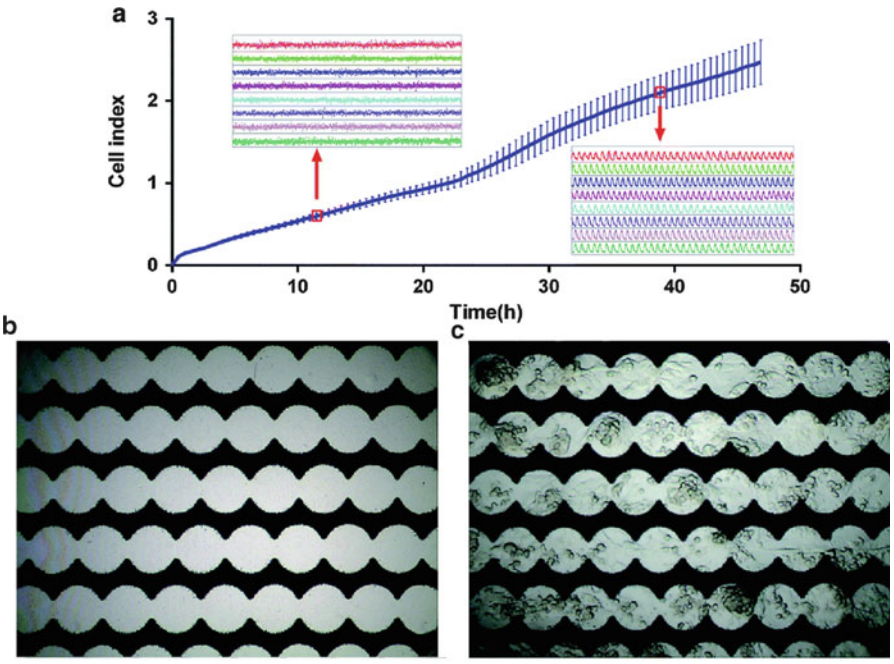

Fig. 4.6 (**a**) Cellular growth curve of rat cardiomyocytes. Images of CIB sensor before (**b**) and after (**c**) cardiomyocytes were loaded onto it (Reproduced with permission from Ref. [59]. 2015 Wang P.)

Verapamil is an L-type calcium channel blocker of the phenylalkylamine class. It can slow down the conduction rate in order to reduce the ventricular rate of patients with chronic atrial fibrillation, atrial flutter, and paroxysmal supraventricular tachycardia frequency. It has been used in the treatment of hypertension, angina pectoris, cardiac arrhythmia, and cluster headaches [60].

To evaluate verapamil effects, different concentrations of verapamil-based culture media were prepared. The verapamil medium was added into the wells, when the cardiomyocytes beat rhythmically with almost the same rate in each well. From the beating status in Fig. 4.7a, verapamil reduced the cardiomyocyte beating rate significantly and showed dose- and time-dependent recovery in the long term. The high-dose verapamil treatment induced the beating stop in the short term. Figure 4.7b displays the normalized CI of cell growth after verapamil treatment. And the cardiomyocytes' impedance growth showed a dose-dependent inhibition effect under verapamil for 24 h culture. The cardiomyocytes were cultured without compound additions as the control group in the whole experiments, and cells were not disturbed by the compound.

The RTCA sensors can evaluate drug effect by simultaneously monitoring cardiomyocyte growth and beating status in long and short time [16]. CI values are calculated by impedance values, which are influenced by a mixture including

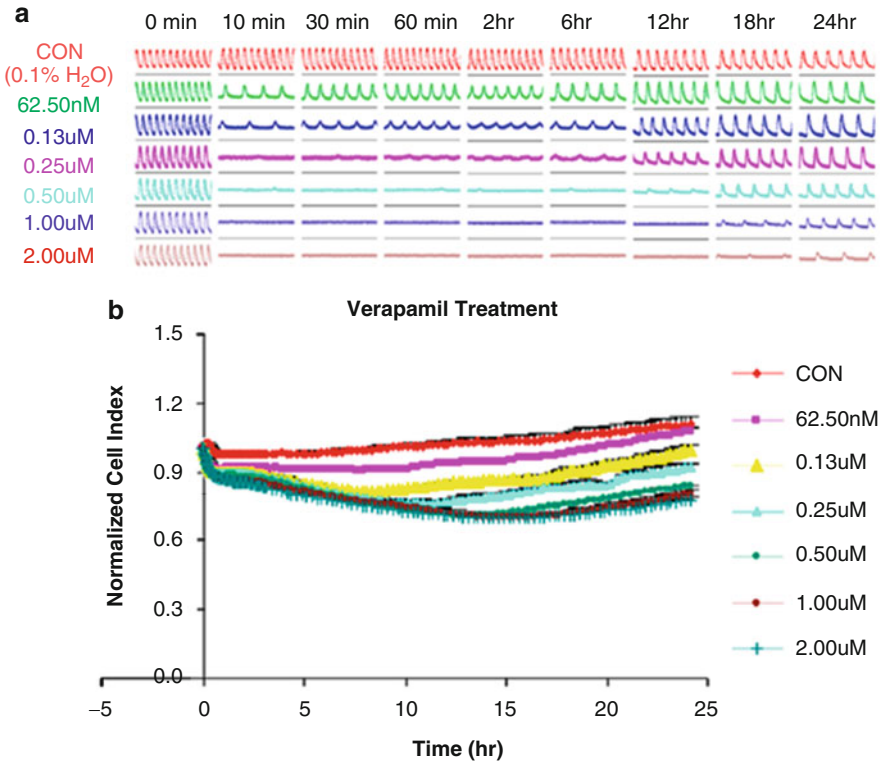

Fig. 4.7 Cardiomyocyte status in the presence of verapamil. (**a**) Snapshot of cardiomyocytes beating profile under verapamil. (**b**) Cardiomyocytes impedance growth curve under verapamil (Reproduced with permission from Ref. [16]. Copyright 2013 Elsevier)

the cardiomyocyte growth, proliferation, and adhesion status. The cardiomyocyte beating status was also monitored in parallel in order to reflect the drug effects on the cardiomyocytes. With the improvement of sensor technology and cell culture, the cardiomyocyte-based biosensor will be a promising tool to preclinical drug screening in the field of pharmaceuticals and medicine.

4.4.2 Environment Monitoring

Protection of drinking water supplies from chemical contaminants can be enhanced by the use of toxicity sensors. Toxicity sensors using enzymes or bacteria are presently in use at some water utilities, but it can only quantify and identify specific chemicals whereas living cell sensors can indicate the presence of a broad range of chemicals (including unknown agents) that cause a toxic response [17, 61, 62].

When maintained on medium alone, impedance values were constant over the 1 h period prior to toxicant exposure. Introduction of pentachlorophenate (PCP) caused a substantial and highly significant decrease in impedance compared to the control values [63].

What's more, the sensor can detect chemical toxicants after long-term storage. When the cells are stored for 16 weeks, PCP still caused a significant change in impedance when compared to controls not exposed to PCP. Although the differences between the control and PCP-treated channels decreased as the age of the chips increased, the differences were still statistically significant, as determined by the curve discrimination software.

This toxicity sensor will be useful for evaluating samples at water utilities and other sites where field toxicity testing with mammalian cells is desired. It can rapidly screen drinking water samples for chemical-related toxicity, and can be used as a toxicity-based indicator of the potential presence of a wide range of toxic chemicals, leading to further analytical evaluation to determine the specific chemical causing the response. Because comprehensive analyte-specific evaluations are too expensive for everyday water utility use (several thousand dollars for both inorganic and organic constituents), the more frequent use of a relatively low-cost toxicity sensor test can be a cost-effective way to improve the odds that potential chemical contamination is discovered before adverse consequences are manifested.

4.4.3 Food Analysis

Marine toxins, produced by algae, are easily accumulated to a high level in filter-feeding fish or shellfish. People commonly are poisoned by eating the contaminated seafood. Among all of the marine toxins, paralytic shellfish poisoning (PSP) toxins are one type of the most widely distributed toxins in the world, and do the most serious harm in public health and marine aquaculture industries [64]. PSP toxins affect the propagation of action potential by blocking sodium channels, which changes the membrane potential on a cellular level and causes neurological symptoms (e.g., numbness and tingling) in humans [65, 66]. Therefore, the detection of marine toxins has great significance in human health and environmental safety.

The official methods for PSP toxin detection are the mouse bioassay (MBA) [67] and precolumn oxidation liquid chromatography with fluorescence detection (ox-LC-FLD) [68–71]. As the most commonly used detection method, MBA can detect the PSP toxins by observing the symptoms and the time of death after injecting shellfish extracts. It can not only detect all of the PSP toxins, but also reflect the actual toxicity. However, the MBA method still has a low-sensitivity problem and ethical problem. Although the ox-LC-FLD method is sensitive and reliable, it is limited by the expensive reference material and chromophore needed to produce fluorescent products [69, 72]. Moreover, these PSP toxins can be converted from one structure to another in preparing samples of ox-LC-FLD.

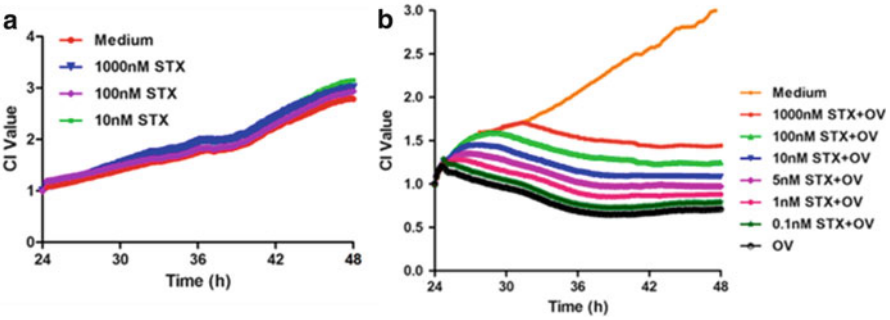

Fig. 4.8 (**a**) A group of normalized cell growth curves of neuro-2a cells responding to different concentrations of STX without OV. (**b**) A group of normalized cell growth curves of neuro-2a cells responding to STX in the presence of OV (Reproduced with permission from Ref. [5]. Copyright 2015 Elsevier)

In addition, the nonanalytical methods, which can only detect a small number of closely related toxins, are insufficient to detect 30 structural variants of PSP toxins [73].

The cell-based assay could improve the detection limit markedly and reduce the number of animals used in experiments [74, 75]. And both the primary cells and continuous cell lines can be used in the cell-based assays. The method based on continuous cell lines might be more promising than primary cells which still need to be derived from laboratory animals. What is more, the continuous cell lines could be applied to detect and screen marine toxins with high throughput. The presence of PSP toxins can be detected by measuring the cell viability cotreated with ouabain and veratridine, which is a widely accepted cell-based assay today [64, 76].

From Fig. 4.8a, it can be seen that there was a neglected effect of STX on cell growth after 24 h of treatment because there were no significant differences in CI values between the high concentration of STX and the control group, indicating that treatment with STX had no effect on the growth and multiplication of cells, which was consistent with previous research [77]. As shown in Fig. 4.8b, each CI value curve provided detailed kinetic information of cells in response to OV and STX with various concentrations, which was ignored in the conventional endpoint assay. CI values measured by the detection system decreased after OV treatment due to the continuous increasing of the intracellular Na^+. And STX inhibited OV-induced cell death by blocking Na^+ inward current. For example, CI value began to decrease within 1 h after OV treatment, whereas the group of 1000 nM and 100 nM STX started to decrease at approximately 8 h and 5 h after STX addition, respectively. Cells cotreated with OV and 1–1000 nM STX present higher CI values than those only OV treated. This result indicated that OV cotreated with a higher concentration of STX needed a longer time to induce neuro-2a cell apoptosis, whereas a lower concentration of STX cotreated with OV induced cell apoptosis quickly. It was suggested that this CIB method can monitor STX-inhibited neuro-2a cell apoptosis

induced by OV dynamically and noninvasively, and provided realtime and dynamic information of the cells' response to different concentration compounds throughout the experiments.

4.4.4 Cancer Research

According to the World Health Organization (WHO), cancer is the leading cause of deaths (8.2 million in 2012) worldwide, with lung, breast, cervical, and liver cancers the most common types. Cancer deaths can be significantly reduced if detected and treated early. Current clinical cancer detection techniques are invasive, costly, time consuming, complex, biomarker labeling, with a false detection rate of 20–50 %. The need for label-free cancer detection methods is increasing which should be minimally invasive, inexpensive, rapid, sensitive, reliable, and easy to use.

Cytotoxic T lymphocytes (CTLs) and natural killer (NK) cells have been implicated in the recognition and annihilation of tumor cells [78]. Traditionally, these assays are conducted by labeling the target cells with a radioactive tracer and then adding the effector cells, such as CTLs or NKs [79]. The extent of CTL and NK cytotoxicity activity towards target cells is assayed by the release of radioactivity by the target cells upon cytolysis [79]. Although the chromium release assay is widely used, it is labor-intensive and cumbersome not only because of the use of radioactivity but also because of high background of noise resulting from the tendency of the label to permeate out of the target cells. Now, both CTL and NK assays can use the RT-CES system to offer an alternative with significant contributions in ease of use and quality of data [80].

The MCF-7 cells were seeded at the wells and continuously monitored. Then different effector-to-target cell ratios of NK-92 cells were added to the wells, and the cytotoxic activity of NK-92 cells towards MCF-7 cells was dynamically monitored. Using this method, it can also be demonstrated that pharmacological inhibitors of signaling proteins such as mitogen-activated protein kinase and phosphoinositide 3-kinase, which control degranulation of NK cells dose-dependently, inhibit NK-mediated cytolysis of target cells. In addition to cell-mediated cytotoxicity, impedance readout can also be utilized to monitor cytotoxicity induced by other nonchemical agents, such as viruses. Because the viral-mediated cytopathic effect on target cells is characterized by rounded cell morphology and de-adhesion, impedance monitoring should be able to detect these changes. As a matter of fact, the RT-CES system was recently used to monitor dynamically both the infection and cytopathic activity of influenza A virus [81] in cultured mammalian cells.

In summary, an impedance readout can profile cell–cell or virus–cell interaction in realtime and allow quantitative detection of both short- and long-term responses.

At present, many studies have used nanoscale coatings to improve the sensitivity of the ECIS electrodes. This strategy is based on two major findings. First, surface

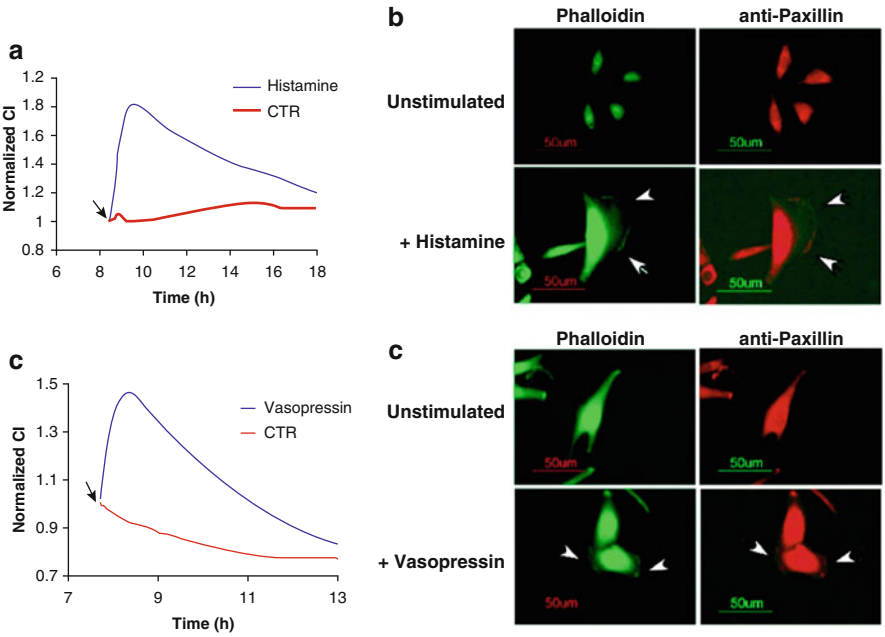

Fig. 4.9 G Protein coupled receptors stimulated by histamine and vasopressin resulting in the changes of cell-substrate impedance (**a–c**) and cell skeleton protein (**b–d**) (Reproduced with permission from Ref. [87]. Copyright 2006 American Chemical Society)

topography can be used specifically to guide the adhesion and spreading of biological cells. Second, the sensitivity of neuronal recordings from implantable microelectrodes was improved using gold nanoparticle and carbon nanotube coatings. In another study, glassy carbon electrodes were coated with polyaniline nanotube membranes and gold nanoparticles and the resulting electrode showed enhanced sensitivity for DNA detection. Coatings consisting of nanocomposites of carbon nanotubes have also been shown to improve sensitivity of electrochemical sensors. The improved sensitivity of the electrodes in these studies was attributed to increased surface roughness and interaction or an enhanced selectivity to the target analyte. These examples provide the rationale for investigation of coatings to modulate the sensitivity of ECIS electrodes to impedance of breast cancer cells. As shown in Fig. 4.9, four nanoscale coatings of gold nanoparticles (AuNP), carbon nanotubes (CNT), and electroplated gold (EPDC) were used to introduce nanoscale roughness on the surface of the gold electrodes and show that the sensitivity of planar gold microelectrodes can be modulated through the use of electrode coatings.

A silicon nanowire-based electrical cell impedance sensor (SiNW-ECIS) is an instrument that detects cancerous cultured living lung cells by monitoring their spreading state at which the cells stretch and become extended on nanowires. The developed device was applied to monitor the spreading-induced electrical

differences between cancerous and normal lung cells in an integral fashion. Detection was performed faster than the time required to complete cell mitosis. Morphology and architecture of doped Si nanowire-covered microelectrodes observably enhance the contact area between cells and electrodes and support accurate signal recording from stretched cells as indicated by SEM and florescent images.

This sensor could be applied to investigate the differences in proliferation rate between normal and malignant cells in the early hours of the culturing process. SiNW-ECIS is suitable for different purposes such as monitoring the effect of anticancer drugs on cell spreading as well as the external stimulating agents on cell proliferation.

4.4.5 Other Applications

GPCRs are an important target for pharmaceutical drug development, and about 50 % of the current drugs on the market are targeted against GPCRs [82]. The vast majority of GPCRs couple to and activate heterotrimeric G proteins and subsequently stimulate second messenger systems [83]. The heterotrimeric G proteins consist of a G_{α} subunit and $G_{\beta/\gamma}$ complex, both of which can activate downstream effectors depending on the receptors being activated [83]. More recently it has become apparent that GPCR signaling either through or in addition to heterotrimeric G-proteins also activate the Rho family of small GTPases [84, 85]. The Rho family of GTPases participates in a number of cellular processes, the main one being regulation and maintenance of specific structures within the actin cytoskeleton framework [86]. GPCRs have been shown to modulate the actin cytoskeleton and hence cell morphology in a very specific manner depending on the Rho family GTPase being activated. Because GPCRs couple to the actin cytoskeletal network and induce very defined morphological changes, it is possible to harness this information as a functional and biologically relevant readout for GPCRs using the RT-CES system [87].

As shown in Fig. 4.9, H1/CHO cells expressing the histamine H1 receptor were seeded in the sensor and continuously monitored. At the indicated timepoint the cells were treated with histamine, and the dynamic cellular response was monitored. The CI curve can reflect the changes of cellular morphology. The important contribution of RT-CES for GPCR cell-based assays is several-fold; first, because the readout is noninvasive, the cells can be stimulated multiple times in order to assess desensitization or crosstalk with other receptor types. Second, in addition to the histamine receptor, which is coupled to the G_q subfamily of G-proteins, cells expressing other receptors coupled to the G_s and G_i families can also be monitored on the RT-CES system [87].

4.5 Summary

In this chapter, the principles of the sensor based on cell electrical impedance, the ECIS cell impedance model, ECIS cell growth detection principle, ECIS cell pulsation measuring principle, and ECIS instrumentation system design and its use in drug testing and food safety are introduced. In the process of cell growth and proliferation, it is controlled by the external environment and chemical molecules. The previous methods of cell measurement are based on the endpoint test, and cannot provide realtime monitoring of the changes of the state of the cells. ECIS can not only monitor cell growth in realtime, and by extension, morphological changes, death, and adherent degree, and with the extracellular matrix molecules can be measured by the use of impedance to analyze the cell growth state and the effect of drugs, and detect myocardial cell rhythm, so that the sensor function ECIS has been further expanded. ECIS has the characteristics of fast, long-term, nondestructive, and high-throughput measurement, which makes it a promising development direction.

References

1. Giaever I, Keese C. Monitoring fibroblast behavior in tissue culture with an applied electric field. Proc Natl Acad Sci. 1984;81(12):3761–4.
2. Keese CR, Bhawe K, Wegener J, Giaever I. Real-time impedance assay to follow the invasive activities of metastatic cells in culture. Biotechniques. 2002;33(4):842–51.
3. Keese CR, Giaever I. A biosensor that monitors cell morphology with electrical fields. Eng Med Biol Magaz IEEE. 1994;13(3):402–8.
4. Wegener J, Keese CR, Giaever I. Electric cell–substrate impedance sensing (ECIS) as a noninvasive means to monitor the kinetics of cell spreading to artificial surfaces. Exp Cell Res. 2000;259(1):158–66.
5. Zou L, Wu C, Wang Q, Zhou J, Su K, Li H, Hu N, Wang P. An improved sensitive assay for the detection of PSP toxins with neuroblastoma cell-based impedance biosensor. Biosens Bioelectron. 2015;67:458–64.
6. Zhou J, Wu C, Tu J, Ling Y, Hu N, Zhang Y, Su K, Wang P. Assessment of cadmium-induced hepatotoxicity and protective effects of zinc against it using an improved cell-based biosensor. Sensors Actuators A Phys. 2013;199:156–64.
7. Wang N, Ostuni E, Whitesides GM, Ingber DE. Micropatterning tractional forces in living cells. Cell Motil Cytoskeleton. 2002;52(2):97–106.
8. Ostuni E, Kane R, Chen CS, Ingber DE, Whitesides GM. Patterning mammalian cells using elastomeric membranes. Langmuir. 2000;16(20):7811–9.
9. Atienza JM, Yu N, Kirstein SL, Xi B, Wang X, Xu X, et al. Dynamic and label-free cell-based assays using the real-time cell electronic sensing system. Assay Drug Dev Technol. 2006; 4(5):597-607.
10. Solly K, Wang X, Xu X, Strulovici B, Zheng W. Application of real-time cell electronic sensing (RT-CES) technology to cell-based assays. Assay Drug Dev Technol. 2004; 2(4):363–72.
11. Dittami GM, Ayliffe HE, King CS, Rabbitt RD. A multilayer MEMS platform for single-cell electric impedance spectroscopy and electrochemical analysis. Microelectromech Syst J. 2008;17(4):850–62.

12. Kurz CM, Büth H, Sossalla A, Vermeersch V, Toncheva V, Dubruel P, Schacht E, Thielecke H. Chip-based impedance measurement on single cells for monitoring sub-toxic effects on cell membranes. Biosens Bioelectron. 2011;26(8):3405–12.
13. Morgan H, Sun T, Holmes D, Gawad S, Green NG. Single cell dielectric spectroscopy. J Phys D Appl Phys. 2007;40(1):61.
14. Han A, Frazier AB. Ion channel characterization using single cell impedance spectroscopy. Lab Chip. 2006;6(11):1412–4.
15. Srinivasaraghavan V, Strobl J, Agah M. Bioimpedance rise in response to histone deacetylase inhibitor is a marker of mammary cancer cells within a mixed culture of normal breast cells. Lab Chip. 2012;12(24):5168–79.
16. Wang T, Hu N, Cao J, Wu J, Su K, Wang P. A cardiomyocyte-based biosensor for antiarrhythmic drug evaluation by simultaneously monitoring cell growth and beating. Biosens Bioelectron. 2013;49:9–13.
17. Kovacs GT. Electronic sensors with living cellular components. Proc IEEE. 2003;91(6):915–29.
18. Zou L, Hu N, Zhou J, Su K, Wang Q, Du L, Wu C, Zhao L, Wang P. A novel electrical cell-substrate impedance biosensor for rapid detection of marine toxins. Sens Lett. 2014;12(6–7):1041–5.
19. Kramer AH, Joos-Vandewalle J, Edkins AL, Frost CL, Prinsloo E. Real-time monitoring of 3T3-L1 preadipocyte differentiation using a commercially available electric cell-substrate impedance sensor system. Biochem Biophys Res Commun. 2014;443(4):1245–50.
20. Tran TB, Cho S, Min J. Hydrogel-based diffusion chip with Electric Cell-substrate Impedance Sensing (ECIS) integration for cell viability assay and drug toxicity screening. Biosens Bioelectron. 2013;50:453–9.
21. Tran TB, Nguyen PD, Um SH, Son SJ, Min J. Real-time monitoring in vitro cellular cytotoxicity of silica nanotubes using electric cell-substrate impedance sensing (ECIS). J Biomed Nanotechnol. 2013;9(2):286–90.
22. Martinsen OG, Grimnes S. Bioimpedance and bioelectricity basics. London: Academic; 2011.
23. Xiao C, Lachance B, Sunahara G, Luong JH. An in-depth analysis of electric cell-substrate impedance sensing to study the attachment and spreading of mammalian cells. Anal Chem. 2002;74(6):1333–9.
24. Xiao C, Luong JH. On-line monitoring of cell growth and cytotoxicity using electric cell-substrate impedance sensing (ECIS). Biotechnol Prog. 2003;19(3):1000–5.
25. Huang X, Nguyen D, Greve DW, Domach MM. Simulation of microelectrode impedance changes due to cell growth. Sensors J IEEE. 2004;4(5):576–83.
26. Yang L, Li Y, Griffis CL, Johnson MG. Interdigitated microelectrode (IME) impedance sensor for the detection of viable Salmonella typhimurium. Biosens Bioelectron. 2004;19(10):1139–47.
27. Giaever I, Keese CR. Micromotion of mammalian cells measured electrically. Proc Natl Acad Sci. 1991;88(17):7896–900.
28. Wang L, Wang H, Mitchelson K, Yu Z, Cheng J. Analysis of the sensitivity and frequency characteristics of coplanar electrical cell–substrate impedance sensors. Biosens Bioelectron. 2008;24(1):14–21.
29. Liu Q, Wu C, Cai H, Hu N, Zhou J, Wang P. Cell-based biosensors and their application in biomedicine. Chem Rev. 2014;114(12):6423–61.
30. Morimoto T, Kinouchi Y, Iritani T, Kimura S, Konishi Y, Mitsuyama N, Komaki K, Monden Y. Measurement of the electrical bio-impedance of breast tumors. Eur Surg Res. 1990;22(2):86–92.
31. Zou Y, Guo Z. A review of electrical impedance techniques for breast cancer detection. Med Eng Phys. 2003;25(2):79–90.
32. Slanina H, König A, Claus H, Frosch M, Schubert-Unkmeir A. Real-time impedance analysis of host cell response to meningococcal infection. J Microbiol Methods. 2011;84(1):101–8.

33. Lyssiotis CA, Lairson LL, Boitano AE, Wurdak H, Zhu S, Schultz PG. Chemical control of stem cell fate and developmental potential. Angew Chem Int Ed. 2011;50(1):200–42.
34. Meyer T, Sartipy P, Blind F, Leisgen C, Guenther E. New cell models and assays in cardiac safety profiling. 2007.
35. Wegener J, Abrams D, Willenbrink W, Galla H-J, Janshoff A. Automated multi-well device to measure transepithelial electrical resistances under physiological conditions. Biotechniques. 2004;37(590):592–4.
36. Abassi YA, Xi B, Li N, Ouyang W, Seiler A, Watzele M, Kettenhofen R, Bohlen H, Ehlich A, Kolossov E. Dynamic monitoring of beating periodicity of stem cell-derived cardiomyocytes as a predictive tool for preclinical safety assessment. Br J Pharmacol. 2012;165(5):1424–41.
37. Bers DM. Cardiac excitation–contraction coupling. Nature. 2002;415(6868):198–205.
38. Braam SR, Tertoolen L, van de Stolpe A, Meyer T, Passier R, Mummery CL. Prediction of drug-induced cardiotoxicity using human embryonic stem cell-derived cardiomyocytes. Stem Cell Res. 2010;4(2):107–16.
39. Sharma R, Blackburn T, Hu W, Wiltberger K, Velev OD. On-chip microelectrode impedance analysis of mammalian cell viability during biomanufacturing. Biomicrofluidics. 2014;8 (5):054108.
40. Ni M, Tong WH, Choudhury D, Rahim NAA, Iliescu C, Yu H. Cell culture on MEMS platforms: a review. Int J Mol Sci. 2009;10(12):5411–41.
41. Guo CX, Ng SR, Khoo SY, Zheng X, Chen P, Li CM. RGD-peptide functionalized graphene biomimetic live-cell sensor for real-time detection of nitric oxide molecules. ACS Nano. 2012;6(8):6944–51.
42. Lim JY, Hansen JC, Siedlecki CA, Hengstebeck RW, Cheng J, Winograd N, Donahue HJ. Osteoblast adhesion on poly (L-lactic acid)/polystyrene demixed thin film blends: effect of nanotopography, surface chemistry, and wettability. Biomacromolecules. 2005;6 (6):3319–27.
43. Ranucci CS, Moghe PV. Substrate microtopography can enhance cell adhesive and migratory responsiveness to matrix ligand density. J Biomed Mater Res. 2001;54(2):149–61.
44. Wan Y, Wang Y, Liu Z, Qu X, Han B, Bei J, Wang S. Adhesion and proliferation of OCT-1 osteoblast-like cells on micro-and nano-scale topography structured poly (L-lactide). Biomaterials. 2005;26(21):4453–9.
45. Wang R, Ruan C, Kanayeva D, Lassiter K, Li Y. TiO2 nanowire bundle microelectrode based impedance immunosensor for rapid and sensitive detection of Listeria monocytogenes. Nano Lett. 2008;8(9):2625–31.
46. Qian Z, Bai H-J, Wang G-L, Xu J-J, Chen H-Y. A photoelectrochemical sensor based on CdS-polyamidoamine nano-composite film for cell capture and detection. Biosens Bioelectron. 2010;25(9):2045–50.
47. Hu N, Wang T, Cao J, Su K, Zhou J, Wu J, Wang P. Comparison between ECIS and LAPS for establishing a cardiomyocyte-based biosensor. Sensors Actuators B Chem. 2013;185:238–44.
48. Limame R, Wouters A, Pauwels B, Fransen E, Peeters M, Lardon F, De Wever O, Pauwels P. Comparative analysis of dynamic cell viability, migration and invasion assessments by novel real-time technology and classic endpoint assays. 2012.
49. Xiao C, Luong JH. Assessment of cytotoxicity by emerging impedance spectroscopy. Toxicol Appl Pharmacol. 2005;206(2):102–12.
50. Arias LR, Perry CA, Yang L. Real-time electrical impedance detection of cellular activities of oral cancer cells. Biosens Bioelectron. 2010;25(10):2225–31.
51. Geldmacher Y, Splith K, Kitanovic I, Alborzinia H, Can S, Rubbiani R, Nazif MA, Wefelmeier P, Prokop A, Ott I. Cellular impact and selectivity of half-sandwich organorhodium (III) anticancer complexes and their organoiridium (III) and trichloridorhodium (III) counterparts. JBIC J Biol Inorg Chem. 2012;17(4):631–46.
52. Mestres P, Morguet A, Schmidt W, Kob A, Thedinga E. A new method to assess drug sensitivity on breast tumor acute slices preparation. Ann N Y Acad Sci. 2006;1091(1):460–9.

53. Atienza JM, Yu N, Kirstein SL, Xi B, Wang X, Xu X, et al. Dynamic and label-free cell-based assays using the real-time cell electronic sensing system. Assay Drug Dev Technol. 2006; 4(5):597–607.
54. Xiao L, Hu Z, Zhang W, Wu C, Yu H, Wang P. Evaluation of doxorubicin toxicity on cardiomyocytes using a dual functional extracellular biochip. Biosens Bioelectron. 2010;26 (4):1493–9.
55. Lawrence C, Pollard C, Hammond T, Valentin JP. In vitro models of proarrhythmia. Br J Pharmacol. 2008;154(7):1516–22.
56. Giorgi MA, Bolanos R, Gonzalez CD, Di Girolamo G. QT interval prolongation: preclinical and clinical testing arrhythmogenesis in drugs and regulatory implications. Curr Drug Saf. 2010;5(1):54–7.
57. Moss AJ, Kass RS. Long QT syndrome: from channels to cardiac arrhythmias. J Clin Investig. 2005;115(8):2018.
58. Smout MJ, Laha T, Mulvenna J, Sripa B, Suttiprapa S, Jones A, Brindley PJ, Loukas A. A granulin-like growth factor secreted by the carcinogenic liver fluke, Opisthorchis viverrini, promotes proliferation of host cells. PLoS Pathog. 2009;5(10):e1000611.
59. Li H, Zou Q, Zou L, Wang Q, Su K, Hu N, Wang P. Detection of cardiovascular drugs and marine toxins using a multifunctional cell-based impedance biosensor system. Anal Methods. 2015;7(18):7715–23.
60. Srinivasan V, Sivaramakrishnan H, Karthikeyan B. Detection, isolation and characterization of principal synthetic route indicative impurities in verapamil hydrochloride. Sci Pharm. 2011;79 (3):555.
61. Newberry J, Wichterman J, Kuchta J. Rapid analytical techniques for drinking water security investigations. Am Water Work Assoc J. 2004;96(1):52.
62. Pancrazio J, Whelan J, Borkholder D, Ma W, Stenger D. Development and application of cell-based biosensors. Ann Biomed Eng. 1999;27(6):697–711.
63. Curtis TM, Widder MW, Brennan LM, Schwager SJ, van der Schalie WH, Fey J, Salazar N. A portable cell-based impedance sensor for toxicity testing of drinking water. Lab Chip. 2009;9 (15):2176–83.
64. Cusick KD, Sayler GS. An overview on the marine neurotoxin, saxitoxin: genetics, molecular targets, methods of detection and ecological functions. Mar Drugs. 2013;11(4):991–1018.
65. Wiese M, D'agostino PM, Mihali TK, Moffitt MC, Neilan BA. Neurotoxic alkaloids: saxitoxin and its analogs. Mar Drugs. 2010;8(7):2185–211.
66. Chen J-H, Yu R-C, Gao Y, Kong F-Z, Wang Y-F, Zhang Q-C, Kang Z-J, Yan T, Zhou M-J. Tracing the origin of paralytic shellfish toxins in scallop Patinopecten yessoensis in the northern Yellow Sea. Food Addit Contam Part A. 2013;30(11):1933–45.
67. Botana LM, Vilariño N, Alfonso A, Vale C, Louzao C, Elliott CT, Campbell K, Botana AM. The problem of toxicity equivalent factors in developing alternative methods to animal bioassays for marine-toxin detection. TrAC Trends Anal Chem. 2010;29(11):1316–25.
68. Rodríguez LP, Vilariño N, Molgó J, Aráoz R, Louzao MC, Taylor P, Talley T, Botana LM. Development of a solid-phase receptor-based assay for the detection of cyclic imines using a microsphere-flow cytometry system. Anal Chem. 2013;85(4):2340–7.
69. Turner AD, Hatfield RG, Rapkova M, Higman W, Algoet M, Suarez-Isla BA, Cordova M, Caceres C, van de Riet J, Gibbs R. Comparison of AOAC 2005.06 LC official method with other methodologies for the quantitation of paralytic shellfish poisoning toxins in UK shellfish species. Anal Bioanal Chem. 2011;399(3):1257–70.
70. Ben-Gigirey B, Rodríguez-Velasco ML, Gago-Martínez A. Extension of the validation of AOAC official method SM 2005.06 for dc-GTX2, 3: interlaboratory study. J AOAC Int. 2012;95(1):111–21.
71. Meneely JP, Campbell K, Greef C, Lochhead MJ, Elliott CT. Development and validation of an ultrasensitive fluorescence planar waveguide biosensor for the detection of paralytic shellfish toxins in marine algae. Biosens Bioelectron. 2013;41:691–7.

72. Humpage A, Magalhaes V, Froscio S. Comparison of analytical tools and biological assays for detection of paralytic shellfish poisoning toxins. Anal Bioanal Chem. 2010;397(5):1655–71.
73. Flanagan A, Callanan K, Donlon J, Palmer R, Forde A, Kane M. A cytotoxicity assay for the detection and differentiation of two families of shellfish toxins. Toxicon. 2001;39(7):1021–7.
74. Okumura M, Tsuzuki H, Tomita B-I. A rapid detection method for paralytic shellfish poisoning toxins by cell bioassay. Toxicon. 2005;46(1):93–8.
75. Hayashi R, Saito H, Okumura M, Kondo F. Cell bioassay for paralytic shellfish poisoning (PSP): comparison with postcolumn derivatization liquid chromatographic analysis and application to the monitoring of PSP in shellfish. J Agric Food Chem. 2006;54(2):269–73.
76. Manger RL, Leja LS, Lee SY, Hungerford JM, Kirkpatrick MA, Yasumoto T, Wekell MM. Detection of paralytic shellfish poison by rapid cell bioassay: antagonism of voltage-gated sodium channel active toxins in vitro. J AOAC Int. 2003;86(3):540–3.
77. Cañete E, Diogène J. Comparative study of the use of neuroblastoma cells (Neuro-2a) and neuroblastoma× glioma hybrid cells (NG108-15) for the toxic effect quantification of marine toxins. Toxicon. 2008;52(4):541–50.
78. Hamerman JA, Ogasawara K, Lanier LL. NK cells in innate immunity. Curr Opin Immunol. 2005;17(1):29–35.
79. Brunner K, Mauel J, Cerottini J-C, Chapuis B. Quantitative assay of the lytic action of immune lymphoid cells of 51Cr-labelled allogeneic target cells in vitro; inhibition by isoantibody and by drugs. Immunology. 1968;14(2):181.
80. Zhu J, Wang X, Xu X, Abassi YA. Dynamic and label-free monitoring of natural killer cell cytotoxic activity using electronic cell sensor arrays. J Immunol Methods. 2006;309(1):25–33.
81. McCoy MH, Wang E. Use of electric cell-substrate impedance sensing as a tool for quantifying cytopathic effect in influenza A virus infected MDCK cells in real-time. J Virol Methods. 2005;130(1):157–61.
82. Nambi P, Aiyar N. G protein-coupled receptors in drug discovery. Assay Drug Dev Technol. 2003;1(2):305–10.
83. Pierce KL, Premont RT, Lefkowitz RJ. Seven-transmembrane receptors. Nat Rev Mol Cell Biol. 2002;3(9):639–50.
84. Hall RA, Premont RT, Lefkowitz RJ. Heptahelical receptor signaling: beyond the G protein paradigm. J Cell Biol. 1999;145(5):927–32.
85. Bhattacharya M, Babwah A, Ferguson S. Small GTP-binding protein-coupled receptors. Biochem Soc Trans. 2004;32(6):1040–4.
86. Etienne-Manneville S, Hall A. Rho GTPases in cell biology. Nature. 2002;420(6916):629–35.
87. Yu N, Atienza JM, Bernard J, Blanc S, Zhu J, Wang X, Xu X, Abassi YA. Real-time monitoring of morphological changes in living cells by electronic cell sensor arrays: an approach to study G protein-coupled receptors. Anal Chem. 2006;78(1):35–43.

Chapter 5
Micro/Nano Cell Potential Biosensors

Jiaru Fang, Qin Wang, and Ning Hu

Abstract As a novel functional bioanalytical method, the cell sensor has become one of the hotspots in the field of biosensors. A cell sensor with high sensitivity can make a quick response to external stimuli, and it has good stability and biocompatibility, is nondestructive, and is used for long-time dynamic monitoring for physiological parameters of different types of cells. In general, a cell sensor can relatively easily achieve miniaturization including batch processing, thereby reducing costs. With the development of microelectromechanical systems technology, the technical means to detect extracellular action potentials emerges, such as microelectrode array (MEA) cell potential sensors. MEA is a commonly used method to detect extracellular action potentials that not only can analyze the electrical activity of electrical excitable cells, but can achieve pharmacology and toxicology analysis of different drugs or toxins. This chapter study further improves the method of the cardiomyocyte and sensor chip coupling, and successfully builds a high stability and consistency of a cardiomyocyte potential sensor. It can explain cell sensor availability that uses a cardiomyocyte sensor for drug analysis and to detect toxins in food, thus by taking advantage of the characteristics, the cell sensor can develop a new testing technology in the food field that has great application prospects in detection analysis.

Keywords Microcell potential biosensors • MEA • Cardiomyocytes

5.1 Introduction

Cell potential recording includes intracellular recording and extracellular recording. Intracellular recording includes the traditional fluorescence imaging method and patch-clamp recording. The shortcoming of the fluorescence imaging method is

J. Fang • Q. Wang • N. Hu (✉)
Biosensor National Special Laboratory, Department of Biomedical Engineering, Zhejiang University, Hangzhou, China
e-mail: huning@zju.edu.cn

P. Wang et al. (eds.), *Micro/Nano Cell and Molecular Sensors*,
DOI 10.1007/978-981-10-1658-5_5

that the fluorescence molecular probes have a certain toxicity to cells. Patch-clamp recording needs to use a glass microelectrode to puncture the cell membrane, resulting in certain damage to cells. This method cannot simultaneously record action potential at different sites of cell networks, and cannot achieve intercellular coupling measurement. Although these intracellular potential detection methods have the advantage of a high signal-to-noise ratio, these methods cannot achieve nondestructive and nontoxic detection. Therefore, with the development of microelectromechanical technology, the technological means used to test extracellular action potential emerged. Since the1990s, Fromherz has used a plane sensor array to detect extracellular action potential, the detection means of which mainly include the microelectrode array (MEA) cell potential sensor and field effect transistor (FET) cell voltage sensor.

MEA is a kind of common extracellular action potential test. The method has simple operation and high flux, and can simultaneously detect dozens or even hundreds of channels of cell electrophysiological signals [1, 2]. In 1972, Thomas et al. first put forward using MEA to record electrical excitation of an in vitro culture cell of extracellular action potential [3]. Thomas and others first deposit a layer of nickel on the glass substrate, then plate an electric layer in the nickel layer, and use a microelectrode array pattern photoresist mask template. In the end they use glass with a beeswax ring fixed on a glass substrate, forming cells to be examined. Before cell culture, they adopted the approach of Gesteland and Robinson in the metal plating platinum electrode surface black. With increasing electrode surface, it reduced electrode impedance [4]. Then they cultured chickens' embryonic myocardial cells in an MEA chip and at the same time recorded multiple microelectrode potentials of the myocardial cell signal. The condition of cell signal detection means in the last few decades has become an important method in the field of research. Currently in cardiac electrophysiological study, neurons, synaptic plasticity, high-throughput drug screening, and other areas of the study are playing more and more important roles [5–7].

MEA electrically excited cells can not only analyze (discharge of myocardial cells, neurons, etc.); they also achieve more differently the pharmacology and toxicology of the drug or toxin analysis. It's simple and easy to detect a variety of parameters of electrical excitation cell networks and to detect the cell layer of action potential propagation. Figure 5.1 shows the MEA chips developed by Multi Channel Systems. The company developed the MEA chip and its planar MEA performance shows the best products on the market at present. FET is another cell that has been announced. As well as MEA, it can grow when the nondestructive detection of extracellular action potential is warranted. However, compared to the MEA, the fabrication of FET is relatively complex, which limits its wide application. In this chapter, MEA is mainly discussed in cell potential detection and biomedical application.

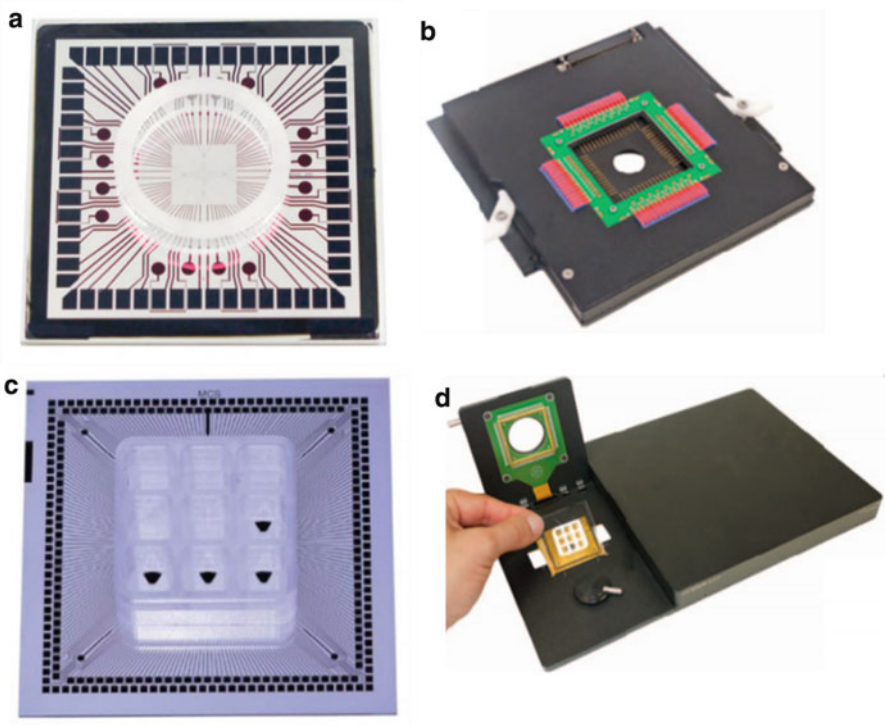

Fig. 5.1 MEA sensor chips developed by multichannel systems (**a**) and (**b**) single-well MEA chip and its detection system (**c**) and (**d**) multiwell MEA chip and its detection system

5.2 Theory of Cell Potential Biosensors

5.2.1 H–H Model of Cardiomyocyte Action Potential

The Na^+ channel, K^+ channel, and Ca^{2+} channel are the three important ion channels in the action potential period of cardiomyocytes. Based on the H–H model of action potential that was put forward by Hodgkin and Huxley, the ion activity of cardiomyocytes in the action potential period is described. Figure 5.2 illustrates the H–H model of cardiomyocyte action potential. In the equivalent circuit, Cm represents membrane capacitance. R_{Na}, R_K, and R_{Ca} represent electrical impedance of sodium channels, the potassium channel, and calcium ion channel, respectively. E_{Na}, E_K, E_{Ca} correspond to the equilibrium potential. I_{total} represents the total membrane current, mainly including capacitive current and ion current, which can be expressed by a mathematical formula as follows.

$$I_{total} = I_{Na} + I_K + I_{Ca} + I_{Cm} \tag{5.1}$$

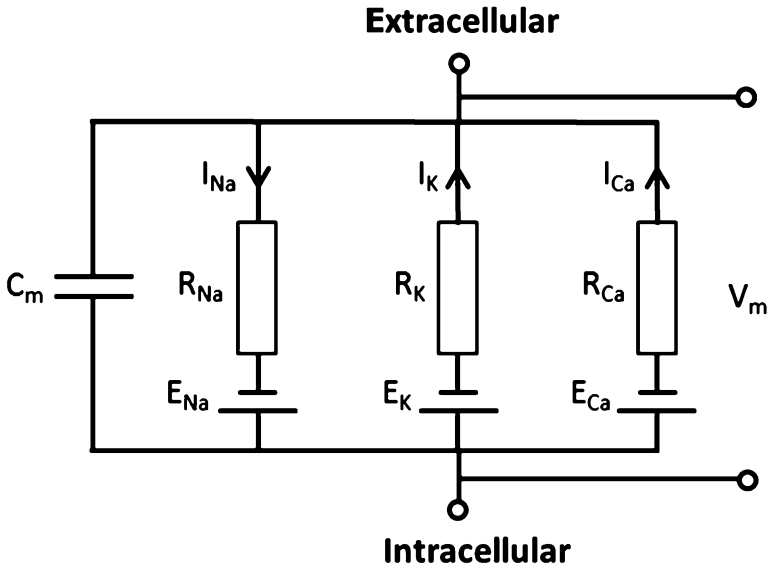

Fig. 5.2 H–H model of cardiomyocyte action potential

$$I_{Cm} = C_m \frac{d_{V_m}}{d_t} \tag{5.2}$$

I_{Cm}: Capacitive current:
I_{Na}, I_K, I_{Ca}:Na^+, K^+, Ca^{2+} current;
V_m: Membrane voltage.

5.2.2 Cell Potential Sensor Model

The cell potential sensor model can be explained by the equivalent circuit in Fig. 5.3. According to the cell–electrode coupling model, the whole circuit can be divided into three parts: (1) the electrophysiological H–H model is the source of the circuit, which mainly includes transmembrane voltage V_m, ion channel current I_{Na}, I_K, I_{Ca}, and membrane capacitance Cm; (2) double electrical layer model of electrode and electrolyte interface (including R_s, R_{ct}, C_l), and sealing resistance R_{seal}. The R_{seal} branch of extracellular voltage is caused by the leakage current of the space between the cells and electrode, which is related to the status of attached cells on the electrodes and the electrode area. Cells are attached more closely and the electrode area is smaller, R_{seal} is bigger, and the leakage current is smaller.

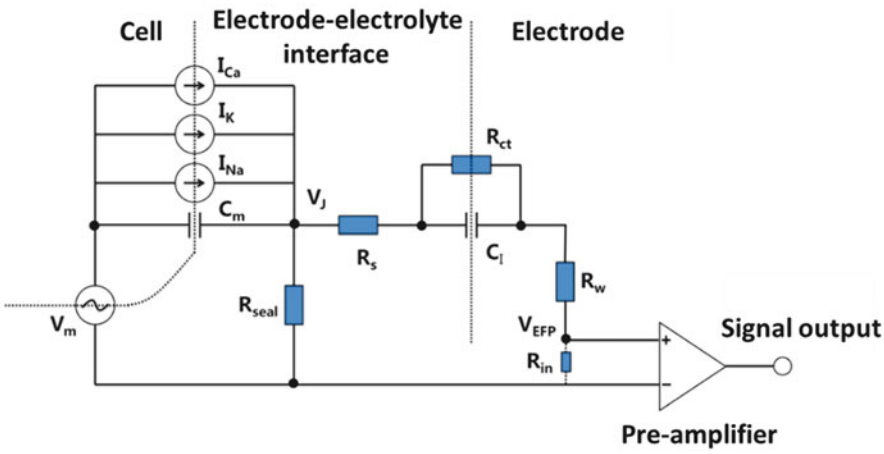

Fig. 5.3 The equivalent circuit model of signaling pathways between extracellular field potential (EFP) and transmembrane potential

(3) R_w as the electrode ontology impedance is very small and negligible. R_{in} is the preamplifier input impedance, and forms a series circuit with R_w. In the equivalent circuit, V_J is the voltage near the cell membrane, which is split into two branches. One branch is a series branch that includes the double electric layer model and R_{in}. Another branch is the R_{seal} branch. V_{EFP} is the R_{in} voltage that is the ultimate detected microelectrode voltage. In order to reduce the loss of signal, the R_{in} value is much higher than the impedance of the other components in the other two branches, so the voltage of the electric double layer is very small and negligible. V_{EFP} and V_J are almost identical. In actual experiments, we usually reduce the electrode area and improve the degree of coupling between the electrodes and cell to increase R_{seal}, and thus improve V_{EFP}, V_{EFP} after amplification, signal amplifier output V_{out}.

In the whole signal transmission process, cell electrical excitation is the source drive, including transmembrane potential and ion channel current. Extracellular field potentials (EFP) and action potential (AP) are synchronous. As shown in Fig. 5.4, cardiomyocytes' EFP spike potential rise is formed through C_{mem}, V_{mem}, and R_{seal}. In the V_{mem} single function, the circuit can be simplified as a C_{mem} and R_{seal} series, the V_{EFP} for R_{seal} voltage on both ends, and the whole circuit can be regarded as a first-order differential of V_{mem}. The action potential fast depolarizes in the composition of EFP Na^+, which wave for the falls of the peak potential plateau of I_{Ca} in the composition of EFP is close to the Na^+ decline in the peak Ca^{2+} wave, phase and fast multipole I_K in EFP ingredients for rising near the Ca^{2+} wave peak K^+ wave. The peak potential, Ca^{2+}, K^+, wave constitute the EFP of myocardial cells.

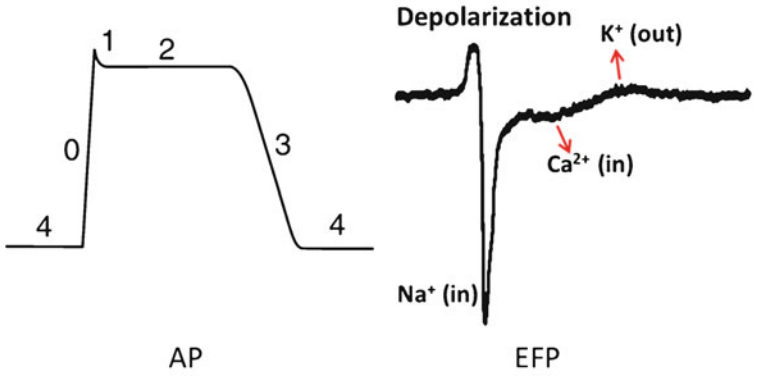

Fig. 5.4 The relationship between cardiomyocyte extracellular field potential and action potential

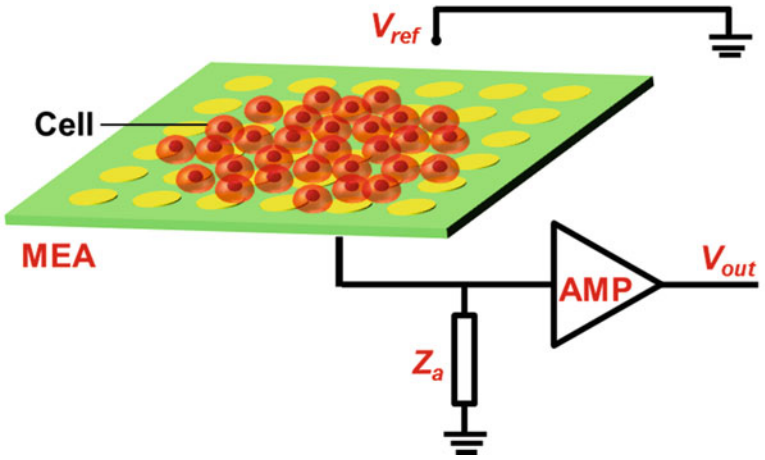

Fig. 5.5 Simplified circuit of EFP of cardiomyocyte by microelectrode array

5.2.3 Detection Principle of EFP

The cell potential sensor can detect with electrical excitation characteristics of extracellular action potential (i.e., cell field potential), such as cardiac muscle cells, nerve cells, and the like. The microelectrode array is now a commonly used cell electric sensor chip. The MEA chip is in the central position of the circular microelectrode array configuration. In Fig. 5.5 for the myocardial cell EFP detection principle, V_{ref} represents the reference voltage in the figure and Z_a represents the preamplifier input impedance. The myocardial cell culture on the MEA chip, through a thin layer of electrolyte electrode coupled with chips. Myocardial cells and MEA couple together, electrical excitation characteristics of myocardial cells producing the action potential. Membrane selectivity of the ion channel opening

and closing causes the cell inside and outside the change of ion concentration. Cell field potential is caused by transmembrane voltage variation and the ion current. Therefore, through the detection of extracellular and ion concentration-related field potential changes, it can effectively record myocardial cell electrophysiological signals.

5.3 MEA-Based Biosensors and Measurement

5.3.1 MEA Chip Design and Fabrication

The design of the MEA chip surface area is 2×2 cm^2, increased four times more than before. In Figs. 5.6 and 5.7 showing MEA chip design, MEA is a 6×6 array configuration, including 32 working electrodes and a single circular electrode size to 30 μm in diameter. The electrode spacing is 300 μm. The configuration of four reference electrodes is in the corners of chip.

MEA mainly consists of three parts: insulating substrate, metal electrode array, and passivation layer. It is produced by the standard microelectronic process (Fig. 5.8). First of all, a 30 nm titanium layer and a 300 nm gold layer are deposited on the glass substrate as the adhesive layer and the electrode layer, respectively. Then electrode sites and lead layout are etched by lithography. After removing the photoresist layer, 1 μm Si_3N_4 is deposited as a passivation layer. And the electrodes and the solder pad are exposed by KOH wet etching technology. Finally, the solder pad of the MEA chip is connected to the PCB pad with gold thread.

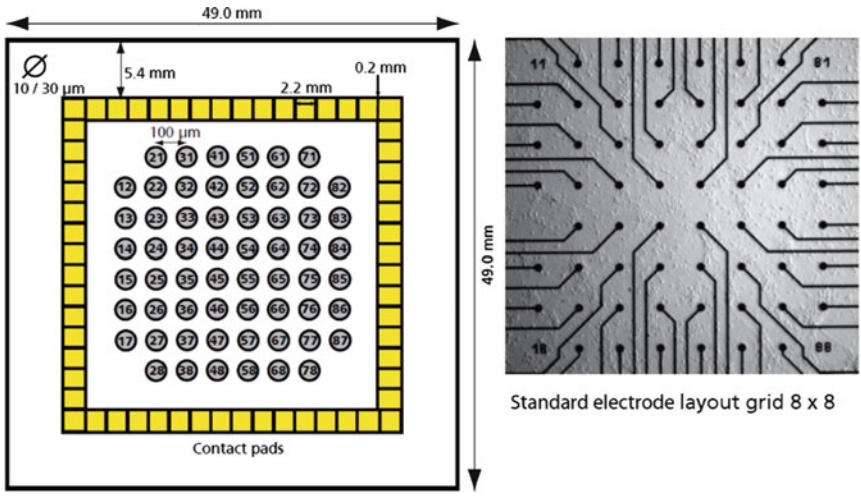

Fig. 5.6 The schematic and optical image of commercial 60-channel MEA chip

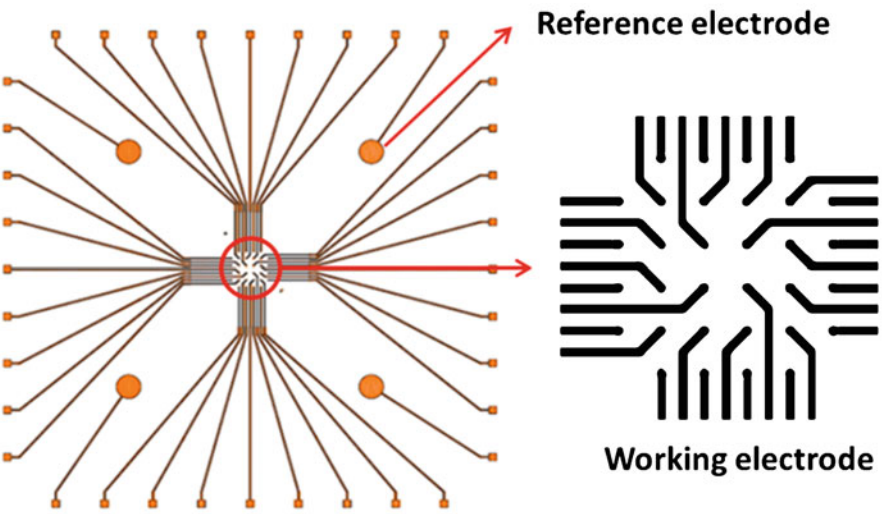

Fig. 5.7 The schematics of 32-channel MEA chip with large reference electrodes and working electrodes

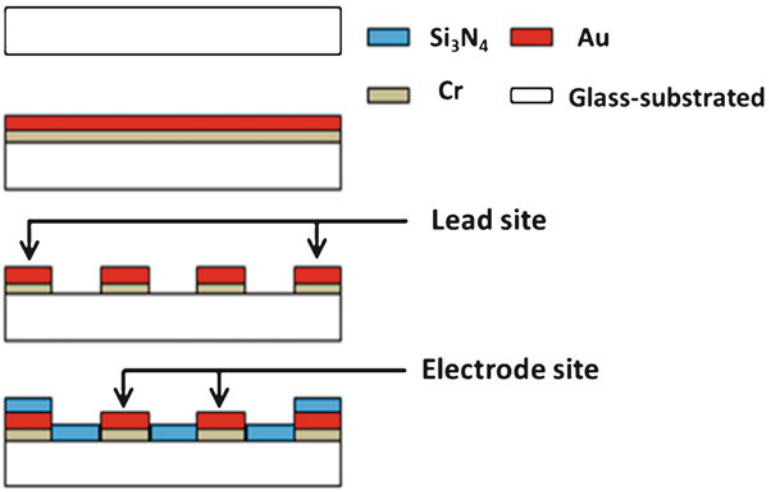

Fig. 5.8 MEA chip processing: (1) Au and Cr deposition. (2) Pattern defined. (3) Lead insulation

Just finished processing the MEA chip, after scribing, SMD, gold spot welding, timely put in vacuum pump. Before using, the cell culture chamber MEA chip package is used in cultured cells. The glue used for silica gel (Dow corning 184) is encapsulated because of its lack of cytotoxicity and it has good biological compatibility that can be widely used. The encapsulation process is as follows.

1. The silicone (Dow corning 184) makeup: 184 silicone including A glue (bottle) and B (small). Before use, it should be in accordance with the proportion of 10 to 1. Because the glue is sticky, the general use of electronic weighing scales is necessary. Preparation: balance, 50 ml tube, size of each disposable syringe (respectively used to take A and B glue, which injector head is cut off, with convenient draw A glue); a glass or metal rod is used for stirring. To formulate A rubber 40 g, 4 g B glue, for example:
    1. Take 50 ml of the tube to add 40 g of a rubber tube.
    2. Add 4 g b rubber tubes.
    3. Use a glass rod to mix glue A and B until both are fully combined. The glue mixture will contain a lot of bubbles, therefore wait for the bubbles as this is commonly used again. The method is to mix good AB glue on 20 spend the night (in room temperature or 4° will solidify).
    4. Use the glue after it has been mixed well and glue bubbles disappear.
2. Gold thread closed and culture chamber encapsulation: with good silica gel that has enclosed bare gold between two rows of solder wire insulated, after being natural cured silicone, then use the same silica gel encapsulation culture chamber. As shown in Fig. 5.9, the MEA chip is suitable for a wireless eight-channel MEA detection system. We use the cell culture chamber disposable plastic syringes after they are equidistant from the electric cutting circular cavity (hole diameter is 1.8 cm, height of 2 cm). The cell cavity is nontoxic, high pressure sterilized, and facilitates the encapsulation.

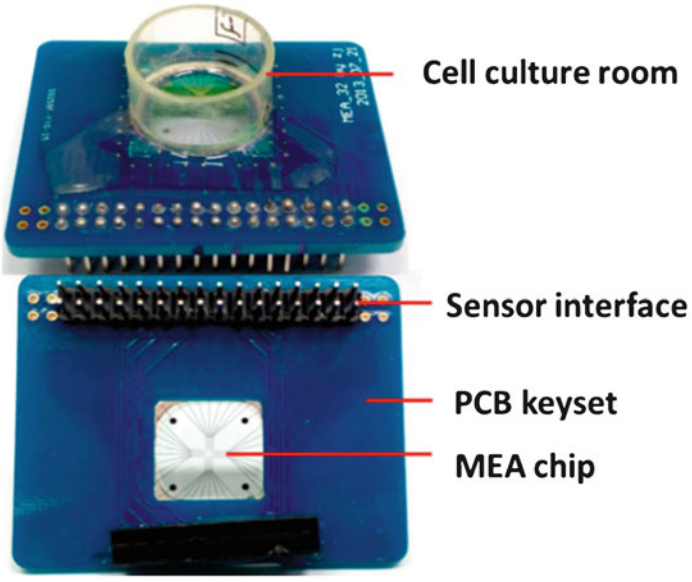

Fig. 5.9 Encapsulation of single-hole MEA sensor with the cell culture chamber and sensor interface of instrument

5.3.2 MEA Chip Surface Modification

At present, the problem on the coupling between the silicon surface and cells is still a major difficulty in the research on cell-based biosensors. The coupling coefficient directly affects the output signal value. It has been demonstrated that loose coupling between the silicon surface and cells will directly lead to a low amplitude signal and make it difficult to extract the useful signals, and even sometimes submerge the useful signals in noise. For example, a microelectrode array is used to detect extracellular field potentials; the amplitude of EFP detected by MEA is low. The signal-to-noise ratio is not high. This is related to the loose coupling between microelectrodes and excitable cells. Therefore, improving the coupling coefficient is the key to building high-performance cell-based biosensors.

In order to reduce the chip contact resistance sensor cells on the surface of a drop, require the cells and tight coupling silicon substrate surface height. The growth of cells on the surface of the sensor, good or bad directly affects the extracellular resistance properties. In order to make the cells better able to grow in what is adhered on the surface of the sensor, there is usually certain physical or chemical processing on the surface. Considering the cell sensors in addition to good adhesion on the surface cells to perform the function of the amplification signal detection box, they cannot be destructive to its surface. For example, in the silicon substrate surface three-dimensional structure, changing the surface pore size and shape will directly affect the detection of the signal. The commonly used methods to promote coupling between the MEA surface and cell are surface hydrophilicity improvement, protein modification, and special structure manufacturing. These three methods are described in detail as follows.

5.3.2.1 Surface Hydrophilicity Improvement Method

The hydrophilic coefficient of the sensor chip surface directly affects cell attachment and cell growth on the sensor surface. Because the cell membrane has a phospholipid bilayer membrane structure, it's hydrophobic towards the cytoplasm and the hydrophilic end towards the extracellular fluid. Therefore cells can only grow on an attached strong hydrophilic surface. When just finished the processing of the surface of the silicon devices is hydrophobic, but the surface hydrophilicity of change can be improved by plasma, by water-based cleaning, hydroxy injection, and other methods. Plasma cleaning refers to the device in the reaction tank after plasma cleaning 2 min, which can remove the organic layer and the oxide that watch is slow, in order to make the material surface activation and rich hydrophilic.

The plasma cleaning with advanced silicon surface cleanliness and sterility, can undertake modification directly. Another method is the hydroxyl injection method, it is to point to in the silicon surface hydroxyl ion implanted directly, thus introduced to the material surface hydrophilicity have the greatest contribution of Si-O-H group. Tsinghua University's Fan Yuwei injected hydroxyl silicon material and

used it for tissue repair engineering. The study found that the surface of the cells' viscosity is greatly increased. For a cell sensor chip, the ion implantation method does not increase the thickness on the surface of the sensor chip; it can improve the signal-to-noise ratio, but will reduce the sensitivity of the sensor to a certain degree.

5.3.2.2 Protein Modification Method

For an ordinary cell line, after plasma cleaning the surface of the material can satisfy the attached growth of cells. With primitive cells (and also a few more delicate cells), after plasma cleaning the surface of the material has difficulty meeting the adhesion for cell growth, so researchers will adopt the method of protein modification to promote the growth of cells in the material surface differentiation. For example, in the microelectrode array chip to cultivate primary hippocampal neurons, the researchers usually use a more poly lysine and laminin modified MEA chip surface. Poly lysine is a richer positively charged group of amino acids, polymers, made from a negatively charged silica surface that becomes positively charged to enhance the surface for cell adhesion.

Laminin (LN) peptides promote the neuron axon growth active site, and in the process of neuronal development stimulate cell adhesion and cell movement. LN can also affect the growth, migration, and differentiation of cells. Again as in the impedance or MEA chip on cultivating the original generation of myocardial cells, researchers usually use fibronectin for material surface modification. Fibronectins (FNs) are the main functions of mediating cell adhesion in the material surface. Purification of FN can promote the connection between the cells and cell adhesion and cells and extracellular matrix. FN can control the shape of the cell signal transduction pathways, regulate cell and cytoskeleton organization, and promote cell spreading.

5.3.2.3 Special Structure Manufacturing Method

In order to make the fixed cell grow in the special structure of the surface of the material, researchers usually keep an independent molecular layer (self-assembled monolayers, SAMs) fixed in the miniature design of the structure of the material surface. At present, the commonly used methods are making the micropattern with laser etching; molecular methods such as sputtering are the microseal. SAMs refers to a thin layer (1–3 nm) of an organic molecular layer. For a cell sensor, SAMs generally refer to the high molecular protein polymers that can enhance cell adhesion.

Natarajan et al. used a laser etching technology on the surface of MEA-carved miniature patterning (Fig. 5.10a), and fibronectin fixed on the surface of the MEA with a good design micropattern, then cultivated the original generation of myocardial cells on the surface to study the functional connection molecules between myocardial cells [8]. As shown in Fig. 5.10b, the myocardial cell after it adhered to

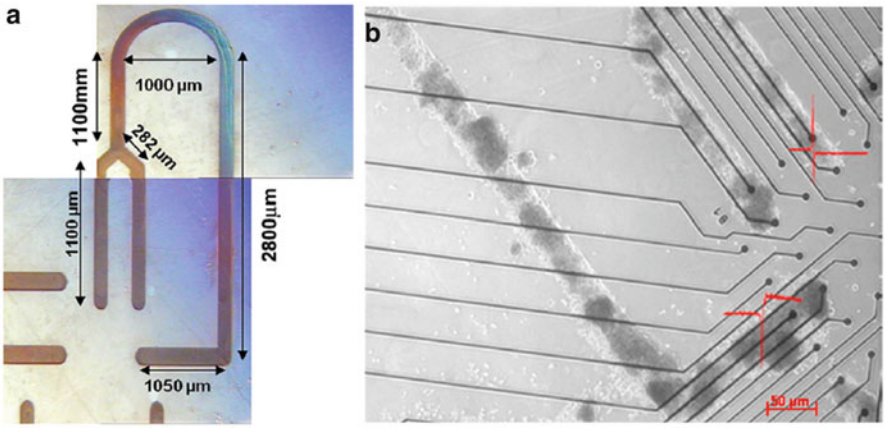

Fig. 5.10 (**a**) Miniature design drawings. (**b**) Cardiomyocytes on a MEA of a micropattern (Reproduced with permission from Ref. [8]. Copyright 2011 Elsevier)

the surface of the SAMs- modified MEA grew well, and almost all cells along the designed pattern structure showed growth differentiation.

Compared with the laser etching technology, microseal (microcontact printing, mμCP) technology is relatively simple. It is a physical method of miniature design manufacturing. In the early 1990s, Kumar and Whitesides' seal method was developed through a miniature design of the structure of the PDMS (polydimethylsiloxane) mercaptan kind of SAMs on Au [9]. μCP are not limited to imprint the mercaptan kind of SAMs on Au. Other SAMs, such as silane coupling agent, lipid, protein, DNA, nanoparticles, and metal film can be covered by mμCP printed on the base of the corresponding. As shown in Fig. 5.11 for the mμCP method of operation process, the preparation of a miniature design of the structure of the PDMS, the PDMS is in the SAMs in the solution. Finally through the PDMS will SAMs on a suitable substrate. Anupama Natarajan et mμCP method MEA surface produces a miniature design structure and cultivates the original generation of hippocampal nerve cells on the surface. Hippocampal neurons grew adhered to the surface of the special structure of the MEA, and most of the cells along the designed pattern tend to the growth of the structure.

5.3.3 Detection System and EFP Measurement

Since its introduction 30 years ago, the technology and related culture methods for electrophysiological cell and tissue assays have been continually improved and have found their way into many academic and industrial laboratories. MEA technology has attracted increased interest because of a growing need to screen selected

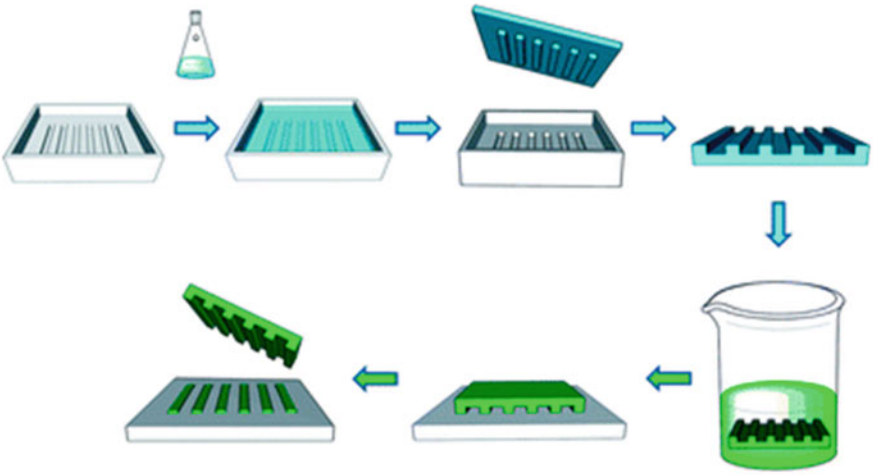

Fig. 5.11 Microcontact printing process based on the PDMS stamp for cell culture ([9] Copyright AIP Publishing LLC)

compounds against ion channel targets in their native environment at the organic, cellular, and subcellular levels.

The microelectrode array system is a compact and innovative tool for in vitro experiments. You can place cell and tissue preparations from heart, brain, and muscle on the MEA and record the electrophysiological signals with the MEA amplifier. The signals are then analyzed with the included software. The modular principle offers various possibilities for a setup extension with perfusion and stimulation devices. The MEA technology is an easy and straightforward approach to apply electrophysiological techniques for drug screening and basic research. Over 600 publications in scientific journals prove its versatility and reliability.

The classical MEA system consists of a data acquisition computer, MEA amplifiers, MEAs, and a temperature controller. The core element is the MEA amplifier with 60 channels. Depending on your experimental need, you can decide whether to build a setup with one, two, or four amplifiers, resulting in a system with 60, 120, or 240 channels, respectively. You can run completely independent experiments on each of the amplifiers. MEA amplifiers are available in two different versions, designed specifically for upright and inverted microscopes. For data acquisition, you can choose either the PCI-bus data acquisition card which is preinstalled in a computer or a USB data acquisition which can easily be connected via USB 2.0 High Speed to any PC or laptop. No matter which option you choose, flexibility, the possibility for setup expansions, and recording and analysis software MC_ Rack are always included (Fig. 5.12).

To establish the portable cardiomyocyte-based potential biosensors, cardiomyocytes and nanoplatinum electroplated MEAs are employed and the portable wireless eight-channel MEA system is used for noninvasively monitoring electrical activity of the cardiomyocytes. Cardiomyocytes are cultured on the

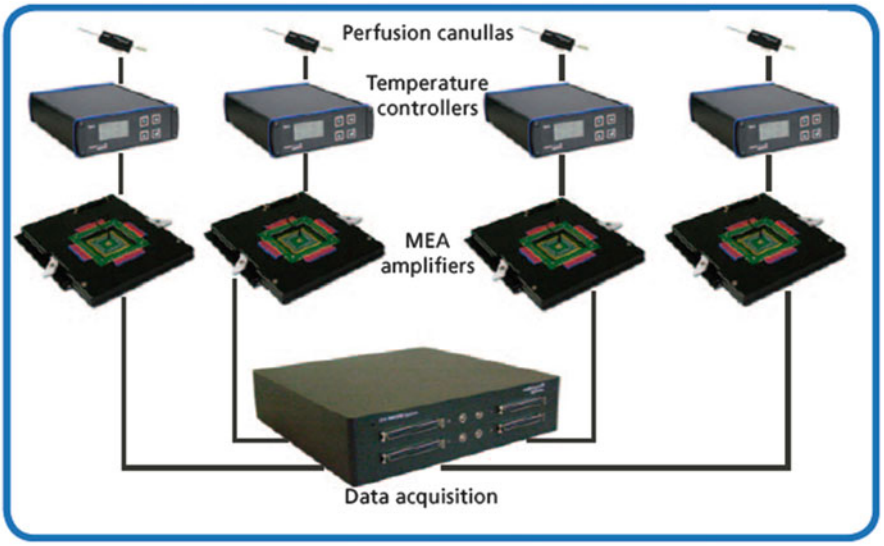

Fig. 5.12 Classical MEA systems developed by the Multi Channel System Company for high-throughput systems

surface of MEA which is modified with a self-assembled monolayer. When cell–electrode coupling forms, there still exists a nanoscale gap between them filled with a trace amount of electrolyte. For electrogenic cells in excitation phase, transient transmembrane potential and ionic current generate and polarize the electrodes by re-establishing the charge distribution at the electrode–electrolyte cell interface. In that way, the electrodes record changes in voltage as EFP. Generally, their components originate from the derivative of the transmembrane potential and ionic flows including Na^+, Ca^{2+}, and K^+ in different phases of action potential [2].

EFP recording is performed by a self-developed portable wireless eight-channel MEA system. The recording system is packaged into a 13 cm long, 10 cm wide, and 4 cm high plastic case that weighs about 400 g with battery packs installed (Fig. 5.13). The recording system consists of three main parts: an eight-channel signal conditioning circuit that amplifies and filters EFP signals from the MEA chip. An embedded Wi-Fi module integrates a Cortex-M3 microcontroller STM32F205 and a user interface to handle the data captured by the STM32F205. The Wi-Fi module acts as an access point, and a PC or iPad device can wirelessly connect to the module directly. The A/D conversion for each channel is set to a 15 kHz sampling rate, and the up to 54 M bits per second (Mbps) wireless link easily supports transmission of eight channels of captured cardiomyocyte EFP data synchronously. The sensor chip mounted onto a sensor interface is connected to the signal conditioning circuit through a zero-insertion-force socket. Cardiomyocyte EFP signals are bandpass-filtered from 0.5 Hz to 4 kHz and are amplified with a total voltage gain of 60 dB. The input-referred noise level of the system is maintained within 20 μV, which can easily afford the measurement of EFP from

Fig. 5.13 Wireless eight-channel MEA detection system (Reproduced with permission from Ref. [10]. Copyright 2015 Elsevier B.V.)

the cardiomyocyte network. Because the packets are transmitted over the wireless local area network, the detection system provides a large transmission distance up to 50 m which enables experimenters to be able to operate the device within almost any laboratory or open field context.

5.4 Application in Biomedicine and Food Analysis

The cell-based potential biosensor is an emerging technology that can be used to noninvasively and instantaneously detect and analyze cell responses to chemical and biological agents. This section highlights the fabrication and measurement technologies of cell impedance sensors, and their application uses in toxin detection and anticancer drug screening. We start with an introduction that describes the capability and advantages of cell-based sensors over conventional sensing technology, followed by a discussion of the influence of cell adhesion, spreading and viability during cell patterning on the subsequent impedance measurements, and sensing applications. We then present an electronic circuit that models the cell–

electrode system, by which the cellular changes can be detected in terms of impedance changes of the circuit. Finally, we discuss the current status of using cell potential sensors for toxin detection and anticancer drug screening.

5.4.1 Cardiac Pathology Research

Cardiomyocytes, isolated from embryonic chicken, neonatal rat or mouse, or cardiac cell lines such as HL-1 cells can be cultured on the MEA dish. The cells couple by gap junctions and form a functional syncytium with one or multiple pacemakers. The cell culture can be paced by external or internal stimulation electrodes. The cardiac cell culture on MEA is a valuable assay system in cardiac toxicity and safety pharmacology research. It can also be used as a model system for arrhythmia research. The multitude of electrodes allows measuring conduction velocity and plotting local activation time maps.

Cultured heart cells are useful for the study of cardiac pathology. Indeed, isolated rat cardiac myocytes have been used as an experimental model in the study of anoxic cell injury since the early 1980s. One major advantage is that these cells can be easily obtained from embryonic or neonatal animals, and they provide the means of studying cellular morphology, biochemistry, and electrophysiological characteristics of the mammalian heart [11]. Thus far, cultured cardiac myocyte models have proven to be very useful for the study of hypoxic injury and hypoxic preconditioning [12–17]. The use of isolated cardiac myocyte models to study cardiac functions has been reviewed [18]. The effects of cardiac hypoxia are often correlated with the functionality of the cells before and after hypoxic episodes using a patch-clamp approach [14]. There is no doubt that the patch-clamp technique can yield important information on the cellular electrophysiology of a few cells. This approach, however, cannot provide a comprehensive picture of cell-to-cell signal propagation characteristics, and continuous long-term recording is not practical; the microelectrode arrays may provide the answers to these problems. The rationale behind the use of MEAs is based on the integration of multiple cells on microchips in order to detect changes of extracellular electrophysiological signals. This system enables the recording of many cells simultaneously, which is useful when a global view of a population of cells is desired as in the case of cardiac hypoxia. Our previous studies have demonstrated the potential application of cultured embryonic cardiac-myocyte–integrated field effect transistor arrays in pharmacological bioassay.

The MEA recording is carried out with integrated metal electrodes that sense the electrical field potentials of spontaneously beating or electrically stimulated clusters of hESC-CM plated directly on the MEA dishes. The cells can be cultured for up to 2 weeks on the MEA dish and subsequent long-term recordings allow monitoring of the differentiation and maturation process. When a sufficiently adult phenotype is established, a cumulative dose-response experiment with increasing concentrations of a pharmacologically relevant drug is performed. In

order to increase the throughput, it is possible to transfer the assay from a multielectrode single-well approach into a multiwell layout with a limited number of electrodes per well. To establish an industry standard high-throughput compatible platform, a 96-well format can be used that matches the standards defined by the Society for Biomolecular Screening (SBS standard). To automate the assay, a liquid handling robot can be added and integrated in the electrophysiological sensing platform. To further enhance the convenience of the assay, data acquisition and analysis software may assist the user in obtaining report sheets with dose-response curves and analysis of the proarrhythmic potential of the drug.

Because the regenerative capacity of adult heart tissue is limited, any substantial cell loss or dysfunction, such as occurs during myocardial infarction, is mostly irreversible and may lead to progressive heart failure, a leading cause of morbidity and mortality. Similarly, tissue loss or dysfunction at critical sites in the cardiac electrical conduction system may result in inefficient rhythm initiation or impulse conduction, requiring the implantation of a permanent electronic pacemaker. Transplantation of excitable myogenic cells within the dysfunctional zone is a possible therapeutic approach to restoring cardiac electromechanical functions. Although several cell types have been proposed, the inherent structural, electrophysiological, and contractile properties of cardiomyocytes strongly suggest that they may be the ideal donor cell type. However, clinical application of this strategy is hampered by the paucity of cell sources for human cardiomyocytes and by the limited evidence of direct functional integration between host and donor cells. Human ES cells represent a promising source of donor cardiomyocytes. These unique cell lines, isolated from human blastocysts, can be propagated in the undifferentiated state in culture and coaxed to differentiate into derivatives of all three germ layers. Recently, a reproducible cardiomyocyte differentiating system was established by culturing hES cells as three-dimensional differentiating cell aggregates termed embryoid bodies. Cells isolated from spontaneously beating areas of the cultures displayed structural, molecular, and functional properties of early-stage cardiomyocytes. More recently, we have demonstrated that this differentiating system generates in vitro a functional cardiomyocyte syncytium with spontaneous pacemaker activity and action-potential propagation. Here we explore the utility of this unique tissue in cell therapy procedures aimed at restoring myocardial electromechanical functions. We show that excitable cardiac tissue generated from hES cells integrates structurally and functionally in vitro over the long term with rat cardiomyocyte cultures. Human ES cell-derived cardiomyocytes were also tested in a large animal model of complete atrioventricular block. The cardiac conduction system consists of specialized cells that generate and conduct the electrical impulse in the heart (Fig. 5.14).

Over the past decades, many novel chemical and therapeutic methods and agents were explored for heart diseases and regeneration. However, a number of cardiovascular or noncardiovascular agents have been withdrawn from the market due to the sudden cardiac death cases, and drug-induced cardiotoxicity became the leading cause of drug withdrawal or development termination [20, 21]. Among these cases, the QT interval prolongation is associated with a trend to develop torsades de

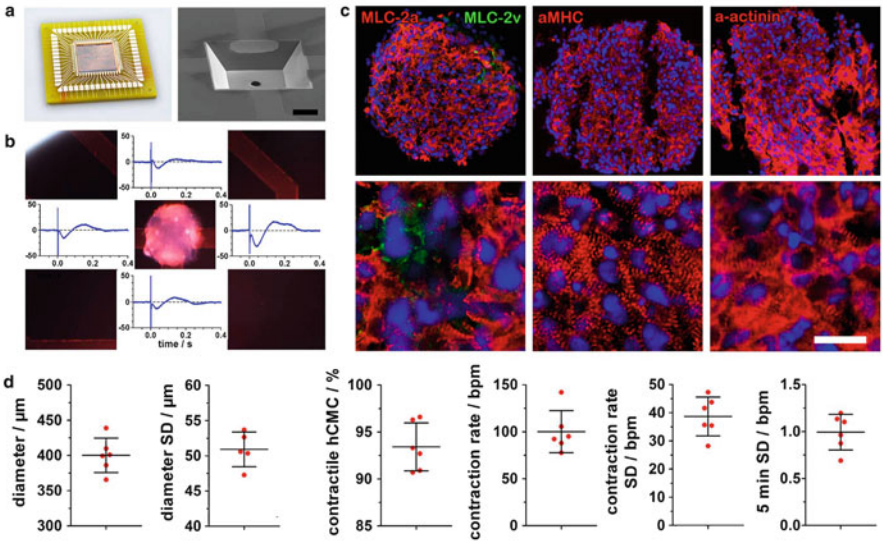

Fig. 5.14 (**a**) Microcavity array and SEM image of an automated positioning hole in a cavity. (**b**) The field potential of cardiomyocytes can be recorded on four electrodes. (**c**) The hCMC consist of highly enriched cardiomyocytes and a smaller amount of ventricular cardiomyocyte characteristics. (**d**) Size and electrophysiological characteristics of differentiation experiments each with 36 hCMC (mean 6 s.d.) (Reproduced with permission from Ref. [19]. Copyright 2013 Jahnke et al.)

pointes (TdP), a ventricular tachyarrhythmia [22, 23]. TdP presents a twisting of the QRS complex in the electrocardiogram (ECG), and TdP can revert to normal sinus rhythm or degenerate into the ventricular fibrillation, which is threatening to human life without prompt medical intervention. The rapid delayed rectifier current I Kr determines the ventricular action potential duration. Conventionally, TdP-risk of new drug candidates should be assessed by high-throughput hERG inhibition screening (e.g., hERG protein drug-binding, noncardiac cell lines hERG overexpression with automated patch-clamp at the early drug development stages).

These early analysis approaches have the features of high throughput and low cost. However, the acquired information is less significant than the study of effects on I Kr by the gold-standard manual patch-clamp [24]. Gradually, automated patch-clamp systems are created to improve the high-quality data and throughput of the manual patch-clamp for assessing hERG inhibition. Human induced pluripotent stem cell-derived cardiomyocytes (iPSC-CMs) can be cultured in vitro for single-cell recording by an automated patch-clamp system and multicellular recording by a microelectrode array system. Most studies focus on the iPSC-CMs electrophysiological measurement that can reflect the drug cardiotoxicity directly [25–27], whereas the beating function of iPSC-CMs is largely ignored. The beating function of iPSC-CMs is similar to the contraction and relaxation of the heart based on the excitation–contraction coupling where Ca2+ is considered to be crucial [28]. In the

former study we had established a cardiomyocyte-based biosensor by primary neonatal rat cardiomyocytes and sensor impedance for monitoring growth and beating of cardiomyocytes simultaneously [29], which can be used for some ion channel drug tests. However, the lack of hERG channels was a significant problem, which was meaningless for hERG inhibitor screening. Hu and his coworker employed the ECIS (electric cell–substrate impedance sensing) technology to screen the hERG inhibitor [30] (Figs. 5.15 and 5.16).

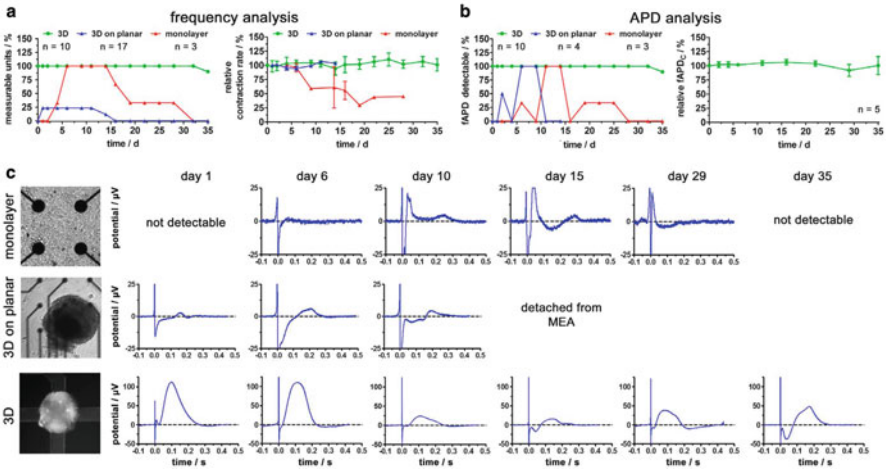

Fig. 5.15 (**a**) EFP firing rate recorded by microelectrode array for 35 days. (**b**) Analysis of the occurrence and stability of fAPD over 35 days. (**c**) The detection of field potentials with three types of microelectrode arrays (Reproduced with permission from Ref. [19]. Copyright 2013 Jahnke et al.)

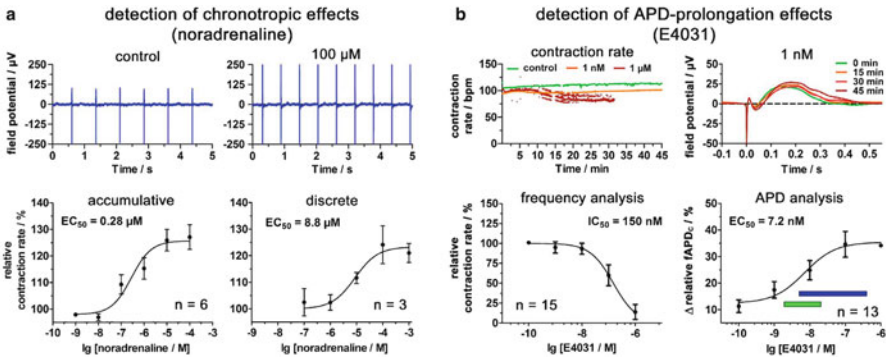

Fig. 5.16 (**a**) Detection field potential of hCMC when it began (control) and after application of 100 µM noradrenaline. The concentration response curves have different EC50 values for the accumulative ($n = 6$ hCMC) and discrete application ($n = 3$ hCMC). (**b**) Analysis of adverse side effects can be detected and quantified with relevant APD prolongation (Reproduced with permission from Ref. [19]. Copyright 2013 Jahnke et al.)

Cardiotoxic chemicals and drugs can cause severe effects on the functions of the heart, such as alteration in the contractility and change in cardiac rhythm that can alter blood pressure and ischemia. These toxic effects range from subclinical abnormalities to life-threatening states. The effects may be related to drug exposure or medical therapy, but also to long-term cardiovascular effects. Safety pharmacology concerns are the major cause of drug attrition during the clinical development phases and account for approximately 35–40 % of all drug attrition. Of these, cardiovascular-related toxicities dominate, with 19 % of the withdrawn drugs. A significant proportion of these toxicities are due to functional and dose-dependent effects. Approximately half of the 19 % withdrawals are caused by arrhythmia effects, including potentially life-threatening states such as drug-induced torsades de pointes (Fig. 5.17).

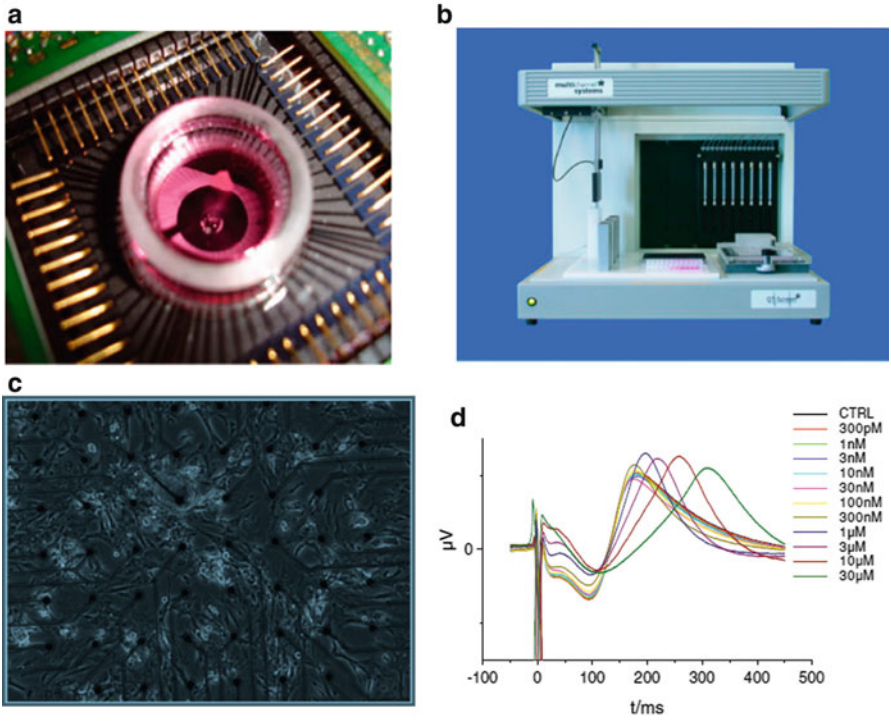

Fig. 5.17 (**a**) High-throughput microelectrode array. (**b**) Instrument of MEA measurement cell. (**c**) MEA under the microscope. (**d**) Graph from a MEA recording at concentrations from 300 pM to 30 µM (Reproduced with permission from Ref. [31]. Copyright 2015 Elsevier B.V.)

5.4.2 Cardiac Safety Evaluation

Cardiac safety plays a significant role in the development and approval of new drug discovery. Many drugs are restricted due to cardiac safety problems, and even withdrawn from the market. According to statistics, about 45 % of approved drugs were withdrawn due to cardiovascular adverse effects. In these cases, most withdrawal drugs can cause the tip of the reverse torsades de pointes. TdP is a life-threatening ventricular tachycardia. It is a term used to describe a form of electrocardiogram (ECG) at the baseline of oscillation. TdP, automatically suppressed, will deteriorate into a life-threatening ventricular fibrillation. The cause of typical TdP is rapidly delayed rectifier K^+ on the myocardial cell membrane ion channel I_{Kr} being restrained. I_{Kr} by human Mr-a-go-go–related gene coding, is the human ventricular myocyte repolarization of the main current. When I_{Kr} is restrained, it causes depolarization and repolarization time extension, namely the QT interval extension, resulting in early after depolarization, eventually leading to TdP. Therefore, hERG channel inhibition assessment is necessary for drug cardiac safety [32].

Drug-induced long QT is most commonly induced by affecting the rapid potassium current Ikr by binding to the hERG ion channel [33]. For both cardiac and noncardiac drugs, primary canine or rabbit Purkinje fibers or cell lines ectopically expressing the hERG ion channel are the preclinical in vitro test systems currently available. Species differences, or the lack of complex ion channel interactions in transgenic cell lines, reduce the predictive value of these systems. For example, determination of the IC50 value for a drug compound in transgenic cell lines oversimplifies a complex process that is state, time, and voltage dependent. Some drugs such as dofetilide require channel activation to reduce the hERG current [34], whereas others, such as fluvoxamine, interact exclusively with a closed channel. Finally, not all drugs that block hERG channels in these cell systems carry an arrhythmogenic risk; one well-known example is verapamil [35]. Also of note: many antiarrhythmics can interact with multiple ion channels simultaneously. In addition to potassium channels, the activity of a heart cell is largely dependent on sodium and calcium channels. Whereas activation of sodium channels is required for the generation of an action potential, inward Ca2+ currents through (L-type) calcium channels counterbalance outward potassium currents in the repolarization phase. To illustrate the complexity of predicting QT prolongation, a recent comparison of 10 drugs on dog Purkinje fibers demonstrated a wide range of effects on QT time, ranging from 158 % prolongation to 16 % shortening, whereas all compounds blocked hERG channels by more than 50 %.

Disinfection by-products (DBPs) are an unintended consequence of drinking water disinfection and are formed when the disinfectant residual reacts with natural organic matter or organic compounds present in the source water. The presence of DBPs in treated drinking water is an important public health concern as many DBPs are associated with adverse health outcomes. Rapid toxicity testing of DBPs is desirable as the number of identified DBPs increases. The N-nitrosamines are a

group of emerging DBPs. N-Nitrosodimethylamine (NDMA) is the nitrosamine most commonly detected as a DBP and has been detected in treated drinking water in California, Ontario, and Alberta [14, 17].

A major limitation to using mammalian cell-based biosensors for field testing of drinking water samples is the difficulty of maintaining cell viability and sterility without an onsite cell culture facility. Curtis describes a portable automated bench-top mammalian cell-based toxicity sensor that incorporates enclosed fluidic biochips containing endothelial cells monitored by electric cell–substrate impedance sensing technology [36]. Long-term maintenance of cells on the biochips is made possible by using a compact, self-contained disposable media delivery system. The toxicity sensor monitors changes in impedance of cell monolayers on the biochips after the introduction of water samples. The fluidic biochip includes an ECIS electronic layer and a polycarbonate channel layer, which together reduce initial impedance disturbances seen in commercially available open-well ECIS chips caused by the mechanics of pipetting while maintaining the ability of the cells to respond to toxicants. Toxicant responses of bovine pulmonary artery endothelial cells grown on fluidic biochips are similar to cells on commercially available open-well chips, and these cells can be maintained in the toxicity sensor device for at least 9 days using an automated media delivery system. Longer-term cell storage is possible; bovine lung microvessel endothelial cells survive for up to 4 months on the fluidic biochips and remain responsive to a model toxicant. This is the first demonstration of a portable bench-top system capable of both supporting cell health over extended periods of time and obtaining impedance measurements from endothelial cell monolayers after toxicant exposure.

5.4.3 Food Analysis

Food analysis includes determination of trace elements, residual pesticides, drugs, toxins (natural toxins), hormones, microbiology, and additives in food. Although the cardiomyocyte-based potential biosensor is rarely used in food analysis currently, it attracts more and more researchers' attention due to its high sensitivity and dynamic detection. With further study in potential biosensors, Wang [10] used a cardiomyocyte-based potential biosensor to detect marine toxins. Marine toxins, mainly produced by algae, are easily accumulated to a high level in filter-feeding fish or shellfish through the food chain. These toxins show no toxicity to shellfish and fish, but they pose high toxicity to humans and even cause human death [37, 38].

In Wang's work, a portable cardiomyocyte-based potential biosensor is designed for rapid detection of saxitoxin (STX) and brevetoxin 2 (PbTx-2). STX and PbTx-2 are two typical and dangerous marine toxins. They exert their biological effects through interactions with sites 1 and 5 of the α subunit of the voltage-dependent sodium channel (VDSC), respectively [39, 40]. VDSC is responsible for the sodium current and depolarization phase of action potential in excitable cells, such as cardiomyocytes and neurons. STX is a potent and selective inhibitor of VDSC, which produces a blockade of action potentials [41], and may affect cardiac and

neural electrophysiological activity. In contrast to STX, PbTx-2 is known as a VDSC activator, which triggers repetitive action potential discharges [42], and leads to action potential depression and complete blockade [43].

The cardiomyocyte-based potential biosensor is constructed of a cardiomyocyte and microelectrode array with a label-free and realtime wireless eight-channel recording system that can dynamically monitor the extracellular field potential of the cardiomyocyte network. When the potential biosensor was exposed to STX or PbTx-2, the EFP signal of this biosensor was affected by the toxins due to their action mechanism. Cell field potential changes in the level can reflect the toxicity level [10] (Figs. 5.18 and 5.19).

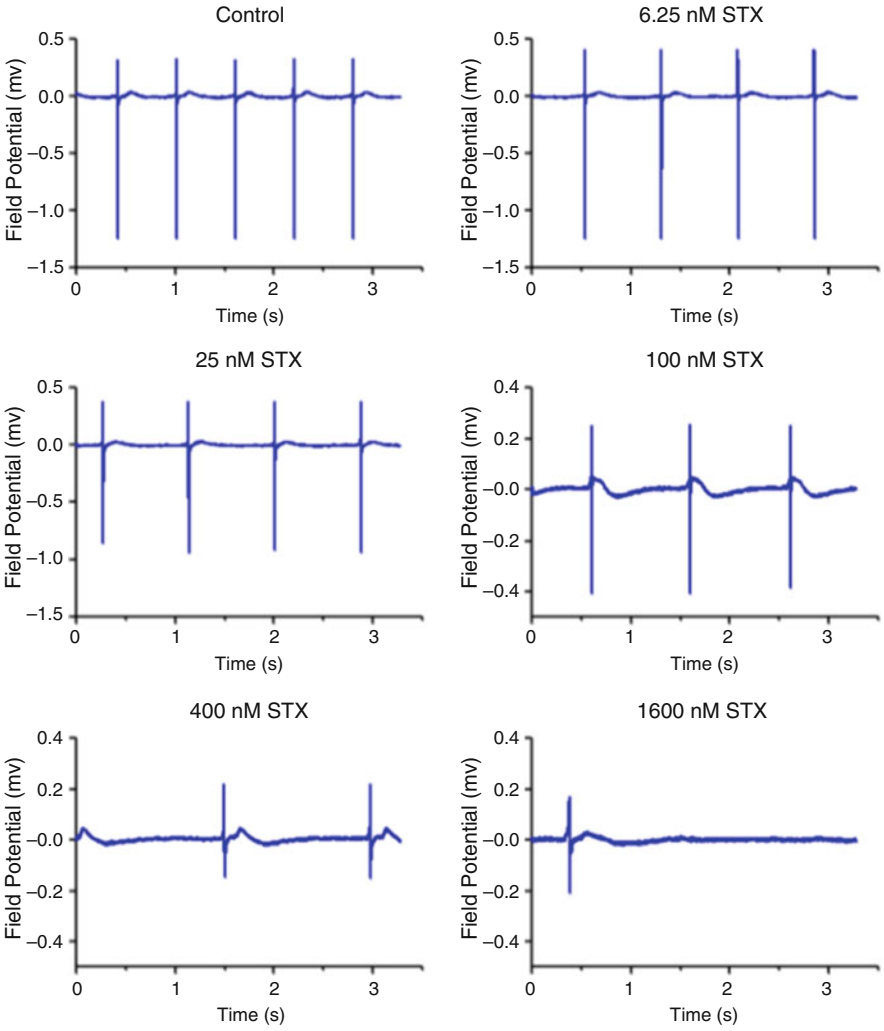

Fig. 5.18 Changes in EFP signals after adding STX with different concentrations (Reproduced with permission from Ref. [10]. Copyright 2015 Elsevier B.V.)

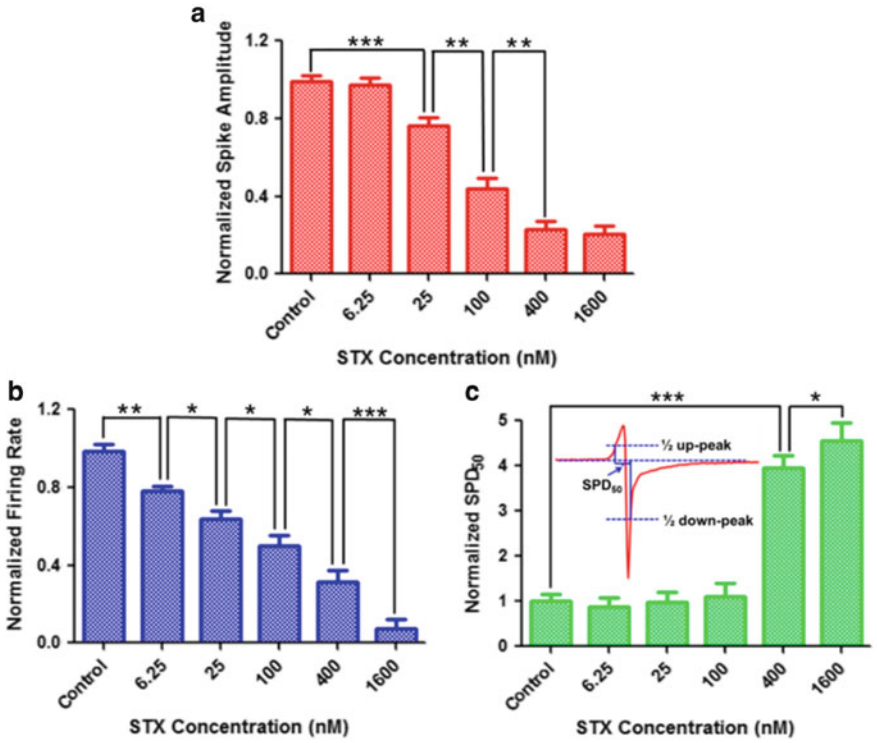

Fig. 5.19 The statistics of the three characteristic parameters of the measured signal change with the different concentrations of STX after 5 min. Data represent six independent experiments from three different isolations (Reproduced with permission from Ref. [10]. Copyright 2015 Elsevier B.V.)

The results show that the most sensitive parameters to STX and PbTX-2 are the firing rate and SPD50, respectively. Consequently, the linear dependence of biosensors is analyzed on the firing rate and SPD50 for STX and PbTX-2, respectively. The recording signal parameters, spike amplitude, firing rate, and 50 % of spike potential duration (SPD50) extracted from the extracelluar field potential signals of the potential biosensor are analyzed to evaluate quantitatively the toxicological risk of STX and PbTx-2. The firing rate of biosensor signals presents high sensitivity to STX with the detection limit of 0.35 ng/ml within 5 min. SPD50 shows high sensitivity to PbTx-2 with the detection limit of 1.55 ng/ml within 5 min. Based on the multiparameter analysis, the cardiomyocyte-based potential biosensor will be a promising tool for rapid detection of these two toxins.

5.4.4 *Other Applications*

Cellular potential biosensors show tremendous promise in quantifying cellular events such as adhesion, spreading, growth, motility, and in serving as a predictor of in vivo responses to environmental toxins, pharmacological drugs, and other chemicals and substances.

5.5 Summary

The broad range of applications is reflected by the variety of MEAs with different geometries that have been developed to cover as many applications as possible. The biological sample can be positioned directly on the recording area; the MEA serves as a culture and perfusion chamber. A temperature controller controls the temperature in the culture chamber. Various culture chambers are available, for example, ones with leakproof lids or with semipermeable seals. An incubator is not necessarily required; long-term recordings in the MEA culture chamber are possible over several weeks or even months. Cellular potential biosensors show tremendous promise in quantifying cellular events such as adhesion, spreading, growth, motility, and in serving as a predictor of in vivo responses to environmental toxins, pharmacological drugs, and other chemicals and substances.

The cardiomyocyte-based potential biosensor offers a unique and powerful method to assess the actions of drugs and chemicals on the function of cardiomyocyte networks. As toxicity testing approaches a transition to higher-throughput predictive approaches in the future there will be a need to address the actions of chemicals on physiological endpoints using reliable in vitro techniques. Few if any physiological approaches offer the potential depth, breadth, and rapid collection of information that can be gained from in vitro MEA approaches.

References

1. Xiao L, Hu Z, Zhang W, Wu C, Yu H, Wang P. Evaluation of doxorubicin toxicity on cardiomyocytes using a dual functional extracellular biochip. Biosens Bioelectron. 2010;26 (4):1493–9.
2. Meyer T, Boven K-H, Günther E, Fejtl M. Micro-electrode arrays in cardiac safety pharmacology. Drug Saf. 2004;27(11):763–72.
3. Thomas C, Springer P, Loeb G, Berwald-Netter Y, Okun L. A miniature microelectrode array to monitor the bioelectric activity of cultured cells. Exp Cell Res. 1972;74(1):61–6.
4. Gesteland R, Howland B, Lettvin J, Pitts W. Comments on microelectrodes. Proc IRE. 1959;11 (47):1856–62.
5. Kornblum A, Pillekamp F, Matzkies M, Fleischmann B, Bonnemeier H, Schunkert H, Brockmeier K, Hescheler J, Reppel M. A new model to perform electrophysiological studies in the early embryonic mouse heart. Cell Physiol Biochem. 2013;32(1):1–10.

6. Johnstone AF, Gross GW, Weiss DG, Schroeder OH-U, Gramowski A, Shafer TJ. Microelectrode arrays: a physiologically based neurotoxicity testing platform for the 21st century. Neurotoxicology. 2010;31(4):331–50.
7. Caspi O, Itzhaki I, Kehat I, Gepstein A, Arbel G, Huber I, Satin J, Gepstein L. In vitro electrophysiological drug testing using human embryonic stem cell derived cardiomyocytes. Stem Cells Dev. 2009;18(1):161–72.
8. Natarajan A, Stancescu M, Dhir V, Armstrong C, Sommerhage F, Hickman JJ, Molnar P. Patterned cardiomyocytes on microelectrode arrays as a functional, high information content drug screening platform. Biomaterials. 2011;32(18):4267–74.
9. Kumar A, Whitesides GM. Features of gold having micrometer to centimeter dimensions can be formed through a combination of stamping with an elastomeric stamp and an alkanethiol "ink" followed by chemical etching. Appl Phys Lett. 1993;63(14):2002–4.
10. Wang Q, Fang J, Cao D, Li H, Su K, Hu N, Wang P. An improved functional assay for rapid detection of marine toxins, saxitoxin and brevetoxin using a portable cardiomyocyte-based potential biosensor. Biosens Bioelectron. 2015;72:10–7.
11. Chlopcikova S, Psotová J, Miketová P. Neonatal rat cardiomyocytes-a model for the study of morphological, biochemical and electrophysiological characteristics of the heart. Biomed Pap Palacky Univ Olomouc. 2001;145(2):49–55.
12. Oshima Y. Postcolumn derivatization liquid chromatographic method for paralytic shellfish toxins. J AOAC Int. 1995;78(2):528–32.
13. Yang J, Lin Y, Guo Z, Cheng J, Huang J, Deng L, Liao W, Chen Z, Liu Z-G, Su B. The essential role of MEKK3 in TNF-induced NF-kB activation. Nat Immunol. 2001;2(7):620–4.
14. Bollensdorff C, Knopp A, Biskup C, Zimmer T, Benndorf K. Na^+ current through KATP channels: consequences for Na^+ and K^+ fluxes during early myocardial ischemia. Am J Phys Heart Circ Phys. 2004;286(1):H283–95.
15. Eigel B, Gursahani H, Hadley R. ROS are required for rapid reactivation of Na^+/Ca^{2+} exchanger in hypoxic reoxygenated guinea pig ventricular myocytes. Am J Phys Heart Circ Phys. 2004;286(3):H955–63.
16. Webster KA, Discher DJ, Bishopric NH. Cardioprotection in an in vitro model of hypoxic preconditioning. J Mol Cell Cardiol. 1995;27(1):453–8.
17. Hausenloy DJ, Yellon DM, Mani-Babu S, Duchen MR. Preconditioning protects by inhibiting the mitochondrial permeability transition. Am J Phys Heart Circ Phys. 2004;287(2):H841–9.
18. Diaz RJ, Wilson GJ. Studying ischemic preconditioning in isolated cardiomyocyte models. Cardiovasc Res. 2006;70(2):286–96.
19. Jahnke H-G, Steel D, Fleischer S, Seidel D, Kurz R, Vinz S, Dahlenborg K, Sartipy P, Robitzki AA. A novel 3D label-free monitoring system of hES-derived cardiomyocyte clusters: a step forward to in vitro cardiotoxicity testing. PLoS ONE. 2013;8(7):e68971.
20. Kola I, Landis J. Can the pharmaceutical industry reduce attrition rates? Nat Rev Drug Discov. 2004;3(8):711–6.
21. Bowes J, Brown AJ, Hamon J, Jarolimek W, Sridhar A, Waldron G, Whitebread S. Reducing safety-related drug attrition: the use of in vitro pharmacological profiling. Nat Rev Drug Discov. 2012;11(12):909–22.
22. Fermini B, Fossa AA. The impact of drug-induced QT interval prolongation on drug discovery and development. Nat Rev Drug Discov. 2003;2(6):439–47.
23. Jeyaraj D, Ashwath M, Rosenbaum DS. Pathophysiology and clinical implications of cardiac memory. Pacing Clin Electrophysiol. 2010;33(3):346–52.
24. Hancox JC, McPate MJ, El Harchi A, Hong Zhang Y. The hERG potassium channel and hERG screening for drug-induced torsades de pointes. Pharmacol Ther. 2008;119(2):118–32.
25. Nattel S, Carlsson L. Innovative approaches to anti-arrhythmic drug therapy. Nat Rev Drug Discov. 2006;5(12):1034–49.
26. Sanguinetti MC, Tristani-Firouzi M. hERG potassium channels and cardiac arrhythmia. Nature. 2006;440(7083):463–9.

27. Itzhaki I, Maizels L, Huber I, Zwi-Dantsis L, Caspi O, Winterstern A, Feldman O, Gepstein A, Arbel G, Hammerman H. Modelling the long QT syndrome with induced pluripotent stem cells. Nature. 2011;471(7337):225–9.
28. Bers DM. Cardiac excitation–contraction coupling. Nature. 2002;415(6868):198–205.
29. Wang T, Hu N, Cao J, Wu J, Su K, Wang P. A cardiomyocyte-based biosensor for antiarrhythmic drug evaluation by simultaneously monitoring cell growth and beating. Biosens Bioelectron. 2013;49:9–13.
30. Hu N, Wang T, Wang Q, Zhou J, Zou L, Su K, Wu J, Wang P. High-performance beating pattern function of human induced pluripotent stem cell-derived cardiomyocyte-based biosensors for hERG inhibition recognition. Biosens Bioelectron. 2015;67:146–53.
31. Mandenius CF, Steel D, Noor F, Meyer T, Heinzle E, Asp J, Arain S, Kraushaar U, Bremer S, Class R. Cardiotoxicity testing using pluripotent stem cell-derived human cardiomyocytes and state-of-the-art bioanalytics: a review. J Appl Toxicol. 2011;31(3):191–205.
32. Rampe D, Brown AM. A history of the role of the hERG channel in cardiac risk assessment. J Pharmacol Toxicol Methods. 2013;68(1):13–22.
33. Moss AJ, Kass RS. Long QT syndrome: from channels to cardiac arrhythmias. J Clin Investig. 2005;115(8):2018.
34. Weerapura M, Nattel S, Chartier D, Caballero R, Hébert TE. A comparison of currents carried by HERG, with and without coexpression of MiRP1, and the native rapid delayed rectifier current. Is MiRP1 the missing link? J Physiol. 2002;540(1):15–27.
35. Redfern W, Carlsson L, Davis A, Lynch W, MacKenzie I, Palethorpe S, Siegl P, Strang I, Sullivan A, Wallis R. Relationships between preclinical cardiac electrophysiology, clinical QT interval prolongation and torsade de pointes for a broad range of drugs: evidence for a provisional safety margin in drug development. Cardiovasc Res. 2003;58(1):32–45.
36. Curtis TM, Widder MW, Brennan LM, Schwager SJ, van der Schalie WH, Fey J, Salazar N. A portable cell-based impedance sensor for toxicity testing of drinking water. Lab Chip. 2009;9(15):2176–83.
37. Fleming LE, Jerez E, Stephan WBB, Cassedy A, Bean JA, Reich A, Kirkpatrick B, Backer L, Nierenberg K, Watkins S. Evaluation of harmful algal bloom outreach activities. Mar Drugs. 2007;5(4):208–19.
38. Hinder SL, Hays GC, Brooks CJ, Davies AP, Edwards M, Walne AW, Gravenor MB. Toxic marine microalgae and shellfish poisoning in the British isles: history, review of epidemiology, and future implications. Environ Health. 2011;10(1):54.
39. Yasumoto T, Murata M, Oshima Y, Sano M, Matsumoto G, Clardy J. Diarrhetic shellfish toxins. Tetrahedron. 1985;41(6):1019–25.
40. Poli M, Mende TJ, Baden DG. Brevetoxins, unique activators of voltage-sensitive sodium channels, bind to specific sites in rat brain synaptosomes. Mol Pharmacol. 1986;30(2):129–35.
41. Lipkind GM, Fozzard HA. A structural model of the tetrodotoxin and saxitoxin binding site of the Na+ channel. Biophys J. 1994;66(1):1.
42. Templeton CB, Poli MA, Solow R. Prophylactic and therapeutic use of an anti-brevetoxin (PbTx-2) antibody in conscious rats. Toxicon. 1989;27(12):1389–95.
43. Huang J, Wu CH, Baden DG. Depolarizing action of a red-tide dinoflagellate brevetoxin on axonal membranes. J Pharmacol Exp Ther. 1984;229(2):615–21.

Chapter 6
Micro/Nano Neuronal Network Cell Biosensors

Liping Du, Liang Hu, and Chunsheng Wu

Abstract Neuronal network cell biosensors were developed by coupling the neuronal network with multisite detection devices. In this chapter, we will mainly focus on three major issues, including the patterned growth of neuronal networks, principles of various detection devices, and the application of neuronal network-based biosensors in the field of neuroscience and biomedicine. In the culture of neuronal networks, several neuronal patterning techniques will be discussed in detail, such as photolithography, micro-contact printing, microfluidics, etc. The transfection methods were employed in the bioengineering of neuronal networks in order to modify the function of neuronal network. In the field of neuronal network-based biosensor, there are two kinds of multisite detection devices: microelectrode array (MEA) and field-effect transistor (FET). The basic working principle of FET and its advantages will be presented. Based on this knowledge, two other emerging FETs-utilized nanomaterials (graphene FET and nanowire FET) will also be introduced. At the end, some examples of neuronal network-based biosensors will be presented by discussing their application in the neuroscience research and drug detection.

Keywords Neuronal network • Neuron patterning • Field-effect transistor • Transfection • Nanomaterials

6.1 Introduction

The neuronal network of the brain can process the received sensory signals and command the movement of the body. Some set of neuronal networks work as an independent subsystem, and different subsystems can coordinate to constitute a complex and highly ordered neuronal system. The neuronal computing, as one of

L. Du • C. Wu (✉)
Institute of Medical Engineering, School of Basic Medical Sciences, Health Science Center, Xi'an Jiaotong University, Xi'an, China
e-mail: wuchunsheng@xjtu.edu.cn

L. Hu
Biosensor National Special Laboratory, Department of Biomedical Engineering, Zhejiang University, Hangzhou, China

P. Wang et al. (eds.), *Micro/Nano Cell and Molecular Sensors*,
DOI 10.1007/978-981-10-1658-5_6

the most powerful system, is related with all the body and mental activities and has the ability of learning and memory. During the information processing, the neuronal network is robust and fault tolerant, reliable, and reproducible. These features make it an ideal candidate as a sensing and processing integrated system in the development of biosensors. On the other hand, lots of mechanisms in the neuronal network are still less studied, for example, how the electrophysiological signals are processed and coded in the neuronal network and how the memory and learning function. It is one possible way to investigate these underlying principles by elucidating the relation between the network function and the activity of individual neuron at high spatial and temporal resolution. Therefore, an efficient investigation platform is urgently needed as well to reveal such basic mechanisms of the brain by high-resolution simultaneous stimulation and recording of neuronal network activities. The neuronal network biosensor is a kind of good candidate from this point of view.

The pioneering work of neuronal network biosensors can date back to 30 years ago, when Tomas [1], Pine [2], and Gross [3] explored the feasibility of simultaneous signal recording from cultured cardiac myocytes, neurons, and isolated ganglia with planar microelectrode arrays. Thereafter much work is focused on the development of recording and stimulation devices and the coupling between neuron networks and sensing devices in this field. In the early research stage of neuronal network biosensors, primary neurons are dissociated from the tissue and cultured homogeneously on the substrates of devices. Even in some cases, brain slices are used directly to investigate the behavior of natural neuronal networks. For the neuronal culture on devices, the coverage proportion of microelectrodes depends on the chance in the specific cell density. The structure of neuronal networks cannot be controlled as well. Thereby the patterned culture of neuronal networks has been intensely investigated, which is fulfilled by the collaboration of the engineering methods and biological experiences. Many techniques are used in this issue, such as photolithography, micro-contact printing, microfluidics, etc. For the development of recording devices, various microelectrode arrays (MEAs) and field-effect transistor (FET) arrays are intensively developed in the neuronal network biosensors due to the rapid development of silicon microfabrication technologies. The substrates of most MEAs are silicon and glass, and the materials of electrodes are mainly gold (Au), platinum (Pt), and titanium nitride (TiN). The diameter of single detection electrode ranges from 10 to 100 μm in general, which corresponds to the size of cells in order to increase the efficiency of signal detection. High-density design is one trend to increase the spatial resolution of signal detection, even for the different parts of single neuron. In the research of MEA-based neuronal network biosensors, the effective coupling between cultured neuronal networks and detection electrodes is a hot issue, and the coupling relates directly with the signal-to-noise ratio. Some 3D nanoscale design of microelectrodes instead of plat microelectrodes have emerged to make larger contact surface between the microelectrode and the cell body, such as needle-like, mushroom-like microelectrodes. In addition, tremendous exploratory work has been done on the field-effect transistor array in order to open up its applications in the neuronal network biosensors. The inherent advantage of the signal amplification makes FETs attractive in the detection of weak biological signals. The foundation of the modern silicon

microfabrication technology provides sufficient technical support for the fabrication of various FETs. The advancement of nanotechnology promotes the use of nanomaterials in the fabrication of FETs, which improves the performance of traditional FETs and makes FETs more suitable in the recording and stimulating of neuronal networks. The current applications of neuronal network biosensors are mainly as a research platform in the field of electrophysiological detection in order to unravel the signal propagation, neuronal coding, and the function of the brain. The responses of neuronal networks to drugs are also studied to search the potential application in the drug screening.

The important aspects of neuronal network-based biosensors will be introduced in this chapter. Here we will focus on three major questions, including the development of patterned neuronal networks, various detection devices, and the application of neuronal network-based biosensors in the field of neuroscience and biomedicine. In the part of patterned culture of neuronal networks, several neuronal culture techniques and the bioengineering methods will be discussed, especially on the preparation of patterned neuronal networks and the transfection methods. For the detection devices, there are two kinds of devices currently used in the field of neuronal network-based biosensor including microelectrode array (MEA) and field-effect transistor (FET). FET will be introduced in detail in this chapter, and MEA has been discussed in detail in other chapters. The basic working principle of FET and its advantages will be presented. Based on this knowledge, two other emerging FETs-utilized nanomaterials (graphene FET and nanowire FET) will also be introduced. In addition, some examples of neuronal network-based biosensors will be presented to discuss their application in the neuroscience research and drug detection. At the end of this chapter, a summary is made and the future development trend will be discussed.

6.2 The Development of Neural Networks

6.2.1 The Culture of Neuronal Networks

The neuronal networks used in biosensors include primary cultured dissociated neurons, brain slices, and related tissues. In this chapter, we will focus on the primary cultured neuronal networks.

In earlier studies, dissociated neurons are plated on the homogeneously coated substrate of the detection devices, and a neuronal network will be formed randomly. Generally, detection electrodes are arranged on the surface of devices in a certain array. For most devices the number of electrodes is less than 100 and the density is not high enough to detect most neurons. Therefore, the neuron deposition on the detection sites is random under the fixed cell density. Especially for the low-density neuronal network, only a small fraction of neurons adheres exactly on the electrodes so that the efficiency of recording is not sufficient. One possible solution is to increase the cell density in order to cover the electrodes as many as possible, but the

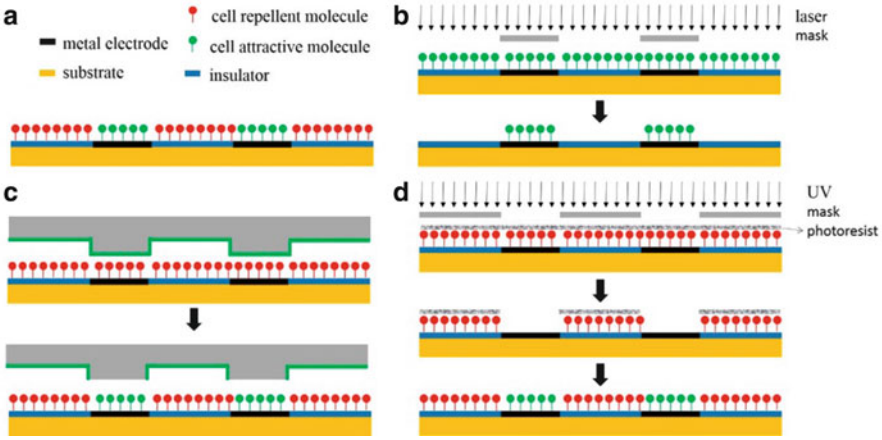

Fig. 6.1 Cell patterning methods on the surface of transducers. (**a**) The illustration of patterning on the surface of electrode arrays; (**b**) photoablation; (**c**) micro-contact printing; (**d**) photolithography

complexity of the networks is also increased, and the structure of the network is not easy to reproduce. In this context the guided growth of neuronal networks becomes a promising approach to develop controlled networks on the surface of transducers. On one hand, neurons can be guided to adhere on the specific sites and grow in a certain pattern; on the other hand, the geometrical structure of neuronal networks can be well controlled and be easy to reproduce.

It has a long history for the controlled cellular growth [4, 5], but the advancement of microfabrication technologies accelerates the research of cellular patterning on substrates greatly [6]. The patterning is mainly based on the following two basic strategies. One is using cell-adhesive and cell-repellent molecules to pattern the substrate (as illustrated in Fig. 6.1a). In this strategy, cell-attractive molecules form the cell-adhesive region, in which cells can adhere and grow to form networks, while the cell-repellent molecules form a repellent region to inhibit the cell deposition and growth. The selection of these substances for cell patterning is based on some initial observations:

1. The hydrophilic surface is more suitable for the cell attachment and growth than the hydrophobic one.
2. Positively charged materials are preferred to negatively charged materials [6].
3. Some proteins and polypeptides are known to control cell attachments and even enhance the axonal growth, such as extracellular matrix (ECM) proteins, polylysine [7], laminin [8], the laminin-derived peptide sequence (P22-2) [9], fibronectin, etc.
4. The cell growth is correlated with the amine group density of substrates.
5. Polyethylene glycol (PEG) can be used to restrict the neurite growth [10, 11].

Therefore, the permissive molecules include polylysine, laminin and related peptides, various aminosilanes, extracellular matrix, positively charged molecules, hydrophilic molecules, and even neural growth factors such as BDNF [12], while the nonpermissive molecules include polyethylene glycol, negative charged molecules, and hydrophobic molecules. The other one strategy is to make some barriers and 3D constraints on the substrate to guide the growth of neurons, such as microfluidic channels, microwells, nanostructured surfaces, etc. This strategy exerts the space constraints for the cells to realize the patterned growth of neurons mainly basing on micro/nano-fabrication techniques.

Several commonly used methods in cell patterning are illustrated in Fig. 6.1. The photoablation is a simple method to produce patterned substrates for cell culture (Fig. 6.1b) [13]. Before photoablation, the substrate is coated with a layer of cell-attractive proteins. It utilizes the laser to inactivate proteins of some regions and protects the non-illuminated area by a mask. At the end a cell-attractive pattern is left on the substrate. This method is noncontact, of high resolution (even down to nanometer), and applicable to any substrates. Though cells prefer to grow on the protected area than laser-illuminated area, the inactivated proteins are not repellent surface strictly. The photolithography method (Fig. 6.1d) is a little bit similar to the photoablation, but the use of photoresist agents will make it possible to pattern cell-attractive and cell-repellent substances at the same time [14]. At the beginning the cell-repellent substances can be coated evenly on the devices. After the spin coating of the positive photoresist and the alignment of mask, UV will erase the positive photoresist of the unprotected area and inactivate the unprotected proteins. Then cell-attractive proteins can be coated on this surface. After removing the photoresist, the patterned surface with two kinds of proteins will be formed. Micro-contact printing (μCP) is one of the mostly used methods to pattern cells (Fig. 6.1c) due to simplicity, cost-effectiveness, and flexibility [15]. In the process of μCP, the pattern structure can be fabricated in the mold and then cased into the PDMS stamps or other elastomeric stamps. Stamps are incubated in the protein-containing ink solution for some minutes and then dried by the nitrogen gas. The protein of the ink solution will coat on the surface of stamps evenly. Afterward the stamp is in contact with the pretreated substrate and is exerted appropriate force. The protein will be transferred onto the substrate in the designed pattern. The whole process is completely like stamping. For the pretreatment of substrates, normally the background of printing should be repellent molecules. For the micro-contact printing on the detection electrode, the stamps should be aligned with the electrodes of substrate under the microscope. Besides, several kinds of proteins can also be printed onto one surface by several micro-contact printing with the assistance of the alignment instrument.

Patterned substrates can also be made by the UV-activation of photoreactive organosilanes under standard fluorescence microscopes. In the strategy, the silane (1-(2-nitrophenyl) ethyl-5-trichlorosilylpentanoate, NPE-TCSP) has a photocleavable 2-nitrobenzyl group. The substrate chemically modified with NPE-TCSP was coated with bovine serum albumin (BSA) to prevent the cell adhesion. UV irradiation will cause 2-nitrobenzyl group to be photocleaved and

BSA to be dissociated from the substrate. Then the vacancy of BAS will be replaced selectively by adding fibronectin, which can promote the cellular adhesion [16].

Besides, patterning can be obtained by "direct writing" as well, that is, to deposit protein molecules directly on the substrate in some certain patterns, such as the dip-pen lithography, the inkjet printing [17]. In these techniques, the substrate acts as the "paper," while the protein molecules act as the "ink." The dip-pen lithography uses an atomic force microscopy (AFM) tip to deposit single protein molecules with features even under 100 nm [18]. It can create high-resolution protein pattern to control the neuronal growth. In the inkjet printing, biologically active proteins can be printed on the substrate using a simple automated printing process with a modified commercial inkjet printer, and the size of the protein pattern is as small as 350 μm [19]. The details of each technique and compares can be found in many reviews [15, 20].

In the strategy of space, constraining microfluidic patterning is a convenient method. Generally, microfluidic channels are formed by bonding a PDMS structure onto a substrate and can restrict the fluidic flow to selected areas of a substrate. In this way neurons can be constrained to growth in these channels. The substrate-coating proteins can be also delivered into the microchannel as well as the culture medium. The elastic nature and hydrophobicity of the PDMS material make it to be self-sealed and separated with the substrate easily. Peyrin et al. presented a microfluidic platform to exploit the directional growth of axons from one chamber (emitting) to the other (receiving) (named "axon diodes"). The microfluidic platform comprises two independent cell culture reservoirs and a series of 500 μm long, 3 μm high, asymmetrical microchannels (as shown in Fig. 6.2a, b). The entrance of microchannel is 15 μm wide to allow optimal axonal collection from the emitting chamber, and the entrance of the receiving chamber is 1–3 μm wide. When neurons are seeded in the emitting chamber of a 15–3 μm diode, the receiving chamber (narrow side of the channel) is massively invaded by axons 8 days after seeding (Fig. 6.2c). In contrast, the number of axons reaching the opposite chamber is greatly reduced when neurons are seeded in the receiving chamber at the same density (Fig. 6.2d). These results demonstrate that the platform allows the construction of oriented neuronal networks [21]. It can also use the laminar flow in microfluidic channels to guide the neuronal growth in selected areas [22]. As shown in Fig. 6.2e, f, a network of microchannel capillaries has three inlet channels and a single main outlet channel, which is initially filled with water by filling the inlet reservoirs, and the fluid is driven by a vacuum at the outlet. Once liquid forms a smooth flow through the channels, a solution of a fluorescent neoglycoprotein (man–FITC–BSA) is added from two side inlets, and a solution of BSA is added from the middle inlet. These solutions will flow into the main channel under the influence of gentle aspiration at the outlet. Proteins adsorbed nonspecifically to the regions of the surface, and fluorescence image of the resulting protein pattern is shown in Fig. 6.2e. When the system of capillaries was then filled with a suspension of *E. coli* RB 128, they can bind to mannose-presenting surfaces. Cells that did not adhere strongly will be washed away with PBS. The fluorescent nucleic acid

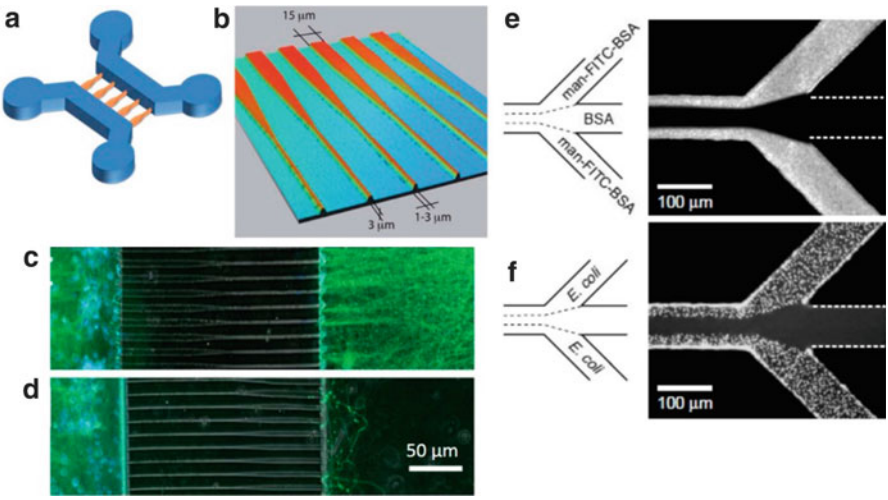

Fig. 6.2 (**a**) Global 3D view of the microfluidic device comprising asymmetrical microchannels. (**b**) 3D view of the funnel-shaped microchannels. (**c**) Immunofluorescent image of microfluidic cultures (*green*, a-tubulin; *blue*, Hoechst), in which neurons were seeded in the emitting chamber. (**d**) The immunofluorescent result when neurons were seeded in the receiving chamber (Reproduced with permission from Ref. [21]. Copyright 2011 Royal Society of Chemistry). (**e**) Laminar flow patterning of the protein and (**f**) cells (Reproduced with permission from Ref. [22]. Copyright 1999 National Academy of Sciences, U.S.A.)

staining of remaining adherent cells is shown in Fig. 6.2f. It can be found that *E. coli* RB 128 adhered only to the regions of man–FITC–BSA.

In some literatures, micro-contact printing (μCP), patterning using microfluidic channels, and laminar flow patterning are also named as "soft lithography," which refers to those methods using stamps or channels fabricated in an elastomeric (soft) material for the patterned protein transfer onto another substrate.

Three-dimensional structures are also used to guide the outgrowth of cells by restricting the cellular morphology. Figure 6.3a, b shows the microscopic picket fences to fix cell bodies mechanically on the chip surface of transistor and stimulator. This chip contains field-effect transistors and capacitance stimulator (St) array. The picket fences of polyimide are placed around the transistor and stimulators in order to trap single neuron on the specific region. Different neurons are fixed in different regions and form a neuronal network. Voltage pulses are applied to a capacitive stimulator to excite the attached neuron. Action potential signal is transmitted in the neuronal network and elicits an action potential in a second neuron, which can be detected by the corresponded transistor. The open picket fences on the chip assist a reproducible formation of silicon–neuron–neuron–silicon circuits by immobilizing the cell bodies on their two-way contacts [23]. Li et al. developed a platform to pattern primary neurons in array formats with single-cell resolution, and the general design schematic is shown in Fig. 6.3c. A PDMS stencil enables the production of through-holes in a thin layer of PDMS with feature

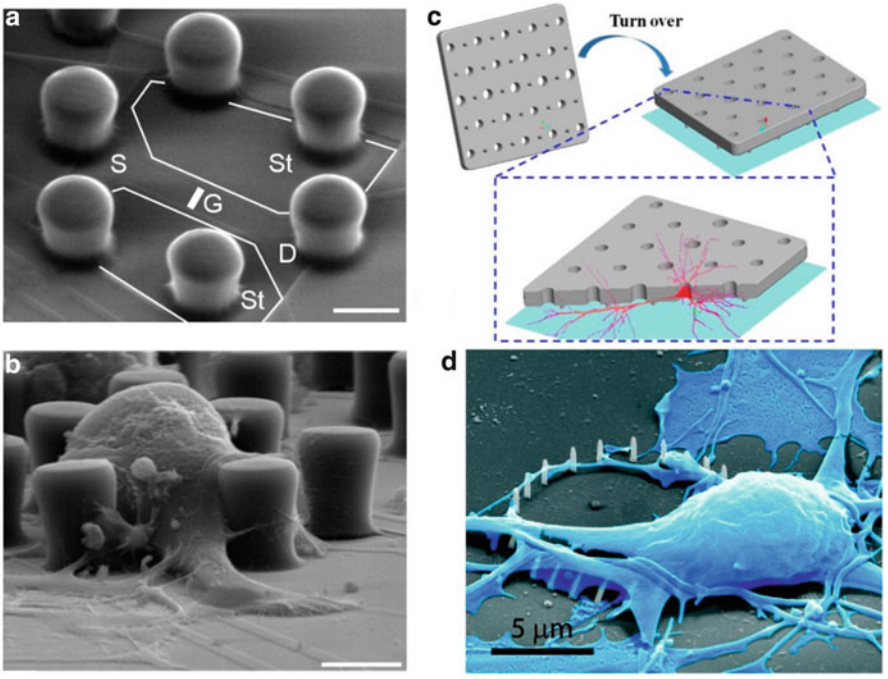

Fig. 6.3 3D microstructures and nanostructures to control the cell growth. (**a**) Electron micrograph of a transistor with the microscopic picket fences of polyimide, scale bar 20 μm, (**b**) electron micrograph of an immobilized snail neuron in the microfences, scale bar 20 μm (Reproduced with permission from Ref. [23]. Copyright 2001 National Academy of Sciences, U.S.A.). (**c**) General design of through-holes for pattering neural network (Reproduced with permission from Ref. [24]. Copyright 2014 Nature publishing group). (**d**) Close contact interface between neuron and nanopillars (Reproduced with permission from Ref. [25]. Copyright 2010 American Chemical Society)

sizes as small as 3 μm, which does not restrict the neurite outgrowth and allows the formation of freely designed, well-connected, and spontaneously active neural network [24]. In addition, vertical nanopillar arrays are designed to pin the position of neurons in a noninvasive manner, as shown in Fig. 6.3d. The cell bodies of neurons are efficiently anchored by the nanopillars, but neurites can also grow and elongate freely into the surrounding area. Moreover, if combining with microelectrode array (MEA), vertical nanopillars would improve the neuron-to-electrode contact and also serve as neuron traps for long-term neuronal network study [25].

6.2.2 The Bioengineering of Neuronal Networks

The introduction of foreign receptors into neurons can enhance the sensitivity of neurons to corresponding ligand substances, and the prerequisite is that the foreign

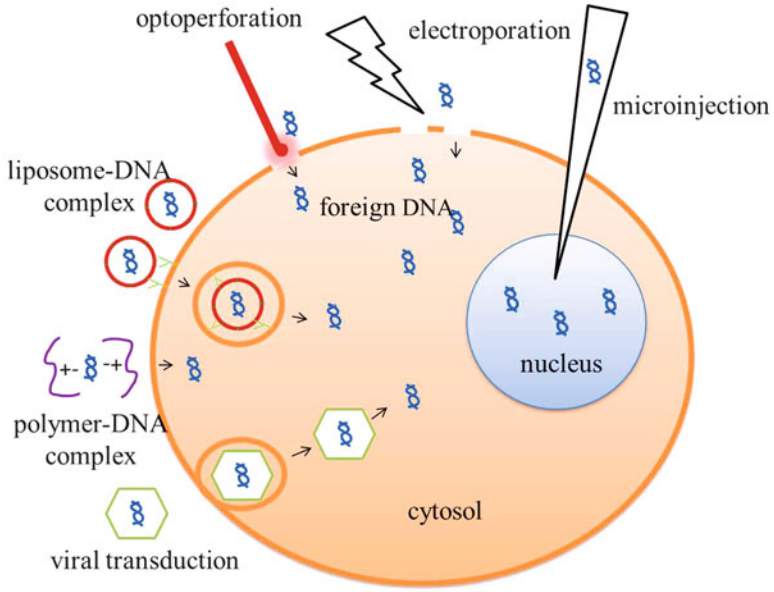

Fig. 6.4 Schematics of current transfection methods

receptors could interact with the intracellular signal transduction system of neurons. Thus, the membrane potentials can be changed once interacting with the substances. Another approach is to couple receptors to native membrane proteins via the fabrication of chimeric receptors. The final goal is to gain supersensitivity of neurons to specific ligand substances. The expression of foreign receptors in neurons needs the bioengineering of neurons by incorporating related genes into neurons, and then the genes are translated into corresponded proteins. Here various methods of bioengineering neurons will be discussed, mainly on several transfection methods.

The transfection, a process of delivering DNAs directly into the nucleus or indirectly into cytosol, is needed for the expression of foreign receptors or ion channels in neurons. The foreign DNAs are incorporated into the genome, inducing the expression of related proteins in cells. The current methods include physical perforation-mediated transfection, chemical-mediated transfection, and virus-mediated transfection, as illustrated in Fig. 6.4. The physical perforation-mediated transfection firstly makes some holes in the cellular membrane and then delivers targeted DNAs into cells. For example, optoperforation uses a highly focused laser to generate a tiny hole in the plasma membrane; electroporation increases the permeability of cell membrane by exposing cells to short pulse of an intense electric field; microinjection can use a microneedle to inject DNA directly into the nucleus. Besides, the holes can also be made by the high-intensity ultrasound and nanofibers. The optoperforation transfection and microinjection method can transfect single

cell effectively and are very suitable for the analysis of single cells. The chemical-mediated methods employ some chemical reagents to transfer the DNA into the nucleus, such as liposome and polymers. These chemical reagents can form a complex with DNAs, and the complex interacts with the cellular membrane. In the lipid-mediated method, the liposome and DNA form a liposome-DNA complex. Some polymers such as calcium phosphate can also form a complex with DNA by the electrostatic interaction. When the complex is incubated with the cell suspension, endocytosis happens and the endosome forms. In the cytosol, the endosome will release the DNA out. The DNA in the cytosol can transport into nucleus through the nuclear pore [26]. In the viral transduction, virus acts as a carrier. Before transfection the foreign DNAs are packaged into the virus. When the packaged virus particle is incubated with cells, endocytosis results in the introduction of exogenous genes [27].

In recent years, optogenetics becomes a very popular technique in the neuronal engineering, which involves the expression of light-sensitive proteins in excitable cells and targeted light illumination to alter cellular behaviors. These light-sensitive proteins can be either naturally occurring or be chemically modified to become photosensitive. Optical controlled cells can be obtained by delivering genes coding for these light-sensitive proteins to the target cells by transfection, viral transduction, or the creation of transgenic animal lines. Restricted expression can be obtained by using specific promoters or recombinase-based conditional systems such as the Cre system. Alternatively, viral transfection can allow targeting of specific cells without specific promoters. The membrane potential or cellular signaling can be controlled by triggering the light-sensitive proteins of targeted cells. One of the most common uses of optogenetics is switching the membrane voltage potential of excitable cells. In general, membrane depolarization leads to the activation of spiking, and membrane hyperpolarization leads to the inhibition of these signals. Controlling the "switch" by light enables neuroscientists to study neuronal communication and neuronal circuit-related behavior.

Figure 6.5 shows the activation and inhibition of neuronal activities by optogenetics. The channelrhodopsin-2 (ChR2) is a nonselective cation channel and sensitive to the blue light (470 nm). Once illuminated by the blue light, it will immediately depolarize the neuron and trigger a spike. There are several variants of ChR2 such as ChETA, SFO, and VVhR1. ChETA is a faster ChR2 variant, which is sensitive to the blue light (470 nm) and can trigger neurons at frequencies greater than 40 Hz, while the step function opsins (SFO) variants are slower versions of ChR2, which can induce prolonged stable excitable activities in neurons upon exposure to blue light (470 nm) and can be reversed by exposing to green light (542 nm). Channelrhodopsin-1 (VChR1) variant is similar to ChR2, but it is sensitive to the red-shifted light (535–589 nm). On the other hand, it is also desirable to inhibit neuronal signaling by specific lights. The photosensitive proteins can inhibit spikes and block signaling by hyperpolarizing neurons in response to specific light, such as a photosensitive chloride pump halorhodopsin (NpHR) (589 nm) and its variants eNpHR2.0 (589 nm) and eNpHR3.0 (589–680 nm),

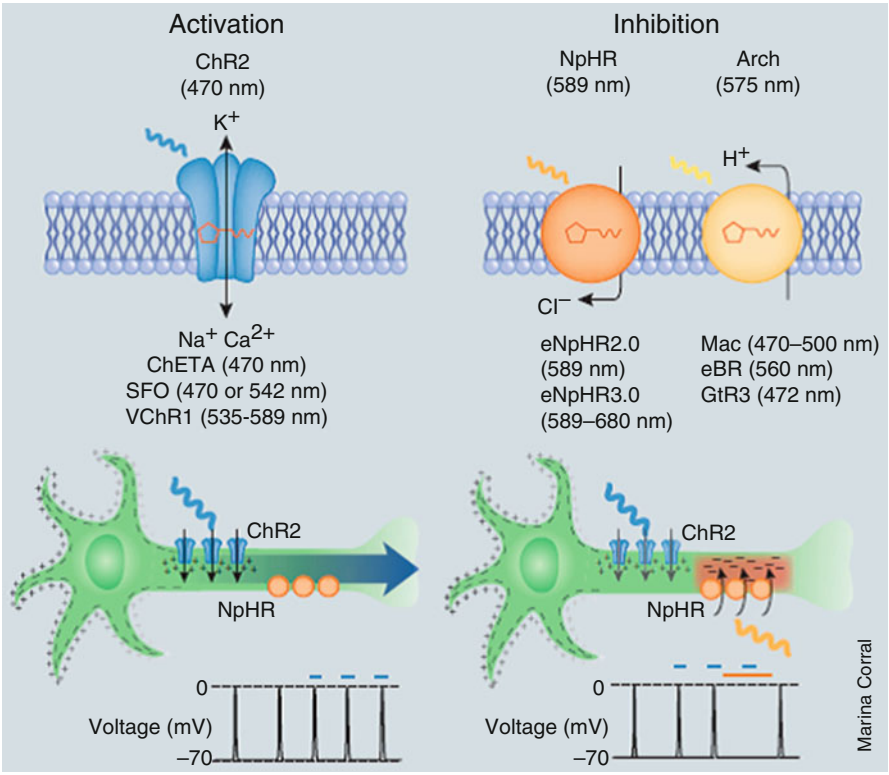

Fig. 6.5 Optogenetic tools control the membrane potential of neurons (Reproduced with permission from Ref. [28]. Copyright 2010 Nature publishing group)

proton pumps archaerhodopsin-3 (Arch) (575 nm), Mac (470–500 nm), bacteriorhodopsin (eBR) (560 nm), and rhodopsin-3 (GtR3) (472 nm). The effect of light-driven activation and inhibition is shown in the lower part of Fig. 6.5. Blue light-stimulated ChR2 induces the increased firing of neurons, while yellow light-driven NpHR results in the decreased firing of neurons. It is also found that the optogenetic tools can also be used to control the intracellular signaling cascades and molecular interactions by general fusions of light-absorbing domains with protein "effector" domains. In this way, the related receptors, G protein-mediated signaling cascades, and even the production of second-messenger molecules can be directly controlled by specific lights [28]. Therefore, optogenetics provides an effective way to engineer neuronal network and would become an important method to realize special control of neuronal activities. Even though optogenetic-engineered neuronal network is still mostly under investigation by the patch clamp, in the development of neuronal network-based biosensors, optogenetics will become a promising tool to research the neuronal communication and neuronal encoding.

6.3 Neural Network Cell Biosensors

6.3.1 The Field-Effect Transistor

For the multisite simultaneous detection of neuronal networks, miniaturized sensor arrays are needed to record the electrophysiological signals of the network. Up to now, two kinds of devices are under use in this field, i.e., microelectrode arrays (MEAs) and field-effect transistor (FET) arrays. Both are fabricated using the microfabrication technology and have their own characteristics. MEA has been introduced in detail in Chap. 5. Therefore, in this chapter we will focus on the basic principles of several FETs and its application in neuronal network biosensors.

An adequate sensitivity and low noise are the prerequisites of microelectronic devices for the local extracellular recording of neuronal excitation in an aqueous environment. In common metal-oxide silicon (MOS) field-effect transistors, the low-frequency noise is mainly caused by the electron tunneling between silicon and traps in the gate oxide. It can be reduced by burying the electron channel of the transistor in the silicon substrate, a few nanometers from the interface. FETs used in the neuronal recording are non-metalized open-gate field-effect transistors. A schematic of cell and n-type silicon bulk open-gate field-effect transistor hybrid was shown in Fig. 6.6a. In the gate area, there is a layer of silicon dioxide insulator. Electrogenic cells (such as neurons) are cultured on top of the non-metalized gate in

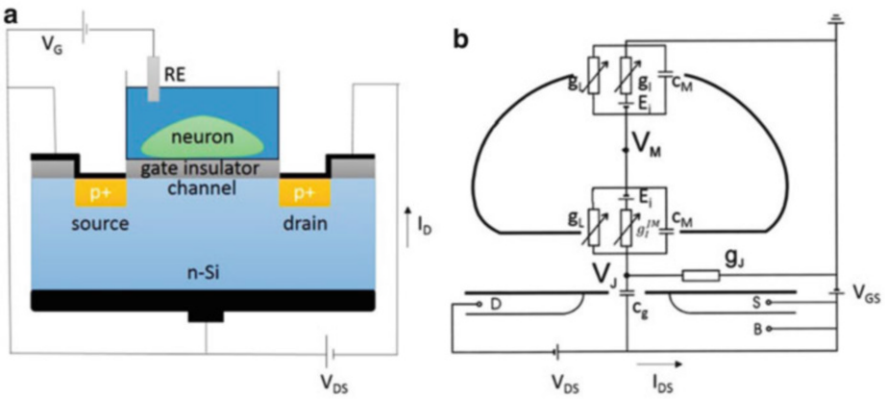

Fig. 6.6 (**a**) Schematic of the cell/FET hybrid (Reproduced with permission from Ref. [30]. Copyright 2012 Noemi Rozlosnik) (**b**) Equivalent circuit of the cell/FET hybrid. The cell membrane and the silicon dioxide on the FET chip are marked as heavy lines. The actual width of the cleft between the insulator and the membrane is around 35–70 nm. P-type source (S) and drain (D) of the transistor are in a bulk substrate (B) of n-type silicon with appropriate bias voltages. The modulation of the source–drain current probes the extracellular voltage VJ in the cleft. The intracellular voltage is VM. g_J is the seal conductance of the junction per unit area. The current balance is described by a two-compartment circuit with capacitances and voltage-dependent conductance of the free and of the attached membrane driven by reversal voltages and with a capacitance of the silicon dioxide

the medium. The current of FET flows along a semiconductor channel under the gate. Two ends of the channel are the source and the drain, respectively. Even though the physical diameter of the channel is fixed, its conductivity can be modulated effectively by the voltage of the gate. A small voltage change in the gate (U_{GS}) will cause a large variation in the current from the source to the drain (I_{DS}). The transconductance (g_m) can depict the sensitivity of the transistor, which is defined as the derivative of I_{DS} with respect to U_{GS}. This intrinsic signal amplification effect makes FET very suitable to detect the weak electrical signals from cells.

An equivalent circuit of cell/FET hybrid is shown in Fig. 6.6b, which is also called the point-contact model. The cell membrane is divided into two parts by the contact of FET, the attached and free membrane. There are various ionic channels incorporated into the cell membrane. The current of ionic channels (i) and the conductance of membrane will be changed with a time- and voltage-dependent manner by the open and close of ionic channels. Both the attached and free membranes are described by a membrane capacitance c_M, a leakage conductance g_L, a specific ionic conductance g_I, and the corresponded electrochemical driving force E_i. An extended layer of electrolyte is in the cleft between the cell membrane and the gate oxide, which can be described by a specific seal conductance g_J and a specific capacitance of the gate c_g. V_J is the extracellular voltage recorded by FET, and V_M represents the intracellular voltage which can be monitored by the patch clamp. Considering that the ion channels in the contact region have different opening properties and/or different densities compared with the free membrane, a scaling factor X_I is used to describe the differences between the conductance of the average cellular membrane and the attached cellular membrane: $g_I^{JM} = X_I g_I$. The extracellular voltage V_J can be determined by Kirchhoff's current law. The capacitive current through the gate and the leakage current through g_L can be neglected. In addition, it can be assumed that the ion concentrations in the cleft are not changed with respect to the bulk electrolyte [29]. Based on these simplifications, the extracellular voltage V_J can be described by the following equation:

$$V_J = \frac{1}{g_J}\left(c_M \frac{dV_M}{dt} + \sum\nolimits_i X_i \cdot i^i\right) \tag{6.1}$$

Besides, the capacitive stimulation of a neuron could be also achieved on the FET device, which opens up the possibility for two-way, nontoxic communication between microelectronic chips and neurons.

Field-effect transistors have an intrinsic advantage over microelectrode arrays (MEAs), which is the signal amplification capability. Since FETs can be fabricated by the standard semiconductor technology, the production of high-density structures becomes relatively easy, and even the integration fabrication with the following signal amplification circuits may be possible, which would enhance the recording ability of cell activity with unprecedented spatial resolution and signal-to-noise ratio.

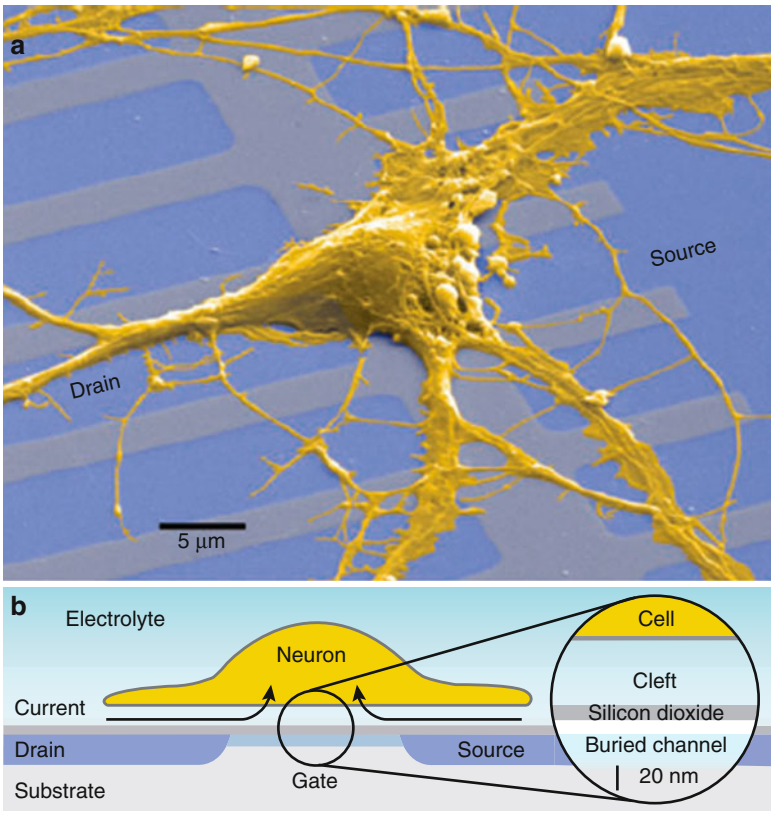

Fig. 6.7 A rat neuron on a field-effect transistor: (**a**) colorized electron micrograph of a hippocampal neuron on a silicon chip; (**b**) schematic cross section of a neuron on buried-channel FET (Reproduced with permission from Ref. [31]. Copyright 2004 John Wiley and Sons)

For the successful recording of firing neurons, the surface of FET should be coated with a thin layer of protein or polypeptide in order to facilitate the growth and adhesion of neurons, such as laminin and poly-L-lysine. After culturing a few days, the extracellular potential recording can be conducted by FET. Figure 6.7a shows the colorized electron micrograph of a rat hippocampal neuron attached directly on the exposed gate oxide of a linear array of p-type buried-channel transistors. The open voltage-sensitive gates are between the source and drain leads. The gate region and the surrounding chip surface are insulated with 10 nm of silicon dioxide. The whole surface of the device is chemically and structurally homogeneous with a surface profile below 20 nm. Figure 6.7b is the schematic cross section of a neuron on a buried-channel field-effect transistor with blowup (drawn to scale) of the contact area. During an action potential, the local extracellular potential changes in the electrolyte of the cleft between cell and chip directly modulate the source–drain current, and the current flows through the adhering cell membrane and along the resistance of the cleft between chip and cell.

6.3.2 Graphene Solution-Gated Field-Effect Transistors

Presently the common problems of FETs are the poor stability and biocompatibility of the ubiquitous semiconductor silicon in the harsh ionic biological environment. It does not only decrease the performance of the transistor but also may damage the surrounding tissue. The good candidate materials for building high-performance electronic devices should be chemically stable and exhibit high charge carrier motilities and low electronic noise which are required for a high signal-to-noise ratio. Besides, it should allow to be fabricated into small devices compatible with the cell dimension. Highly crystalline substrates or even single crystals could be considered; however, mechanical characteristics properties of such good crystalline, like highly rigid and sharp edges, become the major obstacles of application in biological systems [32].

A rapidly rising star on the horizon of materials science, graphene, comes into the sight. Its excellent electronic and mechanical properties comply with all the abovementioned requirements. Graphene is employed rapidly in the field of neuron-transistor hybrids. Graphene is strictly two-dimensional (2D) honeycomb lattice material made of monolayer carbon atoms. For the high flexibility, graphene becomes also the basic building block for graphitic materials of all other dimensionalities (Fig. 6.8). It can be either wrapped up into 0D fullerenes, rolled into 1D carbon nanotubes, or stacked into 3D graphite [33, 34]. Graphene is chemically stable and impervious to the harsh biological environment. In addition, it also has outstanding electronic properties. The charge carrier mobility is extremely high and outnumbers other semiconductors greatly such as silicon, diamond, and AlGaN/GaN. Its interfacial capacitance is almost one order of magnitude higher than other materials. Consequently, graphene has a significantly higher transconductance and sensitivity

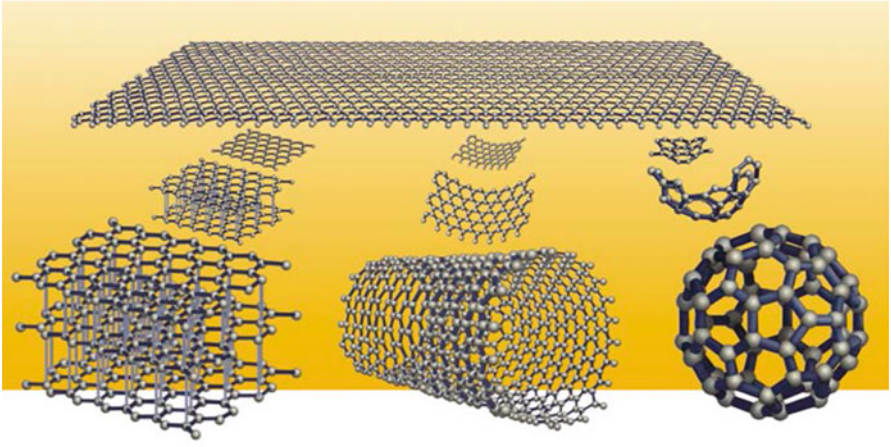

Fig. 6.8 Graphene is a building material for carbon materials of all other dimensionalities (Reproduced with permission from Ref. [34]. Copyright 2008 Nature publishing group)

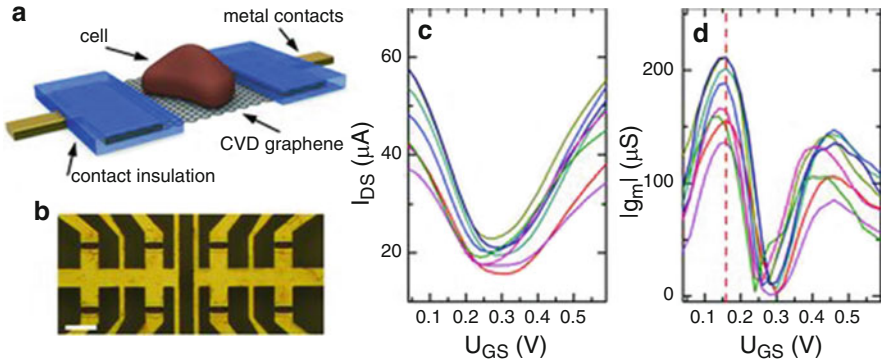

Fig. 6.9 Graphene FET. (**a**) The schematic of a cell-graphene FET hybrid. (**b**) An optical micrograph of graphene FET array. Scale bars are 100 μm. (**c**) The drain-source current (I_{DS}) vs. electrolytic gate voltage for eight different transistors in the same array. The experiments were performed in the cell culture medium and with the confluent layer of HL-1 cells on the array. All curves were recorded at a drain-source voltage $U_{DS} = 100$ mV. The UGS scale refers to the Ag/AgCl redox potential. (**d**) Transconductance vs. gate voltage for the transistor curves depicted in (**c**). The *red line* indicates the operating point for the sensing experiment (Reproduced with permission from Ref. [36]. Copyright 2011 John Wiley and Sons)

than other materials. Besides, graphene is only one atomic layer thick and can be transferred onto almost any substrate even thin flexible polymer film, which allows its application in fabricating high-performance flexible transistors [32]. Moreover, graphene can also record and stimulate any electrogenic cells and is promising in next-generation bionic technology [35].

Figure 6.9a shows a schematic of a neuroelectronic hybrid based on graphene FET. Cells are grown on top of the graphene gate to be stimulated or recorded. Before the fabrication of transistors, the high-quality graphene is grown by chemical vapor deposition (CVD) on a copper foil in a high-temperature (1000 °C) furnace under the flow of methane and hydrogen. Then the graphene/copper stack is coated with a layer of poly(methyl 2-methylpropenoate) (PMMA) as a mechanical support and placed on the surface of an iron (III) chloride solution to etch the copper under the graphene. Afterward, the graphene/PMMA layer is fished on the substrate, and PMMA is removed by solvents. Graphene on the substrate is patterned into defined active area of transistors by optical lithography and an oxygen plasma, and the metal drain and source contacts are made by gold evaporation and etching. Finally, a patterned layer of chemically stable SU8 photoresist is spine coated onto the substrate to protect the metal contacts from electrolyte and prevent the leakage currents. At the same time graphene region is exposed as the sensing area. At the last step the graphene solution-gated FETs will be wire bonded to a chip carrier and packaged with silicone glue. Normally an array of graphene FETs will be fabricated in one substrate to have a high spatial resolution for the cell experiment. One optical micrograph (Fig. 6.9b) shows an eight-transistor array. In the cellular experiment, the size of transistors should be compatible with the size of cells in order to get a

good performance. In this case the transistor has a length of 10 μm and a width of 20 μm in the active area.

Basic characterizations of graphene FETs are performed in the cell culture medium and with the confluent layer of HL-1 cells on the array as shown in Fig. 6.9c, d. The gate voltage U_{GS} is applied between a Ag/AgCl reference electrode in the solution and the source contact of the transistor. The given gate voltages are always referred to this Ag/AgCl reference electrode. The drain-source current (I_{DS}) is proportional to the drain-source voltage (V_{DS}) and can be modulated with the gate voltage (U_{GS}). When the drain-source voltage (V_{DS}) is fixed at 100 mV, the relationship between I_{DS} and U_{GS} is shown in Fig. 6.9c, in which the current shows a minimum value at a certain U_{GS} and increases almost linearly away from this point. As a consequence, the conductance of graphene FET can be modulated by applying a gate voltage between the graphene gate and the Ag/AgCl reference electrode in the electrolyte. Such devices are commonly referred to as solution-gated FETs (SGFETs). In this case, the applied gate voltage between the graphene film and the Ag/AgCl reference electrode shifts the position of the Fermi level in graphene layer, which controls the number and type of charge carriers. When the Fermi level reaches the Dirac point where conduction and valence band meet, the conductivity of graphene reaches its minimal value. When the Fermi level is below the Dirac point, the major charge carriers are holes in the graphene valence band. With the gate voltage further decreasing, the Fermi level is shifted deeper into the valence band, and the charge density increases. When the Fermi level is above the Dirac point, the major charge carriers are electrons in the graphene conduction band, and the charge density is modulated in the same way.

The sensitivity of graphene FETs is evaluated by the transconductance (g_m), which is defined as the derivative of I_{DS} with respect to U_{GS}. The transconductance under different U_{GS} is shown in Fig. 6.9d. This parameter reflects the resulting change in current for a small variation in U_{GS} and is of special importance for sensing applications. It is found that the transconductance of the graphene FET can reach up to 200 μS and is almost one order of magnitude larger than other SGFET technologies such as Si- or AlGaN-based devices [36]. In the experiment, the operating voltage of transistors is set at the point in which the transconductance reaches its maximum value (the red line in Fig. 6.9d). Cardiomyocyte-like HL-1 cells were cultured on the graphene FET array and showed healthy growth after several days in vitro. The action potentials and the temporal propagation were recorded successfully on different transistors across the cell layer [36].

6.3.3 Nanowire Field-Effect Transistors

In recent years, many types of one-dimensional semiconducting nanomaterials, such as silicon nanowires [37], metal-oxide nanowires (e.g., In_2O_3-NW [38] and ZnO-NW [39]), and carbon nanotubes [40], have attracted great attention in the development of FETs. Due to the high surface-to-volume ratios of nanomaterials, a

huge proportion of the constituent atoms are located at or close to the surface of the material, which play an important role in the physical, chemical, or even electronic properties of nanomaterials. Moreover, surfaces of some particular nanomaterials can be easily chemically modified, which makes them suitable for nanoscale sensing applications. FETs with one-dimensional nanomaterials show high selectivity and sensitivity, real-time response, and label-free detection capabilities in many applications, such as nucleic acids, proteins, viruses, and neurotransmitters. Due to the well-developed silicon industry, Si nanowires (SiNWs) can be prepared with parameters precisely controlled. Therefore, SiNW-FETs can be fabricated with mature silicon industry processing techniques. In this section, we will focus on the working mechanisms, fabrications, and application of silicon nanowire FETs.

SiNW-FET biosensors include the source, the drain, and the gate. The silicon nanowires act as the semiconductor channel between the source and the drain electrodes. The channel conductance will be modulated by the solution gate electrode or the back gate. For the fabrication of SiNW-FETs, there are two major techniques: "top-down" and "bottom-up." The "top-down" method is fully based on lithographic processing on a silicon-on-insulator (SOI) wafer, which contains a substrate Si wafer, a buried silicon dioxide layer in the middle (about 200–400 nm), and the top Si layer (about 50–100 nm). Firstly, the top Si layer is doped with low-density boron or phosphorous of $\sim 10^{15}/\text{cm}^3$ (about 10–20 Ω cm) in order to determine the n-/p-type semiconducting property and doping ratio of SiNWs. Then the source and drain leads are defined with heavy density ($10^{19}/\text{cm}^3$) doping to the patterned area drawn with a photomask design. In the third step, the reactive ion etching (RIE) is conducted to make the micrometer-sized source and drain electrodes. Last the nanometer-sized SiNWs is fabricated with an electric-resist pattern and RIE etching. Subsequently, the contact leads and an insulator layer is made on the SiNW-FET devices. The "bottom-up" method begins with the growth of SiNWs, which are synthesized catalytically and well controlled in a chemical vapor deposition (CVD) reaction via the vapor–liquid–solid (VLS) growing mechanism. Subsequently, the SiNWs are suspended in ethanol solution and assembled onto a silicon substrate. The substrate was spin coated with a two-layer photoresist consisting of LOR3A and S1805 using a photomask protect. Then the source–drain contacts were developed by thermal evaporation. At the end the remaining photoresist layer was removed and a SiNW-FET was fabricated successfully. SiNWs by this "bottom-up" method are of high crystallinity, designated dopant density, thin silicon oxide sheaths, and easily controlled diameters in a cost-effective preparation. However, a deliberate alignment is needed for the randomly orientated SiNWs on the silicon substrate, resulting in inefficient fabrication yields in the device fabrication and limiting their development in the industrial applications. Therefore, the production of high-quality SiNW-FETs requires a uniform assembly technique of the "bottom-up"-synthesized SiNWs on the support substrates [41].

6.4 Application in Neuroscience and Biomedicine

6.4.1 The Research Platform of the Neuronal Signal

In the traditional electrophysiological experiments, neuronal signals are detected by intracellular micropipettes of patch clamps, which are the golden standard detection technique of cellular signals. However, patch clamps are invasive and not easy to conduct multisite simultaneous detection of the neuronal signal propagation, especially for the signal propagation along the single neurite. In this aspect, various FET arrays have great advantages. First, microfabrication technology could fabricate the high-density, micrometer (even nanometer) scale sensor array for the noninvasive and simultaneous detection of extracellular signals. Second, the gate dimension can be made in the nanometer scale, and appropriate contact between the neuron and the FET array will make fine signal detection possible. Besides, the signal detection and appropriate stimulation can be done using the same FET array to study the underlying mechanism of signal propagation.

Patolsky et al. developed a silicon nanowire FET (SiNW-FET) array to stimulate, inhibit, and record neuronal signals from numerous locations along the neuronal projections and cell body [37]. The polylysine patterning technique was employed to direct the growth of rat neurons in order to realize the stable contacts between neurites and SiNW-FETs and the high yield of specific SiNW-neuron structures. They designed an aligned NW-neuron device array, in which silicon nanowires lay between the source and drain electrodes of SiNW-FETs, and the polylysine pattern was made by the lithography technique onto the SiNW-FETs. In the polylysine pattern, a square region 30–60 μm on edge was used to promote the cell body adhesion, and 2 μm-wide lines were projected to define subsequent neurite across the silicon nanowires. Neuron suspensions were planted to polylysine-patterned chips for 1 h of incubation, washed to remove excess cells from non-patterned regions, and then incubated for the neuronal growth under growth conditions in the incubator. This overall approach made it possible that the addressable SiNW-neuron FET array was designed in well-defined positions, and the interdevice spacing can be down to at least 100 nm. The contact length along a neurite projection crossing a SiNW was only on the order of 20 nm; thus, these SiNW-FET devices were highly local and noninvasive probes of neuronal projections. The action potentials were elicited by a conventional glass microelectrode impaled at the soma or the SiNW-axon contact. The intracellular potential (IC) was recorded at the glass microelectrode, and extracellular potential was recorded by the conductance of SiNW-FET. The result showed that SiNW-FET can record the extracellular signals, and it was temporal correlated directly with the intracellular action potential spikes in the soma. The single peak from the SiNW-FET exhibited the characteristic shape of neuronal action potentials. For a p-type SiNW of these devices, the relative potential at the outer membrane was opposite to the measured IC potential and became more negative first and then more positive, which caused an enhanced conductance (accumulation of carriers) followed by a

reduced conductance (depletion of carriers), respectively. Therefore, the conductance peak of p-type SiNW was directly correlated with intracellular (IC) potential peak, while the conductance peak of n-type SiNWs was negatively correlated with IC peak. In another hand, SiNW-FETs can also be used to elicit detectable somatic action potential spikes by applying biphasic excitatory pulse sequences. The threshold of excitatory pulses was about 0.4 V. No potential spikes appeared under the threshold, which was similar as in the presence of chemical inhibitor TTX or the absence of the SiNW. When the input voltage of pulses was set at or above 0.9 V, systematic inhibition and ultimately complete blocking of propagation will be observed. The inhibition effect was similar to the chemical inhibitor TTX. Besides, this kind of single SiNWs can also be used for simultaneous stimulation and detection. In the experiment, the stimulation process was carried out at least 30 times over a 4-h period. The results demonstrated that neurons did not lose potential spikes or viability. Thus, the stimulation does not damage the neurons. They also designed a linear SiNW-FETs array including four SiNW-FETs array, one gap, and another five SiNW-FETs array in order to investigate simultaneous and temporally resolved propagation and backpropagation of action potential spikes in axons and dendrites, respectively. The neuron was guided to adhere on the gap region and projected its axon and dendrite in two opposite directions, respectively. The polarity of neuron can be determined by the growing behavior during culture and subsequently by electrical response and fluorescent imaging after measurement. After intracellular stimulation at the soma, the conductance output from SiNW-FETs array was then simultaneously detected. It was found that seven of nine independent addressable SiNW-FETs yielded correlated conductance peaks after stimulation of action potential spikes in the soma. The high-resolution conductance-time data demonstrated that the propagation of spikes can be resolved in the dendrite and axon. There was a clear peak reduction and temporal spreading in the dendrite direction (NW 6–NW9), while little change was found in the axon direction (NW1–NW5). These observations were consistent with passive and active propagation mechanisms of action potential along dendrite and axon, respectively. In addition, the signal propagation rates were calculated by using the first NW (i.e., NW1 and NW6) in each neurite as references, which were 0.16 m/s for dendrites and 0.43 m/s for axons, respectively. The propagation rates have Gaussian distributions of 0.15 ± 0.04 ($\pm$ SD) and 0.46 ± 0.06 m/s for dendrites and axons, respectively. Highly integrated SiNW-FETs array was also designed and fabricated by this approach to investigate the capability of single-cell hybrid structures at high density of nanoelectronic devices. A well-aligned neuron was achieved on a repeating structure that consists of 50 addressable SiNW-axon elements. The conductance spike propagation along with about 500 μm axon was found in 43 out of 50 devices after intracellular stimulation of action potentials in the soma. Little decay in peak amplitude was found from NW1 to NW49, which was consistent with the active propagation process of action potential along the axon [37]. These local SiNW-neurite junctions could detect, stimulate, and inhibit the local signal flow with high spatial and temporal resolution. The good

reproducibility of the SiNW-neuron devices and great integration ability made it promising in developing flexible real-time cellular assays, such as drug discovery and testing.

6.4.2 Drug and Toxicity Analysis

One important application field of neuronal network-based biosensors is the analysis of drug and toxicity. Neurons can be seen as a homeostatic system, which can constantly regenerate biomolecules or structures and are therefore renewable "receptor platforms." The electrophysiological signals of neurons are sensitive to the microenvironment, and any chemical changes of environment will generate the substance- and concentration-specific responses. Therefore, the neuronal network is a fault-tolerant system and could provide high sensitivity, reliability, and reproducibility in identifying substances. The firing pattern of the whole network will reflect the real changes. Such neuronal network-based biosensors have great application prospect in drug screening, toxicity detection, and evaluation [42].

Gross et al. reported the drug and toxin analysis using neuronal network-based biosensors [42]. They cultured spinal cord neurons on a 64-channel microelectrode array to investigate three strategies, including (1) substance-dependent major changes in spontaneous native activity patterns; (2) substance-dependent changes in network oscillations via disinhibition; and (3) detection of paroxysmal responses indicating major, pathological membrane currents in large subpopulation of cells. The results demonstrated that the glycine receptor blocker (strychnine) could reliably generate increased multichannel bursting at 5–20 nM and regular, coordinated bursting above 5 μM. During the blocker of the inhibitory $GABA_A$ receptors (bicuculline), induced network oscillation compounds will alter oscillation frequencies or terminate activity in a substance-specific manner. The gp120 protein of the AIDS virus (at 1 μg/mL) could produce massive, unique paroxysmal discharges. They also reported spontaneously active neuronal networks grown on substrate-integrated thin-film microelectrodes and determine characteristic responses to the cannabinoid agonists anandamide (AN) and methanandamide (MA) [43]. Dissociated embryonic murine spinal cord and auditory cortex neurons were cultured on microelectrodes. Two kinds of drugs (AN and MA) reversibly inhibited spike and burst production in tissue- and substance-dependent manner. Responses showed high intra- and interculture reproducibility at all ages of neurons. In cortical cultures AN and MA were equipotent and terminated bursting and spiking at 2.5 ± 0.9 mM ($n = 10$), while in spinal cultures, activities were shut off by AN at 1.3 ± 0.7 mM ($n = 15$) but required MA at 5.8 ± 1.2 mM. MA demonstrated a biphasic influence on neuronal activities; excitation effects occurred at 0.25–3.5 mM and suppression effects at 4–7.1 mM. But AN does not have this kind effect. Palmitoylethanolamide did not affect network activity at concentrations up to 6.5 mM, which is a related lipophilic molecule with no reported binding to the CB1 receptor (to which AN and MA bind in the central nervous system). In

addition, the rapid and reliable detection of a toxic compound, trimethylolpropane phosphate (TMPP), was also achieved in another experiment [44].

Marine toxins (brevetoxin-3 (PbTx-3) and saxitoxin (STX)) were detected in a seawater matrix using the neuronal network biosensor (NNB) [45]. The mammalian spinal cord neuronal networks were cultured over microelectrode arrays, and the extracellular action potentials were monitored noninvasively. Before and during exposure to the toxins, the mean spike rate was analyzed. The results demonstrated that extracellular action potentials of the network are highly sensitive to STX and PbTx-3 no matter in recording buffer or in combination with matrixes such as natural seawater and algal growth medium. This work provides evidence that the neuronal network biosensors have great capacity to detect marine toxins rapidly and has the potential for monitoring toxin levels during harmful algal blooms.

6.4.3 Detection of Neurotransmitters

Neurotransmitters play important roles in the whole neuronal system. It is crucial to detect the neurotransmitters and analyze their potential roles in the neuronal networks. Hu et al. developed a hippocampal neuronal network biosensor to detect and monitor 5-hydroxytryptamine (5-HT) using microelectrode array (MEA) chip [46]. As shown in Fig. 6.10a, hippocampal neurons were cultured on the surface of MEA chip, and a random neuronal network was formed on the top of microelectrode array. It can be seen clearly that more than one neuron grew on the single microelectrode. Hippocampal neurons express endogenously 5-HT receptors, which could be activated specifically by 5-HT. Spontaneous extracellular electrophysiological signals can be detected by microelectrode array. Here different concentrations of 5-HT ranging from 0.1 to 100 μmol/L were used to stimulate the activity of neuronal network. The characteristics were discussed by analyzing the firing rate and the firing amplitude. The results were shown in Fig. 6.10b, c, indicating the dose-dependent inhibitory effect of 5-HT on the firing rate of electrophysiological signals as well as the firing amplitude. The firing activity was inhibited completely when the concentration was 10 μmol/L, which was also consistent with the former pharmacological study of 5-HT in hippocampal neuron. While 5-HT was washed out of the medium, the electrophysiological activities can be recovered.

In the bitter taste sensing research, taste buds have specific firing patterns under the stimulation of different bitter substances. These firing signals were transmitted into the cortex for processing. Hu et al. applied three simulated bitter firing signals of taste buds into hippocampal neuronal network by electrical stimulation to investigate the characteristics of responses. The simulated signals corresponded to the responses of three bitter substances (cycloheximide, denatonium, and quinine). The results demonstrated that the activities of the neuronal network were changed significantly by these simulated bitter signals, and the hippocampal

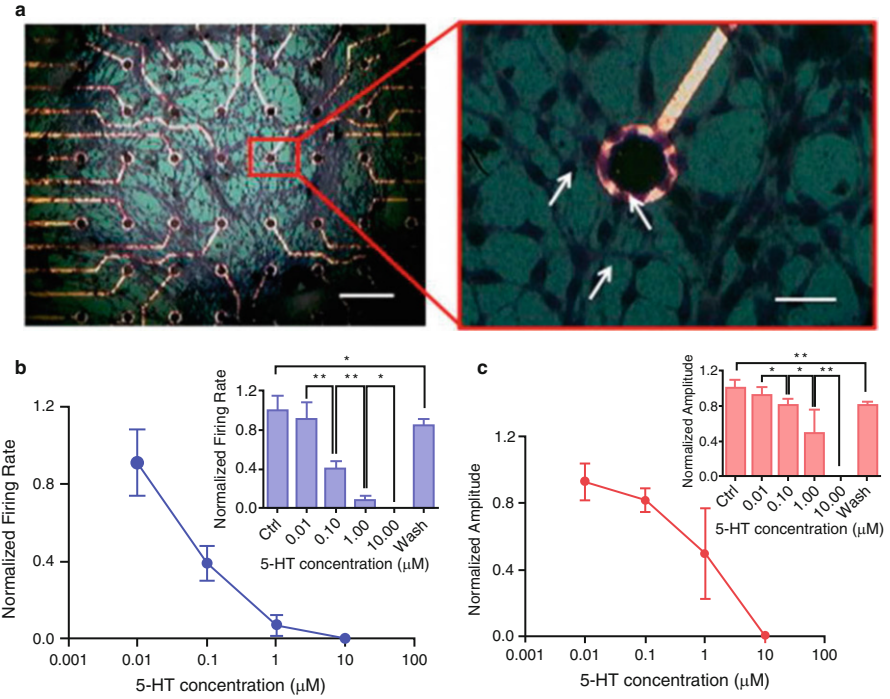

Fig. 6.10 (**a**) Hippocampal neuronal network cultured on microelectrode array (MEA) chip at div14, scale bar 150 μm. The inserted graph illustrated the neurons on the single microelectrode, scale bar 50 μm. (**b**) The relationship curve between the concentration of 5-HT and the firing rate of neuronal network. Inserted graph showed the statistical analysis on the normalized firing rates under concentration gradient. (**c**) The responses of biosensor to 5-HT based on the signal amplitude. Inset is the result of statistical analysis on normalized signal amplitude under concentration gradient (Reproduced with permission from Ref. [46]. Copyright 2015 Elsevier)

neuronal network exhibited specific firing patterns. All these results demonstrated that neuronal network biosensors can be used as a platform to study the neurotransmitter and taste-related researches [47].

6.5 Summary and Outlooks

In this chapter, the neuronal network-based biosensor is well introduced. The pioneering work of early researchers opens a broad field of investigation for neuroscientists and engineers, which combines some traditional research methods of neuroscience and engineering tools. The development of microfabrication makes it possible to detect the weak biological signals in a noninvasive way on the micrometer (even nanometer) level. On one hand, the detection device is developed in the goal of reaching lower signal detection limits and high signal-to-noise ratio.

Various field-effect transistors (FETs) are one major platform of signal detection except microelectrode array (MEA). With the rapid development of semiconductor technologies, the performance of devices becomes more and more efficient and compatible with neurons. The interface between neurons and devices is also well studied in order to increase the efficiency of the signal detection. On the other hand, the neuronal engineering is investigated as well for the specific goals in combination with some advanced biological progress such as optogenetics. In the near future, the application of neuronal network-based biosensor will expand into the standard research platform, such as the neuronal signal propagation and encoding mechanisms, drug screening, odor detection, and even toxicity detection in complex environment.

References

1. Thomas C, Springer P, Loeb G, Berwald-Netter Y, Okun L. A miniature microelectrode array to monitor the bioelectric activity of cultured cells. Exp Cell Res. 1972;74(1):61–6.
2. Pine J. Recording action potentials from cultured neurons with extracellular microcircuit electrodes. J Neurosci Methods. 1980;2(1):19–31.
3. Gross GW. Simultaneous single unit recording in vitro with a photoetched laser deinsulated gold multimicroelectrode surface. Biomed Eng IEEE Trans. 1979;5:273–9.
4. Carter SB. Principles of cell motility: the direction of cell movement and cancer invasion. Nature. 1965;208(5016):1183.
5. Ivanova OY, Margolis L. The use of phospholipid film for shaping cell cultures. Nature. 1973;242:200–1.
6. Kleinfeld D, Kahler K, Hockberger P. Controlled outgrowth of dissociated neurons on patterned substrates. J Neurosci. 1988;8(11):4098–120.
7. Oliva Jr AA, James CD, Kingman CE, Craighead HG, Banker GA. Patterning axonal guidance molecules using a novel strategy for microcontact printing. Neurochem Res. 2003;28 (11):1639–48.
8. Esch T, Lemmon V, Banker G. Local presentation of substrate molecules directs axon specification by cultured hippocampal neurons. J Neurosci. 1999;19(15):6417–26.
9. Matsuzawa M, Tabata T, Knoll W, Kano M. Formation of hippocampal synapses on patterned substrates of a laminin – derived synthetic peptide. Eur J Neurosci. 2000;12(3):903–10.
10. Branch DW, Wheeler BC, Brewer GJ, Leckband DE. Long-term maintenance of patterns of hippocampal pyramidal cells on substrates of polyethylene glycol and microstamped polylysine. Biomed Eng IEEE Trans. 2000;47(3):290–300.
11. Branch DW, Wheeler BC, Brewer GJ, Leckband DE. Long-term stability of grafted polyethylene glycol surfaces for use with microstamped substrates in neuronal cell culture. Biomaterials. 2001;22(10):1035–47.
12. Mai J, Fok L, Gao H, Zhang X, Poo M-M. Axon initiation and growth cone turning on bound protein gradients. J Neurosci. 2009;29(23):7450–8.
13. Hammarback J, Palm S, Furcht L, Letourneau P. Guidance of neurite outgrowth by pathways of substratum-adsorbed laminin. J Neurosci Res. 1985;13(1–2):213–20.
14. Cheng J, Zhu G, Wu L, Du X, Zhang H, Wolfrum B, Jin Q, Zhao J, Offenhäusser A, Xu Y. Photopatterning of self-assembled poly (ethylene) glycol monolayer for neuronal network fabrication. J Neurosci Methods. 2013;213(2):196–203.
15. Falconnet D, Csucs G, Grandin HM, Textor M. Surface engineering approaches to micropattern surfaces for cell-based assays. Biomaterials. 2006;27(16):3044–63.

16. Nakanishi J, Kikuchi Y, Takarada T, Nakayama H, Yamaguchi K, Maeda M. Photoactivation of a substrate for cell adhesion under standard fluorescence microscopes. J Am Chem Soc. 2004;126(50):16314–5.
17. Millet LJ, Collens MB, Perry GL, Bashir R. Pattern analysis and spatial distribution of neurons in culture. Integr Biol. 2011;3(12):1167–78.
18. Lee K-B, Park S-J, Mirkin CA, Smith JC, Mrksich M. Protein nanoarrays generated by dip-pen nanolithography. Science. 2002;295(5560):1702–5.
19. Roth EA, Xu T, Das M, Gregory C, Hickman JJ, Boland T. Inkjet printing for high-throughput cell patterning. Biomaterials. 2004;25(17):3707–15.
20. Nie Z, Kumacheva E. Patterning surfaces with functional polymers. Nat Mater. 2008;7 (4):277–90.
21. Peyrin J-M, Deleglise B, Saias L, Vignes M, Gougis P, Magnifico S, Betuing S, Pietri M, Caboche J, Vanhoutte P. Axon diodes for the reconstruction of oriented neuronal networks in microfluidic chambers. Lab Chip. 2011;11(21):3663–73.
22. Takayama S, McDonald JC, Ostuni E, Liang MN, Kenis PJ, Ismagilov RF, Whitesides GM. Patterning cells and their environments using multiple laminar fluid flows in capillary networks. Proc Natl Acad Sci. 1999;96(10):5545–8.
23. Zeck G, Fromherz P. Noninvasive neuroelectronic interfacing with synaptically connected snail neurons immobilized on a semiconductor chip. Proc Natl Acad Sci. 2001;98 (18):10457–62.
24. Li W, Xu Z, Huang J, Lin X, Luo R, Chen C-H, Shi P. NeuroArray: a universal interface for patterning and interrogating neural circuitry with single cell resolution. Sci Rep. 2014;4:4784.
25. Xie C, Hanson L, Xie W, Lin Z, Cui B, Cui Y. Noninvasive neuron pinning with nanopillar arrays. Nano Lett. 2010;10(10):4020–4.
26. Whitt M, Buonocore L, Rose JK. Liposome – mediated transfection. Curr Protocol Immunol. 2001:10.16. 11–10.16. 14.
27. Labant MA. Transfection methods evolving. Genet Eng Biotechnol News. 2013;33(15):1. 32, 33, 34, 36.
28. Pastrana E. Optogenetics: controlling cell function with light. Nat Methods. 2011;8(1):24–5.
29. Offenhäusser A, Knoll W. Cell-transistor hybrid systems and their potential applications. Trends Biotechnol. 2001;19(2):62–6.
30. Kiilerich-Pedersen K, Rozlosnik N. Cell-based biosensors: electrical sensing in microfluidic devices. Diagnostics. 2012;2(4):83–96.
31. Voelker M, Fromherz P. Signal transmission from individual mammalian nerve cell to field – effect transistor. Small. 2005;1(2):206–10.
32. Hess LH, Seifert M, Garrido JA. Graphene transistors for bioelectronics. Proc IEEE. 2013;101 (7):1780–92.
33. Geim AK, Novoselov KS. The rise of graphene. Nat Mater. 2007;6(3):183–91.
34. Geim AK, Kim P. Carbon wonderland. Sci Am. 2008;298(4):90–7.
35. Schmidt C. Bioelectronics: the bionic material. Nature. 2012;483(7389):S37–7.
36. Hess LH, Jansen M, Maybeck V, Hauf MV, Seifert M, Stutzmann M, Sharp ID, Offenhäusser A, Garrido JA. Graphene transistor arrays for recording action potentials from electrogenic cells. Adv Mater. 2011;23(43):5045–9.
37. Patolsky F, Timko BP, Yu G, Fang Y, Greytak AB, Zheng G, Lieber CM. Detection, stimulation, and inhibition of neuronal signals with high-density nanowire transistor arrays. Science. 2006;313(5790):1100–4.
38. Li C, Curreli M, Lin H, Lei B, Ishikawa F, Datar R, Cote RJ, Thompson ME, Zhou C. Complementary detection of prostate-specific antigen using In2O3 nanowires and carbon nanotubes. J Am Chem Soc. 2005;127(36):12484–5.
39. Choi A, Kim K, Jung H-I, Lee SY. ZnO nanowire biosensors for detection of biomolecular interactions in enhancement mode. Sensors Actuators B Chem. 2010;148(2):577–82.
40. Chen RJ, Choi HC, Bangsaruntip S, Yenilmez E, Tang X, Wang Q, Chang Y-L, Dai H. An investigation of the mechanisms of electronic sensing of protein adsorption on carbon nanotube devices. J Am Chem Soc. 2004;126(5):1563–8.

41. Chen K-I, Li B-R, Chen Y-T. Silicon nanowire field-effect transistor-based biosensors for biomedical diagnosis and cellular recording investigation. Nano Today. 2011;6(2):131–54.
42. Gross GW, Harsch A, Rhoades BK, Göpel W. Odor, drug and toxin analysis with neuronal networks in vitro: extracellular array recording of network responses. Biosens Bioelectron. 1997;12(5):373–93.
43. Morefield S, Keefer E, Chapman K, Gross G. Drug evaluations using neuronal networks cultured on microelectrode arrays. Biosens Bioelectron. 2000;15(7):383–96.
44. Keefer EW, Gramowski A, Stenger DA, Pancrazio JJ, Gross GW. Characterization of acute neurotoxic effects of trimethylolpropane phosphate via neuronal network biosensors. Biosens Bioelectron. 2001;16(7):513–25.
45. Kulagina NV, Mikulski CM, Gray S, Ma W, Doucette GJ, Ramsdell JS, Pancrazio JJ. Detection of marine toxins, brevetoxin-3 and saxitoxin, in seawater using neuronal networks. Environ Sci Technol. 2006;40(2):578–83.
46. Hu L, Wang Q, Qin Z, Su K, Huang L, Hu N, Wang P. Detection of 5-hydroxytryptamine (5-HT) in vitro using a hippocampal neuronal network-based biosensor with extracellular potential analysis of neurons. Biosens Bioelectron. 2015;66:572–8.
47. Hu L. Research on bitter taste cell-based sensing technology and its application in bitter taste transduction mechanism. Zhejiang University, Hangzhou. 2015.

Chapter 7
Micro/Nano Material-Based Biosensors

Xianxin Qiu, Jie Zhou, and Ping Wang

Abstract Novel nanomaterial for use in bioassay applications represents a rapid advancing field. Various kinds of nanomaterial have been investigated to determine their properties and possible applications in biosensor. The nanomaterial's ultrafine grain, high-concentration grain boundary and the adjacent condition of interfacial atoms determine their specific performance which was obviously different from amorphous, normal polycrystal and monocrystal. The common properties of micro/nano material contain volume effect, also known as small size effect, surface effect, quantum size effect, macroscopic quantum tunnel effect, and dielectric confinement effect. Besides, different nanomaterials also have their unique characteristics. Because of these extraordinary effects and properties, nanomaterial shows incredible macroscopic physical properties, which lay a broad prospect for its application. Biosensor is a kind of special sensor which consists of biomolecule recognition element and all kinds of physical or chemical transduces. They are often applied to analyze and detect living and chemical matter with high specificity and accuracy and low cost. Biosensors including electrochemical biosensors, optical biosensor, piezoelectric sensor, and FET-biosensor have got very great developments with the use of micro/nano material. The structures, properties, and applications in biosensors of several main groups, including metal nanomaterial, carbon nanomaterial, semiconductor material, magnetic nanomaterial, etc., are studied in this chapter.

Keywords Nanomaterial • Biosensor • Application

X. Qiu • J. Zhou • P. Wang (✉)
Biosensor National Special Laboratory, Department of Biomedical Engineering, Zhejiang University, Hangzhou, China
e-mail: cnpwang@zju.edu.cn

P. Wang et al. (eds.), *Micro/Nano Cell and Molecular Sensors*,
DOI 10.1007/978-981-10-1658-5_7

7.1 Introduction

The history of biosensors started in 1967 with the development of enzyme electrodes by scientists Updike and Hicks [1]. Since then, research communities from various fields such as very large-scale integration (VLSI), physics, chemistry, and material science have come together to develop more sophisticated, reliable, and mature biosensing devices. Applications for these devices are in the fields of medicine, agriculture, biotechnology, as well as the military and bioterrorism detection and prevention [2].

Biosensors are known as immunosensors, optrodes, chemical canaries, resonant mirrors, glucometers, biochips, and biocomputers. Two commonly cited definitions by S.P.J. Higson [3] and D.M. Frazer [4], respectively, are "a biosensor is a chemical sensing device in which a biologically derived recognition entity is coupled to a transducer, to allow the quantitative development of some complex biochemical parameter," and "a biosensor is an analytical device incorporating a deliberate and intimate combination of a specific biological element (that creates a recognition event) and a physical element (that transduces the recognition event)."

Nanotechnology involves the study, manipulation, creation, and use of materials, devices, and systems typically with dimensions smaller than 100 nm. Nanotechnology is playing an increasingly important role in the development of biosensors [5, 6]. Sensitivity and other attributes of biosensors can be improved by using nanomaterials because of effects such as the quantum size effect, mini size effect, surface effect, and macro-quantum tunnel effect.

Because of their submicron size, nanosensors, nanoprobes, and other nanosystems are revolutionizing the fields of chemical and biological analysis, to enable rapid analysis of multiple substances in vivo and in vitro. As shown in Fig. 7.1, nanoparticles can be modularly assembled from different materials composition with different physical and chemical properties and functionalized with a myriad of ligands for biological targeting [7]. In this chapter, we mainly discuss the structures and properties of nanomaterial and its application in biosensor design.

Nanoparticles can be modularly assembled from different materials composition with different physical and chemical properties and functionalized with a myriad of ligands for biological targeting [7].

7.2 Structures and Properties of Nanomaterial

Novel nanomaterial for use in bioassay applications represents a rapid advancing field. Various kinds of nanomaterial have been investigated to determine their properties and possible applications in biosensor. According to different bulk material, nanomaterial can be classified into several main groups, including metal nanomaterial, carbon nanomaterial, semiconductor material, magnetic nanomaterial, etc. The structures and properties of these nanomaterials are discussed in this section.

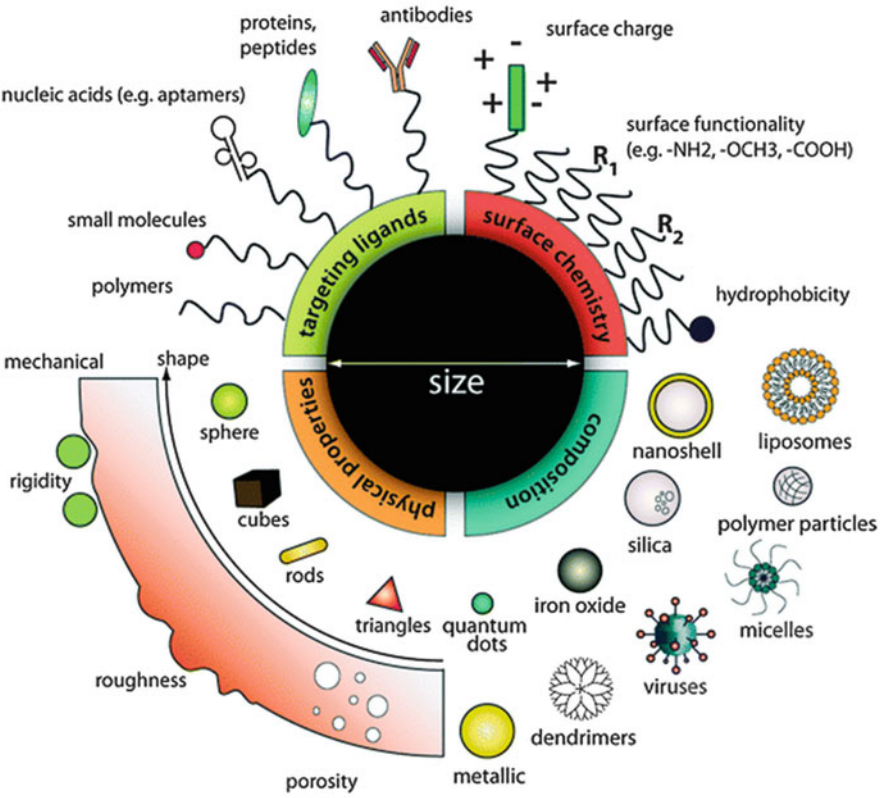

Fig. 7.1 Designing nanoparticles for bioapplications (Reproduced with permission from [7]. Copyright 2010 Royal Society of Chemistry)

7.2.1 Basic Properties of Nanomaterial

The nanomaterial's ultrafine grain, high-concentration grain boundary and the adjacent condition of interfacial atoms determine their specific performance which was obviously different from amorphous, normal polycrystal and monocrystal. We firstly introduce common properties of nanomaterial:

1. Volume effect, also known as small size effect. When the size of nanoparticles is close to or even smaller than the wavelength of conduction electrons and the coherent wavelength of superconducting state, the periodic boundary condition will be destroyed. And the melting point, magnetic properties, optical absorption, heat resistance, chemical activity, and catalytic properties would change significantly.
2. Surface effect. Surface effect refers to the variation of properties induced by the rapid increased ratio of surface atomic number and the total atom number along with the decreasing particle size.

3. Quantum-size effect. When the size of particle decreased to a certain value, the electronic energy levels near Fermi level changed from quasi-continuous energy level to discrete energy level, which makes nanomaterial owning a series of particular properties, such as specific catalysis, strong oxidizability, and reducibility.
4. Macroscopic quantum tunnel effect. It refers to the ability of microscopic particles through the barrier. Magnetic nanoparticles have tunnel effect. So they can pass through the barrier of macroscopic system.
5. Dielectric confinement effect. The dielectric confined effects of nanoparticles have important impacts on the light absorption, photochemical and optical nonlinearity properties of nanoparticles.

Besides, nanomaterial also has other characteristics. Because of these extraordinary effects and properties, nanomaterial shows incredible macroscopic physical properties, which lay a broad prospect for its application.

7.2.2 Metal Nanoparticles

Among all the metal nanomaterials, the precious metal nanomaterial is most widely used. Next we'll primarily introduce the properties of precious metal nanomaterial.

Precious metal nanomaterial refers to material containing precious metal (gold, silver, platinum, palladium, and other expensive elements) and in the size of 0.1–100 nm developed by nanotechnology [8]. Precious metal material itself has unique physical and chemical properties. When the size of the precious metal material is in a state of mesoscopic, its macroscopic properties will change greatly. When the size of precious metal material decreased to nanoscale scope, it not only has all the properties of bulk precious metal but also presents the novel properties of nanomaterial [9]. Thus precious metal nanomaterial has broad application prospect in the field of chemical catalysis, biological medicine, energy and environment, and electronic technology and attracts more and more attention of researchers [10, 11].

7.2.2.1 The Properties of Precious Metal Nanomaterial

Optical Properties

Precious metal nanoparticles have strong light absorption when the size decreased to a certain degree. The smaller the size is, the darker the color is. Besides, compared with bulk material, the light absorption peak of precious metal nanomaterial showed obvious spectral migration properties. It would shift to short-wave direction or long-wave direction that is blue shift or red shift [12]. The quantum confinement effect of precious metal nanoparticles would cause significant quantum energy-level splitting of nanoparticles and the

broadening of bandgap between the conduction band and valence band, inducing the blue shift of spectrum; the interface or surface effect of precious metal nanoparticles leads to increased surface tension of nanoparticles, which further prompts the narrowing of bandgap and causes the red shift of spectrum [13, 14]. The spectral migration characteristics of metal nanomaterial provide solid theoretical support for designing novel nano-optical sensor and colorimetric probe [15–17].

Surface Plasmon Resonance Properties

Under the light exposure, free electrons on metal surface are undergoing electromagnetic disturbance, resulting in the oscillation of partial charges and the formation of plasma [18]. When the frequency of applied electromagnetic wave equals the oscillation frequency of the plasma inside the metal, the surface plasmon resonance (SPR) occurs [19–21].

Noble metal nanoparticles are different from precious bulk metal, for the surface oscillation of electron cannot form electromagnetic wave which oscillated along the surface, but forms electromagnetic wave which oscillated confined on the surface of nanoparticles that is localized surface plasmon resonance (LSPR) [18]. The surface functionalization and modification could be achieved by Au-S bond or electrostatic adsorption, which is the key to its analytical applications. Figures 7.2 and 7.3 show the characteristics of precious metal nanomaterial, respectively, including easy modification and color-gradient characteristics.

Thermal Properties

The melting point of large-sized solid matter is fixed. After it being ultra-micronized, the melting point was significantly decreased, especially when the

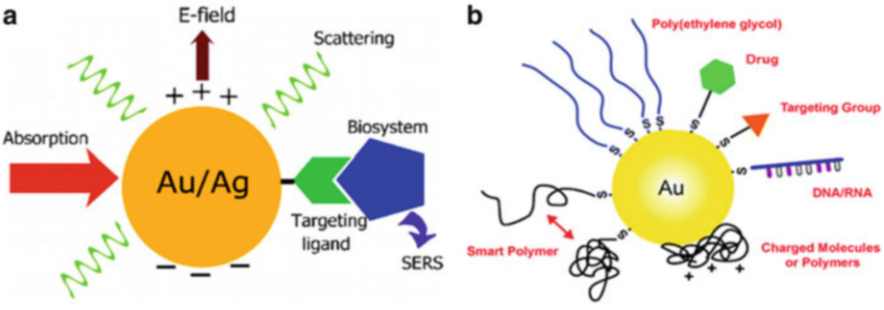

Fig. 7.2 (**a**) The optical properties of noble metal nanomaterial (Reproduced with permission from [10]. Copyright 2008, American Chemical Society); (**b**) NMNMs can be conjugated with a wide variety of functional moieties, both through the gold-thiolate bond and by passive adsorption (Reproduced with permission from [22]. Copyright 2010 Royal Society of Chemistry)

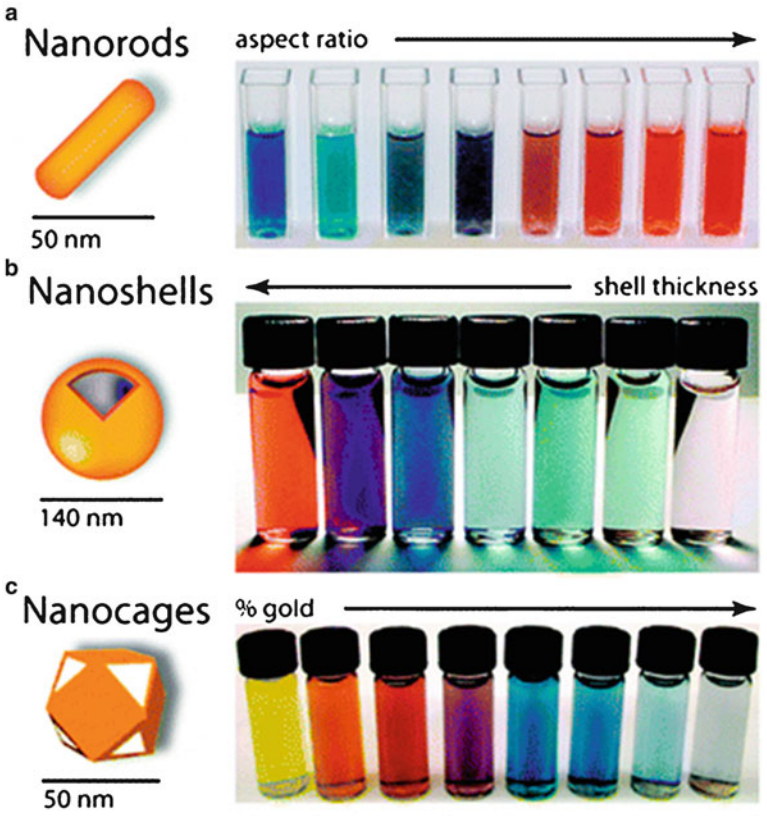

Fig. 7.3 Biomedical applications of gold nanoparticles. (**a**) Gold nanorods, (**b**) nanoshells, and (**c**) gold nanocages. The intense color arises from the collective excitation of their conduction electrons, or surface plasmon resonance modes, because of photon absorption at wavelengths which varies with (**a**) aspect ratio, (**b**) shell thickness, and/or (**c**) galvanic displacement by gold (Reproduced with permission from [23]. Copyright 2011 Royal Society of Chemistry)

particle size is less than 10 nm magnitude. The conductive material made from superfine silver powder can be sintered under low temperature, which could not only save raw material but also produce high-quality membrane with uniform thickness and large coverage [24].

Catalytic Properties

The catalytic activity and selectivity of precious metal nanomaterial can be controlled by regulating its morphology, element composition, and surface modification. The crystal face has important influence on the catalytic activity and selectivity of nanoparticles [24].

7.2.3 *Carbon Nanomaterial*

Carbon nanomaterial refers to carbon material which at least one dimension is smaller than 100 nm. Novel carbon nanomaterial in different structure and morphology has been successively synthesized, such as zero-dimensional fullerenes, one-dimensional carbon nanotubes, two-dimensional graphene, etc.

7.2.3.1 Fullerene

Fullerene is a novel type of all-carbon molecule. And it is the third allotrope of carbon and famous for its unique cage structure, in which one of most prominent representatives is C_{60}. C_{60} is spherical in shape. It could be expressed as that each carbon atom forms two single bonds and one double bond with adjacent three carbon atoms [25]. Because of the structural characteristics of C60 molecule, it presents many special physical and chemical properties such as anti-pressure capacity, the strong intramolecular force, weak molecular pressure, and low surface energy, which make it act as good solid lubricant in the tribology. All π electrons of C_{60} tightly bind together and produce the negative inductive effect. So it has strong electrophilic ability and can be used as electron acceptor. Some kinds of metal atom could be embedded in C60 molecule to form the intercalation compound. In 1991, Hebard first reported the superconducting temperature of potassium-doped C60: $Tc = 18$ K, exceeding the highest organic superconductivity temperature ($Tc = 12.8$ K), which aroused great interest of physicists and materials scientists [26]. Lately the Tc of Rb_3C_{60} was found to be 28 k, the Tc for Rb_2CsC_{60} is 31 k, and the Tc for $RbCs_2C_{60}$ is 33 k.

Fullerene molecules such as C_{60} and C_{70} present a unique performance due to its unique structure. So far C_{60}, C_{70}, and their derivatives have been found to have a series of excellent performance in optical, electrical, and magnetic fields. Especially, the nanotubes prepared by C60 have broad application prospects.

7.2.3.2 Carbon Nanotubes

Carbon nanotube is a one-dimensional quantum material with special structure (the radial size of CNTs is at nanoscale, the axial size of CNTs is at microscale, and both ends of nanotubes are sealed). According to the number of layers of carbon nanotubes, carbon nanotubes can be generally divided into single-walled carbon nanotubes (SWCNTs), double-walled carbon nanotubes (DWCNTs), and multi-walled carbon nanotubes (MWCNTs).

Carbon nanotubes have good electrical conductivity, mechanical properties, and biocompatibility. Researches have showed that carbon nanotubes not only have high strength and toughness but also have excellent electrical and magnetic properties, making it a recognized super one-dimensional reinforced material.

Mechanical Property

CNTs have good mechanical properties. The tensile strength of CNTs is up to 50–200 GPa, 100 times higher than that of steel. The tensile strength of SWCNTs with ideal structure is about 800 GPa. The composite material, which is made by fabricating carbon nanotubes on other engineering materials as matrix, would have excellent strength, elasticity, antifatigue, and isotropic properties, which may greatly improve the performance of composite materials. The hardness of CNTs is comparative to that of diamond, but it has good flexibility and can be stretched. In addition, the melting point of CNTs is the highest among known materials.

Conductive Property

CNTs have good electrical performance due to the lamellar structure similar with graphite. Theories predicted that the conductive properties of CNTs depend on its diameter and helical angle of CNTs. When the diameter of CNTs is greater than 6 nm, the conductivity of CNTs decreased.

Heat-Transfer Properties

CNTs have good heat transfer properties. CNTs have big L/D ratio; thus the heat transfer performance along the length direction is high, and the heat transfer performance along the vertical direction is low. In addition, CNTs have relatively high thermal conductivity. So the thermal conductivity of the composite material could be greatly improved as long as trace CNTs are doped in the composite material.

7.2.3.3 Graphene

For many years it has been used to describe the properties of carbon material, such as fullerenes, carbon nanotubes, and graphite. Almost all allotropes of carbon except diamond can be obtained from graphene, as shown in Fig. 7.4 [27]. Graphene is normally in a thickness of an atomic layer, but can also be collectively called single-layer graphene, double-layer graphene, and graphene with less than ten layers. Ten atomic layers are the critical thickness between the 2D and 3D materials.

Basic Electronic Properties

The most worth exploring physical property of graphene is its electronic properties [27–29]. Firstly, the mostly discussed aspect is the electronic spectroscopy of

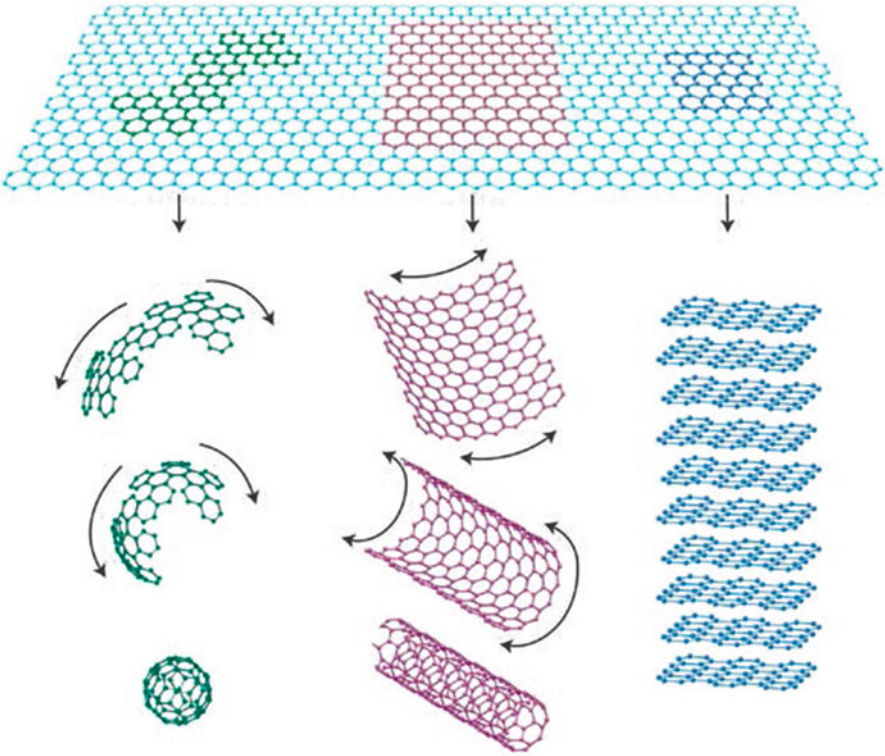

Fig. 7.4 Graphene is a 2D building material. It can be changed into 0D buckyballs, rolled into 1D nanotubes or stacked into 3D graphite (Reproduced with permission from [27]. Copyright 2007 Nature Publishing Group)

graphene (dispersion relations). Secondly, the propagation of electronic wave in graphene is confined in a one-atom thick layer, making them detectable by a variety of probes. At the same time, it makes them sensitive to other materials close to graphene, such as dielectric, superconductor, ferromagnetic, etc. Thirdly, electrons of graphene can transmit in submicron range without scattering; even graphene is put on rough substrate. Fourthly, the quantum effect of graphene is very strong even at room temperature.

Electron Transport Properties

Owing to highly symmetric crystal structure of graphene, at room temperature, the mobility of graphene almost has nothing to do with temperature and is mainly influenced by impurities and defects [30].

Nonelectronic Properties

In 2008, C. Lee reported the first measurement on the mechanical and thermal properties of graphene. The breaking strength of graphene is ~40 N/m and reaches the theoretic limit [31]. He also reported that the thermal conductivity of graphene was recorded at room temperature ($-5000\ \mathrm{Wm^{-1}\ K^{-1}}$) [32] and Young's modulus (~1.0 TPa) [31]. Graphene can be elastically stretched up to 20 %, which is larger than most crystals [31, 33]. Similarly, graphene has both high flexibility and high vulnerability [34]. In addition, graphene is composed of single-atom thick layers, which make it impermeable to gas, including helium [35].

7.2.4 Semiconductor Nanomaterial

The size of particles is greater than that of atom clusters and less than usual particles, generally 0.1–100 nm. It includes two parts with similar volume: one is particles in a diameter of several or dozens of nanometer and the other is the interface between particles.

It is more sensitive to confined space. Semiconductor nanomaterial doesn't exist in nature and it is mainly artificially made by energy-band engineering. The unique properties of semiconductor nanomaterial make it play an important role in the development of various functional devices. Except the common properties of nanoparticles, semiconductor nanoparticles also have special optical effects and photoelectrochemical properties.

Among many outstanding optical properties, the ultrafast optical nonlinear response and photoluminescence (room temperature) features have attracted most attentions. The blue shift of absorption spectrum and fluorescence spectrum forms a series of discrete energy levels in the band.

7.2.5 Magnetic Nanomaterial

The properties of nanomaterial are different from that of conventional magnetic material. The reason is that the characteristic physical length associated with magnetism is exactly at the nanometer level. Magnetic nanomaterial has many special properties, such as superparamagnetism, quantum size effect, macroscopic quantum tunneling effect, small size effect, etc. Among them, its magnetic properties are the most outstanding property distinguishing it from any other nanomaterial.

When nanoparticles' size reaches a critical value, it will enter the super paramagnetic state and coercive force is nearly zero. When there is no additional magnetic field, the particles (domain) are in disordered arrangement showing paramagnetism. When magnetic field is applied, the particles are ordered in terms of magnetic field showing the ferromagnetism (but weaker than block).

There are mainly five kinds of magnetic material, metal alloy (Fe, Co, Ni), ferric oxide (Fe_20_3, Fe_30_4), iron nitride (FeN), ferrite ($CoFe_20_4$, $BaFe_{12}0_{19}$), and chrome oxide ($Cr0_2$). Among them, Fe_30_4 is mostly used magnetic nanoparticles. It can be easily prepared by coprecipitation or oxidative coprecipitation in aqueous solution. And its size, shape, and composition can be controlled by adjusting the reaction conditions.

Ferroferric oxide crystal can be expressed as $Fe(III)[Fe(II)Fe(III)]O_4$. The size of ferromagnetic oxide nanoparticle normally distributed at around 5–100 nm. Owing to the small size effect and surface effect, when the diameter of ferroferric oxide nanoparticle is smaller than 16 nm, it presented superparamagnetism [36]. The unique performance of ferromagnetic oxide nanoparticles affords great potential in biomedical research and separation process study [37]. The nanoparticles are easily to be synthesized and functionalized, which provides great commonality for research. Figure 7.5 shows the properties and modification of ferroferric oxide nanoparticles [38].

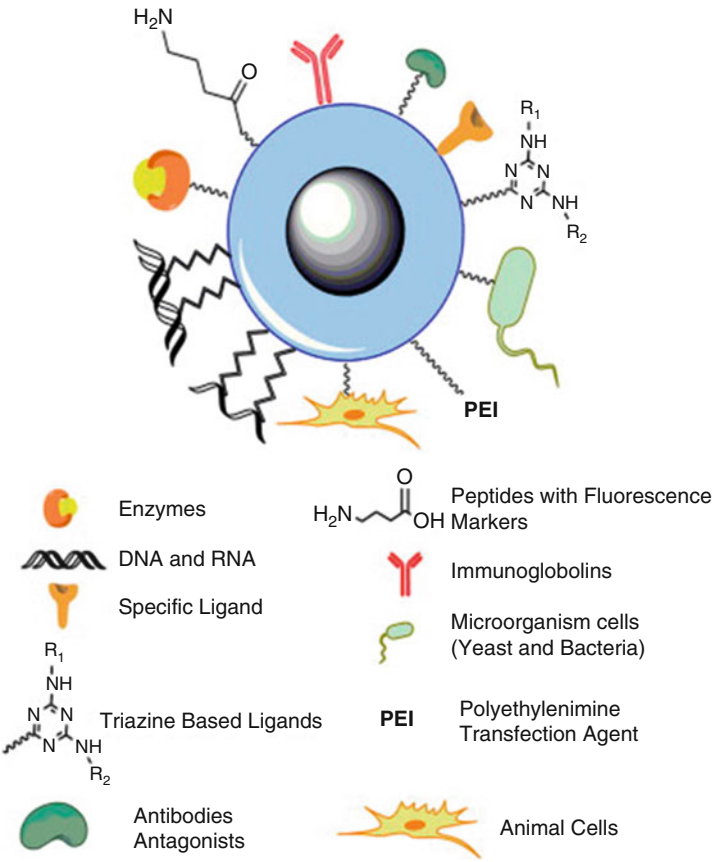

Fig. 7.5 Magnetic nanoparticles decorated with multifunctional receptors and polysaccharides (Reproduced with permission from [38]. Copyright 2008 Elsevier B.V.)

7.3 Recent Developments in the Use of Micro/Nano Material in Biosensors

7.3.1 Electrochemical Biosensors

Nanomaterials mainly have the following functions when it is applied in the field of electrochemical biosensor: (1) accelerate electron transfer and increase the reaction reversibility of redox on electrode surface, (2) catalyze reaction, (3) act as the carrier of biological molecules, (4) label biological molecules, (5) control chemical reaction, and (6) act as reactants.

7.3.1.1 Accelerating Electron Transfer

Metal nanoparticles (such as gold, silver, etc.) and carbon nanotubes can be used as a conductor which connects protein (enzyme) and electrodes and promotes the electron transfer between electrodes and the active center of protein, making it applicable to prepare biological sensors with special performance. Willner et al. [39] linked 1.4 nm gold nanoparticles with flavin adenine dinucleotide (FAD), the cofactor of glucose oxidase (GOx) together, and then recombine FAD-AuNPs composite and cofactor-deleted GOx into new GOx. The recombinant enzyme was assembled onto the gold electrode through double thiol molecules. When detecting glucose with this electrode, the electrons were transferred between enzyme and electrodes through AuNPs making electron transfer rate seven times higher than that between a natural enzyme and the natural oxygen. Because the electron transfer rate of AuNPs is quicker than that of oxygen, the sensor is not affected by the concentration of dissolved oxygen and the interference of reducing substances – ascorbic acid when detecting glucose. After that, they fixed one end of carbon nanotubes on electrodes, while connecting the other end to the FAD, and to form a new GOx like AuNPs [40]. Carbon nanotubes can also transfer electrons between recombinant enzyme and electrodes like a wire. And the electron transfer rate is six times faster than that between a natural enzyme and its oxygen substrate. What's more, the electron transfer rate is related to the length of carbon nanotubes. For example, the electron transfer rate of carbon nanotubes with the length of 25 nm is 1.5 times than that with a length of 50 nm. Xu et al. introduced 17 nm AuNPs into assembled composite membrane for fabricating a glucose biosensor [41].

In addition, the direct electrochemical reaction of many biological molecules such as myoglobin (Mb), hemoglobin (Hb), cytochrome C (Cyt C), and horseradish peroxidase (HRP) on the electrode can also be conducted through the conduction of the metal, metal oxide nanoparticles, or carbon nanotubes. Ju et al. fixed a hybrid composite membrane of zirconium dioxide and Mb on the surface of graphite electrode [42]. The existence of composite membrane accelerated the electron transfer between the electrode and Mb, making the sensor catalyze the reduction of hydrogen peroxide in the absence of any medium. Li et al. [43] assembled gold

nanoparticles on gold electrode using thiol-DNA and then immobilized Cytc. Gold nanoparticles transfer electrons between Cytc and electrode, by which we can observe the direct electrochemistry of Cytc. And in a certain range, with the increased layer of gold nanoparticle, the electrochemical current of Cytc increased.

In addition to being electronic wire, metal nanoparticles [44] and carbon nanotubes can also help improve oxidation-reduction reversibility of active substances in electrochemical sensitive membranes.

7.3.1.2 Acting as Catalyst

Metal nanomaterial could catalyze the oxidation or reduction of various electroactive substances (e.g., nicotinamide adenine dinucleotide (NADH) and H_2O_2) and reduce its overpotential in electrochemical reactions. Raj et al. [45] found that NADH was oxidized at −0.3 V on electrodes modified with sol-gel film doped with gold nanoparticles and reached the maximum value at 0 V. Compton et al. [46] found that the silver nanoparticles can catalyze the reduction of H_2O_2, based on which the electrodes have a detection limit of 2.2 μmol/L for H_2O_2. Platinum nanoparticles can also catalyze the oxidation of H_2O_2. Halaoui et al. [47] prepared a highly sensitive H_2O_2 sensor by immobilizing platinum nanoparticles on indium tin oxide (ITO) electrode surface modified with poly diene propyl dimethylamine (PDDA) by self-assembly method. Since NADH is coenzyme for more than 300 kinds of dehydrogenase. While H_2O_2 is the reaction product of oxidase and the substrate of peroxidase, through the high selective determination of NADH and H_2O_2, we can effectively detect the concentration of many kinds of enzymes or the substrate. Palladium and iridium nanoparticles have similar functions with platinum, so they are frequently used as material to immobilize oxidase on electrodes.

Because of the small diameter, high surface energy, and the insufficient atom ligand, carbon nanomaterial such as carbon nanotubes are easily to transfer electron with other substances, making it suitable for broad applications in electrocatalysis. Gorski et al. [48] dissolved carbon nanotubes in chitosan, forming carbon nanotubes-chitosan composites. The compound had good film-forming property and showed the good catalytic capability on the oxidation of NADH. The NADH oxidation potential on the composite membrane was reduced by 300 mV. After fixing glucose dehydrogenase on the electrode surface, the sensor can quantitatively detect glucose of 5.0–300 μmol/L. Chen et al. [49] fixed carbon nanotubes-chitosan composites on glassy carbon electrode surface with one step of electrodeposition method, which can catalyze the reaction of O_2 and H_2O_2 at the same time. The prepared biosensor can be used to detect the substrate at different potentials, which effectively eliminates the interference of electroactive material such as ascorbic acid. Using electrical catalysis of carbon nanotubes modified electrodes on H_2O_2 or NADH, we can indirectly detect substrates and inhibitors of many enzymes, such as choline, ethanol, organophosphorus pesticide, and so on.

7.3.1.3 The Immobilization of Biomolecules

With such features as large specific surface area, high surface free energy, good biocompatibility, and rich in functional groups on surface, nanomaterial makes it possible to fix a large number of biological molecules on the electrode surface and keeps its good biological conformation and activity, which plays a vital role in the construction of biosensor.

Gold nanoparticles were widely applied in immobilizing protein. AuNPs have been used to immobilize a lot of protein, such as Hb, HRP, tyrosinase, and glucose oxidase on the electrode surface. Studies have shown that protein (enzyme) can attach on the surface of AuNPs well through the interaction between groups like NH_2 and SH and gold atom. What's more, AuNPs have good biocompatibility. So, fixed biological molecules can maintain their biological activity. Chen et al. [50] deposited chitosan-AuNPs-GOx composite on electrode surface using electrodeposition method and prepared an amperometric sensor with fast response for the determination of glucose. Recently, they used AuNPs which was synthesized in situ on the surface of polydimethylsiloxane (PDMS) to develop polymer-nanomaterial composite film-modified electrodes with good biocompatibility and strong protein adsorption ability [51]. Taking advantage of different adsorption sites of choline oxidase and acetyl cholinesterase on composite membrane, the selective detection of acetyl cholinesterase in homogenate neural tissue can be realized. Except for immobilizing protein, gold nanoparticles have also played a huge role in immobilizing antigen, antibody, DNA, and cells. Zhu et al. [52] synthesized a three-dimensional nanostructured gold film which provided a biocompatible microenvironment for antibodies and then developed a novel unlabeled immunosensor. Ju et al. [53] built a bionic interface using AuNP-chitosan gel and cultured K562 leukemia cells on the interface. The number of cells, the proliferation, and apoptosis of cells can be reflected by the change of impedance value.

Oxide nanomaterial is mainly used for protein immobilization in the field of electrochemical biosensors. Because of the good hydrophilicity and biological compatibility of nano-oxides' surface, nano-oxides are beneficial for maintaining the biological configuration of proteins and can realize the direct electron transfer between active center of protein and the electrode surface. Hu et al. [54] immobilized heme proteins on the graphite electrode through layer-by-layer assembly method by using the interaction between SiO_2 nanoparticles and Hb, which realized direct electrochemistry of HB. In addition, they have discussed the immobile driving force of the protein on oxide nanoparticles based on the model of heme protein [55]. In 2004, for the first time, by introducing SiO_2 nanoparticles and GOx onto grid surface of FET, Chen et al. [56] prepared enzyme-based FET which presented increased sensitivity and prolonged service life for glucose determination compared to enzyme-based FET without SiO_2 nanoparticles. Besides the electrostatic interaction, there is chelation between transitional metal nanoparticles and proteins. Therefore, they are more suitable for immobilizing protein. Nanomaterials such as TiO_2, Fe_3O_4, ZrO_2, and MnO_2 also achieved good results for immobilizing protein on electrochemical biosensors.

7.3.1.4 Biomolecule Labeling

Among metal nanomaterials, gold and silver nanoparticles can be used as biomarkers in electrochemical analysis by labeling biomolecules with molecular recognition ability, such as antigen, antibody, DNA, etc., which play a role in electrochemical immunoassay and DNA testing. Limoges et al. [57] labeled antibody with gold nanoparticles and assembled gold nanoparticles on electrode surface through the immunoreaction between antibody and antigen. Then the concentration of gold ions was determined by anodic stripping voltammetry, thus indirectly measuring the concentration of antibody. The method is of high sensitivity and can be used to measure pmol/L level of immunoglobulin. On the basis of that, the developed AgNP- and CuNP-enhanced stripping method was also applied to the antigen and antibody detection.

With multiple energy state, semiconductor nanomaterials such as CdS, CdTe, PbS, and ZnS can glow when they are excited at multiple wavelengths. The nanoparticle biomarkers used in electrochemical analysis are mainly metal nanoparticle and semiconductor nanoparticles, namely, quantum dots. In the field of electrochemical biosensors, quantum dots are often applied to label biological molecules. Biological molecules labeled by quantum dots were assembled to the sensor interface through specific interaction between antigen and antibody or biotin and avidin. After that, the concentration of targets can be quantitatively detected through stripping voltammetric response of the constituent elements of a quantum dot. Wang et al. [58] labeled CdS quantum dots onto polysaccharides. Due to the specific interaction between the polysaccharide and lectins fixed on surface of gold electrode, CdS quantum dots labeled polysaccharide (fixed concentration) and unlabeled polysaccharide (concentration need to be detected) competitively combined with lectins. So concentration of polysaccharide can be indirectly measured by measuring the stripping voltammetric response of Cd caught by lectins. In addition, they developed an electrochemical method which can detect a variety of kinds of DNA at the same time [59]. Recently, Ju et al. [60] assembled a novel sugar monolayer film that established a method for in situ detection of sugar on cell surface by using CdTe quantum dots as the biomarker.

7.3.1.5 Acting as Reactant

It is known that the chemical properties of nanoparticles are different from that of its body material. Due to high surface energy, the chemical activity of nanomaterial is usually higher than its ontology. As is known to all, MnO_2 can catalyze the decomposition of H_2O_2, but MnO_2 nanoparticles can directly react with H_2O_2, generating Mn^{2+} and O_2, while consuming H^+. Obviously, the consumption of H^+ will cause the change of pH, which can be monitored by H^+-sensitive FET. Based on this principle, Chen et al. [61, 62] prepared glucose biosensor and lactic acid biosensor with high sensitivity and good selectivity. In addition, MnO_2

nanoparticles can also react with ascorbic acid. Taking advantage of this property, Chen et al. [63] deposited a layer of MnO_2-chitosan composite film on the surface of prepared glucose sensor, which can effectively eliminate the influence of ascorbic acid and improve the precision of the sensor in the determination of glucose. More recently they developed H_2O_2 sensor with double catalytic ability by using the property of changing valence of MnO_2 nanoparticles, which were successfully applied for detection of choline at low potential [64].

7.3.2 Optical Biosensor

7.3.2.1 The Application of Metal Nanoparticles in Optical Biosensor

Photochemical sensing research of precious metal nanoparticles has attracted much attention in recent years. Applications of precious metal nanomaterial in the field of optical sensing are mainly concentrated in the following aspects:

1. The optical colorimetric analysis
2. The surface plasmon resonance detection
3. Local surface plasmon resonance (LSPR) and surface-enhanced Raman scattering (SERS)
4. The fluorescence detection

Chromaticity sensor has attracted many attentions due to its simplicity, high sensitivity, low cost, easiness to read by naked eyes, no need for complex instruments, etc. Metal nanoparticles, due to its high extinction coefficient in visible light area, have become one kind of colorimetric probe. The dispersion of AuNP solution presents a red color, while the aggregation of AnNPs presents a purple or blue color. So far, AuNPs modified by different functional molecules with high recognition ability have been widely used.

For the first time, Mirkin et al. [65–67] used thiol-DNA-modified AuNP probe, since DNA can combine with a lot of target molecules, causing the cross-link of AuNPs. So they can detect different kinds of target materials such as oligonucleotides, proteins, small molecules, enzyme activity, metal ion, etc. AuNPs modified with thiolated aptamer acted as colorimetric probe. Based on the color changes in the process of gathering and depolymerization, sensitive colorimetric detection of adenosine can be realized.

Xia group established a universal colorimetric sensor platform by using unlabeled ssDNA, unmodified AuNPs, and cationic conjugated polymers, which can be used in the detection of a variety of target materials including DNA, proteins, small molecules, and inorganic ions [68].

In 2010, Parab et al. reported an optical sensor to detect target DNA by using gold nanorods as molecular probe. This sensor is based on that the hybridization of target DNA with two different DNA probes leads to the aggregation of gold nanorods. This sensor has been successfully applied to detect pathogen gene of

Chlamydia trachomatis in human urine samples with a detection range of 0.25–20 nM.

Surface plasmon resonance sensor is a new type of biological sensing technology which appeared in the 1980s. By utilizing SPR principle, SPR sensor transferred the interaction of biological molecules into optical signal. SPR sensor owns the advantage of real-time, online detection and highly sensitive detection.

Localized surface plasmon resonance refers to a physical optic phenomenon when the incident light radiates on the surface of nanoparticles, in which occasion the frequency of incident light resonates with the oscillation frequency of metal free electron aggregation and presents strong absorption spectra in specific wavelength range.

In addition to the inheritance of SPR sensor's merits, LSPR sensor also has the following features:

1. Small test instrument and simple system setup
2. High sensitivity and strong anti-interference ability
3. Rapid and multichannel detection

The biomacromolecular detection based on the technology of LSPR is an important branch of LSPR sensing research. Gold nanorods are the most commonly used LSPR sensing substrate which is easy to be prepared. Gold nanorods own strong local surface plasmon resonance absorption peak and can be assembled into a one-dimensional (1D), two-dimensional (2D), and three-dimensional (3D) structure under suitable conditions. The resonance absorption peak of gold nanorods is relatively sensitive to shape, size, and space between nanorods and the surrounding medium environment. Using this feature, LSPR sensors based on gold nanorods has begun to be widely used in biological macromolecules detection, immunoassay, etc. [69].

In 1996, Mirkin et al. [65] firstly reported gold nanoparticle-based DNA detection by LSPR method. He added a single-stranded DNA sequence which was complementary to different DNA fragments modified on the surface of AuNPs to the AuNPs solution, leading to the red shift of the absorption peak of LSPR. At the same time, the color of AuNP solution turned from red to blue. Although this method is sensitive, the surface of AuNPs needs complex modification process and the operation is complicated. In 2000, by using gold nanoparticles with negative charge on its surface, Li et al. [70] wrapped single-stranded DNA on the surface of AuNPs through electrostatic interactions. When target DNA fragments appeared in the system, the hybridization of target DNA with DNA probe on the surface of AuNPs would occur, which would induce the aggregation and color change of gold nanoparticles. Immune analysis based on the technology of LSPR is an important branch of LSPR sensing research. In 2002, Thanh et al. [71] develop a method which can detect anti-protein antibody at 1 ug/mL based on the aggregation of AuNPs.

Huang et al. [72] prepared a photochemical biosensor based on unlabeled and high-throughput LSPR for the first time. The author prepared five LSPR sensors with different throughput by using five kinds of gold nanorods with different length

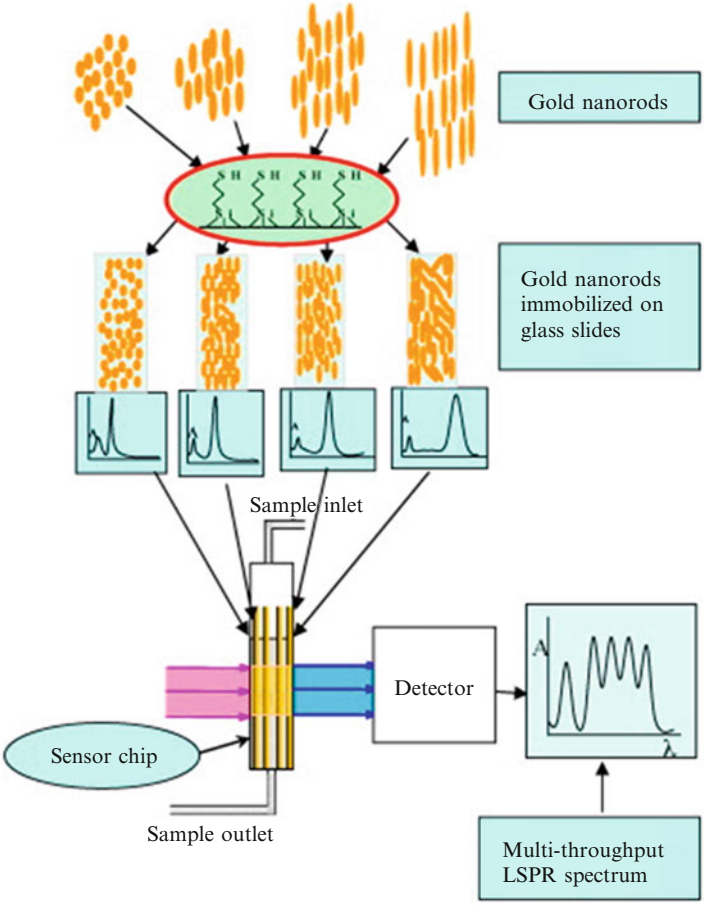

Fig. 7.6 Multi-throughput localized surface plasmon resonance (MLSPR) (Reproduced with permission from [72]. Copyright 2008 Elsevier B.V.)

to diameter ratio. Different receptor-ligand pairs can be detected in the wavelength range from 530 to 940 nm at the same time. And the sensor can also detect three pairs of the antigen antibody simultaneously. Wang et al. [73] applied LSPR sensors based on gold nanorods for the detection of hepatitis B virus (HBV) in buffer, serum, and plasma. Harshala et al. [74] prepared an optical DNA sensor for pathogen diagnosis (Fig. 7.6).

With the development of surface modification technology and nanofabrication technology, by controlling the array distribution, structure, and the surrounding medium of the precious metal nanoparticles and increasing the breadth and depth of LSPR technology, LSPR technology will become a forefront research hotspot in sensing fields.

Compared to other spectral methods, fluorescence analysis is very popular due to its inherent advantages such as high sensitivity, easiness to operate, and the diversity of the measurable parameters. Especially in recent years, some progresses in research of properties of nanomaterial give a new thought for designing chemical and biological fluorescent sensing scheme.

In 2005, Chen et al. [75] found that there are two fluorescence emission belts at 743 nm and 793 nm with different intensity for gold nanorods whose length to diameter ratio is greater than 1:13. The larger the length to diameter ratio is, the higher fluorescent efficiency gold nanorods have. The hybridization between DNA probe and target molecules can be detected through the changing of fluorescence intensity of gold nanorods which is labeled by DNA molecule.

In 2010, Gouet et al. [76] detected the human single-stranded DNA, double-stranded DNA, and G-quadruplex by using the positively charged gold nanorods as optical labels. The conformation changes of telomere DNA are converted to multiple optical signals such as fluorescence quenching, near-infrared absorption, plasma resonance light scattering, and dynamic light scattering. The formation of double-stranded DNA and G-quadruplex, accompanied by strength decreases, leads to the fluorescence quenching and blue shift of longitudinal absorption peak of gold nanorods.

Surface-enhanced Raman scattering (SERS) is an important tool for studying surface molecules. Raman spectrum analysis method is based on the Raman scattering effect found by Indian scientists C.V. Raman. By analyzing the scattering spectrum which is different with incident light, we can get the information of molecular vibration and rotation. And the information is helpful for us to study the structure of molecules. While using normal Raman spectrometry to detect the sample adsorbed on colloidal metal particles such as silver, gold, or copper or on the rough surface of metal, the Raman spectrum intensity of the sample can be improved by 10^3–10^6 times. This phenomenon is called surface-enhanced Raman effect.

SERS overcomes the drawback of low sensitivity of Raman spectrum, so it can get the structural information which cannot be easily retrieved from the conventional Raman spectrum, resulting its wide use in the study of biological molecular interface orientation, configuration, structure, etc. Relative information in vivo about biomacromolecule such as protein, nucleic acid, and phospholipid can be accurately obtained by stimulating the near-infrared light which has less damage to organisms. Surface-enhanced Raman scattering can be used in biological research of complex system.

Due to its nanoscale rough surface and good water solubility of AuNPs, it has been widely used as SERS-active substrate which can be applied to study soluble adsorption molecules in solution system in the fields of biochemistry, trace analysis, etc. The study found that the size, shape, and surface topography of gold nanoparticles will greatly influence the SERS enhancement effect. Also, although the SERS enhancement factor of a single gold particle is small, the enhancement of AuNP aggregation is obvious. The aggregation of AuNPs can be obtained by adding some inorganic salts (KCl, NaCl, $NaNO_3$) and organic amine into the AuNP solution. Nie et al. [77] designed a new kind of SERS AuNP probe. Through

the specific hybridization of DNA, the distance between AuNPs was adjusted, which would change SERS signal and then realize molecular recognition and signal amplification. Besides being used as SERS substrate in the solution system, AuNPs can also be used in the preparation of solid base. Porter et al. [78] proved that the gold substrate assembled by AuNPs can become good solid-phase SERS substrate. Meanwhile they found that SERS substrate with gold basement and gold nanoparticles has strong SERS effect and proved that coupled vibration of these two kinds of surface electron cloud of the basement and gold nanoparticles played an important role in SERS effect.

7.3.2.2 The Application of Semiconductor Nanoparticles in Optical Biosensor

Quantum dots, QD for short, also called the semiconductor nanoparticles or semiconductor nanocrystals, are a kind of nanoparticles composed of VI and V elements [79]. With high fluorescence quantum productivity and better fluorescence lifetime, core-shell type quantum dots have many advantages as fluorescent probes compared with traditional fluorescent dyes and are often used for the detection of biological macromolecules [80].

QD assay labeling uses QDs for in vitro assay detection of DNA, proteins, and other biomolecules. DNA-coated QDs have been shown as sensitive and specific DNA labels for in situ hybridizations, as probes for human metaphase chromosomes, and in single-nucleotide polymorphism and multi-allele DNA detection. Conversely, DNA linked to QD surfaces has been used to code and sort the nanocrystals. These results demonstrate that DNA-conjugated QDs specifically bind their complements both in fixed cells and in vitro. For proteins, our group uses a self-assembled electrostatic protein QD functionalization strategy to create QD-based fluoro-immunoassay reagents. Using antibodies conjugated to QDs by an adaptor protein, we have carried out multiple demonstrations of analyte detection in numerous immunoassays including a four-color multiplex toxin analysis [81, 82]. For bioassays, the ability to excite QDs at almost any wavelength below the band edge combined with high photo bleaching resistance and "multiplexing" capabilities highlights the unique combination of spectral properties that make QD fluorophores of interest to biologist.

Luminescent quantum dots have many applications in nucleic acid detection. DNA molecules labeled with QDs can be used as a fluorescent probe of oligonucleotide which could hybrid specifically with its complementary oligonucleotide. After DNA molecules labeled with QDs match with its complementary DNA, the fluorescence spectrum of QDs will change. It's the arrangement change of QDs that cause changes of their fluorescence [83]. Han et al. [84] assembled QDs which emit different fluorescence on the surface of polymer microspheres and encode according to the type of QDs and the ratio of fluorescence intensity through hybridization reaction, which can provide corresponding fluorescence information

for each of the DNA sequence with 99.99 % accuracy. Patolsky et al. monitored the dynamics of DNA replication by using resonance energy transfer between CdSe/ZnS quantum dots and organic fluorescence [85].

7.3.2.3 The Application of Carbon Nanomaterial in Optical Biosensor

Resonance energy transfer, a kind of non-radiation energy transfer process, is when the donor on excited state transfers energy to receptors on the ground state. When the donor is a kind of fluorescent substance, whether the receptor is a kind of fluorescent substance or not, this process is called fluorescence resonance energy transfer (FRET). The efficiency of FRET is affected by many factors, such as the degree of spectrum overlapping, the orientation of quadrupole on transition state, the distance between the donor and receptor molecules, etc. Donor and receptor are usually two kinds of dye molecules whose charge is limited to the zero dimension in traditional FRET, in which the energy transfer rate (k) is inversely proportional to the six powers of molecule distance. The effective distance of energy transfer is between 1 and 10 nm. When the distance is more than 10 nm, effective FRET process will not happen. According to the report of Sebastian et al. [86, 87], when either receptor or donor has off-domain charge, the rate of energy transfer will deviate from the traditional law of FRET. For example, when the donor is dye molecule and the receptor is CNTs with one-dimensional structure, the rate of energy transfer is inversely proportional to five powers of distance. When the receptor is graphene, the rate of energy transfer is inversely proportional to four powers of the distance. In these systems, even when effective energy transfer distance is far greater than 10 nm, the transfer efficiency is much higher than that of the traditional energy transfer efficiency between dye molecules. Therefore, donor-recipient type based on nanomaterials such as CNTs and graphene has broad application prospects in the chemical and biological sensing.

In terms of CNTs, in recent years, research about the interaction between some biological molecules such as nucleic acids, proteins, and CNTs is very attractive which can be used for the separation of CNTs, biological sensing, and drug transmission. Among them, the ssDNA was proved to have the ability to interact with CNTs non-covalently. ssDNA could wrap around the surface of CNTs to form stable compounds through the π-π stack between its nucleotide bases and sidewall of CNTs. However, the affinity of double-stranded DNA (dsDNA) to CNTs is very small, so it cannot wrap on the surface of CNTs [88, 89]. The differences of affinity properties to CNTs between single- and double-stranded DNA combine with specificity of aptamer to interact its target resulting to the CNTs wide use in chemical biology sensing. For example, Yang et al. built donor-receptor type nanohybrid through the interaction between CNTs and SWCNTs both labeled by fluorophore. As shown in Fig. 7.7, after the formation of dsDNA based on hybridization with the target sequence, fluorescence recovery can be detected. In addition, the detection range of this sensing strategy to detecting target material molecules can expand by utilizing aptamer. For example, Yang et al. [90] detected adenosine

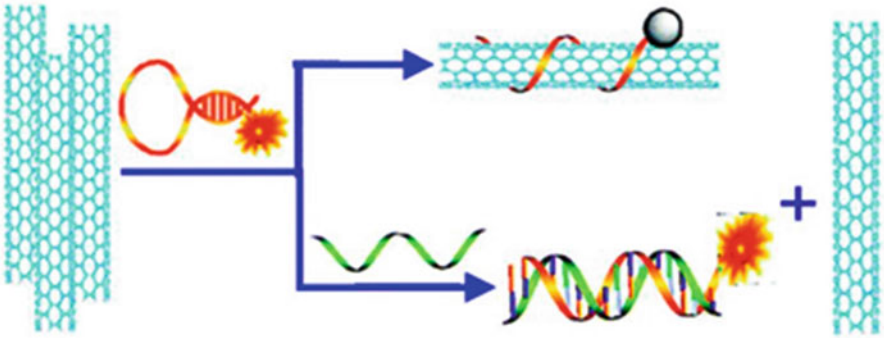

Fig. 7.7 Scheme of the SWCNTs-based fluorescence sensor for DNA detection (Reproduced with permission from [90]. Copyright 2008 American Chemical Society)

triphosphate by assembling aptamer molecular beacon (MAB) and MWCNTs. Not only the problem of high fluorescent background signal and low efficiency of energy transfer between the dye of the traditional molecular beacon can be overcame; the cost was also reduced greatly by using MWCNTs as energy receptors. In addition, by using different Aptamer, the detection range of molecules increased greatly.

Similarly, FRET sensor based on graphene especially graphene oxide (GO) is widely used. They are usually consisted of three parts:

1. Recognition probe, such as ssDNA or aptamer which can respectively combine with the corresponding target sequence or specific molecular targets
2. The report fluorophore which usually coupled on the probe
3. GO

First of all, the DNA probes labeled with fluorescent molecules interact with GO plane through nucleotide bases, forming donor-receptor type GO hybridization and inducing fluorescence quenching. While target molecules were combined with DNA probe, the conformation of DNA probe changed, inducing the dissociation of DNA probe. Finally, the FRET process is terminated, so is the fluorescence recovery of quenching fluorophore led by. Tang et al. [91] reported such kind of sensor system based on the recovery of quenching fluorophore to detect specific ssDNA sequences, whose detection limit can reach nanomole level. The author also discovered that DNA adsorbed on the surface of GO can protect it from nuclease degradation, confirmed that specific detection of target sequences in the presence of nuclease can also be realized. Similarly, the other two DNA sensing methods were further proved that they can be used to detect the mismatch of single base.

In order to further improve the sensitivity of the method, Li et al. [92] built double-quenching fluorescence sensing system by combining GO and molecular beacon (MS), which greatly improves the SNR, and the detection limit can reach 0.1 nM. Dong et al. [93] took CdTe QDs as fluorescent report group and detected target molecules by building the GO/MB-QDs energy transfer quenching system.

Similarly, this method can be used to detect proteins and metal ions by using aptamer as the recognition probe. Lu et al. [94] designed a fluorescent sensor based on the GO/aptamer for thrombin detection whose performance is obviously better than that of purely fluorescent sensor based on traditional fluorescent dye [95] and optical sensing method based on aptamer-CNT hatch. In addition, Chang et al. [96] also developed fluorescence sensing method by using surfactant decentralized reduced graphene oxide (RGO) rather than GO, which improve the detection sensitivity up to picomole. And Wen also developed a FRET method for sensitive detection of Ag by using specific aptamer of Ag labeled by fluorescence and GO (Fig. 7.8).

7.3.3 Piezoelectric Sensor and FET Biosensor

7.3.3.1 The Application of Nanomaterial in Piezoelectric Sensor

The term "piezoelectric" derived from the Greek word piezen meaning "to press." The first investigation on the piezoelectricity was performed in 1880 by Jacques and Pierre Curie [98], who observed that a mechanical stress is applied to the surfaces of various crystals, caused by a corresponding electrical potential across the crystal, whose magnitude was proportional to the applied stress. Many types of materials (quartz, tourmaline, lithium niobate or tantalate, oriented zinc oxide, or aluminum nitride) exhibit the piezoelectric effect, but the properties of quartz make it the most common crystal type used in analytical applications. The most used devices in biosensors are generally bulk acoustic wave-based and surface acoustic wave-based biosensor.

Surface acoustic wave (SAW) is a kind of acoustic wave that spreads along the surface of medium, and its amplitude decreases rapidly with depth. As early as 100 years ago, people had known the properties of this wave theoretically, but until 1965 the technology of generating surface wave had been broken through by using interdigital transducer. Since then, SAW device obtained rapid development. Now it has been widely used in fields such as radar, satellite, communication, electronic countermeasure, and sensor technology, becoming a new kind of promising device.

Typical quartz crystal SAW devices mainly include delay lines, resonators, oscillators, band-pass filter, etc. And the main component of SAW is piezoelectric substrate and interdigital transducer (IDT). IDT is one kind of ultrasonic transducer that could directly excite surface acoustic wave. Because of its low dissipation of electroacoustic conversion, design flexibility, simple fabrication, and certain working frequency range, it has become one of mostly used technologies for the excitation and detection of surface acoustic wave. Firstly, a layer of metal film was fabricated on piezoelectric substrate by vacuum vapor deposition. Then the interdigital fork electrodes were made by photolithography method.

Nanomaterials have incomparable excellent properties, so they are often used for signal amplification of piezoelectric biosensor. Wang et al. [99] deposited amino

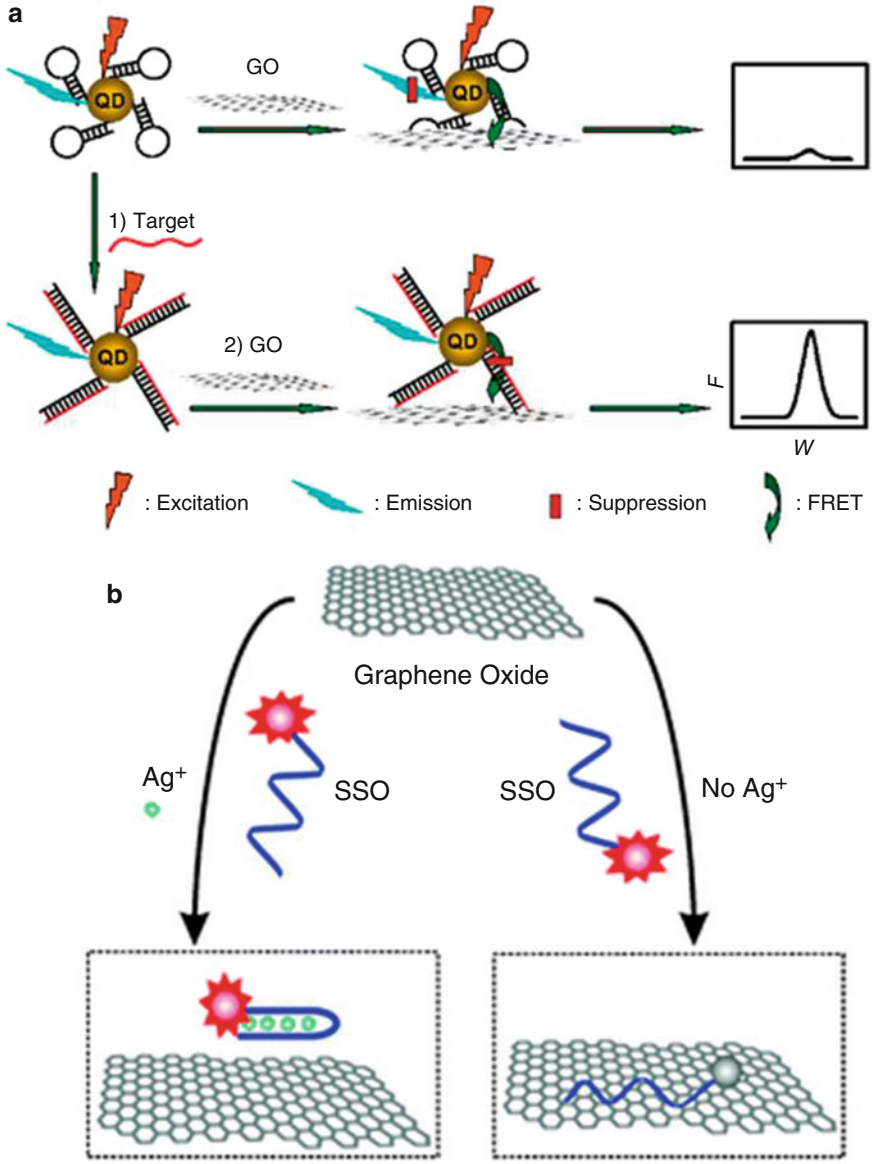

Fig. 7.8 (**a**) Schematic illustration of DNA hybridization using a double-quenching system consisting of GO and molecular beacon (MB) (Reproduced with permission from [93]. Copyright 2015 2010, American Chemical Society). (**b**) Schematic illustration of the fluorescence sensor for Ag(I) ions based on the target-induced conformational change of a silver-specific cytosine-rich oligonucleotide (SSO) and the interactions between the fluorogenic SSO probe and graphene oxide (Reproduced with permission from [97]. Copyright 2010 Royal Society of Chemistry)

plasma polymer film on the gold electrode surface of a piezoelectric crystal and then assembled nanoparticles on film to develop an immobilization technology based on the multiplication of gold nanoparticles.

Jin et al. [100] labeled antihuman IgG antibody with nanoscale SiO_2 particles instead of traditional latex and established an improved liquid piezoelectric immune agglutination technology based on piezoelectric immune agglutination sensing for direct and rapid detection for human IgG. Meanwhile, they investigate immune agglutinate phenomenon between nanogold-labeled antibody and lgG and compared its result with that of antibody labeled with SiO_2 nanoparticles. Hua Wang et al. [101] covalently fixed the predominant antigens of schistosome on the surface of functional SiO_2 particles and rapidly detected the concentration of schistosome antibody in infectious rabbit serum by sensitive sensing the changes of non-quality parameters such as density, viscosity induced by agglutination action events of immune particle using piezoelectric crystal, and then successfully developed a piezoelectric sensor-based assay for the diagnosis of schistosomiasis. Compared with normal immune sensing method, this kind of non-mass effect piezoelectric sensor has the advantage of fast and sensitive detection, simple operation, low cost, portable detection instrument, real-time detection, etc.

7.3.3.2 The Application of Carbon Nanomaterial in Field-Effect Transistor-Based Biosensors

Among diverse electrical biosensing architectures, devices based on field-effect transistors (FETs) have attracted great attention because they are an ideal biosensor that can directly translate the interactions between target biological molecules and the FET surface into readable electrical signals. There has been an explosion of interest in using carbon nanomaterials in FET-based biosensors. Owing to their unique physicochemical properties, SWNTs and graphene are in the forefront of this explosion. The major advantages of SWNTs and graphenes are their high conductivity, well biocompatibility, molecule compatibility size, high chemical stability, and easy availability, which suggest that carbon nanomaterial-based FETs have promised as paradigms for device architecture, yielding devices that are capable of converting biological information to easily detectable electrical signals.

The properties of SWNTs can be leveraged by combining them with other functional materials, such as small molecules, lipid membrane, or aptamers, to enhance the biosensing performance and install new functionalities. Kim et al. coated SWNT surfaces with human olfactory receptor 2AG1 and reported the real-time detection of specific odorant molecules (such as amyl butyrate, butyl butyrate, propyl butyrate, and pentyl valerate) [102]. The observed femtomolar sensitivity resulted from the deformation of the human olfactory receptor 2AG1 protein when the WNT-bound protein and the odorants docked.

Previous reports indicated that single-stranded DNA can form a stable complex with individual SWNTs by wrapping around them, the interaction being driven by

the aromatic interactions between nucleotide bases and SWNT sidewalls. Label-free electrical detection of DNA hybridization utilizing SWNT FET-based biosensors suggests a new generation of DNA chips that can give direct electrical readouts. This could provide fast and inexpensive analyses of nucleic acid samples. In 2006, Star et al. [103] used SWNT FETs to study interactions between single-stranded DNA oligonucleotides and SWNTs and the subsequent DNA hybridization processes that occurred on the device surface. They showed that SWNT FETs could be selectively modified with DNA oligonucleotides and maintain hybridization specificity.

Recently, Goldsmith et al. have developed an electrochemical method to create single-point defects in SWNTs in a controllable manner and then covalently bind biomolecules at this scattering site [104]. Using these devices, they also demonstrated continuous, multihour monitoring of the binding of a single molecule with high sensitivity (a conductance change of >100 nS for binding of a reactive carbodiimide). Sorgenfrei et al. [105] covalently attached a single-stranded probe DNA sequence, which was terminated with an amine group, to a carboxylic acid functionalized point defect in a carbon nanotube using a standard amide-formation coupling reaction.

Recently, the increasing interest in graphene for biosensing applications seems to have overtaken the corresponding interest in SWNTs. The first graphene FET-based electrical biosensors were demonstrated by Mohanty et al. [106]. They immobilized GO and GA sheets on silica substrates with either predeposited or postdeposited gold electrodes and used silicon as a back gate for electrical measurements. They exploited the functional groups on GOs or GAs to fabricate three CMG-based biosensors:

1. A single-bacterium biodevice
2. A label-free DNA sensor
3. A bacterial DNA/protein and a polyelectrolyte chemical transistor

The bacteria biodevice was highly sensitive; just a single-bacterium attachment caused a sharp (42 %) increase in conductivity of CMG sheets. To improve the detection sensitivity, Dong et al. [107] used large, CVD-grown graphene films to fabricate biosensors, thereby achieving DNA sensing with a concentration as low as 0.01 nM. They attribute this marked increase in sensitivity to the electronic n-doping to the devices. They further found that adding AuNPs on the surface of graphene devices could extend the upper limit of DNA detection from 10 to 500 nM due to the increase in loading of probe DNA molecules onto the AuNPs. This AuNP strategy is apparently widely applicable.

Ohno et al. [108] developed label-free immunosensing based on an aptamer-modified graphene FETs. The aptamer-modified graphene FETs showed selective electrical detection of immunoglobulin E protein. From the dependence of the drain current variation on the immunoglobulin E concentration, the dissociation constant was estimated to be 47 nM, indicating good affinity. In a similar way, Agarwal et al. [109] recently demonstrated the biocompatibility of reduced GOs with proteins and further used them after protein functionalization to create biosensors for detecting various metals in real time with high sensitivity [110] (Fig. 7.9).

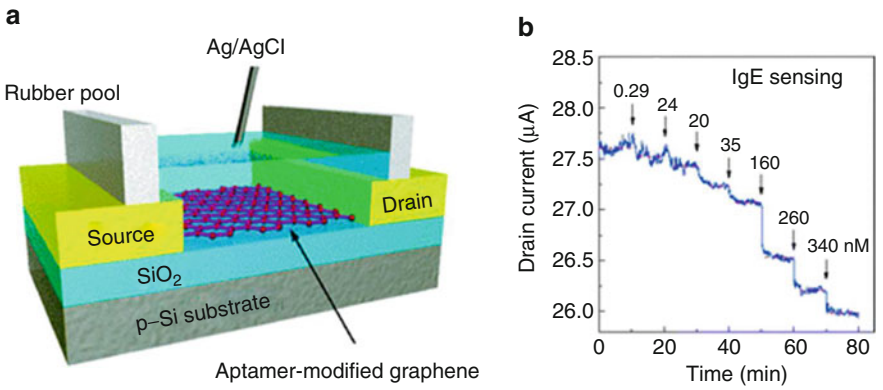

Fig. 7.9 (**a**) Schematic illustration of aptamer-modified electrolyte-gated graphene FETs. (**b**) Time course of ID for an aptamer-modified graphene FET. At 10-min intervals, various concentrations of IgE were injected (Reproduced with permission from [108]. Copyright 2010 American Chemical Society)

7.3.3.3 The Application of Silicon Nanowire in Field-Effect Transistor-Based Biosensors

Silicon nanowire field-effect transistors (SiNW-FETs) have recently drawn tremendous attention as a promising tool in biosensor design for their ultrasensitivity, selectivity, and label-free and real-time detection capabilities [111]. In the fields of biological research, SiNW-FETs are employed in the detections of proteins, DNA sequences, small molecules, cancer biomarkers, and viruses.

SiNW-FET has been widely used lately for studying protein interaction mechanisms, not only because of its real-time and label-free detection but also due to its high sensitivity and selectivity. An early measurement made by Cui et al. demonstrated the real-time detection of streptavidin binding to biotin-modified SiNWFET [112]. They also explored the ability of biotin-modified SiNW-FET to detect streptavidin at the concentration of 10 pM, which is much lower than the nanomolar-range detection level obtained from other techniques, such as the stochastic sensing of single molecules [113]. Lately, Zheng et al. have also demonstrated a new methodology based on a frequency (f) domain electrical measurement utilizing a SiNW-FET for protein detection [114]. In the presence of the protein (antigen) which can be recognized specifically by the antibody-functionalized SiNW-FET, the frequency spectrum exhibits a Lorentzian shape with a characteristic frequency of several kHz. They observed the shape of the frequency spectrum to monitor the binding events and further to determine the detection limit.

In addition to the protein-protein interactions mentioned above, SiNW-FETs were adapted for the detection of DNA or RNA. Due to the large amount of negative charges in the phosphate backbones of DNA or RNA, SiNW-FETs offer a good candidate for monitoring DNA or RNA hybridizations, because the

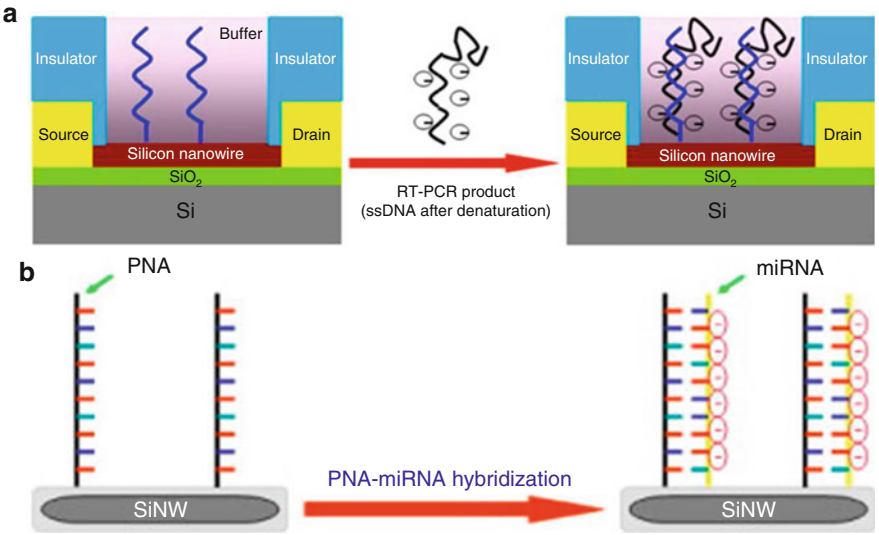

Fig. 7.10 (**a**) A schematic diagram of the RT-PCR product of DEN-2 hybridized to a PNA-functionalized SiNW-FET sensor (Reproduced with permission from [116]. Copyright 2008 Elsevier B.V.) (**b**) Label-free direct hybridization for the ultrasensitive detection of miRNA (Reproduced with permission from [117]. Copyright 2008 Elsevier B.V.)

hybridizations cause the accumulation or depletion of charge carriers in the SiNW-FET, leading to a conductance change. Hahm et al. have reported the real-time and label-free detection of DNA with a PNA (peptide nucleic acid)-modified SiNW-FET [115]. In that study, PNA was anchored to the SiNW surface by the strong interaction between avidin and biotin. The successful PNA-DNA duplex formation was demonstrated by the observation of a sizable increase in conductance in the p-type PNA-modified SiNW-FET, because of the negatively charged phosphate backbones of DNA. This ultrasensitive biosensor for sensing DNA is capable of detecting down to 10 fM.

Specific PNA-modified SiNW-FET sensors have recently been established to diagnose dengue virus infection [116]. As represented schematically in Fig. 7.10a, the synthetic PNA receptors were first anchored to the SiNW-FET surface. A specific fragment (69 bp) derived from dengue serotype2 (DEN-2) virus genome sequences was selected as the target DNA and amplified by the reverse transcription polymerase chain reaction (RT-PCR). The detection limit of this biosensor based on SiNW-FET was claimed to be 10 fM. In addition, this promising method allows the detection of microRNAs (miRNAs) for early cancer diagnosis [117]. As illustrated in Fig. 7.10b, a PNA-immobilized SiNW-FET was used to probe miRNA by detecting PNA-miRNA hybridization via base pairing. This approach exhibits an excellent detecting specificity capable of discriminating a single-base mismatch in miRNA.

The SiNW-FET system has also been applied to disease screening. Recently, Zheng et al. utilized a SiNW-FET array for the detection of multiple cancer markers [117]. This SiNW-FET array, shown in Fig. 7.10, is composed of three independent SiNW-FET devices on which different antibodies were immobilized. The conductance vs. time measurements showed the simultaneous recording of the PSA, CEA, and mucin-1 solutions, which were delivered sequentially to the SiNW-FET arrays. By virtue of the ultrasensitive SiNW-FET, the detection limit for these three cancer markers has advanced to the pg/mL scale.

Using nano- and neuro-technologies to couple electrical interfacing with neural systems has great potential to unveil many details of neuron studies [118]. In the past few years, SiNW-FETs and CNT-FETs have been applied for electrophysiological measurements by recording signals from neuron cells and tissues, e.g., recording the electrical signal from a single neuron and cardiomyocyte cells and detecting the released neurotransmitter of CgA from living neurons.

7.4 Summary and Outlooks

Nanomaterial, especially the combination of nanomaterial with other materials or different nanomaterial (such as carbon nanotubes and nanoparticles, quantum dots and nanoparticles) combinations increasing the immobilization amount of bioactive substances and surface active sites, provides good reaction microenvironment, accelerates the electron transfer process, and shortens the response time of signal. The sensitivity, detection range, and repeatability of biosensor have been dramatically enhanced, which broaden the application fields of biosensors. As more and more nanomaterials were discovered and used, biosensors have become a new detection technology. It has broad application prospect in the field of life science and engineering technology.

In the future, the study of novel biosensor design based on nanomaterial can focus on the following aspects:

1. The synthesis of nanomaterial with uniform distribution and obvious physiochemical response, which may play a role in the multi-protein and multi-gene detection simultaneously.
2. The use of nanomaterial for constructing bionic interface, which can be applied to the study of artificial simulation of neural activity.
3. The combination of nanomaterial, microfluidic chip, and ultramicroelectrode technology, which can be applied for real-time monitoring chemical activity of single cell.
4. The combination of nanomaterial and biosensing technology and MEMS technology, which can be utilized to develop biosensors for real-time and on-site detection of complicated real samples. With the deepening of the study, the nanotechnology-based biosensor will play a more important role on the research and exploring of life process and will be widely applied in the areas closely related to people's daily life such as clinical diagnosis, environmental monitoring, and food safety.

References

1. Updike S, Hicks G. The enzyme electrode. Nature. 1967;214:986–8.
2. Mohanty SP, Kougianos E. Biosensors: a tutorial review. Potentials IEEE. 2006;25(2):35–40.
3. Higson SP, Reddy SM, Vadgama P. Enzyme and other biosensors: evolution of a technology. Eng Sci Educ J. 1994;3(1):41–8.
4. Fraser D. Glucose biosensors: the sweet smell of success. Med Device Technol. 1994;5:44–7.
5. Cullum BM, Griffin GD, Miller GH, Vo-Dinh T. Intracellular measurements in mammary carcinoma cells using fiber-optic nanosensors. Anal Biochem. 2000;277(1):25–32.
6. Haruyama T. Micro-and nanobiotechnology for biosensing cellular responses. Adv Drug Deliv Rev. 2003;55(3):393–401.
7. Chou LY, Ming K, Chan WC. Strategies for the intracellular delivery of nanoparticles. Chem Soc Rev. 2011;40(1):233–45.
8. Guo S, Wang E. Noble metal nanomaterials: controllable synthesis and application in fuel cells and analytical sensors. Nano Today. 2011;6(3):240–64.
9. Burda C, Chen X, Narayanan R, El-Sayed MA. Chemistry and properties of nanocrystals of different shapes. Chem Rev. 2005;105(4):1025–102.
10. Jain PK, Huang X, El-Sayed IH, El-Sayed MA. Noble metals on the nanoscale: optical and photothermal properties and some applications in imaging, sensing, biology, and medicine. Acc Chem Res. 2008;41(12):1578–86.
11. Giljohann DA, Seferos DS, Daniel WL, Massich MD, Patel PC, Mirkin CA. Gold nanoparticles for biology and medicine. Angew Chem Int Ed. 2010;49(19):3280–94.
12. Kelly KL, Coronado E, Zhao LL, Schatz GC. The optical properties of metal nanoparticles: the influence of size, shape, and dielectric environment. J Phys Chem B. 2003;107(3):668–77.
13. Murphy CJ, Sau TK, Gole AM, Orendorff CJ, Gao J, Gou L, Hunyadi SE, Li T. Anisotropic metal nanoparticles: synthesis, assembly, and optical applications. J Phys Chem B. 2005;109 (29):13857–70.
14. Huang X-J, Choi Y-K. Chemical sensors based on nanostructured materials. Sensors Actuators B Chem. 2007;122(2):659–71.
15. Cao YC, Jin R, Mirkin CA. Nanoparticles with Raman spectroscopic fingerprints for DNA and RNA detection. Science. 2002;297(5586):1536–40.
16. Nam J-M, Thaxton CS, Mirkin CA. Nanoparticle-based bio-bar codes for the ultrasensitive detection of proteins. Science. 2003;301(5641):1884–6.
17. Zhang J, Wang L, Zhang H, Boey F, Song S, Fan C. Aptamer-based multicolor fluorescent gold nanoprobes for multiplex detection in homogeneous solution. Small. 2010;6(2):201–4.
18. Jain PK, Huang X, El-Sayed IH, El-Sayed MA. Review of some interesting surface plasmon resonance-enhanced properties of noble metal nanoparticles and their applications to biosystems. Plasmonics. 2007;2(3):107–18.
19. Link S, El-Sayed MA. Optical properties and ultrafast dynamics of metallic nanocrystals. Annu Rev Phys Chem. 2003;54(1):331–66.
20. Kreibig U, Vollmer M. Optical properties of metal clusters. Berlin: Springer; 1995.
21. Eustis S, El-Sayed MA. Why gold nanoparticles are more precious than pretty gold: noble metal surface plasmon resonance and its enhancement of the radiative and nonradiative properties of nanocrystals of different shapes. Chem Soc Rev. 2006;35(3):209–17.
22. Cobley CM, Chen J, Cho EC, Wang LV, Xia Y. Gold nanostructures: a class of multifunctional materials for biomedical applications. Chem Soc Rev. 2011;40(1):44–56.
23. Dreaden EC, Alkilany AM, Huang X, Murphy CJ, El-Sayed MA. The golden age: gold nanoparticles for biomedicine. Chem Soc Rev. 2012;41(7):2740–79.
24. Daniel M-C, Astruc D. Gold nanoparticles: assembly, supramolecular chemistry, quantum-size-related properties, and applications toward biology, catalysis, and nanotechnology. Chem Rev. 2004;104(1):293–346.

25. Ruoff R, Beach D, Cuomo J, McGuire T, Whetten R, Diederich F. Confirmation of a vanishingly small ring-current magnetic susceptibility of icosahedral buckminsterfullerene. J Phys Chem. 1991;95(9):3457–9.
26. Hebard A, Rosseinky M, Haddon R, Murphy D, Glarum S, Palstra T, Ramirez A, Karton A. Potassium-doped c60. Nature. 1991;350:600–1.
27. Geim AK, Novoselov KS. The rise of graphene. Nat Mater. 2007;6(3):183–91.
28. Neto AC, Guinea F, Peres N, Novoselov KS, Geim AK. The electronic properties of graphene. Rev Mod Phys. 2009;81(1):109.
29. Ferrari AC. Raman spectroscopy of graphene and graphite: disorder, electron–phonon coupling, doping and nonadiabatic effects. Solid State Commun. 2007;143(1):47–57.
30. Tombros N, Jozsa C, Popinciuc M, Jonkman HT, Van Wees BJ. Electronic spin transport and spin precession in single graphene layers at room temperature. Nature. 2007;448 (7153):571–4.
31. Lee C, Wei X, Kysar JW, Hone J. Measurement of the elastic properties and intrinsic strength of monolayer graphene. Science. 2008;321(5887):385–8.
32. Balandin AA, Ghosh S, Bao W, Calizo I, Teweldebrhan D, Miao F, Lau CN. Superior thermal conductivity of single-layer graphene. Nano Lett. 2008;8(3):902–7.
33. Pereira VM, Neto AC, Peres N. Tight-binding approach to uniaxial strain in graphene. Phys Rev B. 2009;80(4):045401.
34. Booth TJ, Blake P, Nair RR, Jiang D, Hill EW, Bangert U, Bleloch A, Gass M, Novoselov KS, Katsnelson MI. Macroscopic graphene membranes and their extraordinary stiffness. Nano Lett. 2008;8(8):2442–6.
35. Bunch JS, Verbridge SS, Alden JS, van der Zande AM, Parpia JM, Craighead HG, McEuen PL. Impermeable atomic membranes from graphene sheets. Nano Lett. 2008;8(8):2458–62.
36. Leslie-Pelecky DL, Rieke RD. Magnetic properties of nanostructured materials. Chem Mater. 1996;8(8):1770–83.
37. Woo K, Hong J, Choi S, Lee H-W, Ahn J-P, Kim CS, Lee SW. Easy synthesis and magnetic properties of iron oxide nanoparticles. Chem Mater. 2004;16(14):2814–8.
38. Dias A, Hussain A, Marcos A, Roque A. A biotechnological perspective on the application of iron oxide magnetic colloids modified with polysaccharides. Biotechnol Adv. 2011;29 (1):142–55.
39. Xiao Y, Patolsky F, Katz E, Hainfeld JF, Willner I. "Plugging into enzymes": nanowiring of redox enzymes by a gold nanoparticle. Science. 2003;299(5614):1877–81.
40. Patolsky F, Weizmann Y, Willner I. Long-range electrical contacting of redox enzymes by SWCNT connectors. Angew Chem Int Ed. 2004;43(16):2113–7.
41. Zhao W, Xu J-J, Chen H-Y. Extended-range glucose biosensor via layer-by-layer assembly incorporating gold nanoparticles. Front Biosci. 2005;10:1060–9.
42. Zong S, Cao Y, Zhou Y, Ju H. Reagentless biosensor for hydrogen peroxide based on immobilization of protein in zirconia nanoparticles enhanced grafted collagen matrix. Biosens Bioelectron. 2007;22(8):1776–82.
43. Zhao J, Zhu X, Li T, Li G. Self-assembled multilayer of gold nanoparticles for amplified electrochemical detection of cytochrome c. Analyst. 2008;133(9):1242–5.
44. Pandey P, Upadhyay S. Bioelectrochemistry of glucose oxidase immobilized on ferrocene encapsulated ormosil modified electrode. Sensors Actuators B Chem. 2001;76(1):193–8.
45. RetnaáRaj C, KumaráJena B. Efficient electrocatalytic oxidation of NADH at gold nanoparticles self-assembled on three-dimensional sol-gel network, Chem Commun. 2005, (15):2005–2007.
46. Welch C, Banks C, Simm A, Compton R. Silver nanoparticle assemblies supported on glassy-carbon electrodes for the electro-analytical detection of hydrogen peroxide. Anal Bioanal Chem. 2005;382(1):12–21.
47. Karam P, Halaoui LI. Sensing of H_2O_2 at low surface density assemblies of Pt nanoparticles in polyelectrolyte. Anal Chem. 2008;80(14):5441–8.

48. Zhang M, Smith A, Gorski W. Carbon nanotube-chitosan system for electrochemical sensing based on dehydrogenase enzymes. Anal Chem. 2004;76(17):5045–50.
49. Luo X-L, Xu J-J, Wang J-L, Chen H-Y. Electrochemically deposited nanocomposite of chitosan and carbon nanotubes for biosensor application. Chem Commun. 2005;16:2169–71.
50. Luo X-L, Xu J-J, Du Y, Chen H-Y. A glucose biosensor based on chitosan–glucose oxidase–gold nanoparticles biocomposite formed by one-step electrodeposition. Anal Biochem. 2004;334(2):284–9.
51. Zhao W, Sun S-X, Xu J-J, Chen H-Y, Cao X-J, Guan X-H. Electrochemical identification of the property of peripheral nerve fiber based on a biocompatible polymer film via in situ incorporating gold nanoparticles. Anal Chem. 2008;80(10):3769–76.
52. Chen X, Wang Y, Zhou J, Yan W, Li X, Zhu J-J. Electrochemical impedance immunosensor based on three-dimensionally ordered macroporous gold film. Anal Chem. 2008;80 (6):2133–40.
53. Ding L, Hao C, Xue Y, Ju H. A bio-inspired support of gold nanoparticles-chitosan nanocomposites gel for immobilization and electrochemical study of K562 leukemia cells. Biomacromolecules. 2007;8(4):1341–6.
54. He P, Hu N. Electrocatalytic properties of heme proteins in layer-by-layer films assembled with SiO_2 nanoparticles. Electroanalysis. 2004;16(13-14):1122–31.
55. He P, Hu N, Rusling JF. Driving forces for layer-by-layer self-assembly of films of SiO_2 nanoparticles and heme proteins. Langmuir. 2004;20(3):722–9.
56. Luo X-L, Xu J-J, Zhao W, Chen H-Y. Glucose biosensor based on ENFET doped with SiO_2 nanoparticles. Sensors Actuators B Chem. 2004;97(2):249–55.
57. Dequaire M, Degrand C, Limoges B. An electrochemical metalloimmunoassay based on a colloidal gold label. Anal Chem. 2000;72(22):5521–8.
58. Dai Z, Kawde A-N, Xiang Y, La Belle JT, Gerlach J, Bhavanandan VP, Joshi L, Wang J. Nanoparticle-based sensing of glycan-lectin interactions. J Am Chem Soc. 2006;128 (31):10018–9.
59. Wang J, Liu G, Merkoçi A. Electrochemical coding technology for simultaneous detection of multiple DNA targets. J Am Chem Soc. 2003;125(11):3214–5.
60. Ding L, Cheng W, Wang X, Ding S, Ju H. Carbohydrate monolayer strategy for electrochemical assay of cell surface carbohydrate. J Am Chem Soc. 2008;130(23):7224–5.
61. Xu J-J, Zhao W, Luo X-L, Chen H-Y. A sensitive biosensor for lactate based on layer-by-layer assembling MnO_2 nanoparticles and lactate oxidase on ion-sensitive field-effect transistors. Chem Commun. 2005;6:792–4.
62. Luo X-L, Xu J-J, Zhao W, Chen H-Y. Ascorbic acid sensor based on ion-sensitive field-effect transistor modified with MnO_2 nanoparticles. Anal Chim Acta. 2004;512(1):57–61.
63. Xu J-J, Luo X-L, Du Y, Chen H-Y. Application of MnO_2 nanoparticles as an eliminator of ascorbate interference to amperometric glucose biosensors. Electrochem Commun. 2004;6 (11):1169–73.
64. Bai Y-H, Du Y, Xu J-J, Chen H-Y. Choline biosensors based on a bi-electrocatalytic property of MnO_2 nanoparticles modified electrodes to H_2O_2. Electrochem Commun. 2007;9 (10):2611–6.
65. Mirkin CA, Letsinger RL, Mucic RC, Storhoff JJ. A DNA-based method for rationally assembling nanoparticles into macroscopic materials. Nature. 1996;382:607–9.
66. Elghanian R, Storhoff JJ, Mucic RC, Letsinger RL, Mirkin CA. Selective colorimetric detection of polynucleotides based on the distance-dependent optical properties of gold nanoparticles. Science. 1997;277(5329):1078–81.
67. Rosi NL, Mirkin CA. Nanostructures in biodiagnostics. Chem Rev. 2005;105(4):1547–62.
68. Xia F, Zuo X, Yang R, Xiao Y, Kang D, Vallée-Bélisle A, Gong X, Yuen JD, Hsu BB, Heeger AJ. Colorimetric detection of DNA, small molecules, proteins, and ions using unmodified gold nanoparticles and conjugated polyelectrolytes. Proc Natl Acad Sci. 2010;107:10837–41.
69. Nie S, Emory SR. Probing single molecules and single nanoparticles by surface-enhanced Raman scattering. Science. 1997;275(5303):1102–6.

70. Li H, Rothberg L. Colorimetric detection of DNA sequences based on electrostatic interactions with unmodified gold nanoparticles. Proc Natl Acad Sci U S A. 2004;101(39):14036–9.
71. Thanh NTK, Rosenzweig Z. Development of an aggregation-based immunoassay for anti-protein A using gold nanoparticles. Anal Chem. 2002;74(7):1624–8.
72. Huang H, He C, Zeng Y, Xia X, Yu X, Yi P, Chen Z. A novel label-free multi-throughput optical biosensor based on localized surface plasmon resonance. Biosens Bioelectron. 2009;24(7):2255–9.
73. Wang X, Li Y, Wang H, Fu Q, Peng J, Wang Y, Du J, Zhou Y, Zhan L. Gold nanorod-based localized surface plasmon resonance biosensor for sensitive detection of hepatitis B virus in buffer, blood serum and plasma. Biosens Bioelectron. 2010;26(2):404–10.
74. Parab HJ, Jung C, Lee J-H, Park HG. A gold nanorod-based optical DNA biosensor for the diagnosis of pathogens. Biosens Bioelectron. 2010;26(2):667–73.
75. John H. Fluorescence properties of gold nanorods and their application for DNA biosensing. Chem Commun. 2005;31:3924–6.
76. Gou X-C, Liu J, Zhang H-L. Monitoring human telomere DNA hybridization and G-quadruplex formation using gold nanorods. Anal Chim Acta. 2010;668(2):208–14.
77. Qian X, Zhou X, Nie S. Surface-enhanced Raman nanoparticle beacons based on bioconjugated gold nanocrystals and long range plasmonic coupling. J Am Chem Soc. 2008;130(45):14934–5.
78. Driskell JD, Lipert RJ, Porter MD. Labeled gold nanoparticles immobilized at smooth metallic substrates: systematic investigation of surface plasmon resonance and surface-enhanced Raman scattering. J Phys Chem B. 2006;110(35):17444–51.
79. Klimov V, Mikhailovsky A, Xu S, Malko A, Hollingsworth J, Leatherdale C, Eisler H-J, Bawendi M. Optical gain and stimulated emission in nanocrystal quantum dots. Science. 2000;290(5490):314–7.
80. Bruchez M, Moronne M, Gin P, Weiss S, Alivisatos AP. Semiconductor nanocrystals as fluorescent biological labels. Science. 1998;281(5385):2013–6.
81. Goldman ER, Balighian ED, Mattoussi H, Kuno MK, Mauro JM, Tran PT, Anderson GP. Avidin: a natural bridge for quantum dot-antibody conjugates. J Am Chem Soc. 2002;124(22):6378–82.
82. Goldman ER, Clapp AR, Anderson GP, Uyeda HT, Mauro JM, Medintz IL, Mattoussi H. Multiplexed toxin analysis using four colors of quantum dot fluororeagents. Anal Chem. 2004;76(3):684–8.
83. Mitchell GP, Mirkin CA, Letsinger RL. Programmed assembly of DNA functionalized quantum dots. J Am Chem Soc. 1999;121(35):8122–3.
84. Han M, Gao X, Su JZ, Nie S. Quantum-dot-tagged microbeads for multiplexed optical coding of biomolecules. Nat Biotechnol. 2001;19(7):631–5.
85. Patolsky F, Gill R, Weizmann Y, Mokari T, Banin U, Willner I. Lighting-up the dynamics of telomerization and DNA replication by CdSe-ZnS quantum dots. J Am Chem Soc. 2003;125(46):13918–9.
86. Swathi R, Sebastian K. Distance dependence of fluorescence resonance energy transfer. J Chem Sci. 2009;121(5):777–87.
87. Swathi R, Sebastian K. Excitation energy transfer from a fluorophore to single-walled carbon nanotubes. J Chem Phys. 2010;132(10):104502.
88. Wang S, Humphreys ES, Chung S-Y, Delduco DF, Lustig SR, Wang H, Parker KN, Rizzo NW, Subramoney S, Chiang Y-M. Peptides with selective affinity for carbon nanotubes. Nat Mater. 2003;2(3):196–200.
89. Zheng M, Jagota A, Semke ED, Diner BA, McLean RS, Lustig SR, Richardson RE, Tassi NG. DNA-assisted dispersion and separation of carbon nanotubes. Nat Mater. 2003;2(5):338–42.
90. Yang R, Jin J, Chen Y, Shao N, Kang H, Xiao Z, Tang Z, Wu Y, Zhu Z, Tan W. Carbon nanotube-quenched fluorescent oligonucleotides: probes that fluoresce upon hybridization. J Am Chem Soc. 2008;130(26):8351–8.

91. Sutton DJ, Tchounwou PB, Ninashvili N, Shen E. Mercury induces cytotoxicity and transcriptionally activates stress genes in human liver carcinoma (HepG2) cells. Int J Mol Sci. 2002;3(9):965–84.
92. Li F, Huang Y, Yang Q, Zhong Z, Li D, Wang L, Song S, Fan C. A graphene-enhanced molecular beacon for homogeneous DNA detection. Nanoscale. 2010;2(6):1021–6.
93. Dong H, Gao W, Yan F, Ji H, Ju H. Fluorescence resonance energy transfer between quantum dots and graphene oxide for sensing biomolecules. Anal Chem. 2010;82(13):5511–7.
94. Lu CH, Yang HH, Zhu CL, Chen X, Chen GN. A graphene platform for sensing biomolecules. Angew Chem. 2009;121(26):4879–81.
95. Jhaveri SD, Kirby R, Conrad R, Maglott EJ, Bowser M, Kennedy RT, Glick G, Ellington AD. Designed signaling aptamers that transduce molecular recognition to changes in fluorescence intensity. J Am Chem Soc. 2000;122(11):2469–73.
96. Chang H, Tang L, Wang Y, Jiang J, Li J. Graphene fluorescence resonance energy transfer aptasensor for the thrombin detection. Anal Chem. 2010;82(6):2341–6.
97. Wen Y, Xing F, He S, Song S, Wang L, Long Y, Li D, Fan C. A graphene-based fluorescent nanoprobe for silver (I) ions detection by using graphene oxide and a silver-specific oligonucleotide. Chem Commun. 2010;46(15):2596–8.
98. Curie J, Curie P. An oscillating quartz crystal mass detector. Rendu. 1880;91:294–7.
99. Wang H, Wang C, Lei C, Wu Z, Shen G, Yu R. A novel biosensing interfacial design produced by assembling nano-Au particles on amine-terminated plasma-polymerized films. Anal Bioanal Chem. 2003;377(4):632–8.
100. Jin XY, Jin XF, Ding YJ, Jiang JH, Shen GL, Yu RQ. A piezoelectric immunosensor based on agglutination reaction with amplification of silica nanoparticles. Chin J Chem. 2008;26 (12):2191–6.
101. Wang H, Zhang Y, Yan B, Liu L, Wang S, Shen G, Yu R. Rapid, simple, and sensitive immunoagglutination assay with SiO_2 particles and quartz crystal microbalance for quantifying Schistosoma japonicum antibodies. Clin Chem. 2006;52(11):2065–71.
102. Kim TH, Lee SH, Lee J, Song HS, Oh EH, Park TH, Hong S. Single-carbon-atomic-resolution detection of odorant molecules using a human olfactory receptor-based bioelectronic nose. Adv Mater. 2009;21(1):91–4.
103. Star A, Tu E, Niemann J, Gabriel J-CP, Joiner CS, Valcke C. Label-free detection of DNA hybridization using carbon nanotube network field-effect transistors. Proc Natl Acad Sci U S A. 2006;103(4):921–6.
104. Goldsmith BR, Coroneus JG, Khalap VR, Kane AA, Weiss GA, Collins PG. Conductance-controlled point functionalization of single-walled carbon nanotubes. Science. 2007;315 (5808):77–81.
105. Sorgenfrei S, Chiu C-y, Gonzalez Jr RL, Yu Y-J, Kim P, Nuckolls C, Shepard KL. Label-free single-molecule detection of DNA-hybridization kinetics with a carbon nanotube field-effect transistor. Nat Nanotechnol. 2011;6(2):126–32.
106. Mohanty N, Berry V. Graphene-based single-bacterium resolution biodevice and DNA transistor: interfacing graphene derivatives with nanoscale and microscale biocomponents. Nano Lett. 2008;8(12):4469–76.
107. Dong X, Shi Y, Huang W, Chen P, Li LJ. Electrical detection of DNA hybridization with single-base specificity using transistors based on CVD-grown graphene sheets. Adv Mater. 2010;22(14):1649–53.
108. Ohno Y, Maehashi K, Matsumoto K. Label-free biosensors based on aptamer-modified graphene field-effect transistors. J Am Chem Soc. 2010;132(51):18012–3.
109. Agarwal S, Zhou X, Ye F, He Q, Chen GC, Soo J, Boey F, Zhang H, Chen P. Interfacing live cells with nanocarbon substrates. Langmuir. 2010;26(4):2244–7.
110. Sudibya HG, He Q, Zhang H, Chen P. Electrical detection of metal ions using field-effect transistors based on micropatterned reduced graphene oxide films. ACS Nano. 2011;5 (3):1990–4.

111. Chen K-I, Li B-R, Chen Y-T. Silicon nanowire field-effect transistor-based biosensors for biomedical diagnosis and cellular recording investigation. Nano Today. 2011;6(2):131–54.
112. Cui Y, Wei Q, Park H, Lieber CM. Nanowire nanosensors for highly sensitive and selective detection of biological and chemical species. Science. 2001;293(5533):1289–92.
113. Movileanu L, Howorka S, Braha O, Bayley H. Detecting protein analytes that modulate transmembrane movement of a polymer chain within a single protein pore. Nat Biotechnol. 2000;18(10):1091–5.
114. Zheng G, Gao XP, Lieber CM. Frequency domain detection of biomolecules using silicon nanowire biosensors. Nano Lett. 2010;10(8):3179–83.
115. Hahm J-i, Lieber CM. Direct ultrasensitive electrical detection of DNA and DNA sequence variations using nanowire nanosensors. Nano Lett. 2004;4(1):51–4.
116. Zhang G-J, Zhang L, Huang MJ, Luo ZHH, Tay GKI, Lim E-JA, Kang TG, Chen Y. Silicon nanowire biosensor for highly sensitive and rapid detection of Dengue virus. Sensors Actuators B Chem. 2010;146(1):138–44.
117. Zhang G-J, Chua JH, Chee R-E, Agarwal A, Wong SM. Label-free direct detection of MiRNAs with silicon nanowire biosensors. Biosens Bioelectron. 2009;24(8):2504–8.
118. Rutten WL. Selective electrical interfaces with the nervous system. Annu Rev Biomed Eng. 2002;4(1):407–52.

Chapter 8
Micro/Nano Electrochemical Sensors for Ion Sensing

Jiawei Tu, Hao Wan, and Ping Wang

Abstract The developments in micro/nano electrochemical sensors have large impact on ion sensing research. Significant advances in the fabrications of micro/nano electrochemical sensors are being persistently made. Micro/nano electrochemical sensors play a very significant role in electrochemistry for ion sensing. Compared to conventional electrochemical sensors, micro/nano sensors exhibit nonlinear diffusion with higher sensitivity, higher current density, faster mass transfer, and higher signal-to-noise ratio. Hence, micro/nano electrochemical sensor is widely applied for various ion sensings. The theory of electrochemical sensors for ion sensing, which contains potentiometric sensors, voltammetric sensors, microelectrode array, and LAPS, is described in this chapter. Also a self-designed integrated sensor with microelectrode array (MEA) and light-addressable potentiometric sensor (LAPS) for heavy-metal ion and pH detection is introduced, and its fabrication and the characterization of MEA and LAPS are described. Electrochemical measurements have shown numerous advantages for trace heavy-metal detection, including rapid analysis, good selectivity, andsensitivity. Therefore, some applications in environment and food analysis related to the electrochemical analysis of ion sensing are discussed in this chapter.

Keywords Ion sensing • Microelectrode array (MEA) • Light-addressable potentiometric sensor (LAPS)

8.1 Introduction

Micro/nano electrochemical sensors have been applied in various fields, in which ion sensing in water environment has received extensive concerns for researchers. Among all these ions in water, heavy metals are especially concerned due to the

J. Tu • H. Wan • P. Wang (✉)
Biosensor National Special Laboratory, Department of Biomedical Engineering, Zhejiang University, Hangzhou, China
e-mail: cnpwang@zju.edu.cn

P. Wang et al. (eds.), *Micro/Nano Cell and Molecular Sensors*,
DOI 10.1007/978-981-10-1658-5_8

properties of high toxicity, bioaccumulation, and nonbiodegradability. Extensive heavy metals such as zinc, copper, cadmium, lead, mercury, and chromium can result in severe hazards to the ecosystem and human health. For instance, excessive intake of lead can lead to neurological, neurobehavioral, hematological, and renal diseases, especially potentially harmful to neurodevelopment of infants and children [1, 2]. Copper poisoning may cause hepatitis, liver cirrhosis, jaundice, and hemolytic crisis [3, 4]. Mercury poisoning could lead to damage of the brain, kidneys, and lungs, which resulted in the Minamata Bay tragedy in the 1950s. Thus, heavy-metal ion sensing is of great significance and urgency for human and the environment. Among all approaches for heavy-metal analysis such as atomic absorption spectroscopy (AAS) and inductively coupled plasma mass spectroscopy (ICP-MS), electrochemistry demonstrates its superior merits in terms of sensitivity, detection of limit, and low cost. Besides, heavy-metal sensing is easily implemented with simultaneous detection of several heavy-metal ions. Micro/nano electrochemical sensors play a very significant role in electrochemistry for ion sensing. Compared to conventional electrochemical sensors, micro/nano sensors exhibit nonlinear diffusion with higher sensitivity, higher current density, faster mass transfer, and higher signal-to-noise ratio. Hence, micro/nano electrochemical sensor is widely applied for various ion sensings.

8.2 Theory of Electrochemical Sensors for Ion Sensing

Based on different parameters measured in electrochemical analysis, electrochemical sensors mainly embrace three different sensors, potentiometric sensor, voltammetric sensor, and conductometric sensor. In this chapter, we mainly discuss potentiometric sensor and voltammetric sensor.

8.2.1 Potentiometric Sensors

In potentiometry, a potential is measured between two electrodes under the conditions of no current flow. The measured potential may then be used to determine the analytical quantity of interest, generally the concentration of some component of the solution. The potential that develops in the electrochemical cell is the result of the free energy change that would occur if the chemical phenomena were to proceed until the equilibrium condition has been satisfied.

The largest group among potentiometric sensors is represented by ion-selective electrodes (ISEs), the oldest and most widely used among them being a pH-sensitive glass electrode. Different approaches of potentiometric electronic tongues and taste sensors have been demonstrated. They have in common that they all measure the potential over a charged membrane. These membranes can be of different materials, which provide enough selectivity to different classes of chemical substances. Electronic tongues have, thus, been described based on an

Fig. 8.1 ISEs and the measuring system (Reproduced with permission from [5]. Copyright 2015 Elsevier B.V.)

array of chalcogenide glass sensors, including conventional electrodes such as chloride-, sodium- and potassium-selective sensors, combined with a pattern-recognition routine. The photograph of ISEs' array and the measuring system in the group of Andrey Legin, St. Petersburg University (Russia), is shown in Fig. 8.1. The chalcogenide sensors show cross sensitivity, which has been preferably used for measurement of metal ions in river water, and suggested or environmental and process-monitoring purposes. This type of electronic tongues has also been combined with PVC membranes for testing of beverages.

Potentiometric ion and chemical sensors based on field-effect devices form another group of transducers that can be easily miniaturized and are fabricated by means of microelectronic technology. Among them the most studied are the ion-sensitive field-effect transistors (ISFETs) with different ion-selective membranes (often also called chemically sensitive field-effect transistors or Chem-FETs). ISFETs with bare gate insulator (silicon oxide, silicon nitride, aluminum oxide, etc.) show intrinsic pH sensitivity due to electrochemical equilibrium between the protonated oxide surface and protons in the solution. To obtain sensitivity to other ions, a polymeric membrane containing some ionophore may be deposited.

Light-addressable potentiometric sensor (LAPS) is a semiconductor-based device with an electrolyte-insulator-semiconductor (EIS) structure, which is similar to ISFET in function. A DC bias voltage is applied to LAPS, so that a depletion layer appears at the insulator-semiconductor interface. When a modulated light irradiates LAPS from the front or back side, an AC photocurrent inside the depletion layer could be induced as a measured signal. The amplitude of the photocurrent is sensitive to the surface potential and thus LAPS is able to detect the potential variation caused by an electrochemical even. Therefore, in principle,

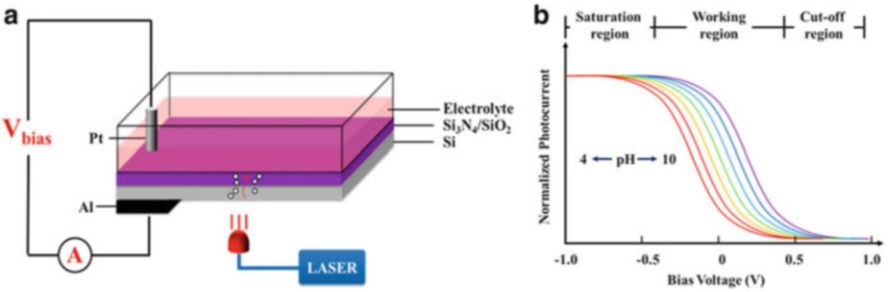

Fig. 8.2 (**a**) Working principle of the LAPS. (**b**) Characteristic I–V curve of N-type LAPS (Reproduced with permission from [6]. Copyright 2015 Science Press, Beijing and Springer Science + Business Media Dordrecht)

any electrochemical reaction that results in the change of surface potential can be detected by LAPS, including the ionic change and redox effect, shown in Fig. 8.2a. By modifying the individual sensitive region with the polymer membrane or chalcogenide glass membrane which contains specific receptor molecules, relevant cations could be detected simultaneously. Most of the solid-state-based thin-film sensors suffer from an insufficient selectivity. Compared to the inorganic membrane, the organic one can overcome the problem with reasonable good selectivity. The characteristic I–V curve of N-type LAPS is shown in Fig. 8.2b.

8.2.2 Voltammetric Sensors

Voltammetry, in which a current is measured at a fixed potential, is a very powerful and often used technique in analytical chemistry. Depending on the potential applied and type of working electrode, redox active compounds are either oxidized or reduced at the working electrode, giving rise to a current. The sensitivity of voltammetric methods is often very high. The selectivity is, however, in many cases poor, since all compounds in a measured solution that are electrochemically active below the applied potential will contribute to the measured current. Different ways to surmount this is, e.g., to cover the working electrode with a gas permeable membrane, only letting gases pass through, or to use pulse voltammetry. Voltammetry appears to have several advantages; the technique has been extensively used in analytical chemistry due to features such as its very high sensitivity, versatility, simplicity, and robustness. Besides, voltammetry offers a widespread number of different analytical possibilities, including cyclic, stripping, and pulse voltammetry. Depending on the technique, various kinds or aspects of information can be obtained from the measured solution. Normally, redox active species are being measured at a fixed potential, but by using, e.g., pulse voltammetry, studies of transient responses when Helmholtz layers are formed also give information concerning diffusion coefficients of charged species. Further information is also

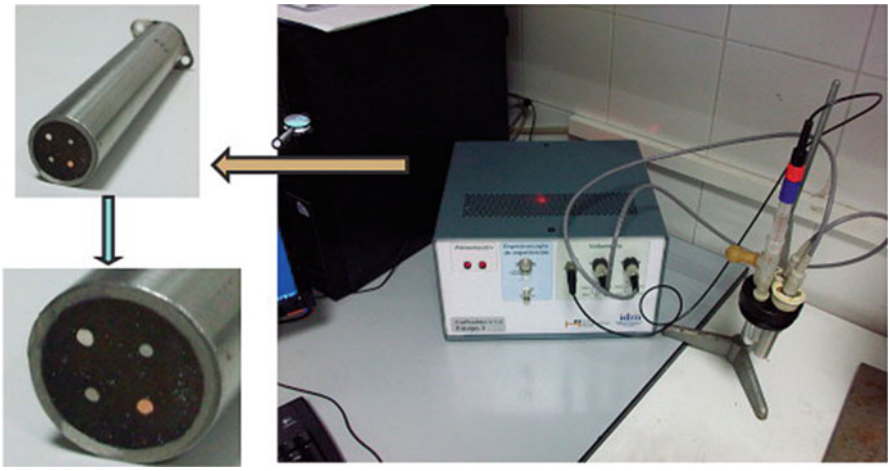

Fig. 8.3 A developed voltammetric electronic tongue for water quality monitoring (Reproduced with permission from [7]. Copyright 2013 by the authors; licensee MDPI, Basel, Switzerland)

obtainable by the use of different types of metals for the working electrodes. Different metal electrodes can be used together with voltammetric measurements to classify different liquids. Still, the voltammograms contain a large amount of information, and to extract this information, multivariate calibration methods have been shown to be rather efficient. A developed voltammetric electronic tongue for water quality monitoring is shown in Fig. 8.3.

In our group, we mainly use voltammetric sensors for heavy-metal analysis, specifically stripping voltammetry. The principle of stripping voltammetry includes three steps: heavy-metal reduction, equilibrium, and reoxidation. First, heavy-metal ions are reduced on the surface of working electrodes under a constant potential. In this step, stirring is generally used to further enhance the mass transfer rate. The equilibrium step ensures an equilibrium reaction in samples without stirring and reduction. Then a positive scanning potential is applied on the working electrode in order to reoxidate the heavy metal, and oxidation current is recorded in this step. Thus, voltammograms are obtained and stripping peaks are linearly correlated with concentrations of heavy metals, by which quantification of heavy metals in a sample is implemented. Specific detection is implemented based on the characteristic oxidation potential. In this deposition step, heavy-metal ions are reduced on a very small working electrode, thus resulting in the enrichment of heavy metals. The detection of limit is about 10^{-8}–10^{-9} mol/L for trace heavy-metal analysis. And in stripping voltammetry, several factors can affect the performance in heavy-metal analysis:

1. Deposition potential. Deposition potential is generally optimized due to its impact on the reduction rate. Besides, more positive deposition potential can lead to unstable reduction reaction, affecting the reproducibility of stripping

analysis. More negative deposition potential may lead to hydrogen evolution and reduction of other heavy-metal ions, by which interferences may be introduced.
2. Deposition time. In a certain range of deposition time, the stripping current of heavy metals is linearly correlated with deposition time. Longer deposition time can lead to the saturation of the working electrode due to the small effective area of working electrodes, which affects the linear detection range in heavy-metal analysis. Short deposition time leads to a decrease of sensitivity and current response in stripping analysis.
3. Scanning rate. Generally, the stripping peak current is linearly correlated with the scanning rate, while faster scanning rate may introduce larger background noise and charging current.
4. Stirring rate. The stirring rate is the essential factor to the reproducibility in heavy-metal analysis and faster stirring rate can also result in higher current response. In our study, differential pulse stripping voltammetry (DPSV) and square wave stripping voltammetry (SWSV) are mainly utilized in our research, which can effectively decrease the background current and increase the signal-to-noise ratio.

8.2.3 Characterizations of Micro/Nano sensors

Well-designed micro/nano sensors usually have the following characteristics: large mass transfer rate and current density, low time constant and IR voltage drop, low charging current, and high signal-to-noise ratio. These characteristics can be described by the corresponding radius diffusion which is dependent on the shape of sensors. Furthermore, the characteristics of microelectrode array are quite more complex than a single electrode.

8.2.3.1 Radius Diffusion

For conventional macroelectrodes, when the active concentration on the surface of working electrode is 0, the relationship between current response and time could be described using Cottrell equation:

$$i(t) = \frac{zFAD^{1/2}C}{\pi^{1/2}t^{1/2}} \tag{8.1}$$

Under this condition, the active substances on the surface of working electrodes diffuse vertical to the surface due to the macro-size of working electrodes shown in Fig. 8.4a. This phenomenon is called linear diffusion. When the size of working electrodes decreases to the size of diffusion layer, mass transfer occurs according to

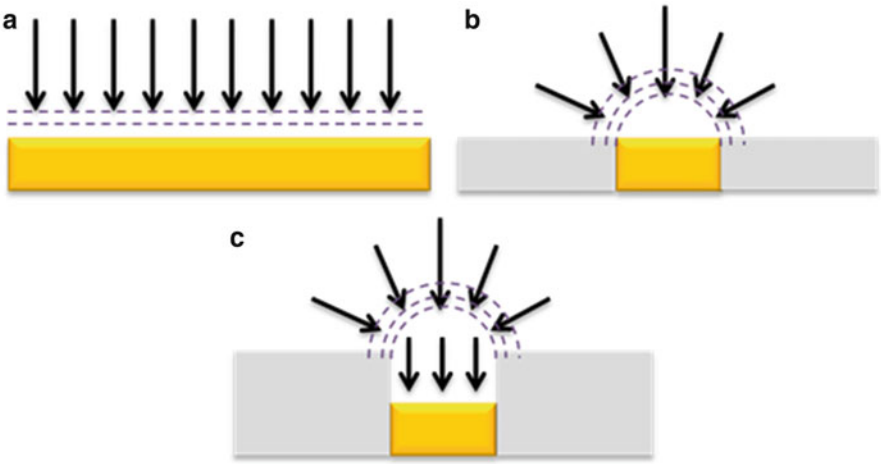

Fig. 8.4 Different shapes of working electrodes. (**a**) Linear diffusion, the active substances on the surface of working electrodes diffuse vertical to the surface; (**b**) radius diffusion, the active substances diffuse around the surface; (**c**) radius diffusion in recessed electrodes, the active substances diffuse upon the surface similar to radius diffusion

the radius direction on the surface, called radius diffusion. In this situation, the Cottrell equation is revised:

$$i(t) = \frac{zFAD^{1/2}C}{\pi^{1/2}t^{1/2}} + \frac{4zFADC}{\pi r} \tag{8.2}$$

where the first item represents the current produced by linear diffusion and the current decreases with the increasing of time. The second item represents the current produced by radius diffusion, which is not related with time, shown in Fig. 8.4b. In electrochemical analysis, the current produced by linear diffusion decreases to 0 after reaction for a period of time. Then the total current is mainly produced by radius diffusion and the current is called steady-state current, which is not changed with time variation. The steady-state current is only related to the radius of micro/nano electrodes. For instance, when using micro/nano disk electrodes for electrochemical analysis, the steady-state current could be described in the equation:

$$i_d = 4zFDCr \tag{8.3}$$

In some cases, recessed micro/nano electrodes are applied in electrochemical analysis since an insulation layer is deposited on the working electrode region shown in Fig. 8.4c. In this situation, the equation is revised in which L represents

the depth of the recessed electrodes and r represents the radius of working electrodes:

$$i_d = \frac{4zFDCr}{\left(\frac{4L}{\pi r} + 1\right)} \tag{8.4}$$

8.2.3.2 Large Mass Transfer Rate and Current Density

According to Eq. 8.4, the steady-state current is linearly correlated with the radius of micro/nano electrodes. Since the size of micro/nano electrodes is usually microscale or nanoscale, the produced current is very low between 10^{-9} and 10^{-12} A. The current density is inversely proportional to the radius of the electrodes, which means larger current density is produced with smaller size. Hence, very large current density could be acquired with micro/nano electrodes compared to conventional macroelectrodes.

The mass transfer rate on the surface of working electrodes can be expressed by Eq. 8.5, where D represents the diffusion coefficient of different active substances and δ is the thickness of diffusion layer. Mass transfer rate represents the spread rate of active substances in the diffusion. For macroelectrodes, the mass transfer rate decreases with the increasing of time due to the linear diffusion as expressed in Eq. 8.6. For micro/nano electrodes, the mass transfer rate is expressed in Eq. 8.7 with the radius diffusion on the surface of working electrodes. In these cases, the mass transfer rate keeps steady and is not related with the time variation, only dependent on the diffusion coefficient and radius of micro/nano electrodes. Compared to macroelectrodes, micro/nano electrodes have large mass transfer rate, which ensures the steady state in a very short time. Hence, instead of stirring and rotating in macroelectrode application, micro/nano electrodes present extraordinary performance in electrochemical analysis without any stirring:

$$M = \frac{D}{\delta} \tag{8.5}$$

$$M = \frac{D^{1/2}}{\pi^{1/2} t^{1/2}} \tag{8.6}$$

$$M = \frac{4D}{\pi r} \tag{8.7}$$

8.2.3.3 Low Time Constant and IR Voltage Drop

In electrochemical analysis, the charging current is produced in the electric double layer on the surface of working electrodes during step-potential scanning. The

relationship between the charging current and time is expressed in Eq. 8.1. As shown in the equation, the charging current is exponential to the capacitance of electric double layer and related with the resistance of the working cell. The time constant is expressed as $\tau = RC_s$, indicating that the charging current decays rapidly with a small time constant. The capacitance of electric double layer is proportional to the area of working electrodes. Hence, the time constant is very small due to the microscale or nanoscale size of micro/nano electrodes, which means the charging current could decrease to 0 in a very short time. For instance, in a micro-disk electrode with radius of 2.5 μm, the charging current of electric double layer could decrease to 1 % in only 12 ns.

In the electrochemical reaction, when the step of micro- and nanoelectrode potential sweep, this will result in the charging current in the electric double layer electrode surface. Charging current versus time is shown in Eq. 8.1. By the above equation, the charging current exponentially changes with the electric double-layer capacitor and is closely related to the internal resistance of the cell. The time constant $\tau = \mathrm{RCs}$, the smaller the time constant, the faster the charging current decays. Since the electric double-layer capacitor Cs is directly proportional to the electrode area, and the area of micro/nano electrode is very small, a very small time constant, the charging current decays to near zero within a very short time [8]. For example, the charging current of the electric double layer decays to 99 % need only 12 ns for a radius 2.5 μm micro-disk electrode. Therefore, the scan rate can be very fast during step-potential scanning, without worrying about the introduction of excessive charging current component because of the fast scan rate. Compared to conventional large electrode, micro/nano electrodes are more suitable for a variety of transient electrochemical analysis methods, such as differential pulse stripping voltammetry and square wave stripping voltammetry. Micro/nano electrodes also greatly reduce the time required for voltammetry in fast potential sweep.

i_R drop is due to the pressure drop in the internal resistance of the cell caused by the current flowing through, so that the voltage actually applied to the working electrode is different from the expected value. Since the current real-time changes in the process of electrochemical reaction, the working electrode voltage varies with time and greatly affects the accuracy of electrochemical analysis. The introduction of a three-electrode system is to solve the problem of i_R drop by using the reference electrode to provide a constant potential for the working electrode. For micro/nano electrodes, the current strength is typically 10^{-9}–10^{-12} A, so i_R drop is very small. For conventional electrodes, the i_R drop is generally up to 5–10 mV. The i_R drop of the micro/nano electrodes is typically several μV or less and is negligible for electrochemical analysis. Therefore, we could use two-electrode system when using a micro/nano electrode as the working electrode. It also simplifies instrument configuration and maintenance procedures without the reference electrode. In addition, the microelectrodes can be applied in the electrochemical analysis of a high-impedance state media.

8.2.3.4 Low Charging Current, High Signal-to-Noise Ratio

The charging current is shown in Eq. 8.1. The time constant of micro/nano electrodes is small, so the charging current is small. The current in the electrochemical reaction is composed of Faraday current and charging current. Faraday current will decay with $t^{1/2}$, and the charging current will decay exponentially with time. So the ratio of the Faraday current and charging current is very large in the step scan. In the case study of micro-disk electrode, Faraday current is independent of time under steady-state conditions. In a single-sweep voltammetry, the SNR of the electrode is:

$$\eta = \frac{i_f}{i_c} = \frac{4zFDC}{\pi C_s r v} \tag{8.8}$$

By the above equation, the SNR of the electrode increases with the decreasing radius. For conventional electrodes, according to the Randles-Sevcik equation, the SNR is:

$$\eta = 0.446\left(\frac{\mathrm{zFD}}{RT}\right)^{1/2}\frac{zFC}{v^{1/2}C_s} \tag{8.9}$$

The radio of micro/nano electrode's SNR and conventional electrode's SNR is:

$$\xi = \frac{\eta_m}{\eta_n} = \frac{(DRT)^{1/2}}{0.1114\pi r(zFv)^{1/2}} \tag{8.10}$$

For an example of radius 5 μm disk microelectrode, when the scan rate is 20 mV/s, $\xi = 20$. That means micro/nano electrode's SNR is 20 times the conventional electrode's SNR under the same conditions. Micro/nano electrodes have a very high SNR [8]; it helps to reduce the detection limit and can be used for qualitative and quantitative analysis of trace substances.

8.2.3.5 Microelectrode Array Characteristics

Single micro/nano electrode's current response strength is very small. The direct detection of the detection circuit has a very high demand. Thus, microelectrode array which is composed of a plurality of micro/nano electrodes is used in actual electrochemical analysis. Microelectrode array has the characteristic of a single electrode, but also has the following features:

1. Current additivity. In microelectrode array, micro/nano electrodes are connected in parallel; when there is no interaction between the electrodes, the total current is the sum of a plurality of micro/nano electrodes.
2. i_R drop and the time constant do not change. In microelectrode array, the total current is the sum of a plurality of micro/nano electrodes. Current increases n

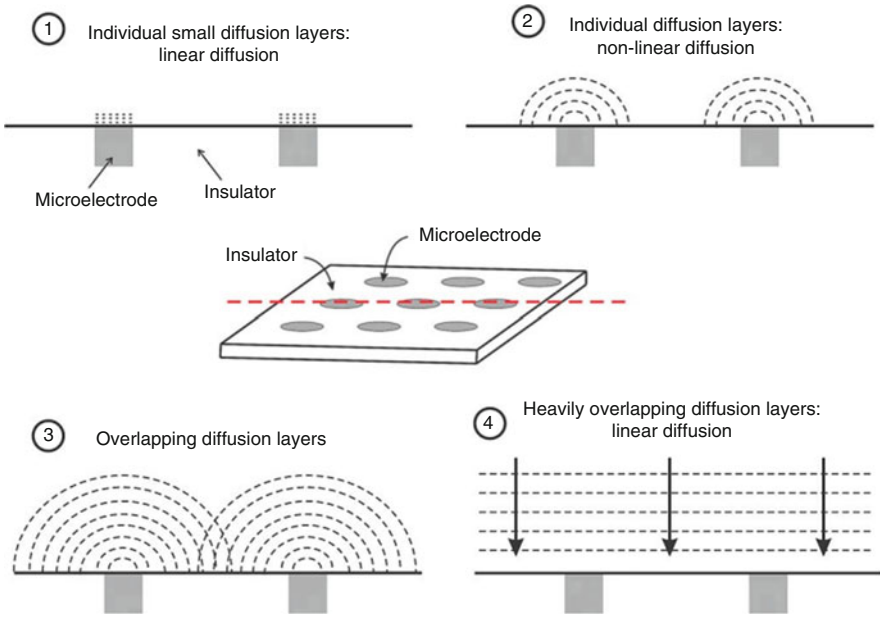

Fig. 8.5 Diffusion characteristics of microelectrode array under different circumstances (Reproduced with permission from [10]. Copyright 2005 Elsevier B.V.)

times, and the resistance is reduced to one n-th. Therefore, i_R drop remains unchanged. Similarly, the total capacitor increases n times because of electrodes are parallel. So the time constant RCs is also unchanged.

3. The shielding effect. Diffusion layer appeared on each micro/nano electrode surface because of substance diffusion. When the pitch of micro/nano electrodes is too close, it will lead to a diffusion layer between the electrode overlap. The response current of the electrode decreases, resulting in shielding effect.

How to avoid the shielding effect of the microelectrode array is an important research to study the characteristics of microelectrode array. The shielding effect is related to the size of micro/nano electrodes, electrode spacing, and diffusion layer thickness. Figure 8.5 shows the diffusion characteristics of microelectrode array under different circumstances [9]. In picture 1, diffusion layer thickness is much smaller than the size of the electrodes so that the linear diffusion appeared on the electrode surface; when the size of the electrode is reduced to the diffusion layer thickness in picture 2, nonlinear diffusion appeared on the electrode surface with the characteristics of low time constant and high SNR. No overlap between the diffusion layer since the distance between the electrodes is far. The distance between electrodes is too close in picture 3, resulting in the shielding effect because of diffusion layer overlap. The distance between electrodes is close but far less than the thickness of the diffusion layer in picture 4, and the diffusion layer has heavily overlap, resulting in linear diffusion instead of nonlinear diffusion. Thus, in the

design of micro/nano electrode array, we should ensure that the small size of the electrodes and the distance between electrodes are sufficiently large that a single micro/nano electrode has nonlinear dispersion characteristics.

8.3 Electrochemical Ion Sensors and Measurement

In this part, we introduce a self-designed integrated sensor with microelectrode array (MEA) and LAPS for heavy-metal ion and pH detection. Au-MEA was utilized for quantitative determination of zinc, lead, and copper, while hydrogen sensitive LAPS was deployed for pH detection in the meanwhile. Due to the significant influence of pH variation to heavy-metal detection, pH value provided by LAPS can be used as the guidance in heavy-metal analysis and further data calibration can be introduced to enhance the accuracy of sensors for heavy-metal quantification.

8.3.1 Fabrication of the Hybrid Sensor

The detailed process for the hybrid chemical sensor fabrication is shown in Fig. 8.6. A 430 μm N-type single crystal silicon wafer was used as the substrate. After RCA clean, LAPS sensing area on the back was etched to 100 μm thick for the enhancement of light permeability, while the rest was protected by photoresist. Thus, the induced alternating photocurrent by illuminating with a modulated light from the back would increase accordingly. Thermal oxidation was employed afterward to form a 50 nm SiO_2 layer in dry oxygen. A 100 nm Si_3N_4 layer was deposited by plasma enhanced chemical vapor deposition (PECVD) upon the SiO_2 layer. The notch, the 100 μm thick area of wafer, and the layers of SiO_2 and Si_3N_4 formed a preliminary structure of LAPS.

A 500 nm SiO_2 layer was deposited by PECVD to eliminate adverse effects on LAPS during the fabrication of MEA and form the insulation between the silicon and MEA. The metal layer was composed of gold and titanium, by which the Ti layer enhanced the adhesion between Au and the substrate. The sensing area of MEA was retained with photoresist while the rest areas were etched. An additional 800 nm Si_3N_4 layer was deposited for the insulation of signal conducting, while the Si_3N_4 layer upon the sensing sites of MEA was etched by photolithographic masks. An aluminum layer was evaporated for Ohmic contact by thermal evaporation. The fabrication of hybrid sensor array was accomplished and utilized for further electrochemical analysis.

The structure of the hybrid sensor fabricated is shown in Fig. 8.7. Section 1 in Fig. 8.7a represents the LAPS sensing areas for pH detection. The sensing area of

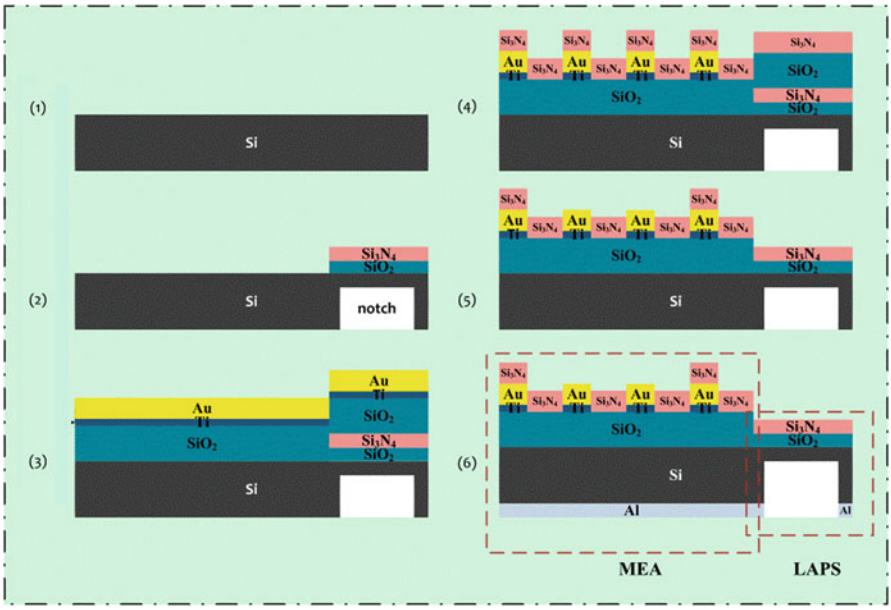

Fig. 8.6 The detailed process for the hybrid chemical sensor fabrication (Reproduced with permission from [11]. Copyright 2013 Elsevier B.V.)

each LAPS was 3.5 × 3.5 mm, while the modulated light (LED) was fixed in the notch behind each sensing surface to engender photocurrent. Two different MEA patterns were fabricated on the sensor in which one was micro-disk electrode array (MEAs 2–5) with the same gold substrate in Fig. 8.7c and the other was consisted of individual disk microelectrodes (MEAs 6–7) in Fig. 8.7d. MEAs 2–3 have a diameter of 50 μm and 30 μm, respectively, while 4 × 4 microelectrodes with interelectrode spacing of 200 μm were fabricated on individual sensing area. By contrast, MEAs 4–5 were consisted of 5 × 5 microelectrodes. MEAs 6–7 were in the same parameters with MEAs 2–3 except for the different patterns. Thus, characterizations of microelectrodes with different sizes, numbers, and patterns can be investigated. The circumambient gold electrodes (Sect. 8) of MEA and LAPS were deployed as the counter electrode. The packaged hybrid sensor is shown in Fig. 8.7b for practical electrochemical analysis.

The scheme of the hybrid sensor is shown in Fig. 8.8. MEA, LAPS, and counter electrode (CE) are integrated on the sensor, and signals are acquired through corresponding bonding pads by signal acquisition module. External reference electrode (RE) immersed in saturated KCl was used, thus constituting a three-electrode system with the working electrode and CE on the sensor. Light source for LAPS was placed at the back of etched LAPS sensing area with light modulation.

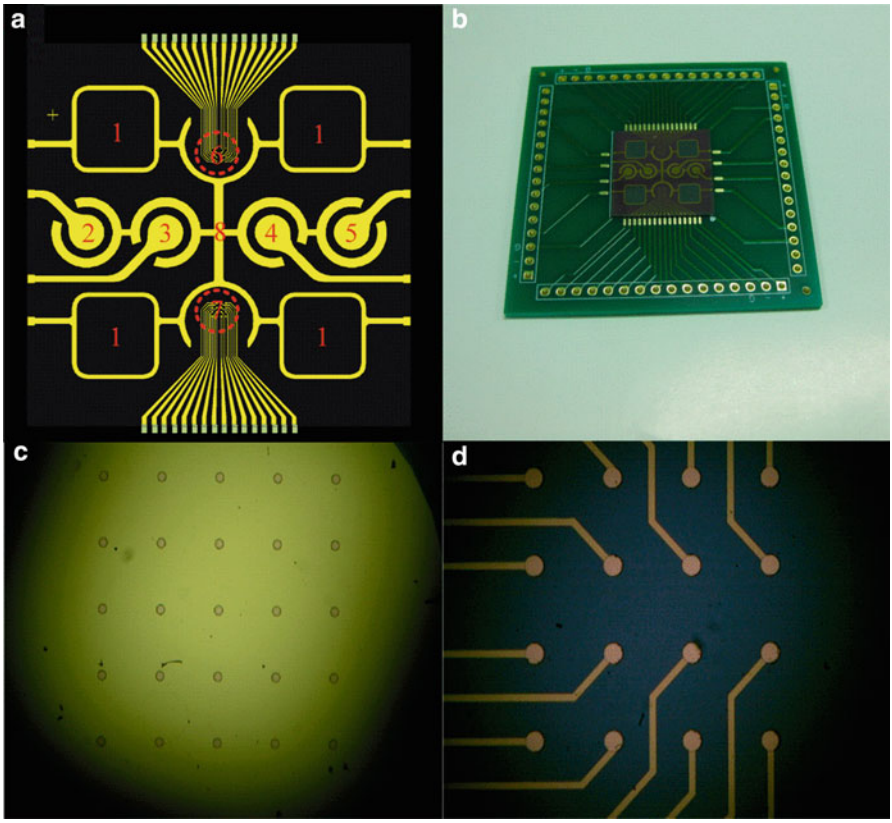

Fig. 8.7 The structure of the hybrid sensor (Reproduced with permission from [11]. Copyright 2013 Elsevier B.V.)

8.3.2 Characterization of MEA

Gold MEA was characterized primarily by cyclic voltammetry to assure electrochemical behavior in SV analysis. Activation procedure was conducted in 0.5 M H_2SO_4 with cyclic voltammetry and the sweep rate was 0.1 V/s. No significant difference was observed in different MEAs and typical cyclic voltammogram was obtained after about 20 times sweep and is shown in Fig. 8.9. Three repetitive cyclic voltammograms present good stability, and well-defined redox reaction of Au-MEA is observed in which oxidation potential (A) and reduction potential (B) are around 1.3 V and 1.0 V.

Subsequent to the activation and cleaning, cyclic voltammetry with different sweep rates (SR) was deployed in 2 mM $K_3[Fe(CN)_6]$ using 0.1 M KCl as the supporting electrolyte. Comparison experiments were conducted between MEAs 2–3 and MEAs 4–5, indicating no significant difference except for the amplitude of

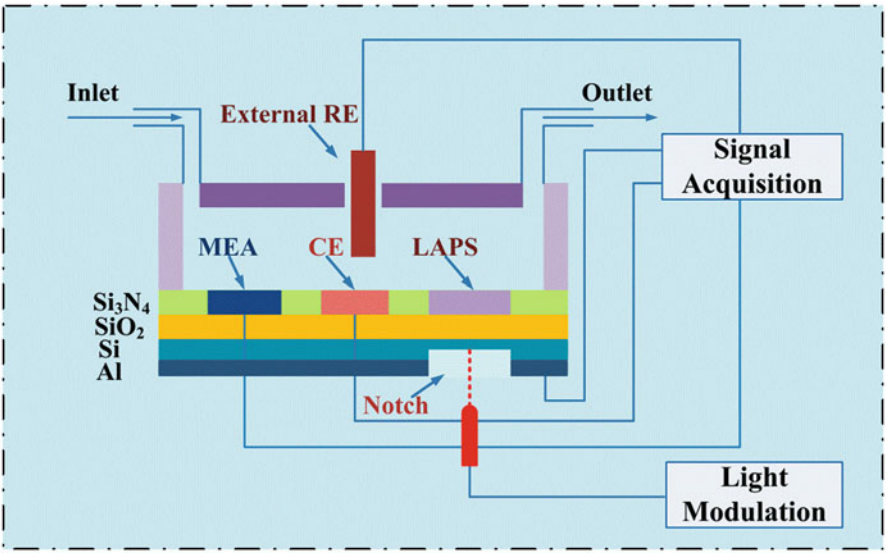

Fig. 8.8 The scheme of the hybrid sensor. *MEA*, *LAPS*, and counter electrode (*CE*) are integrated on the sensor, and signals are acquired through corresponding bonding pads by signal acquisition module (Reproduced with permission from [11]. Copyright 2013 Elsevier B.V.)

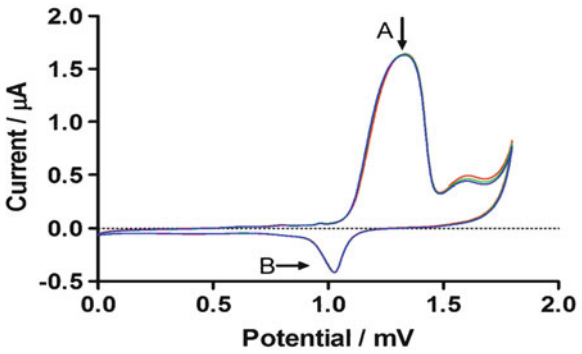

Fig. 8.9 Different MEAs' cyclic voltammograms (Reproduced with permission from [11]. Copyright 2013 Elsevier B.V.)

steady-state current. The difference is attributed to the different numbers of microelectrodes in the array. Therefore, for simplicity, electrochemical behavior of MEA 2 and 3 in Fig. 8.7a was mainly discussed. The cyclic voltammograms of MEA 2 are shown in Fig. 8.10a. Under the condition of low sweep rates, sigmoidal voltammograms were recorded due to the microsize electrode dimensions, and no diffusion overlap occurred in hemispheric diffusion, which is in contrast to macroelectrodes. With the increase of sweep rate, legible peak-shaped voltammogram (SR 0.1 V/s) arose which is in consistent with findings by A. Berduque and coworkers [12]. This is attributed to the decrease of diffusion layer as the increase of sweep rate and monodimensional diffusion became

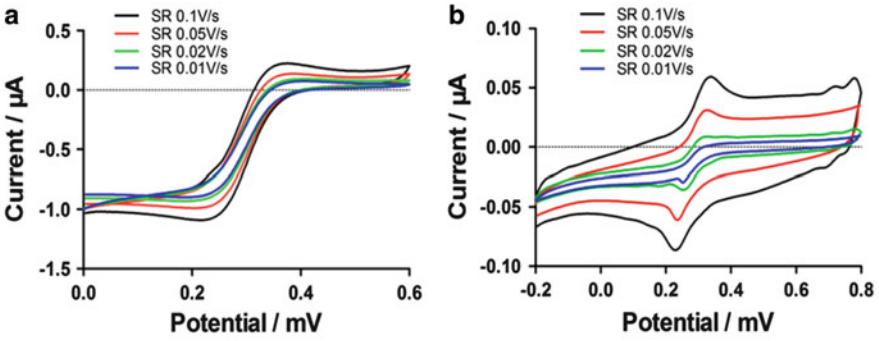

Fig. 8.10 (**a**) The cyclic voltammograms of MEA 2. (**b**) Peak-shaped voltammograms in MEA 3 [11]

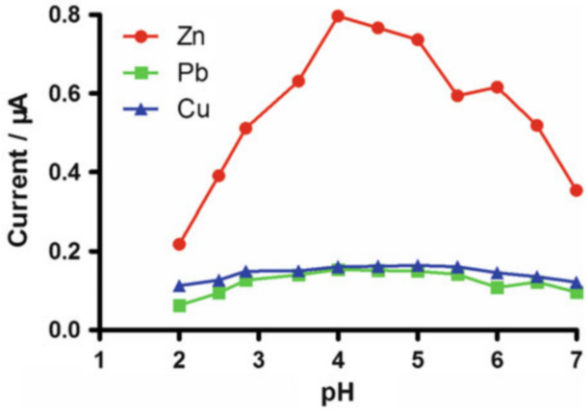

Fig. 8.11 Plots of peak current versus pH (Reproduced with permission from [11]. Copyright 2013 Elsevier B.V.)

predominant similar to macroelectrodes. Peak-shaped voltammograms in MEA 3 with different sweep rates were observed (shown in Fig. 8.10b). This is due to the overlap of diffusion layer with insufficient interelectrode spacing even in high sweep rate. MEA 3 presented a monodimensional diffusion predominantly in analysis of cyclic voltammetry. In summary, characterizations of MEA are affected by the ratio of interelectrode spacing to the size of microelectrode to a great extent. Concerning time costs and maintaining characterizations of microelectrode, MEA 2 was used in further analysis of stripping voltammetry, and the sweep rate was set to 0.05 V/s.

Considering the significant influence of pH variation to the stripping of heavy metal, the impact of different pH on stripping current of heavy metals was discussed to optimize the working condition and utilized for further calibration. Plots of peak current versus pH are shown in Fig. 8.11. As clearly evident, the highest peak current was achieved in the pH range of 4–5, indicating the optimum performance of Au-MEA under solutions with different acidity. When pH was 2, the stripping

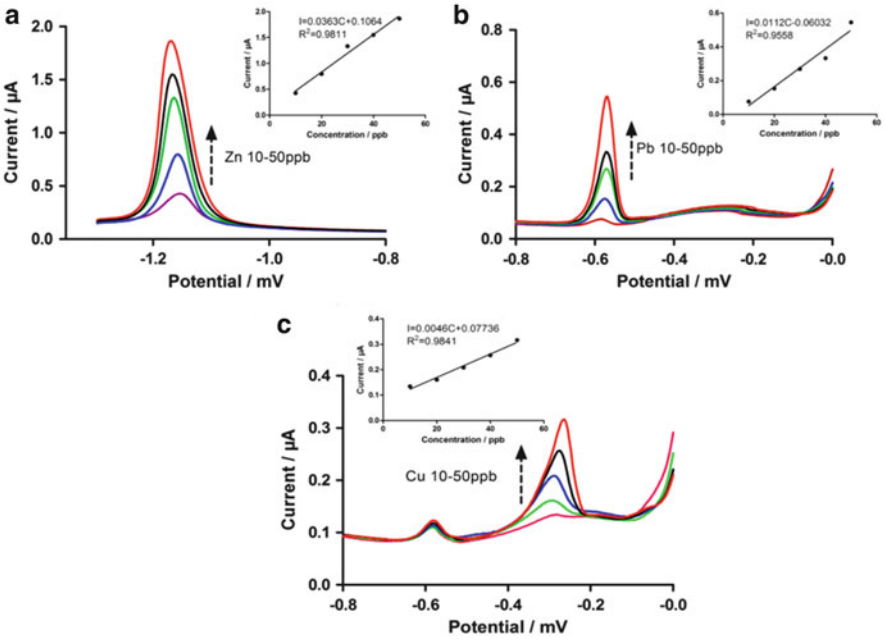

Fig. 8.12 Standard calibration curves of zinc, lead, and copper in 0.5 M KCl with pH 4 acetate buffer (Reproduced with permission from [11]. Copyright 2013 Elsevier B.V.)

peak currents of Zn, Pb, and Cu were relatively low due to the effect of hydrogen reduction. Notably, the peak current of Zn suffered from severe interference attributed to its negative oxidation potential, which approached the reduction potential of hydrogen. The process of hydrogen reduction was dominant on the sensing surface of Au-MEA compared to the oxidation of zinc, thus suppressing the oxidation. The peak current of heavy metal decreased in the pH range of 5–7 and the plausible explanation is the prevailing effect of hydrolysis of heavy metals. Allowing for the stripping currents of Zn, Pb, and Cu with the varying of pH, a pH 4 acetate buffer was applied for further electrochemical analysis.

The standard calibration curves of zinc, lead, and copper were obtained in 0.5 M KCl with pH 4 acetate buffer shown in Fig. 8.12. The deposition potential was −1.35 V and the deposition time was 120 s. The characteristic stripping potentials of zinc, lead, and copper are around −1.1, −0.56, and −0.28 V, respectively. With linear regression, calibration equations for heavy metals were achieved in Fig. 8.12 (inset). The correlation coefficient of zinc is 0.9811 and the sensitivity is 36.3 nA/ppb which is satisfactory for quantitative analysis. The correlation coefficients of lead and copper are 0.9558 and 0.9841, presenting a good linear relationship in the scope of selected concentrations. The sensitivity of lead and copper is 11.2 nA/ppb and 4.6 nA/ppb. The calibration equations acquired by standard curve method (SCM) can be used for quantitative detection of samples and further comparison between different calibration methods.

8.3.3 *Characterization of LAPS*

LAPS on the hybrid sensor was microfabricated for pH detection. The light frequency and light intensity of illuminating light were optimized concerning their vital impacts on the induced photocurrent. The light frequency of 4000 Hz was adopted with best performance and the light intensity was set under the voltage of 1.4 V. In the pH range of 3–8, plots of the photocurrent versus potential were acquired for the calibration of standard curve shown in Fig. 8.13a after normalization. Well-defined drift was observed in the linear working region under solutions with different acidity, suggesting good sensitivity for pH detection. The saturation region and cut-off region were in good coincidence, facilitating the identification of the sensitive point. The sensitive points were located by seeking the inflection point of the I–V curve, and the corresponding potential was recognized as the characteristic value under different pH. The calibration plot of the potential versus pH is shown in Fig. 8.13b. The correlation coefficient between the potential and pH is 0.9986, demonstrating a good linear correlation for pH detection. The sensitivity of LAPS for pH is 52.1 mV/pH, which is in accordance with the Nernst equation for monovalent ion. LAPS presents good sensitivity and performance for pH detection and the typical standard curve is acquired for pH analysis in the samples. To validate the consistency of LAPS, the four sensing areas were all tested for pH detection, and the sensitivity are 50.9 mV/pH, 53.7 mV/pH, and 49.2 mV/pH, respectively. The maximum relative deviation of the sensitivity is less than 5 %, indicating good consistency for pH detection.

The stability and reproducibility of LAPS were evaluated in view of the requirements for practical application. Five repetitive tests were conducted in a sample (pH 7) to validate the behavior of the sensor and the plot is shown in Fig. 8.14a. I–V curves are overlapped in the working region, and slight fluctuations are observed in the saturation region, which is possibly due to the variation of the total ion concentration after each adjustment of pH. The characteristic potential is extracted of which the relative standard deviation (RSD) is 1.45 % in Fig. 8.12 (inset) and good repeatability of plots is presented overall. Subsequently, long-term stability of

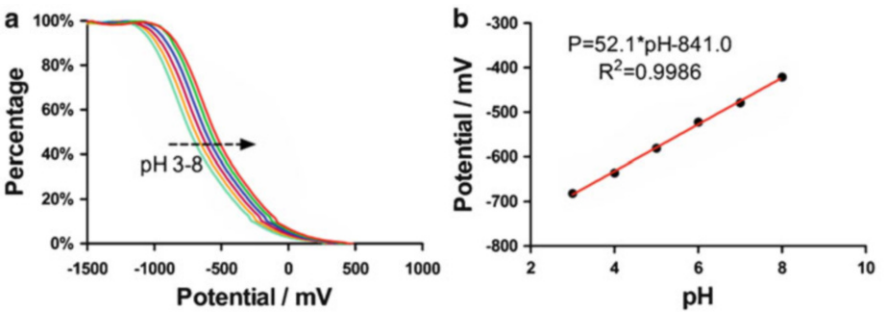

Fig. 8.13 (**a**) The plots of the photocurrent versus potential. (**b**) The calibration plot of potential versus pH [11] (Reproduced with permission from [11]. Copyright 2013 Elsevier B.V.)

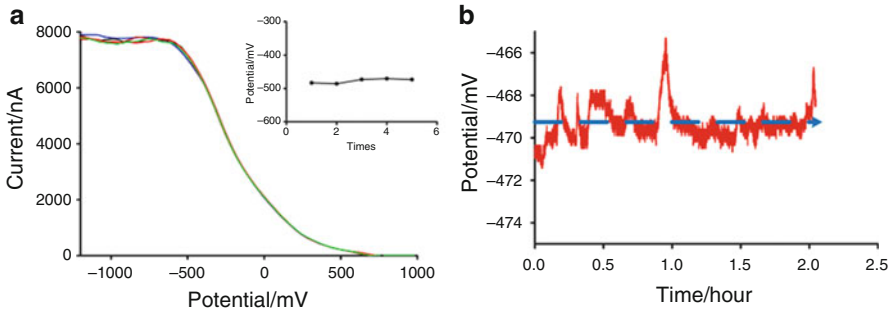

Fig. 8.14 (**a**) The plot of five repetitive tests. (**b**) The deviation of potential versus time (Reproduced with permission from [11]. Copyright 2013 Elsevier B.V.)

LAPS was investigated in a period of 2 h shown in Fig. 8.14b. The deviation of potential in a continuous detection of 2 h is less than 4 mV, while single detection is accomplished in merely 5 min that satisfies practical measurement. LAPS demonstrates good stability and reproducibility for pH detection.

8.4 Application in the Environment and Food Analysis

8.4.1 Heavy-Metal Detection

Electrochemical measurements have shown numerous advantages for trace heavy-metal detection, including rapid analysis, good selectivity, and sensitivity. Therefore, some works related to the electrochemical analysis of ion sensing are discussed in this section [5].

8.4.1.1 Chemically and Biochemically Modified Electrodes

Modified electrodes for electroanalytical determination of heavy metals using stripping voltammetry are commonly employed and present many advantages over the nonmodified electrodes, such as the enhancement of the sensibility and selectivity of the technique. A wide range of modifications have been reported in the literature with the aim of electrochemical detection of heavy metals, ranging from synthetic metal ionophores to biological receptors such as DNA or proteins.

α-Cyclodextrin or *β-cyclodextrin*-modified carbon paste electrodes have been used to determine Pb^{2+} by means of anodic stripping voltammetry [13, 14]. Both modified electrodes display good resolution of the lead oxidation peak. The analysis of the results indicates that the carbon paste electrodes modified with β-cyclodextrin exhibit a better analytical response than the ones modified with *α*-cyclodextrin. Detection limits of 6.30×10^{-7} M and 7.14×10^{-7} M of Pb^{2+},

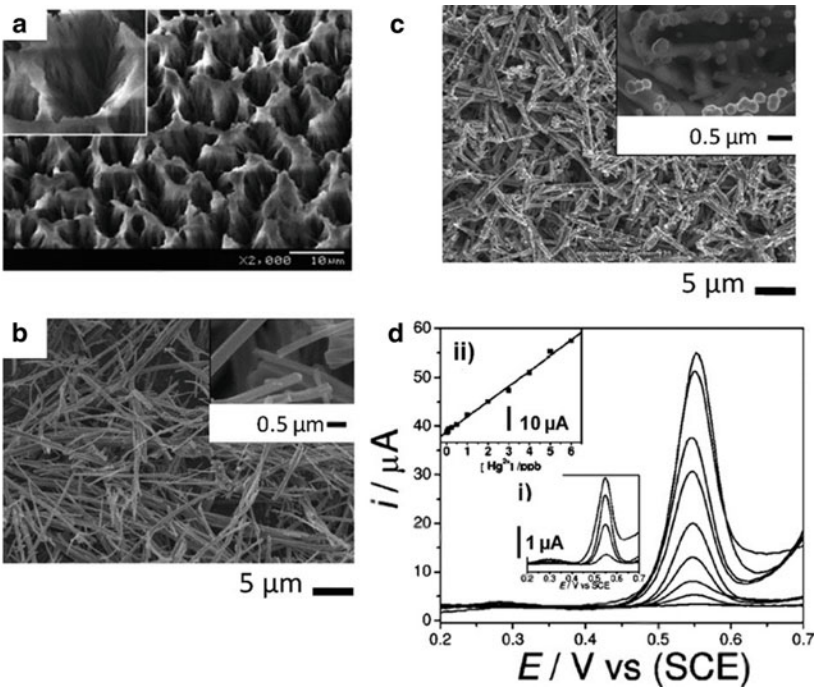

Fig. 8.15 Typical SEM images: (**a**) the bunch-like Bi composed of Bi nanowires, (**b**) the as-synthesized 3,30,5,50-tetramethylbenzidine (*TMB*)-based nanofibers (*NFs*), (**c**) Au-PtNPs/NF inorganic-organic hybrid nanocomposite on a glassy carbon electrode (*GCE*), (**d**) stripping voltammograms of increasing mercury concentrations (Reproduced with permission from [5]. Copyright 2011 American Chemical Society)

respectively, are obtained. The principal factors involved in guesthost complex formation are covalent bonds formed between metal ions and deprotonated $^{-}$O-groups of cyclodextrins.

Although the modified carbon paste electrodes are still being used for sensing purposes, due to their mode of preparation, these devices usually lack reproducibility between batches, and their use is time consuming. While this is not a big problem for in-lab research, it would be a considerable burden in mass production systems.

Because of their exceptional selectivity and sensibility, biomodified electrodes involving DNA, proteins, and antibodies have emerged as a new type of electrochemical sensing strategy for heavy-metal ions. Sensors based on proteins with distinct binding sites for heavy-metal ions are being developed and characterized. A capacitive signal transducer is used to measure the conformational change following heavy-metal binding (Fig. 8.15b). The proteins can be immobilized in different ways on a self-assembled thiol layer on a gold electrode placed as the working electrode in a potentiostatic arrangement in a flow analysis system. Metal ions can be detected down to femtomolar concentration using the biosensor described by

Bontidean et al. [15]. Figure 8.15a shows a developed electrochemical sensor based on cooperative coordination with Hg^{2+} by a pair of short poly-T oligonucleotides that induce conformational switching of the ferrocene-tagged probes from a single-strand to a duplex-like structure, modulating the electron-transfer efficiency [16]. This strategy exploits the cooperation of proximate poly-T oligonucleotides in coordination with Hg^{2+}. Ferrocene (Fc)-tagged poly-T oligonucleotides are immobilized on the electrode surface via self-assembly of the terminal thiol moiety. In the presence of Hg^{2+}, a pair of poly-T oligonucleotides can cooperatively coordinate with Hg^{2+}, which triggers a conformational reorganization of the poly-T oligonucleotides from flexible single strands to relatively rigid duplex-like complexes, thus drawing the Fc tags away from the electrode with a substantial decrease of the redox current. Figure 8.15b1 shows typical differential pulse voltammetry (DPV) curves of the sensor in response to Hg^{2+} ions of varying concentrations, while Fig. 8.15b2 is a plot of DPV peak currents versus Hg^{2+} concentrations. A similar design was proposed for Pb^{2+} detection using methylene blue as electrochemical label [17].

Other approaches related with biochemically modified electrodes involve enzyme-based biosensors, such as oxidase, dehydrogenase, and urease, which detect metal ions by relying on their inhibition of enzymatic reactions [18–20]. The enzyme glucose oxidase has been recently used by Willner et al. (Fig. 8.15c). The system is based on the use of a DNA scaffold for the amplified detection of Hg^{2+} using an electrically contacted relay/enzyme structure as a transducing element [21]. The detection limit for Hg^{2+} corresponds to 100 ± 10 pM. This great sensitivity originates from the amplification path provided by the biocatalytic system. Although the system has high sensitivity, working with enzymes requires narrow operation parameters (e.g., of pH, temperature, ionic strength) and long incubation times. In this context, the application of the enzyme-based system in real samples might be difficult or even impossible if the sample is under extreme conditions. Point-of-care devices are being developed nowadays to provide low-cost analytical systems useful for environmental monitoring of heavy metals. In this context, paper-based systems are highly novel and important [22, 23].

8.4.1.2 Metal Nanoparticle-Modified Electrodes

MNP-modified electrodes may serve as random arrays of microelectrodes. They show distinct advantages over the conventional macroelectrodes, such as increased mass transport, decreased influence of the solution resistance, low detection limit, and better signal-to-noise ratio.

Bismuth and antimony nanoparticles have been proven to be highly sensitive and reliable for trace analysis of heavy metals in conjunction with anodic stripping voltammetry. The attractive and unique behavior of bismuth and antimony nanomodified electrodes is attributed to the formation of multicomponents alloys, as well as the enhanced sensibility coming from the combination of the great

properties of the nanostructured material [24–27]. A new self-organized morphology of Bi (called bunch-like bismuth, see Fig. 8.15a) grown in a bare electrode has been recently described by Zhang et al. and exhibits a good performance for detection of heavy-metal ions [28].

In a parallel way, AuNPs-based electrodes have been proven to be a promising approach for heavy-metal detection [29–31]. Recently, bimetallic NPs have been extensively investigated due to their extraordinary properties, such as good conductivity, and better catalytic activities than their monometallic counterparts. Gong et al. have just reported the use of a bimetallic Au-PtNPs inorganic-organic hybrid nanocomposite-modified glassy carbon electrode for Hg^{2+} ion determination [32]. Bimetallic Au-PtNPs are homogenously distributed in the interlaced nanofiber (NF) matrix (see Fig. 8.15b, c), building a 3D porous network. Such 3D porous nanostructured composite film greatly facilitates electron-transfer processes and the sensing behavior for Hg^{2+} detection, leading to a remarkably improved sensitivity and selectivity. The calibration plot is linear up to 10 ppb, and the detection limit of 0.008 ppb (8 ppt) is obtained with the calculation based on a signal-to-noise ratio equal to 3 (see Fig. 8.15d).

In the same field, Domínguez et al. reported a novel method for the anodic stripping voltammetry determination of Sb^{3+} using AgNPs-modified screen-printed electrodes [33]. The detection limit for Sb^{3+} using the silver and gold modified electrode was 6.79×10^{-10} M for an accumulation time of 200 s.

8.4.1.3 Nanomaterials Combined with Synthetic Receptor-Modified Electrodes

The use of nanomaterials combined with the specific complexing ability of the receptors results in an improved electrochemical sensing platform toward heavy metals with high sensitivity and excellent selectivity for stripping analysis. Pan et al. reported a nanosized hydroxyapatite/ionophore-modified glassy carbon electrode for the determination of lead [34]. The nanostructurated material provides a unique three-dimensional network structure and particular multiadsorbing sites, while the specific complexing ability of the ionophore for lead enhances the sensibility and selectivity of the electrochemical platform for this metal [35]. The electrode has a linear range of response from 5.0 nM to 0.8 μM with a 10 min accumulation time at open-circuit potential. The sensitivity and detection limit of the proposed sensor are 13 μA/μM and 1.0 nM, respectively. Interferences from other heavy-metal ions such as Cd^{2+}, Cu^{2+}, and Hg^{2+} ions associated with lead analysis can be effectively diminished.

A similar work presented by Huang et al. for trace detection of mercury ions combining the use of 2-mercaptobenzothiazole adapters in a SiO_2 3D gold micro/nano pore array has been recently reported showing an excellent linear range (0.05–10 nM) and a good repeatability (relative standard deviation of 2.10 %) [36].

8.4.1.4 Nanobiomodified Electrodes

Electrochemical biosensors based on modifications with DNA and nanomaterials have received increasing attention, mainly for mercury detection [37, 38]. During the past decade, oligonucleotide-functionalized gold nanoparticles have been employed as amplifying tags for novel biosensing protocols due to their unique properties. Recently, Kong et al. have reported a highly selective electrochemical biosensor based on the strong and specific interaction of Hg^{2+} ions by two DNA thymine bases and the use of AuNP-functionalized reporter DNA to achieve signal amplification (see Fig. 8.16a) [39]. The electrochemical mercury biosensor is composed of three elements: a 50-thiol-modified oligonucleotide containing six T-bases for Hg^{2+} binding as a capture probe (DNA 1), an appropriate oligonucleotide linker (DNA 2) with the 30-terminal partially complementary with the capture probe sequence except six T-T mismatches, and finally a DNA 3 functionalized with AuNPs, which could specifically hybridize with the partial linker sequence close to the 50-terminal. When the sensing platform is incubated with solutions containing mercury and the DNA linker, the capture probe can hybridize with the linker via specific T-Hg-T interaction, and the AuNP-functionalized reporter DNA subsequently hybridizes with the linker. In the absence of mercury, the linker does not hybridize with the capture probe, because the melting temperature is lower than

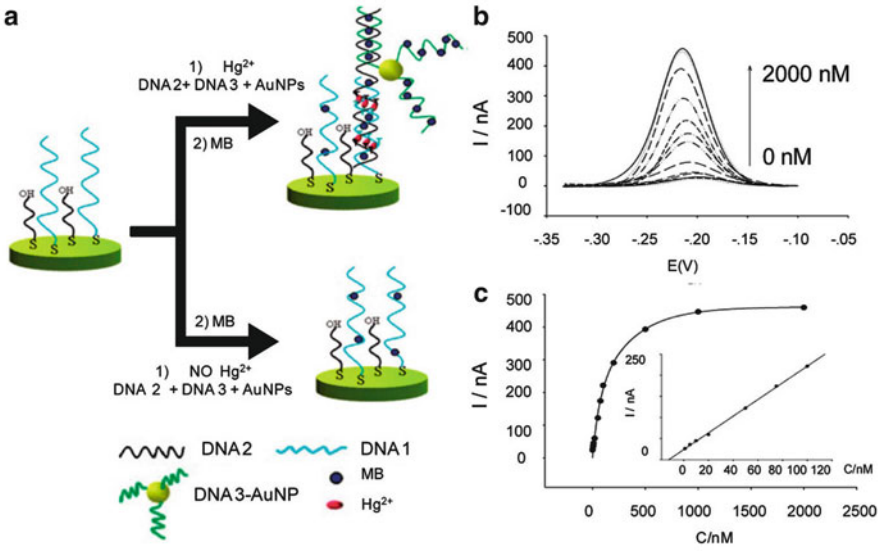

Fig. 8.16 (**a**) A description of the electrochemical Hg^{2+} sensing strategy based on the signal amplification of AuNP-functionalized reporter DNA. (**b**) DPV responses of the sensor after the addition of different concentrations of Hg^{2+} ions. (**c**) Calibration curves of peak current as a function of Hg^{2+} concentration. *Inset*: the linearity of the relative peak current with respect to the Hg^{2+} concentration over the concentration range 1–100 nM (Reproduced with permission from [5]. Copyright 2011 American Chemical Society)

the incubating temperature due to the T-T mismatches. Figure 8.16b shows DPV responses of the sensor after the addition of different concentrations of Hg^{2+} ions (0, 0.5, 1, 5, 10, 20, 50, 75, 100, 200, 500, 1000, and 2000 nM). Moreover, Fig. 8.16c shows the calibration curves of peak current as a function of Hg^{2+} concentration and the linearity of the relative peak current with respect to the Hg^{2+} concentration over the concentration range 1–100 nM. The described electrochemical sensor can achieve a detection limit of 0.5 nM, which makes the detector favorable for Hg^{2+} ion assays in practical samples, such as tap or river water with very low Hg^{2+} concentrations. Even though the system presents low detection limits, issues related with the reusability (by immersing the electrode into 1 M NaOH at 50 C) would represent a drawback for long-term and in-field applications.

8.4.2 Mycotoxin Determination

8.4.2.1 Biosensors as Diagnostic Tools

A biosensor is defined as a bioanalytical device incorporating a molecular recognition element associated or integrated with a physicochemical transducer [40]. To date there are five types of transducers used in biosensor devices, and these include electrochemical, optical, mass-sensitive, calorimetric, and magnetic transducers. The official IUPAC definition states "A biosensor is a self-contained integrated device, which is capable of providing specific quantitative or semiquantitative analytical information using a biological recognition element (biochemical receptor) which is retained in direct spatial contact with a transduction element" [41]. Figure 8.17 shows the concept of constructing a biosensor device where a biorecognition material is selected and then immobilized on the chosen sensor platform surface. The assay is then developed and optimized, and this is then combined with the instrument which will produce the digital signal. The use of these devices allows the capability of analyzing food and feed samples on-site such as on the farm or at the food factory [42]. That is because biosensors have the advantages over traditional methods of being, simple, rapid, cost-effective, and portable devices that are sensitive and specific for the target analyte, e.g., the mycotoxin. These devices can also be designed to be disposable for single use and reusable for several analyses or for continuous monitoring. A range of biosensors have now been developed and reported in the literature for mycotoxin analysis, some of which have the capability of multi-array mycotoxin diagnosis (multiplexing capabilities). The sample preparation can usually be incorporated as part of the sensor procedure system. Some of the extraction and cleanup procedures may be similar to the procedures used for HPLC or GC analysis especially if the samples are of solid food nature. Some sensors have been developed to be applied directly for liquid samples without the need for extraction of the sample. To date sensors can be designed to handle the sample through the inclusion of a microfluidic

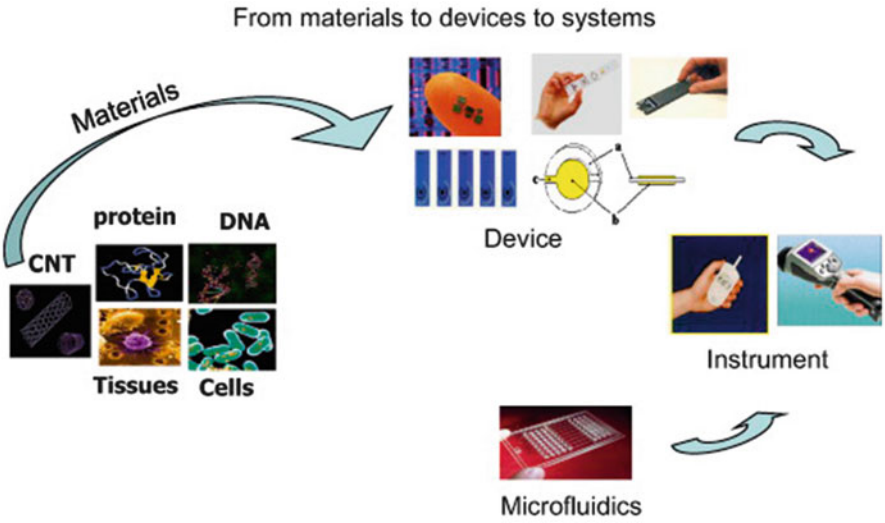

Fig. 8.17 Biosensor construction: a biorecognition material is selected and immobilized on the chosen sensor platform surface, then the assay is developed and optimized and this is then combined with the instrument which will produce the digital signal (Reproduced with permission from [43]. Copyright 2009 Elsevier Ltd.)

system or membrane separation system as part of their design for extracted food sample handling.

8.4.2.2 Micro/Nano electrode Arrays

Nanotechnology has the potential to improve food quality and safety significantly through the use of advanced micro- and nanosensors and tracking systems. Nanotechnology is research at the interface between chemistry, biology, material science, physics, and engineering where ultraprecision engineering can be combined with nanostructured materials and molecular manipulation to produce novel devices. The National Nanotechnology Initiative (NNI) defines nanotechnology as "Research and technology development at the atomic, molecular or macromolecular scale leading to the controlled creation and use of structures, devices and systems with a length scale of 1–100 nanometers (nM)" [44]. Interest in nanotechnology relies on the new properties that materials exhibit when reduced to the nanometer scale compared to the bulk materials. Lab-on-a-chip devices are examples of micro/nano technology systems approaches which can be used for the analysis of food contaminants such as mycotoxins for on-site analysis. These devices can be cost-effective and highly beneficial for the food industry in ensuring high safety and quality of the food and also for risk assessment and management. The use of nanomaterials and structures such as semiconductors and conducting polymer nanowires and nanoparticles (carbon nanotubes, silica nanoparticles,

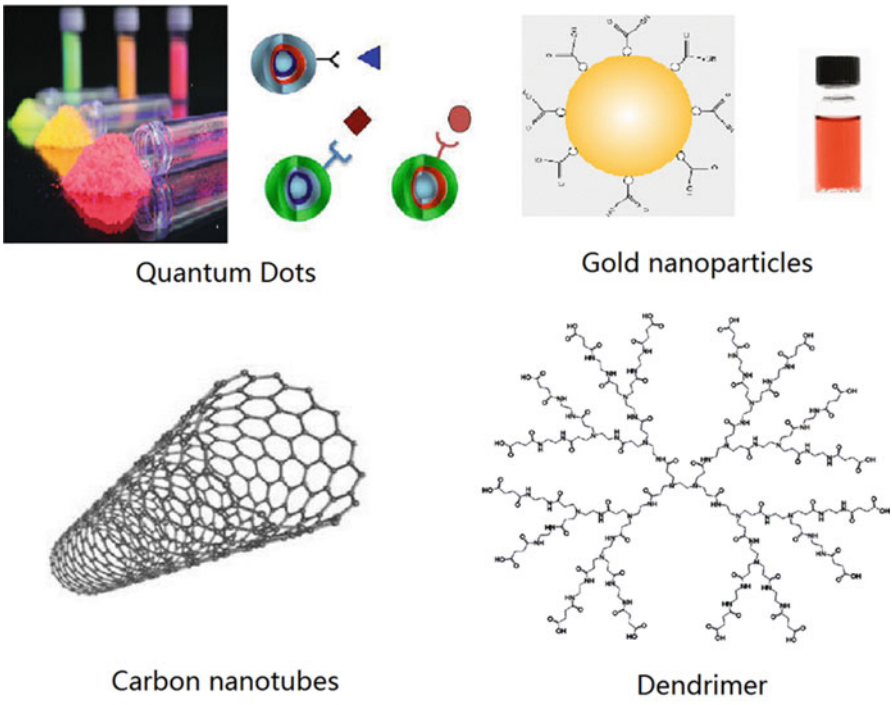

Fig. 8.18 Examples of nanoparticles used in sensor developments: they are quantum dots, carbon nanotubes, gold nanoparticles, and dendrimer

dendrimers, noble metal nanoparticles, gold nanoshells, superparamagnetic nanoparticles, quantum dots, polymeric nanoparticles) for biosensor applications is expanding rapidly. Figure 8.18 shows examples of some nanoparticles used for sensor applications. To date many comprehensive review articles have been published in this area [45–48].

The development of micro/nano sensor devices for toxins analysis is increasing due to their extremely attractive characteristics for this application. In principle these devices are miniature transducers fabricated using conventional thin and thick film technology. Their novel electron transport properties make them highly sensitive for low-level detection [49, 50]. The multiplex analysis capability is also very attractive for multi-biomarker analysis. Micro/nano electrodes can be classified as small electrodes in which at least one dimension is in the μm or nm range, respectively. These can also be fabricated using different materials such as platinum, gold, iridium, and carbon on silicon wafers. Microelectrode arrays (MEA) have been fabricated to produce miniaturized electrochemical sensors [12, 51]. Different shapes and sizes of these electrodes have been fabricated using standard deposition, etching, lithography, and photolithography techniques, including micro-disk electrodes [52], microband electrodes [53], interdigitated electrodes, and three-dimensional MEA [54]. The devices can be based on macro-type of

transducers such as receptor spots on glass slide or can be easily fabricated using screen-printing technology with multi-working electrode array. In order to develop practical devices for commercial developments, problems of binding between heterogeneous antigens and antibodies used in the sensor assays and also the high background signals need to be eliminated and controlled. Multi-toxin detection (e.g. mycotoxins) in foods can be conducted using single micro/nano electrode array chip with high sensitivity and rapid analysis time. The use of micro/nano arrays for analysis applications in foods can produce highly sensitive sensors.

Multi-mycotoxin detection has also been reported in the literature using different sensor platforms combined with multi-ELISA assays. Therefore, multi-toxins can be detected on a single microelectrode array chip with multi-array working electrode, where different antibody is immobilized to detect a specific mycotoxin. Micro/nano electrode arrays have unique properties which include small capacitive charging current and faster diffusion of electro-active species which will result in an improved response time and greater sensitivity [12]. The use of lab-on-a-chip is expanding in all areas of analysis due to the advantages of using small samples to analyze several markers/toxins, i.e., offer high-throughput analysis [55]. These types of devices will be attractive for mycotoxin analysis since several toxins may exist in the same food or feed sample. Examples are the electrochemical assay developed by Piermarini et al. [56], using a 96 well screen-printed microplate to detect aflatoxin B1 in corn samples. Detection was carried out using alkaline phosphatase as the label enzyme with the array used to detect the toxins in several samples simultaneously. Other examples of multi-mycotoxin analysis sensors include those reported by Ngundi et al. [57, 58], using a fluorescence-labeled antibody with a sensor arrays to detect ochratoxin A and deoxynivalenol. Also Gaag et al. [59] developed an SPR biosensor array to monitor aflatoxin B1 and deoxynivalenol. However, no real samples were analyzed using this sensor. Ligler et al. [60] reported on the use of biosensor consisting of a patterned array of capture antibody immobilized on planar waveguide. A fluorescent assay is then performed and the spots are captured using a CCD camera. Several authors reported the use of competitive immunofluorescent assays on a biosensor array for the simultaneous detection of several mycotoxins such as aflatoxin B1, fumonisin, ochratoxin A, and deoxynivalenol [60, 61]. Recently, Bayer Technology Services GmbH has developed a mycotoxin biochip platform based on planar waveguide technology, which is able to analyze multiple mycotoxins based on fluorescently labeled antibodies and consists of a reader and a lab-on a-chip cartridge.

We have developed an electrochemical microarray with 35 arrays and which was used for the detection of aflatoxin M1 [62] (Fig. 8.19). Each array consisted of 35 microsquare electrodes with 20×20 μm dimensions and edge-to-edge spacing of 200 μm (an electrode width to spacing ratio of 10). These dimensions and spacings were chosen to avoid overlapping diffusion layers between neighboring electrodes in the array. The whole microarray was used to immobilize the antibody for aflatoxin M1 analysis with very sensitive detection limit achieved (8 ng L-1 in milk) using amperometry as the detection system. This has now been also used for aflatoxin B1 and fumonisin detection (unpublished data). The use of microarrays

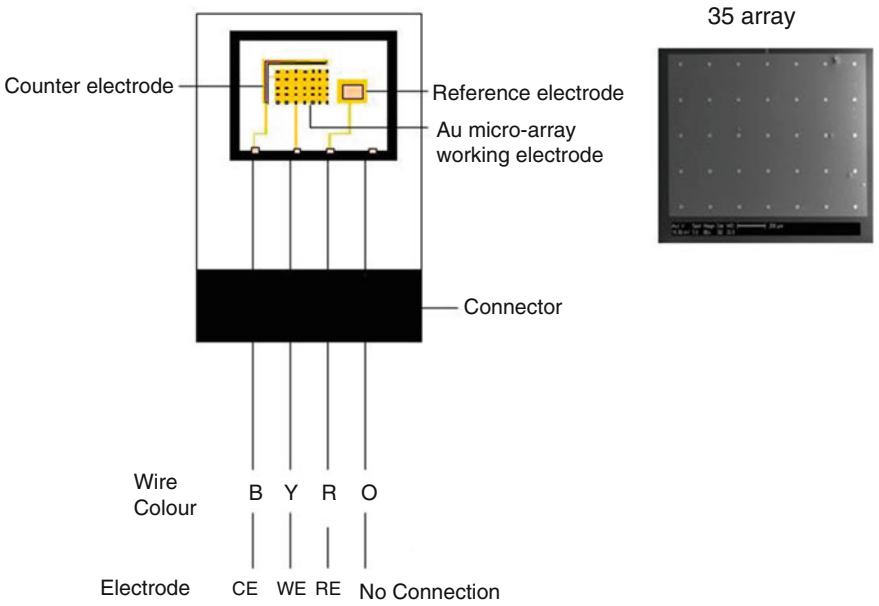

Fig. 8.19 A three-electrode chips with a working electrode area (35 electrodes in the array), a counter electrode, and a reference electrode area (Reproduced with permission from [62]. Copyright 2009 American Chemical Society)

for mycotoxin analysis is still progressing, and as shown above it can produce very highly sensitive sensors for mycotoxin analysis.

8.4.3 Application of the LAPS

The LAPS was first proposed by Hafeman in 1988 as a semiconductor device for biochemical systems [63, 64]. In the following 20 years, LAPS was widely studied in biological analysis and commonly used as an ISFET [65]. Different LAPS systems are designed to obtain better sensitivity, stability, and compatibility for bioassays. The cytosensor microphysiometer for extracellular acidification and the threshold unit for immunoassays have been commercialized by Molecular Devices Corp. (Sunnyvale, CA) [64]. The potentiometric alternating biosensor system has also been commercialized by Technobiochip (Marciana, Livorno, Italy) [66]. These systems have been used widely in various areas, including cellular physiology, toxicology, and pharmacology.

8.4.3.1 Typical LAPS

An LAPS is typically structured as a conventional electrolyte-insulator-semiconductor (EIS) sensor (Fig. 8.20a) [65], and the LAPS surface is chemically deposited with silicon oxynitride as an insulating layer, which can also be silicon oxide and silicon nitride. The insulating layer separates the silicon chip from the solution. The sensor surface forms silamine and silanol groups under hydration. The solution pH can affect the surface potential by changing the proportion of silamine and silanol groups. In the high-pH condition, the LAPS surface has a strong negative charge. In the low-pH condition, the LAPS surface has a weak charge. An electric field is generated in the LAPS when a DC voltage is applied on the sensor chip. A photocurrent is produced by a pulsing infrared light from a light-emitting diode (LED) at the backside of the chip. The photocurrent amplitude depends on the sum of the surface potential and applied potential, and the former depends on the solution pH of the insulating layer [67] (Fig. 8.20b). In the conventional detection mode, a DC voltage is used to keep the LAPS photocurrent constant, and the voltage changes correspond to the pH changes (60 mV/pH unit). Therefore, biological events could induce corresponding fluctuations in the photocurrent output by modifying the electrochemical parameters of the interface.

In the biological application, the LAPS commonly monitors the cellular metabolism, especially energy metabolism. The heterotrophic cells obtain various

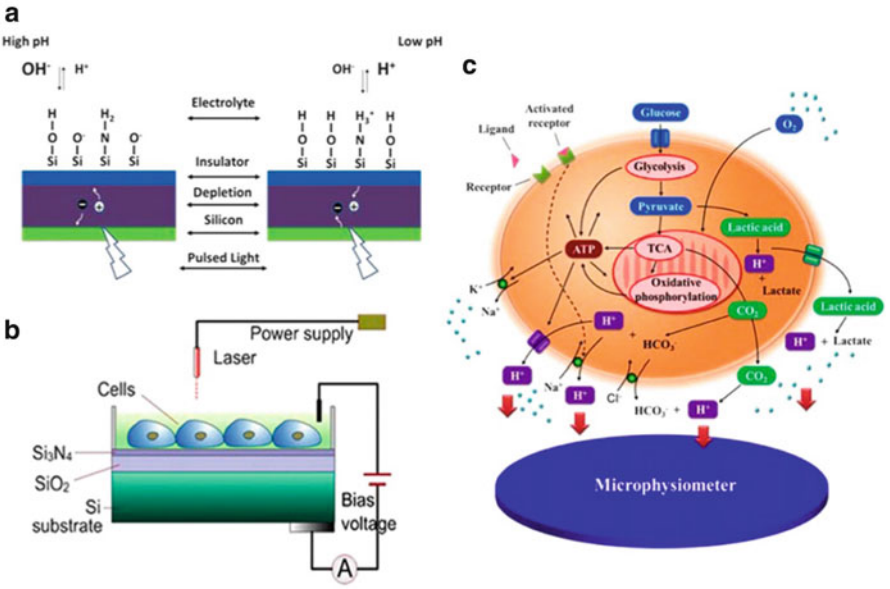

Fig. 8.20 Illustration of a LAPS as a microphysiometer: (**a**, **b**) principle and structure of the LAPS (Reproduced with permission from [65]. Copyright 2000 Elsevier S.A.) (**c**) proton release in cellular metabolism (Reproduced with permission from [67]. Copyright 2011 Elsevier B.V.)

nutrients, produce the energy, and release the wastes for growth. The carbon source (e.g., sugars, amino acids, and fatty acids) mainly produces metabolic energy. The schematic overview of the cellular metabolic process is presented in Fig. 8.20c. In the natural aerobic condition, cells convert glucose into CO_2. In the anaerobic condition, cells convert glucose into lactic acid. The acidic products (e.g., H+, CO_2, and lactic acid) generated by cellular energy metabolism induce a pH drop in the extracellular microenvironment, which can be detected by a microphysiometer.$_{309}$ On the basis of this principle, a large amount of experiments have been carried out to monitor the extracellular acidification rate (ECAR), which is the most significant parameter indicating the state of cellular metabolism. Many biochemical factors, such as receptor-ligand reactions, will affect the ECAR of the cells, and the effects of these factors can be measured via a microphysiometer. Additionally, a microphysiometer can analyze and evaluate pharmaceutical effects on ECAR, such as antitumor drugs for chemotherapy [68, 69].

In constructing cell-based biosensors for extracellular microenvironment monitoring, the LAPS is preferred over the ISFET because of its compatibility with MEMS fabrication, less critical and easier encapsulation, and incorporation into microvolume measuring chambers for bioassays. Also, when cells are cultured on a silicon surface, extracellular action potential coupled to the sensor surface can also generate corresponding spikes in the photocurrent output [70]. Electrophysiological study with the LAPS can overcome the geometric restrictions of MEAs and FETs.

8.4.3.2 Microphysiometers Based on the LAPS

The LAPS is sensitive to pH variation in the electrolyte solution. By encapsulating the LAPS and cells in a microvolume chamber, the microphysiometer is used to indicate the ECAR (Fig. 8.21) [71]. In the microphysiometer, cells are cultured in the microvolume chamber, which is formed by a multiporous polycarbonate membrane and an O-ring spacer. The microvolume chamber is tightly fixed on the LAPS chip, and H+ can diffuse adequately in the small volume, so the ECAR can be directly measured by the LAPS. A modulated infrared LED (light-emitting diode) illuminates the backside of the LAPS, and thus, the LAPS will generate a photocurrent with the same frequency. All of the experimental data are transmitted into a computer by the detection and analysis instrument. The culture medium is injected into the flow chamber by the peristaltic pump, the degasser, and finally the injection valve. The ECAR can be continually measured by refreshing the culture medium cycle.

The basic function of the microphysiometer is to study the metabolic activities responsive to agents. The metabolic activity responses of different cells to many different agents have been successfully monitored [72, 73]. For example, for fibroblast cells, 2-deoxy-D-glucose reduces the acidification rate from −90 to −40 μV/s, which is directly induced by the decrease of lactic acid. Also, fluoride acts as a metabolic inhibitor which binds to the enolase and affects pyruvate formation, which subsequently decreases the ECAR significantly.

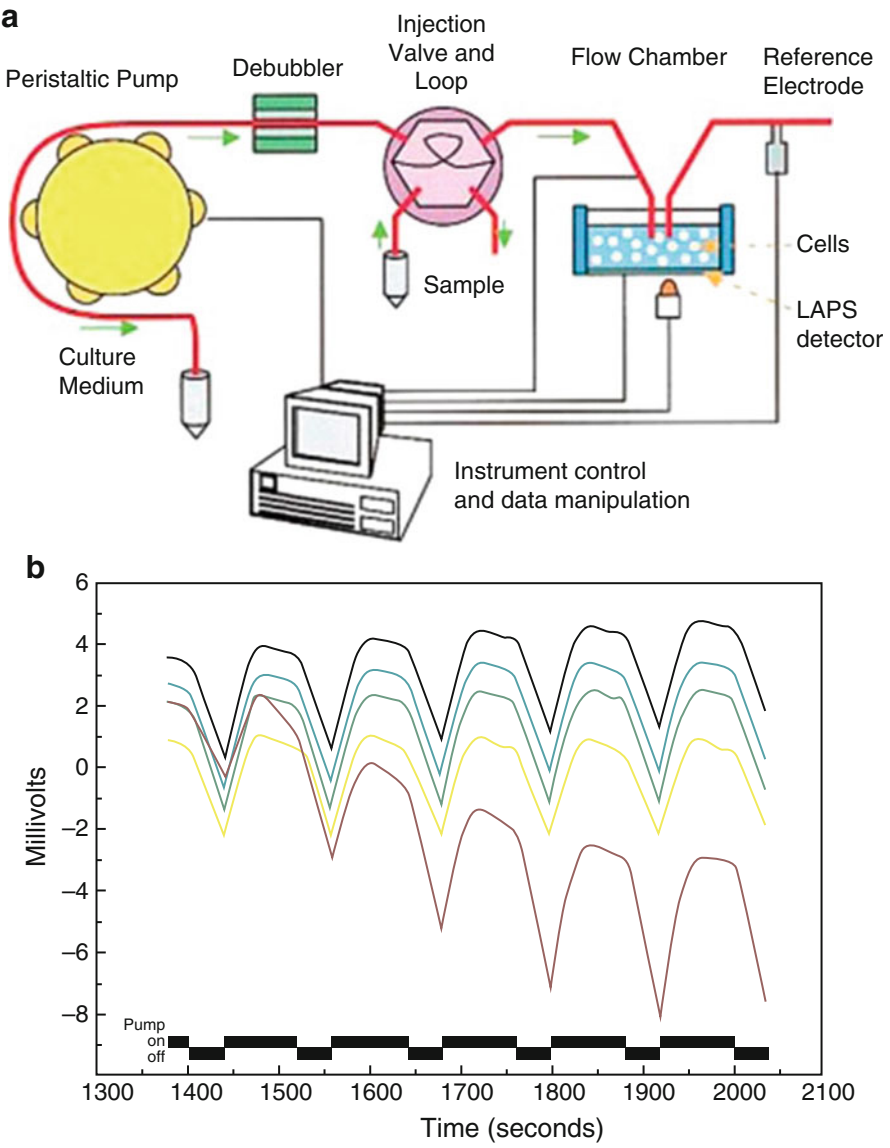

Fig. 8.21 Microphysiometer for extracellular acidification based on the LAPS: (**a**) schematic of the cytosensor microphysiometer, (**b**) ECAR measured by the flow-on/flow-off cycle of the microphysiometer (Reproduced with permission from [71]. Copyright 1999 John Wiley & Sons, Inc.)

Changes in the ECAR typically ranged from 110 to 200 % of the basal ECAR in the receptor activations [74]. Pharmacology assays with microphysiometers can measure the functional consequence of extracellular acidification by drugs binding to molecules. Additionally, microphysiometers can measure the ECAR induced by many receptors (e.g., cAMP and mitogenesis). Cells maintain homeostasis by releasing H+, so the overall cellular metabolism can be reflected by the ECAR. Applications have been proposed in studies including pharmacology-related signaling mechanisms [75], functional characterizations of ligand-receptor binding [76, 77], and identification of specific and functional orphan receptors [78, 79]. Many activations of protein tyrosine kinases have been investigated using the effects of pharmacological factors and receptors, such as epidermal growth factor (EGF) receptor tyrosine kinase [75, 76], epidermal growth factor [80], insulin-like growth factor-1 (IGF-1) [81], ligand-gated ion channels [82], leptin receptor [83], T-cell receptor [84], G-protein-coupled receptors of angiotensin II receptor, type 1 (AT1) receptor [85, 86], and bradykinin receptor B2 [87].

When the signaling pathways are coupled, the receptor activation-induced cellular responses can be studied with the ECAR. For example, dimethyl amiloride (DMA) was used to study Na^+/H^+ exchanger activities in cells growing at different cell densities [88]. Exposing cells at low density (10^4 cells/mL) to dust induced an initial release of acid not involving the exchanger, followed by a sustained DMA-sensitive Na^+/H^+ exchanger activation. In cells near high density (10^6 cells/mL), the Na^+/H^+ exchanger was not activated during exposure, resulting in a modest increase in the ECAR. Exposing cells at high density resulted in a biphasic ECAR pattern, and an initial increase in proton release was followed by an inhibition of the ECAR below baseline. Polar amino acids are important in the proton flux activity of Na^+/H^+ exchangers [89]. A large number of G-protein- and non-G-protein-coupled hormone and neuropeptide receptors which activate the signal transduction mechanisms have been investigated [90]. Signal pathways of gp130 family cytokines (interleukin-6 (IL-6), oncostatin M) and IL-1 were probed by the ECAR of HepG2 cells [91]. Extracellular acidification measurement is a kind of in vitro bioassay, and H+ is used as an indicator of overall cellular metabolism. Initial studies of irritancy testing using human keratinocytes grown on coverslips tested half-log serial dilutions of eight irritants previously characterized as having in vivo ocular irritancy ranging from mild to severe [92]. Ocular and skin irritancy testing materials represent the range of effects commonly encountered in cleaning products [93, 94]. Other cell sources, including hepatic cells and cancer cell lines [91, 95], were treated with various toxins and drugs to evaluate their effects. The microphysiometer is a useful platform to monitor metabolic disturbance by measuring the recovery of the extracellular microenvironment.

Further improvements of the microphysiometer system were proposed for monitoring several parameters in the extracellular microenvironment related to ATP usage and metabolic processes. A multianalyte microphysiometer has been proposed to simultaneously measure the acidification rate, glucose consumption, oxygen uptake, and lactate production in the extracellular environment by modifying the cytosensor microphysiometer system to study the cellular metabolism more

comprehensively [72, 73]. Another attempt to use a multiparameter microphysiometer was made using poly(vinyl chloride)-based ion-sensitive membranes on the LAPS surface for extracellular monitoring of ions such as K^+, Na^+, Ca^{2+}, and Cl− [96, 97]. These multianalyte and multiparameter detections can provide more biological information about cellular responses to achieve better evaluation of drug effects. Especially, if modified with a porous structure, the LAPS could display highly enhanced performance attributed to morphological changes in the sensing units [98].

8.4.3.3 Cell-Semiconductor Hybrid for Electrophysiological Detection

In the above section, the microphysiometer is introduced to monitor metabolism in a cell population. However, it is far from the ability of cell-semiconductor hybrid systems to detect ion channels or potentials of cells. The LAPS surface is totally flat without any special structures, so the cells can easily culture and freely attach to the LAPS. Recently, the LAPS was used to study excitable cells by monitoring extracellular potentials [99, 100]. In principle, the modulated infrared laser is focused by the microscope to illuminate the position of the target cell. The inflow or outflow of cellular ionic currents (e.g., Na^+, K^+, and Ca^{2+}) will induce fluctuation of the LAPS response signals.

The LAPS consists of an EIS structure (Fig. 8.22a, b) [101]. The insulator (SiO_2 layer) is suitable for the attachment of cells without the addition of special structures. Therefore, the ionic current induced by the extracellular potential will couple with the LAPS surface, and the corresponding photocurrent change can be detected by the LAPS. This simple model of the cell-sensor interface is shown in Fig. 8.22c. The LAPS has the light-addressable function, and the laser can scan at arbitrary positions on the LAPS surface. On the basis of the working principle, the extracellular potential of the cell can be detected when the focused laser illuminates the sensitive region of a cell [101]. Thus, a membrane potential change can cause

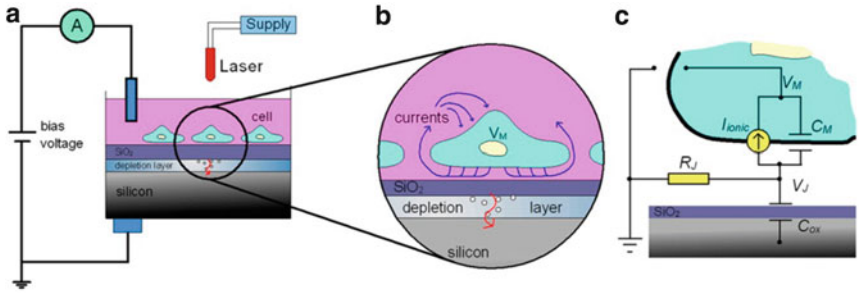

Fig. 8.22 Extracellular potential monitored with the LAPS: (**a**) schematic of the cell-based biosensor and LAPS detection system, (**b**) cell-sensor interface with the EIS structure, (**c**) simplified model of the cell-LAPS biosensor (Reproduced with permission from [101]. Copyright 1999 2006 Elsevier B.V.)

corresponding turbulence in the LAPS output. In recent research, cell-LAPS hybrid biosensors have been proposed as superior instruments for extracellular recording of potential signals [70, 99, 102, 103]. Most recordings were performed with excitable cells, such as ardiomyocytes and neurons.

As discussed in this review, the FET array and MEA are at present the two main types of cell-semiconductor hybrid biosensor systems for extracellular detection. However, the MEA and FET are typically restricted by their surface structure because only a few electrodes are fabricated. Thus, a small effective detection region can be used to monitor the cellular state. Moreover, microelectronic fabrication restricts the distance of the electrodes on the MEA and FET [104], which ranges from 50 to 200 μm [100]. Consequently, the spatial resolution of the sensor is restricted significantly, and it will hamper the development of the biosensors. However, the LAPS is different from the MEA and FET due to its special working mode. The surface potential of the LAPS can be monitored and detected by a scanning focused laser beam. The illuminated site will generate a photocurrent signal which reflects the surface potential. Taking this characteristic into consideration, the spatial resolution will be much improved. Therefore, an arbitrary site on the LAPS can sense the cellular state, so all of the cells cultured on the LAPS can be studied.

The majority of related studies are focused on self-exciting cells such as neurons and cardiomyocytes [105]. Stem cells and tissues are also used as new sources for LAPS biosensors [67, 106, 107]. Liu et al. have cultured the mouse embryoid bodies on the LAPS and induced them to differentiate into cardiomyocytes and neurons in vitro (Fig. 8.23a) [67]. Typical signals of cardiomyocytes recorded are shown in Fig. 8.23b. The spikes can be sorted and analyzed by several parameters shown in Fig. 8.23c. Differences in these parameters can reflect cellular responses to drugs in a way similar to that of MEA- and FET-based biosensors. Electrophysiological responses are monitored using amiodarone, noradrenaline, sparfloxacin, and levofloxacin as cardiotoxic drugs.

An obvious disadvantage of the LAPS is its single-channel output, which makes it difficult to record extracellular potentials of multisite cells simultaneously. The LAPS with submicrometer electrodes has been reported with a light-addressable function [108]. This novel design concept will even benefit MEA systems to solve the problem of lower spatial resolution. Moreover, the functions and performance of the LAPS can be enhanced by modifying specific bioactive units and other materials, such as biological enzymes and ion-selective membranes, to detect many physiological parameters of cells simultaneously.

Alongside parallel detection, another promising field is using the LAPS as a virtual electrode to stimulate excitable cells. The extracellular potential is determined by the membrane potential and ionic current. One group has developed the LAPS biosensor technology by recording the extracellular stimulations of discrete neurons [109]. The complicated spatiotemporal patterns of cell networks can be investigated by scanning the desired sites on the LAPS. Therefore, information at any site will be monitored continually. Compared to the site-restricted MEA, the LAPS can serve as a useful biosensor to carry out the spatiotemporal analysis.

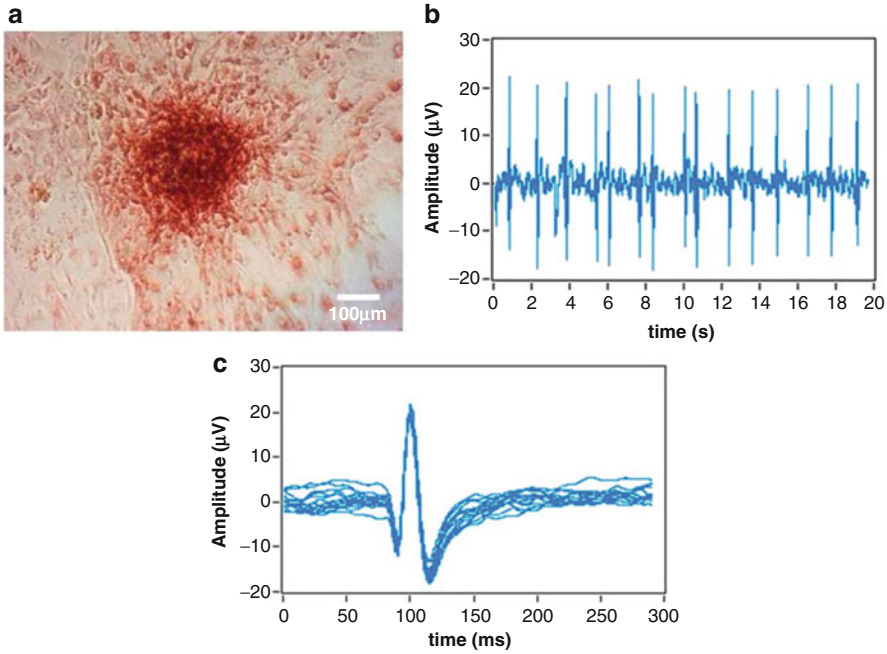

Fig. 8.23 Embryonic stem cells differentiated into cardiomyocytes and extracellular potentials detected by the LAPS: (**a**) mouse embryoid bodies differentiated into cardiomyocytes on the LAPS, (**b**) typical signals recorded, (**c**) automatic spike sorting (Reproduced with permission from [67]. Copyright 2011 Elsevier B.V.)

Additionally, visualized research on cells and tissues may be improved by the technology. The bioelectronics and bioelectrochemical imaging will facilitate the study of cell networks with the development of spatiotemporal pattern studies.

The cell-silicon junction plays a significant role in the combination of neuronal dynamics and electronics. The integration of excitable cells and sensors will be used to exploit a new approach for both eliciting and recording neuronal networks on the same chip simultaneously. The neuronal networks can be formed on the sensors, and the signaling pathway of the neuronal networks can also be modeled and computed in further investigations.

8.5 Summary

The developments in micro/nano electrochemical sensors have large impact on ion sensing research. Significant advances in the fabrications of micro/nano electrochemical sensors are being persistently made. In this chapter, we briefly described the theory of electrochemical sensors for ion sensing, which contain potentiometric sensors, voltammetric sensors, and microelectrode array. A detailed analysis of

these sensors has been carried out on the latest research advancement made in the development of ion sensing-based sensors/biosensors. The characteristics of these sensors are also described in detail.

As more and more nanomaterials were discovered and used, micro/nano electrochemical sensors have become a new detection technology. It has broad application prospect in the field of environment and food analysis. The application of LAPS, heavy-metal detection, and mycotoxin determination has been described in detail in this chapter.

References

1. Goyer RA. Nutrition and metal toxicity. Am J Clin Nutr. 1995;61(3):646S–50.
2. Goyer RA, Clarkson TW. Toxic effects of metals', Casarett & Doull's toxicology. In Klaassen, CD, editor.The basic science of poisons, 5th ed. McGraw-Hill Health Professions Division, New York; 1996. ISBN, 71054766.
3. Goyer RA. Toxic and essential metal interactions. Annu Rev Nutr. 1997;17(1):37–50.
4. Gaetke LM, Chow CK. Copper toxicity, oxidative stress, and antioxidant nutrients. Toxicology. 2003;189(1):147–63.
5. Aragay G, Pons J, Merkoci A. Recent trends in macro-, micro-, and nanomaterial-based tools and strategies for heavy-metal detection. Chem Rev. 2011;111(5):3433–58.
6. Wang P, Liu Q, Wu C, Hsia KJ. Bioinspired smell and taste sensors. In Editor (Ed.)^(Eds.). Book bioinspired smell and taste sensors. Dordrecht: Springer; 2015, edn. pp.
7. Campos I, Pascual L, Soto J, Gil-Sánchez L, Martínez-Máez R. An electronic tongue designed to detect ammonium nitrate in aqueous solutions. Sensors. 2013;13(10):14064–78.
8. Weber SG. Signal-to-noise ratio in microelectrode-array-based electrochemical detectors. Anal Chem. 1989;61(4):295–302.
9. Ramos A, Morgan H, Green NG, Castellanos A. Ac electrokinetics: a review of forces in microelectrode structures. J Phys D Appl Phys. 1998;31(18):2338.
10. Davies TJ, Compton RG. The cyclic and linear sweep voltammetry of regular and random arrays of microdisc electrodes: theory. J Electroanal Chem. 2005;585(1):63–82.
11. Wan H, Ha D, Zhang W, Zhao H, Wang X, Sun Q, Wang P. Design of a novel hybrid sensor with microelectrode array and LAPS for heavy metal determination using multivariate nonlinear calibration. Sens Actuators B. 2014;192:755–61.
12. Berduque A, Lanyon YH, Beni V, Herzog G, Watson YE, Rodgers K, Stam F, Alderman J, Arrigan DW. Voltammetric characterisation of silicon-based microelectrode arrays and their application to mercury-free stripping voltammetry of copper ions. Talanta. 2007;71(3):1022–30.
13. Norkus E. Metal ion complexes with native cyclodextrins. An overview. J Incl Phenom Macrocycl Chem. 2009;65(3–4):237–48.
14. Fragoso A, Ortiz M, Sanromà B, O'Sullivan CK. Multilayered catalytic biosensor self-assembled on cyclodextrin-modified surfaces. J Incl Phenom Macrocycl Chem. 2011;69(3–4):355–60.
15. Bontidean I, Berggren C, Johansson G, Csöregi E, Mattiasson B, Lloyd JR, Jakeman KJ, Brown NL. Detection of heavy metal ions at femtomolar levels using protein-based biosensors. Anal Chem. 1998;70(19):4162–9.
16. Liu S-J, Nie H-G, Jiang J-H, Shen G-L, Yu R-Q. Electrochemical sensor for mercury (II) based on conformational switch mediated by interstrand cooperative coordination. Anal Chem. 2009;81(14):5724–30.

17. Xiao Y, Rowe AA, Plaxco KW. Electrochemical detection of parts-per-billion lead via an electrode-bound DNAzyme assembly. J Am Chem Soc. 2007;129(2):262–3.
18. Zhylyak G, Dzyadevich S, Korpan Y, Soldatkin A, El'Skaya A. Application of urease conductometric biosensor for heavy-metal ion determination. Sens Actuators B. 1995;24 (1):145–8.
19. Rodriguez BB, Bolbot JA, Tothill IE. Development of urease and glutamic dehydrogenase amperometric assay for heavy metals screening in polluted samples. Biosens Bioelectron. 2004;19(10):1157–67.
20. Fennouh S, Casimiri V, Geloso-Meyer A, Burstein C. Kinetic study of heavy metal salt effects on the activity of L-lactate dehydrogenase in solution or immobilized on an oxygen electrode. Biosens Bioelectron. 1998;13(7):903–9.
21. Mor-Piperberg G, Tel-Vered R, Elbaz J, Willner I. Nanoengineered electrically contacted enzymes on DNA scaffolds: functional assemblies for the selective analysis of Hg^{2+} ions. J Am Chem Soc. 2010;132(20):6878–9.
22. Nie Z, Deiss F, Liu X, Akbulut O, Whitesides GM. Integration of paper-based microfluidic devices with commercial electrochemical readers. Lab Chip. 2010;10(22):3163–9.
23. Tan SN, Ge L, Wang W. Paper disk on screen printed electrode for one-step sensing with an internal standard. Anal Chem. 2010;82(21):8844–7.
24. Rico MÁG, Olivares-Marín M, Gil EP. Modification of carbon screen-printed electrodes by adsorption of chemically synthesized Bi nanoparticles for the voltammetric stripping detection of Zn (II), Cd (II) and Pb (II). Talanta. 2009;80(2):631–5.
25. Lee G-J, Lee HM, Uhm YR, Lee MK, Rhee C-K. Square-wave voltammetric determination of thallium using surface modified thick-film graphite electrode with Bi nanopowder. Electrochem Commun. 2008;10(12):1920–3.
26. Stozhko NY, Malakhova NA, Fyodorov MV, Brainina KZ. Modified carbon-containing electrodes in stripping voltammetry of metals. J Solid State Electrochem. 2008;12 (10):1185–204.
27. Toghill KE, Xiao L, Wildgoose GG, Compton RG. Electroanalytical determination of cadmium (II) and lead (II) using an antimony nanoparticle modified boron-doped diamond electrode. Electroanalysis. 2009;21(10):1113–8.
28. Zhang Z, Yu K, Bai D, Zhu Z. Synthesis and electrochemical sensing toward heavy metals of bunch-like bismuth nanostructures. Nanoscale Res Lett. 2010;5(2):398–402.
29. Kumar Jena B, Retna Raj C. Gold nanoelectrode ensembles for the simultaneous electrochemical detection of ultratrace arsenic, mercury, and copper. Anal Chem. 2008;80 (13):4836–44.
30. Orozco J, Fernández-Sánchez C, Jiménez-Jorquera C. Underpotential deposition − anodic stripping voltammetric detection of copper at gold nanoparticle-modified ultramicroelectrode arrays. Environ Sci Technol. 2008;42(13):4877–82.
31. Gong J, Zhou T, Song D, Zhang L. Monodispersed Au nanoparticles decorated graphene as an enhanced sensing platform for ultrasensitive stripping voltammetric detection of mercury (II). Sensors Actuators B Chem. 2010;150(2):491–7.
32. Gong J, Zhou T, Song D, Zhang L, Hu X. Stripping voltammetric detection of mercury (II) based on a bimetallic Au− Pt inorganic− organic hybrid nanocomposite modified glassy carbon electrode. Anal Chem. 2009;82(2):567–73.
33. Renedo OD, Martínez MJA. A novel method for the anodic stripping voltammetry determination of Sb (III) using silver nanoparticle-modified screen-printed electrodes. Electrochem Commun. 2007;9(4):820–6.
34. Pan D, Wang Y, Chen Z, Lou T, Qin W. Nanomaterial/ionophore-based electrode for anodic stripping voltammetric determination of lead: an electrochemical sensing platform toward heavy metals. Anal Chem. 2009;81(12):5088–94.
35. Jang SH, Min BG, Jeong YG, Lyoo WS, Lee SC. Removal of lead ions in aqueous solution by hydroxyapatite/polyurethane composite foams. J Hazard Mater. 2008;152(3):1285–92.

36. Fu X-C, Chen X, Guo Z, Kong L-T, Wang J, Liu J-H, Huang X-J. Three-dimensional gold micro-/nanopore arrays containing 2-mercaptobenzothiazole molecular adapters allow sensitive and selective stripping voltammetric determination of trace mercury (II). Electrochim Acta. 2010;56(1):463–9.
37. Zhu Z, Su Y, Li J, Li D, Zhang J, Song S, Zhao Y, Li G, Fan C. Highly sensitive electrochemical sensor for mercury (II) ions by using a mercury-specific oligonucleotide probe and gold nanoparticle-based amplification. Anal Chem. 2009;81(18):7660–6.
38. Miao P, Liu L, Li Y, Li G. A novel electrochemical method to detect mercury (II) ions. Electrochem Commun. 2009;11(10):1904–7.
39. Kong R-M, Zhang X-B, Zhang L-L, Jin X-Y, Huan S-Y, Shen G-L, Yu R-Q. An ultrasensitive electrochemical "turn-on" label-free biosensor for Hg^{2+} with AuNP-functionalized reporter DNA as a signal amplifier. Chem Commun. 2009;37:5633–5.
40. Chianella I, Piletsky S, Tothill I, Chen B, Turner A. MIP-based solid phase extraction cartridges combined with MIP-based sensors for the detection of microcystin-LR. Biosens Bioelectron. 2003;18(2):119–27.
41. Thevenot DR, Toth K, Durst RA, Wilson GS. Electrochemical biosensors: recommended definitions and classification. Pure Appl Chem. 1999;71(12):2333–48.
42. Tothill IE. Biosensors developments and potential applications in the agricultural diagnosis sector. Comput Electron Agric. 2001;30(1):205–18.
43. Tothill IE. Biosensors for cancer markers diagnosis. Semi Cell Dev Biol. 2009; 20(1):55–62.
44. McNeil SE. Nanotechnology for the biologist. J Leukoc Biol. 2005;78(3):585–94.
45. Katz E, Willner I. Biomolecule-functionalized carbon nanotubes: applications in nanobioelectronics. ChemPhysChem. 2004;5(8):1084–104.
46. Katz E, Willner I, Wang J. Electroanalytical and bioelectroanalytical systems based on metal and semiconductor nanoparticles. Electroanalysis. 2004;16(12):19–44.
47. Willner I, Baron R, Willner B. Integrated nanoparticle–biomolecule systems for biosensing and bioelectronics. Biosens Bioelectron. 2007;22(9):1841–52.
48. Kerman K, Saito M, Tamiya E, Yamamura S, Takamura Y. Nanomaterial-based electrochemical biosensors for medical applications. TrAC Trends Anal Chem. 2008;27(7):585–92.
49. Wang J. Nanomaterial-based electrochemical biosensors. Analyst. 2005;130(4):421–6.
50. Logrieco A, Arrigan D, Brengel-Pesce K, Siciliano P, Tothill I. Microsystems technology solutions for rapid detection of toxigenic fungi and mycotoxins. Food Addit Contam. 2005;22:335–44.
51. Huang XJ, O'Mahony AM, Compton RG. Microelectrode arrays for electrochemistry: approaches to fabrication. Small. 2009;5(7):776–88.
52. Aguiar FA, Gallant A, Rosamond M, Rhodes A, Wood D, Kataky R. Conical recessed gold microelectrode arrays produced during photolithographic methods: characterisation and causes. Electrochem Commun. 2007;9(5):879–85.
53. Ordeig O, Godino N, del Campo J, Muñoz FX, Nikolajeff F, Nyholm L. On-chip electric field driven electrochemical detection using a poly (dimethylsiloxane) microchannel with gold microband electrodes. Anal Chem. 2008;80(10):3622–32.
54. Xu H, Malladi K, Wang C, Kulinsky L, Song M, Madou M. Carbon post-microarrays for glucose sensors. Biosens Bioelectron. 2008;23(11):1637–44.
55. Kress-Rogers E, Brimelow CJ. Instrumentation and sensors for the food industry. Cambridge: Woodhead Publishing; 2001.
56. Piermarini S, Micheli L, Ammida N, Palleschi G, Moscone D. Electrochemical immunosensor array using a 96-well screen-printed microplate for aflatoxin B 1 detection. Biosens Bioelectron. 2007;22(7):1434–40.
57. Ngundi MM, Shriver-Lake LC, Moore MH, Lassman ME, Ligler FS, Taitt CR. Array biosensor for detection of ochratoxin A in cereals and beverages. Anal Chem. 2005;77 (1):148–54.
58. Ngundi MM, Shriver-Lake LC, Moore MH, Ligler FS, Taitt CR. Multiplexed detection of mycotoxins in foods with a regenerable array. J Food Prot. 2006;69(12):3047–51.

59. van der Gaag B, Spath S, Dietrich H, Stigter E, Boonzaaijer G, van Osenbruggen T, Koopal K. Biosensors and multiple mycotoxin analysis. Food Control. 2003;14(4):251–4.
60. Ligler FS, Taitt CR, Shriver-Lake LC, Sapsford KE, Shubin Y, Golden JP. Array biosensor for detection of toxins. Anal Bioanal Chem. 2003;377(3):469–77.
61. Sapsford KE, Ngundi MM, Moore MH, Lassman ME, Shriver-Lake LC, Taitt CR, Ligler FS. Rapid detection of foodborne contaminants using an array biosensor. Sens Actuators B. 2006;113(2):599–607.
62. Parker CO, Lanyon YH, Manning M, Arrigan DW, Tothill IE. Electrochemical immunochip sensor for aflatoxin M1 detection. Anal Chem. 2009;81(13):5291–8.
63. Hafeman DG, Parce JW, Mcconnell HM. Light-addressable potentiometric sensor for biochemical systems. Science. 1988;240(4856):1182–5.
64. Owicki JC, Bousse LJ, Hafeman DG, Kirk GL, Olson JD, Wada HG, Parce JW. The light-addressable potentiometric sensor: principles and biological applications. Annu Rev Biophys Biomol Struct. 1994;23(23):87–113.
65. Hafner F. Cytosensor microphysiometer: technology and recent applications. Biosens Bioelectron. 2000;15(3–4):149–58.
66. Adami M, Sartore M, Nicolini C. PAB: a newly designed potentiometric alternating biosensor system. Biosens Bioelectron. 1995;10(95):155–67.
67. Liu Q, Yu H, Tan Z, Cai H, Ye W, Zhang M, Wang P. In vitro assessing the risk of drug-induced cardiotoxicity by embryonic stem cell-based biosensor. Sensors Actuators B Chem. 2011;155(1):214–9.
68. Wang P, Xu G, Qin L, Xu Y, Li Y, Li R. Cell-based biosensors and its application in biomedicine. Sensors Actuators B Chem. 2005;108(1–2):576–84.
69. Miller D. Cholinergic stimulation of the Na^+/K^+ adenosine triphosphatase as revealed by microphysiometry. Biophys J. 1993;64(3):813–23.
70. Xu G, Ye X, Qin L, Ying X, Yan L, Rong L, Ping W. Cell-based biosensors based on light-addressable potentiometric sensors for single cell monitoring. Biosens Bioelectron. 2005;20 (20):1757–63.
71. Cowey A, V.L.M. Instrumental biosensors: new perspectives for the analysis of biomolecular interactions. Bioessays 1999;21(4):339–52.
72. Eklund SE, Snider RM, Wikswo J, Baudenbacher F, Prokop A, Cliffel DE. Multianalyte microphysiometry as a tool in metabolomics and systems biology. J Electroanal Chem. 2006;587(2):333–9.
73. Eklund SE, Thompson RG, Snider RM, Carney CK, Wright DW, John W, Cliffel DE. Metabolic discrimination of select list agents by monitoring cellular responses in a multianalyte microphysiometer. Sensors. 2009;9(3):2117–33.
74. Mcconnell HM, Owicki JC, Parce JW, Miller DL, Baxter GT, Wada HG, Pitchford S. The cytosensor microphysiometer: biological applications of silicon technology. Science. 1992;257(5078):1906–12.
75. Garnovskaya MN, Mukhin YV, Vlasova TM, Raymond JR. Hypertonicity activates $Na^{+/}H^+$ exchange through Janus kinase 2 and calmodulin. J Biol Chem. 2003;278(19):16908–15.
76. Ellis AG, Doherty MM, Walker F, Weinstock J, Nerrie M, Vitali A, Murphy R, Johns TG, Scott AM, Levitzki A. Preclinical analysis of the analinoquinazoline AG1478, a specific small molecule inhibitor of EGF receptor tyrosine kinase. Biochem Pharmacol. 2006;71 (10):1422–34.
77. Okada Y, Taniguchi T, Akagi Y, Muramatsu I. Two-phase response of acid extrusion triggered by purinoceptor in Chinese hamster ovary cells. Eur J Pharmacol. 2002;455 (1):19–25.
78. Fujii R, Hosoya M, Fukusumi S, Kawamata Y, Habata Y, Hinuma S, Onda H, Nishimura O, Fujino M. Identification of neuromedin U as the cognate ligand of the orphan G protein-coupled receptor FM-3. J Biol Chem. 2000;275(28):21068–74.

79. Kramarenko I, Bunni M, Morinelli TA, Raymond J, Garnovskaya M. Identification of functional bradykinin B(2) receptors endogenously expressed in HEK293 cells'. Biochem Pharmacol. 2009;77(77):269–76.
80. Coaxum SD, Garnovskaya MM. Epidermal growth factor activates Na(+/)H(+) exchanger in podocytes through a mechanism that involves Janus kinase and calmodulin. Biochim Biophys Acta. 2009;1793(7):1174–81.
81. Gonzalo A, Tze-Jen H, Catherine W, Alex V, Paul F, Gibson RM. Insulin-like growth factor-1-dependent maintenance of neuronal metabolism through the phosphatidylinositol 3-kinase-Akt pathway is inhibited by C2-ceramide in CAD cells. Eur J Neurosci. 2007;25(10):3030–8.
82. Fischer H, Seelig A, Beier N, Raddatz P, Seelig J. New drugs for the Na^+/H^+ exchanger. Influence of Na^+ concentration and determination of inhibition constants with a microphysiometer. J Membr Biol. 1999;168(1):39–45.
83. V.X.D.O. Jr, Fázio MA, Santos EL, Pesquero JB, Miranda A. In vitro evaluation of leptin fragments activity on the ob receptor. J Pept Sci Off Publ Eur Pept Soc. 2008;14(5):617–25.
84. Douglas ES, Hsiao SC, Onoe H, Bertozzi CR, Francis MB, Mathies RA. DNA-barcode directed capture and electrochemical metabolic analysis of single mammalian cells on a microelectrode array. Lab Chip. 2009;9(14):2010–5.
85. Cunha FM, Berti DA, Ferreira ZS, Klitzke CF, Markus RP, Ferro ES. Intracellular peptides as natural regulators of cell signaling. J Biol Chem. 2008;283(36):24448–59.
86. Santos EL, Reis RI, Silva RG, Shimuta SI, Pecher C, Bascands JL, Schanstra JP, Oliveira L, Bader M, Paiva ACM. Functional rescue of a defective angiotensin II AT1 receptor mutant by the Mas protooncogene. Regul Pept. 2007;141(1–3):159–67.
87. Santos EL, Souza KDP, Sabatini RA, Martin RP, Fernandes L, Nardi DT, Malavolta L, Shimuta SI, Nakaie CR, Pesquero JB. Functional assessment of angiotensin II and bradykinin analogues containing the paramagnetic amino acid TOAC. Int Immunopharmacol. 2008;8 (2):293–9.
88. Karin B, Lena P, Kjell L. Metabolic activation of A549 human airway epithelial cells by organic dust: a study based on microphysiometry. Life Sci. 2002;71(3):299–309.
89. Belgin S, Ismail B, Ahmet G, Khan O. Functional analysis of amino acids of the Na^+/H^+ exchanger that are important for proton translocation. Mol Cell Biochem. 2003;254 (1–2):117–24.
90. Smart D, Wood MD. Cytosensor techniques for examining signal transduction of neurohormones. Biochem Cell Biol. 2000;78(78):281–8.
91. Roth C, Kohen R, Walton S, Yarmush M. Coupling of inflammatory cytokine signaling pathways probed by measurements of extracellular acidification rate. Biophys Chem. 2001;89(1):1–12.
92. Parce JW, Owicki JC, Kercso KM, Sigal GB, Wada HG, Muir VC, Bousse LJ, Ross KL, Sikic BI, Mcconnell HM. Detection of cell-affecting agents with a silicon biosensor. Science. 1989;246(4927):243–7.
93. Bruner LH, Miller KR, Owicki JC, Parce JW, Muir VC. Testing ocular irritancy in vitro with the silicon microphysiometer. Toxicol In Vitro Int J Publ Assoc Bibra. 1991;5(4):277–84.
94. Landin W, Mun G, Nims R, Harbell J. Use of the cytosensor microphysiometer to predict results of a 21-day cumulative irritation patch test in humans. Toxicol In Vitro. 2007;21 (6):1165–73.
95. Waldenmaier DS, Babarina A, Kischkel FC. Rapid in vitro chemosensitivity analysis of human colon tumor cell lines. Toxicol Appl Pharmacol. 2003;192(3):237–45.
96. Yicong W, Ping W, Xuesong Y, Qingtao Z, Rong L, Weimin Y, Xiaoxiang Z. A novel microphysiometer based on MLAPS for drugs screening. Biosens Bioelectron. 2001;16 (4–5):277–86.
97. Wu Y, Wang P, Ye X, Zhang G, He H, Yan W, Zheng X, Han J, Cui D. Drug evaluations using a novel microphysiometer based on cell-based biosensors. Sensors Actuators B Chem. 2001;80(3):215–21.

98. Siqueira JR, Werner CF, Bäcker M, Poghossian A, Zucolotto V, Oliveira ON, Schöning MJ. Layer-by-layer assembly of carbon nanotubes incorporated in light-addressable potentiometric sensors. J Phys Chem. 2009;113(33):14765–70.
99. Ismail ABM, Yoshinobu T, Iwasaki H, Sugihara H, Yukimasa T, Hirata I, Iwata H. Investigation on light-addressable potentiometric sensor as a possible cell-semiconductor hybrid. Biosens Bioelectron. 2003;18(12):1509–14.
100. Stein B, George M, Gaub HE, Parak WJ. Extracellular measurements of averaged ionic currents with the light-addressable potentiometric sensor (LAPS). Sensors Actuators B Chem. 2004;98(2):299–304.
101. Liu Q, Cai H, Xu Y, Li Y, Li R, Wang P. Olfactory cell-based biosensor: a first step towards a neurochip of bioelectronic nose. Biosens Bioelectron. 2006;22(2):318–22.
102. George M, Parak WJ, Gerhardt I, Moritz W, Kaesen F, Geiger H, Eisele I, Gaub HE. Can the light-addressable potentiometric sensor (LAPS) detect extracellular potentials of cardiac myocytes? Sensors Actuators A Phys. 2000;47(8):1106–13.
103. Zhang W, Li Y, Liu Q, Xu Y, Cai H, Wang P. A novel experimental research based on taste cell chips for taste transduction mechanism. Sensors Actuators B Chem. 2008;131(1):24–8.
104. George M, Parak WJ, Gaub HE. Highly integrated surface potential sensors. Sensors Actuators B Chem. 2000;69(3):266–75.
105. Liu Q, Cai H, Xu Y, Xiao L, Yang M, Wang P. Detection of heavy metal toxicity using cardiac cell-based biosensor. Biosens Bioelectron. 2007;22(12):3224–9.
106. Liu Q, Cai H, Xiao L, Li R, Yang M, Wang P. Embryonic stem cells biosensor and its application in drug analysis and toxin detection. Sensors J IEEE. 2007;7(12):1625–31.
107. Liu Q, Ye W, Yu H, Hu N, Du L, Wang P, Yang M. Olfactory mucosa tissue-based biosensor: a bioelectronic nose with receptor cells in intact olfactory epithelium. Sensors Actuators B Chem. 2010;146(2):527–33.
108. Bucher V, Leibrock C, Schubert MNW, Brunner B. Electrical properties of a light-addressable microelectrode chip with high electrode density for extracellular stimulation and recording of excitable cells. Biosens Bioelectron. 2001;16(3):205–10.
109. Artem S, Jung C, Sebastian HS. Light-directed electrical stimulation of neurons cultured on silicon wafers. J Neurophysiol. 2005;93(2):1090–8.

Chapter 9
Future Trends of Micro/Nano Cell and Molecule-Based Biosensors

Ping Wang, Ning Hu, Chunsheng Wu, and K. Jimmy Hsia

Abstract The novel micro/nano cell- and molecule-based biosensors are powerful tools in cell and molecule study, ranging from the traditional microbiosensors and novel nanotechnology. In this chapter, intelligent micro/nano cell- and molecule-based biosensor biosystems, including intelligent multiparameter biosensors, intelligent high-throughput biosensor array, and intelligent multifunction biosensors, are introduced. Moreover, application perspective in biomimetic devices, health care, and rehabilitation was further discussed. These micro/nano cell and molecular biosensors have demonstrated excellent performance in cell and molecule applications and will pave a wide way in biomedicine and environmental applications.

Keywords Intelligent biosensors biosystem • Nano-micropatterned cell culture • Nano-sensors

9.1 Introduction

Biosensors will develop rapidly in the future and will become more powerful and versatile by using bioactive elements such as tissues, cells and molecules, and even organoid as sensing elements combined with microfabrication and nanotechnology to produce biomimetic sensors. These cell- and molecule-based biosensors have superior performance such as high sensitivity and selectivity to environment and other objects, which may be similar as or even superior to sensing performance of human and animals. Cell- and molecule-based biosensors employ living cells and bioactive molecule components to qualitatively and quantitatively detect and

P. Wang (✉) • N. Hu
Biosensor National Special Laboratory, Department of Biomedical Engineering, Zhejiang University, Hangzhou, China
e-mail: cnpwang@zju.edu.cn

C. Wu
Institute of Medical Engineering, School of Basic Medical Sciences, Health Science Center, Xi'an Jiaotong University, Xi'an, China

K.J. Hsia
Department of Biomedical Engineering, Carnegie Mellon University, Pittsburg, PA, USA

P. Wang et al. (eds.), *Micro/Nano Cell and Molecular Sensors*,
DOI 10.1007/978-981-10-1658-5_9

measure the presence of substances and their concentrations. These cell- and molecule-based biosensors can sense much functional information from external physical or chemical stimulations. Besides, cell- and molecule-based biosensors as biomimetic sensors will also be used in biomedical practical application. Significantly, the performance of these biosensors can be enhanced to very high levels by nanotechnology and nanomaterial, which dramatically improved the sensitivity and selectivity of cell- and molecule-based biosensors.

Future trends of cell- and molecule-based biosensors will be tightly combined with the state-of-the-art technologies, e.g., microfabrication, nanotechnology, and molecular biology to build the multifunctional, integrated, and intelligent biosensor. In this chapter, we will discuss the novel trends in micro/nano cell- and molecule-based biosensors in the near future.

9.2 Intelligent Micro/Nano Cell- and Molecule-Based Biosensors and Biosystems

Integrated cell- and molecule-based biosensors can be divided into three types: integrated multiparameter biosensors, high-throughput biosensor arrays, and multifunctional biosensors. Both integrated and multifunctional cell-based biosensors can provide either high-throughput information or different functional parameters of living cells and bioactive molecules. Nowadays, micro/nano sensors integrated with cells and molecules for biomedical applications have attracted broad attention of researchers in a variety of fields.

For compound assessment, it is important to select the suitable model to evaluate the compound effect, so the integrated multifunctional sensors can be employed in these cases to determine the right compound analysis models. After these bioassays, multiparameter data can be collected for further study. Thus, the suitable models or screening methods can be determined for the subsequent high-throughput analysis with sensor array. These intelligent biosensors could significantly reduce the cost for compound analysis. For example, in vitro cellular bioassay can be performed prior to using the drug candidates on animal models, which is time-consuming and expensive. Consequently, nowadays researches are focused to integrate different sensors into miniaturized biochips for a multiparameter online analysis of living cells and bioactive molecules for physiological and environmental monitoring. The throughput of extracellular parameters can be greatly enhanced, and molecule concentration can be measured by these intelligent sensors. It is a different approach in functional online analysis of living cells and bioactive molecule in physiologically controlled environments for extended periods of time.

9.2.1 Intelligent Multiparameter Biosensors

Different biosensors and detection technologies are used to obtain more information about living cells and bioactive molecules. Bernhard Wolf et al. [1, 2]

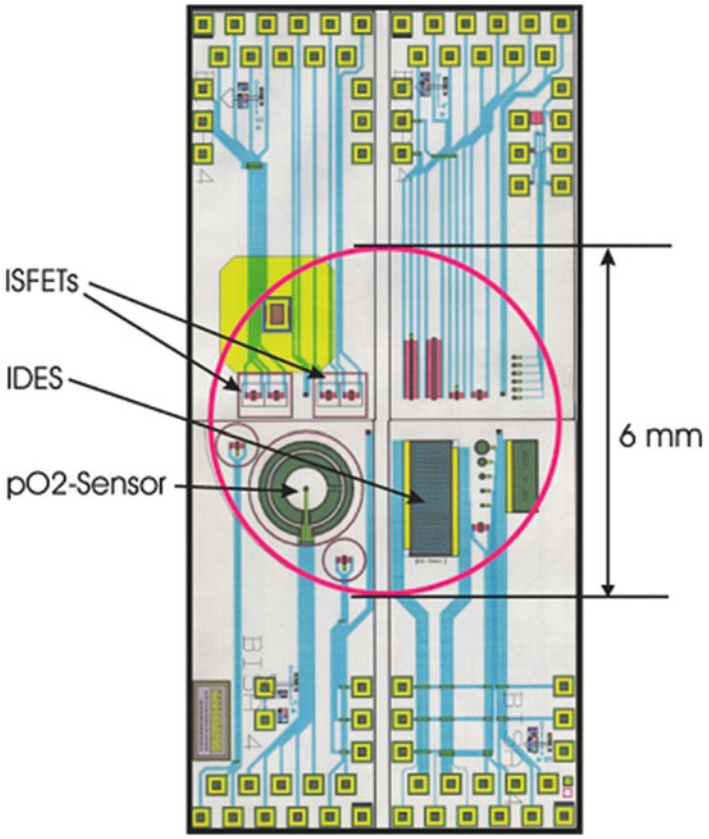

Fig. 9.1 Intelligent sensor chips based on integration of potentiometric, amperometric, and impedance sensor (Reproduced with permission from Ref. [5]. Copyright 2003 Royal Society of Chemistry)

fabricated several types of integrated chips, which contain interdigitated electrodes (IDES), ISFET, O_2 sensor, and temperature sensors as shown in Fig. 9.1. This intelligent miniaturized biosystem can obtain sufficient information from cells and their metabolic molecules. These various cell- and molecule-based biosystems allowed online and noninvasive measurements of different parameters of signaling based on cells and molecular detection [3, 4].

These multiparameter integrated sensors are used for investigations of cells by real-time recording extracellular physiological status and molecular changes in the microenvironment. Potentiometric, amperometric, and impedance sensors are designed on the single chip for multiparameter monitoring [5]. Extracellular acidification rates (by ion-sensitive field-effect transistors), oxygen consumption rates (by Pt electrode), and cell morphology (by impedance electrode) can be simultaneously monitored on single chips for days.

Integrated cell- and molecule-based biosensors with multiparameter biosensors play a significant role in recent decade. Multiparameter biosensors can provide

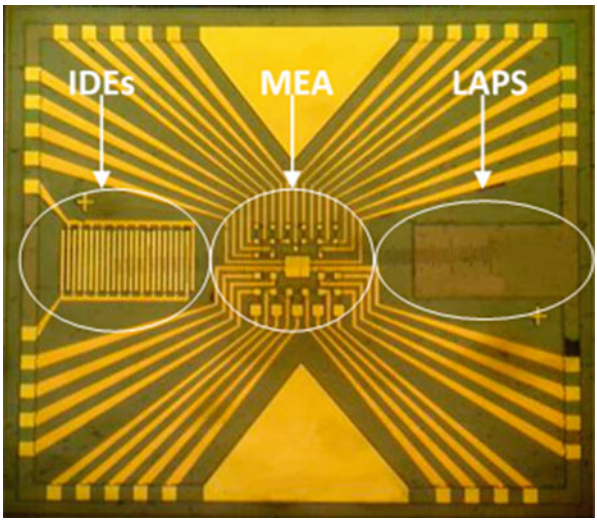

Fig. 9.2 Integrated cell- and molecule-based biosensors including ECIS, MEA, and LAPS

more information on the status of cells and molecules. As shown in Fig. 9.2, the integrated chip is integrated by interdigitated electrodes (IDEs) that measure the impedance of cells for growth evaluation, microelectrode array (MEA) which detects the extracellular potential of cells, and light-addressable potentiometric sensor (LAPS) which monitors the cellular metabolites in microenvironment. In a multiparameter integrated chip, these three biosensors are incorporated into a single chip. After living cells are seeded on this chip, both chemical and electrical parameters can be recorded. Living conditions of the target cells, including the cell growth and metabolism, can be analyzed from the data of IDA and LAPS part. The extracellular potential can be detected by the MEA part.

9.2.2 Intelligent High-Throughput Biosensor Array

Intelligent cell- and molecule-based biosensors array is utility for high-throughput bioassays after the model determination, and biosensor array can dramatically improve the efficiency of bioassays. MEA, FET, LAPS, and ECIS array are commonly used in cell and molecule detection and measurement. These high-throughput cell- and molecule-based biosensor arrays can provide extracellular information of living cells and bioactive molecules.

Thomas Geisler et al. integrated multiparameter, bioelectrical, and biochemical sensors for the analytical monitoring of intra- and extracellular parameters, as shown in Fig. 9.3 [6, 7]. The intelligent multiparameter biosensor array can provide more information on cells and molecules and has the high-throughput analysis data, and thus more information can be derived for further analysis. The extracellular potential, growth, and metabolism status can be monitored in real time, which

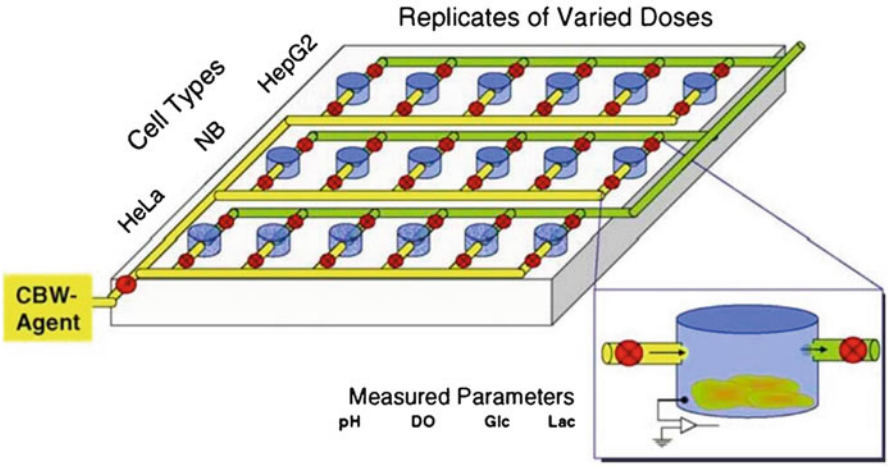

Fig. 9.3 High-throughput multiparameter biosensor array (Reproduced with permission from Ref. [8]. Copyright 2006 Elsevier B.V.)

reflected extracellular status. These high-throughput cell- and molecule-based biosensor arrays can not only improve the efficiency of bioassays but enrich the high-content analysis as well.

Multifunction cell- and molecule-based biosensors are another important advancement, which is different from the multiparameter sensors. They can perform different functions through different working modes. ECIS can monitor the cell growth status and record the cardiomyocyte beating status under the high-speed mode. LAPS is another typical multifunction sensor. Usually, LAPS is used to monitor the cellular metabolic molecules, while it also can be used to detect the cardiomyocyte beating status. Higher and higher levels of integration are the most important feature of the requirement of integrated cell- and molecule-based biosensors. Most integrated cell-based biosensors involve all three types of intelligent cell- and molecule-based sensors at the same time. High level integration can provide more comprehensive information to give precise determination of cell and molecular functions. Therefore, more precise and rigorous preselection of identified compounds can be achieved with these integrated cell- and molecule-based biosensors.

9.2.3 Devices Through Integrating MEMS/Micro/Nano Technologies and Live Cells for Cell Behavior Measurements and Manipulation

Hybrid systems and devices through integrating MEMS/micro/nano technologies and live cells have been actively developed in recent years. Although many studies

focus on biological and biochemical properties of cells, several recent studies utilize mechanical principles of such devices to perform certain functions [9–11], including measuring cell properties and manipulating cell responses. One such device is a novel vibrational platform developed using MEMS technology for cell mass measurements as shown in Fig. 9.4 [9]. Cell growth and cell division are highly complex biological processes that are critical in all living systems. However, there were no reliable techniques to accurately measure the mass of individual live cells as they grow and thus to determine the cell growth rate. The vibrational platform developed by Park et al. makes use of the mechanical principle of resonance frequency to measure the mass of individual live cells. The method took into account cell elasticity and cell viscosity and was able to follow the cell

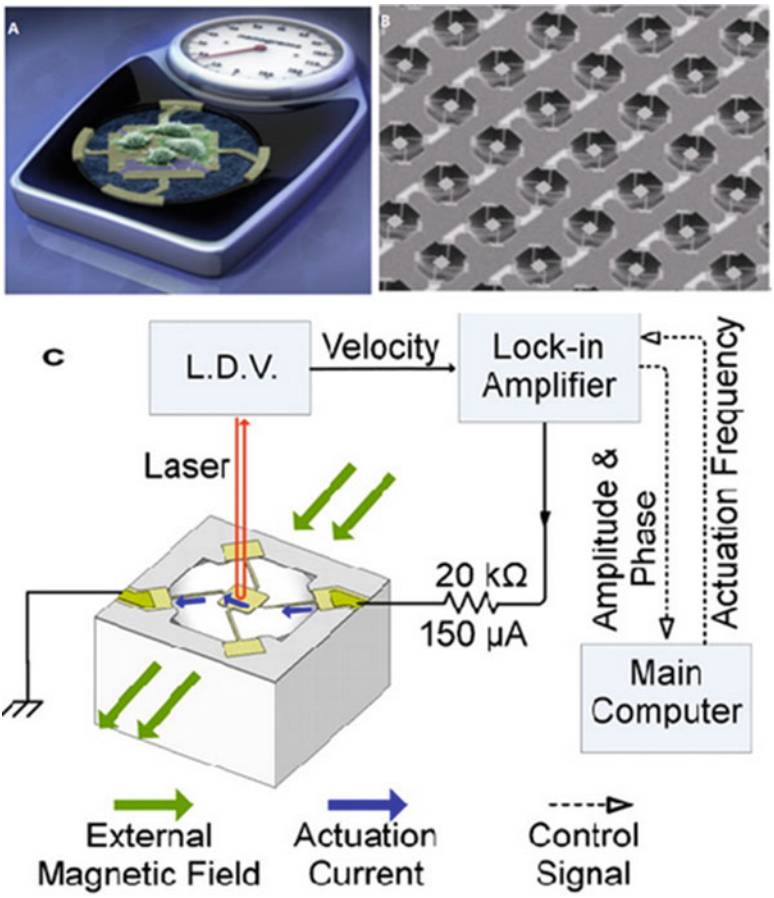

Fig. 9.4 A novel vibrational platform developed using MEMS technology for cell mass measurements: (**a**) scheme of cell mass measurement, (**b**) SEM of the array chip for cell mass measurements, and (**c**) schematic diagram of an integrated chip for cell mass measurements (Reproduced with permission from Ref. [9]. Copyright 2010 National Academy of Sciences)

growth → cell division → daughter cell growth cycles in real time. Mechanics modeling was carried out to interpret the measurement results. Understanding of what control cell growth and division processes in mammalian cells will have tremendous impact on issues like cancer cell growth and proliferation.

9.3 Application Perspective in Biomimetic Devices, Health Care, and Rehabilitation

In recent decades, nanotechnology and nanomaterials have been driving the development in science and technology. A nanometer (nm) is a billionth of a meter ($1\ \text{nm} = 10^{-9}$ m). However, nanostructure dramatically enhances the performance of the cell- and molecule-based biosensors. Nanotechnology contains the investigation, manipulation, fabrication, and employment of materials, devices, and systems under 100 nm in one dimension. Nanomaterials, e.g., nanotubes, nanopillars, nanowire, nanorods, nanocapsules, nanoparticles, and nanoporous membrane, are widely used in design and fabrication of sensors. Besides, nanotechnology also plays an increasingly significant role in the progress of cell- and molecule-based biosensors. Performance of these biosensors will be wonderfully improved by using nanomaterials or nanostructures. Nanomaterials and nanostructures present superior physical and chemical characteristics due to size effects like the quantum size effect, minisize effect, surface effect, and macro-quantum tunnel effect.

Many studies have reviewed the various nanomaterial and nanostructure-based biosensors, even at the molecular level [12]. Moreover, the nano-based biosensors also revolutionize research, analysis, and application at the cellular level. The convergence of MEMS, nanotechnology, and biology leads a new way to manipulate nanomaterial for a wide variety of biomedical applications for living cells and bioactive molecules. Nano-based biosensors will be promising tools for monitoring in vivo and in vitro biological processes, which will greatly improve our understanding of cellular function, thereby promoting cell biology.

9.3.1 Nano-micropatterned Cell Cultures

The nano-micropatterned biosensors become popular for cell cultures due to their good biocompatibility based on the characteristics for study of sensor arrays, tissue engineering, and cellular physiology in recent years. Nanomaterials and nanostructure-based biosensors have been employed in vitro and in vivo experiments, which construct the bioactive tissues and organs, improve biocompatible characteristics, and perform the relative biomedical researches. Properties of nanomaterials and nanostructures are extremely important to the design, fabrication, and use of nano-based devices. Some researches [13–15] have reported the perspective of integrated

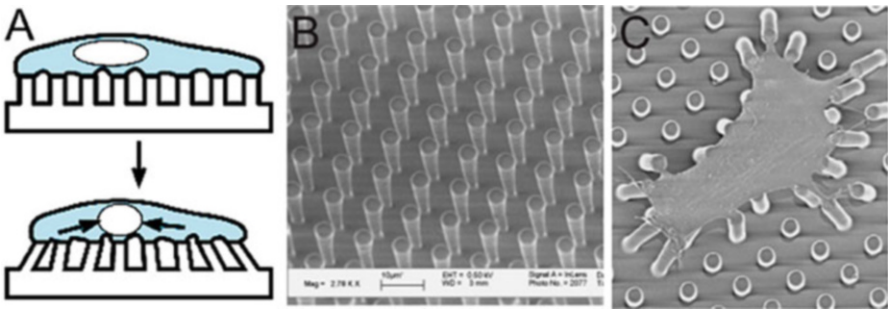

Fig. 9.5 Smooth muscle cell culture on micropillars: (**a**) cell behavior on the micropillars; (**b**) a uniform array of micropillars; and (**c**) SEM of the cell deforming the micropillar after adhesion (Reproduced with permission from Ref. [16]. Copyright 2003 National Academy of Sciences)

nanomaterials and nanostructures to sense living cells. In many researches, the nanoparticles are assembled to pattern and fabricate the substrate for cell study. The nanomaterials and nanostructures can significantly increase the surface area which can enhance the performance of biosensors for detection and measurement. Furthermore, a nanomaterial or nanostructure substrate can affect the conformation and functionality of proteins which attach onto its surface. Moreover, cell status in terms of morphology, adhesion, proliferation, differentiation, etc. can be influenced by micro- and nano-modified surfaces.

Researchers [16] described a method to measure mechanical interactions of cell-cell attachment and cell-substrate attachment by using microfabricated arrays of elastic PDMS micropillars (Fig. 9.5). Cells cultured on the surface can attach and spread on the micropillars. The deformation of the micropillars occurred independently of neighboring micropillars; therefore, the deformation of micropillars directly reflects the subcellular distribution of interaction forces. By controlling cell attachment on these micromechanical sensors, cell morphology regulates the magnitude of interaction force generated by cells. These results demonstrate a coordination of biochemical and mechanical signals to regulate cell attachment, and micropillar array is introduced to fabricate mechanically isolated sensors to measure the mechanical interactions of cells.

9.3.2 Nanoporous-Based Biosensor

The high surface area-to-volume ratio is one of the most important characteristics of nanomaterials. The increased nanomaterial or nanostructure surface can act as the adsorbents to embed small molecular particles into the pores. The properties of nanoporous, e.g., pore size, morphology, structure, and specific distribution which directly interact with cells or molecule, enhance absorption and ultimately result in

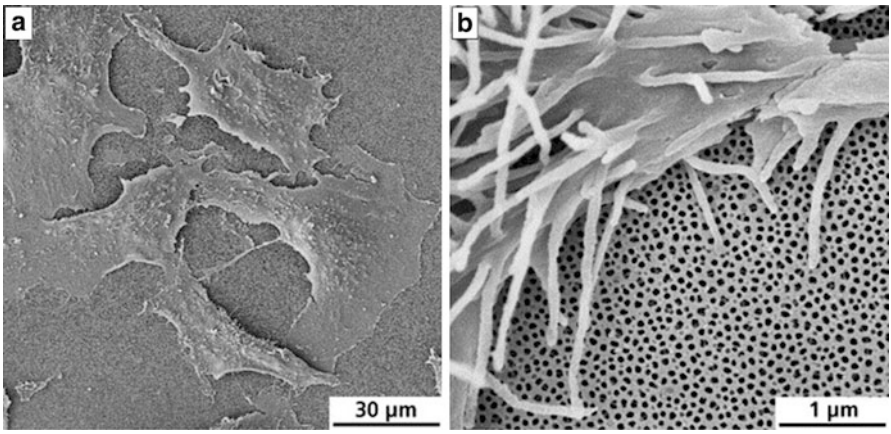

Fig. 9.6 HepG2 cells on self-supporting aluminum oxide membrane 1 (pore diameter is about 75 nm). Overview (**a**) and magnification of a cell border (**b**) (Reproduced with permission from Ref. [18]. Copyright 2007 Elsevier B.V.)

substantial improvements on functional applications such as reaction catalysis, membrane attachment, electrode sensitivity, and so on.

Nanoporous materials are not only used in biomedical fields but other research fields as well. Nanoporous anodic aluminum oxide (AAO), or known as alumina, attracted more attention due to excellent biocompatibility and fabrication process, as shown in Fig. 9.6 [11, 17, 18]. Alumina has already been extensively employed as a sensor substrate for cell and tissue culture. To achieve applications of cell or tissue engineering, the biocompatibility of the nanostructure surface is one of the most important factors for cell study. For example, osteoblast has been used in the study of alumina surfaces in different labs. In some study, a two-step anodization process was optimized with uniform pore dimension and distribution in the fabrication of nanoporous alumina membranes. The impact of the nanopores was studied by evaluating osteoblast adhesion, morphology, and proliferation via different methods. The results show that alumina surfaces have significant biointegration for cell growth and the measurement of cell response can be greatly improved with nanoscale structure.

Our research group has successfully fabricated AAO using a two-step anodization procedure, with pores sized between 50 and 120 nm. A cell molecule-based biosystem was established with PDMS chamber to perform the cell culture and molecule measurement [19]. Different cells were cultured on the AAO surface of sensor, and cell responses to specific compounds have been observed. In our new analytical biosystem based on this, the cancer cells' response to anticancer drug can be found in multifrequency electrical impedance spectra. The new nanostructure biosensor will be promising to enhance the sensor performance and replace the traditional time-consuming cell bioassays or microscopic techniques in anticancer drug screening in the future.

9.3.3 Nanoprobes to Intracellular Nano-sensors

With the advancement of nanotechnology, nanoscale devices can be used to probe the intracellular environmental status of single living cells, leading to more true information of the whole cell. It can greatly improve our understanding of cellular function as a novel method. Those nano-sensors could be fabricated to nanoscale size, which makes them suitable for sensing and measuring intracellular physiological parameters of single cell.

Zinc oxide (ZnO) is popular in the sensor fabrication due to its semiconducting, unique optical, piezoelectric, and magnetic properties. ZnO nanostructures present good characteristic including high catalytic efficiency and strong adsorption ability. In the recent years, the interest has been focused toward the application of ZnO in biosensing based on its high isoelectric point, biocompatibility, and fast electron-transfer kinetics, indicating the potential applications of ZnO as one of the promising materials for biosensor applications [20].

Nanostructure ZnO nanorods are suitable for intracellular pH measurement. Some authors have reported ZnO nanorods as an intracellular sensor for pH measurements [21]. Main effort has been made to construct nanorod tips, which are capable of penetrating the cell membrane as well as optimization of the electrode properties. ZnO nanorods are grown on the tip of a borosilicate glass capillary (0.7 μm in diameter), and a highly sensitive ZnO nanorod pH sensor is created for monitoring intracellular environment of single cell. The ZnO nanorods, functionalized by proton H^+ and hydroxyl OH^- groups, present a pH-dependent behavior versus an Ag/AgCl reference electrode (Fig. 9.7). The pH potential difference is linear over a large dynamic range. Therefore, these nanoelectrode devices can carry out analytical measurements in single living cells and sense individual chemical species in specific locations within a cell.

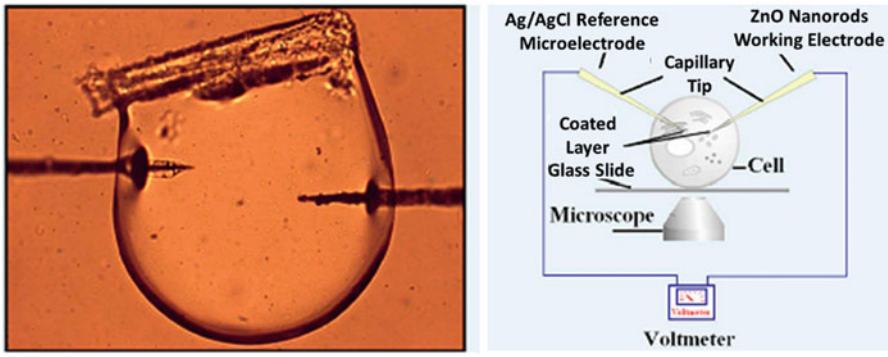

Fig. 9.7 Optical image and schematic diagram illustrating intracellular pH measurements performed in a single human fat cell using ZnO nanorods (Reproduced with permission from Ref. [21]. Copyright 2007 American Institute of Physics)

9.3.4 *Nano- and Micro-patterned Surface for Cell Behavior Manipulation*

Micro/nano technologies have also been used to control cell behavior. By seeding C2C12 cells on a surface with submicron-/micron-scale waviness, Grigola et al. [10] succeeded in aligning the migrating cells along the wavy directions. More importantly, they were able to identify the critical conditions governing cell alignment. C2C12 are skeletal muscle cells. Being able to align them allows us to form precursor tissues that can be differentiated into muscle strips. This technology is potentially very useful to constructing integrated cell-nanostructure machines capable of performing mechanical functions. Another technique to form elongated cell clusters with MCF10a cells (breast cells) was developed by Joaquin et al. [11]. Instead of submicron waviness, they produced a surface with submillimeter-scale waviness. They showed that, in a 3D in vitro culture environment, these breast cells migrate following mechanical stiffness gradient to form elongated cell clusters, a precursor to ductal shaped tissues. MCF10a cells cluster into acini, i.e., hollow spheres in common 3D culture environment in vitro. However, they form hollow ducts in an in vivo culture environment, through which milk is transported in female mammals. The technique developed by Joaquin et al. [11] not only helps us understand the ECM microenvironment governing duct formation in breast cells but also has potential for tissue engineering to reconstruct breast tissues. These hybrid bio-micro/nano structured systems and devices have opened up doors for vast varieties of different functionalities to be achieved, including sensing, actuation, and shape and form manipulations.

9.4 Summary

The novel micro/nano cell and molecule-based biosensors are discussed in this book, ranging from the traditional microbiosensors to novel nanotechnology. Traditional biosensors, such as microelectode array (MEA), impedance sensor, field-effect transistor (FET), and light-addressable potentiometric sensor (LAPS), are useful tools in cell and molecule analysis, and the nanostructures and nanomaterials-based biosensors emerge gradually with the advance of nanotechnology. These nanostructure and nanomaterial-based biosensors have demonstrated excellent performance in cell and molecule applications. With a combination of sensor technology and nanotechnology, the novel micro/nano cell and molecule biosensors can explore a wide way in biomedicine and environment monitoring applications.

References

1. Baumann W, Lehmann M, Schwinde A, Ehret R, Brischwein M, Wolf B. Microelectronic sensor system for microphysiological application on living cells. Sens Actuators B. 1999;55 (1):77–89.
2. Wolf B, Brischwein M, Lob V, Ressler J, Wiest J. Cellular signaling: aspects for tumor diagnosis and therapy. Biomed Tech. 2007;52(1):164–8.
3. Henning T, Brischwein M, Baumann W, Ehret R, Freund I, Kammerer R, Lehmann M, Schwinde A, Wolf B. Approach to a multiparametric sensor-chip-based tumor chemosensitivity assay. Anticancer Drugs. 2001;12(1):21–32.
4. Otto AM, Brischwein M, Motrescu E, Wolf B. Analysis of drug action on tumor cell metabolism using electronic sensor chips. Arch Pharm. 2004;337(12):682–6.
5. Brischwein M, Motrescu E, Cabala E, Otto A, Grothe H, Wolf B. Functional cellular assays with multiparametric silicon sensor chips. Lab Chip. 2003;3(4):234–40.
6. Geisler T, Ressler J, Harz H, Wolf B, Uhl R. Automated multiparametric platform for high-content and high-throughput analytical screening on living cells. Autom Sci Eng IEEE Trans. 2006;3(2):169–76.
7. Becker D-IB, Lob V, Janzen N, Grundl D, Ilchmann F, Wolf B. Automated multi-parametric label free 24 channel real-time screening system. In Editor (Ed.)^(Eds.) Book automated multi-parametric label free 24 channel real-time screening system. Springer; 2008, edn, p. 186–189.
8. Eklund SE, Snider RM, Wikswo J, Baudenbacher F, Prokop A, Cliffel DE. Multianalyte microphysiometry as a tool in metabolomics and systems biology. J Electroanal Chem. 2006;587(2):333–9.
9. Park K, Millet LJ, Kim N, Li H, Jin X, Popescu G, Aluru N, Hsia KJ, Bashir R. Measurement of adherent cell mass and growth. Proc Natl Acad Sci. 2010;107(48):20691–6.
10. Grigola MS, Dyck CL, Babacan DS, Joaquin DN, Hsia KJ. Myoblast alignment on 2D wavy patterns: dependence on feature characteristics and cell-cell interaction. Biotechnol Bioeng. 2014;111(8):1617–26.
11. Joaquin D, Grigola M, Kwon G, Blasius C, Han Y, Perlitz D, Jiang J, Ziegler Y, Nardulli A, Hsia KJ. Cell migration and organization in three-dimensional in vitro culture driven by stiffness gradient. Biotechnol Bioeng. 2016;9999:1–11.
12. Jianrong C, Yuqing M, Nongyue H, Xiaohua W, Sijiao L. Nanotechnology and biosensors. Biotechnol Adv. 2004;22(7):505–18.
13. Helmke BP, Minerick AR. Designing a nano-interface in a microfluidic chip to probe living cells: challenges and perspectives. Proc Natl Acad Sci. 2006;103(17):6419–24.
14. Kriparamanan R, Aswath P, Zhou A, Tang L, Nguyen KT. Nanotopography: cellular responses to nanostructured materials. J Nanosci Nanotechnol. 2006;6(7):1905–19.
15. Yap F, Zhang Y. Protein and cell micropatterning and its integration with micro/nanoparticles assembly. Biosens Bioelectron. 2007;22(6):775–88.
16. Tan JL, Tien J, Pirone DM, Gray DS, Bhadriraju K, Chen CS. Cells lying on a bed of microneedles: an approach to isolate mechanical force. Proc Natl Acad Sci. 2003;100 (4):1484–9.
17. Swan EEL, Popat KC, Grimes CA, Desai TA. Fabrication and evaluation of nanoporous alumina membranes for osteoblast culture. J Biomed Mater Res A. 2005;72(3):288–95.
18. Hoess A, Teuscher N, Thormann A, Aurich H, Heilmann A. Cultivation of hepatoma cell line HepG2 on nanoporous aluminum oxide membranes. Acta Biomater. 2007;3(1):43–50.
19. Yu J, Liu Z, Liu Q, Yuen KT, Mak AF, Yang M, Leung P. A polyethylene glycol (PEG) microfluidic chip with nanostructures for bacteria rapid patterning and detection. Sensors Actuators A Phys. 2009;154(2):288–94.
20. Kumar SA, Chen SM. Nanostructured zinc oxide particles in chemically modified electrodes for biosensor applications. Anal Lett. 2008;41(2):141–58.
21. Al-Hilli SM, Willander M, Öst A, Stralfors P. ZnO nanorods as an intracellular sensor for pH measurements. J Appl Phys. 2007;102(8):4304.

Index

P. Wang et al. (eds.), *Micro/Nano Cell and Molecular Sensors*,
DOI 10.1007/978-981-10-1658-5